IMPROVED SEISMIC DESIGN OF STRUCTURES USING RISK-TARGETING AND COST-MINIMIZATION CONSIDERATIONS

BY

ATHANASIOS GKIMPRIXIS

A DISSERTATION SUBMITTED TO THE DEPARTMENT OF CIVIL AND ENVIRONMENTAL ENGINEERING OF THE UNIVERSITY OF STRATHCLYDE, GLASGOW FOR THE DEGREE OF DOCTOR OF PHILOSOPHY

JUNE 2020

This thesis is the result of the author's original research. It has been composed by the author and has not been previously submitted for examination which has led to the award of a degree.

Signed: Athanasios Gkimprixis

Date: 29/06/20

Abstract

This thesis addresses various topics in the context of seismic design of structures with risk and loss considerations. Three design philosophies are investigated: the one based on uniform-hazard spectra, the risk-targeting technique, and an approach that minimizes the life-cycle costs.

While the "uniform-hazard" approach is embedded in most of seismic design regulations, many studies have highlighted the need for a more rigorous and explicit control of the structural performance and of the consequences of seismic damage, not only at the assessment but also at the design stage. Thus, in this context, the risk-targeting philosophy has emerged and has been implemented in US regulations. This approach is thoroughly reviewed herein, together with alternative risk-targeting techniques. Various case studies and European-wide investigations are performed to compare the results obtained with the risk-targeting and the uniform hazard approaches, evaluate the strengths and limitations of the techniques, and show possible steps forward.

Acknowledging the significant financial implications of earthquakes, more advanced frameworks have been developed to account also for losses from future earthquake events in the design. A life-cycle cost optimization technique that considers the initial construction costs and the expected losses is studied in this work. A benchmark building is designed and analysed for different seismic levels and the results are compared against those obtained with the uniform-hazard and the risk-targeting approaches.

Subsequently, an investigation is carried out on how the epistemic uncertainty inherent in seismic hazard models influences the structural design and the attained risk and loss estimates. The topic is investigated through different case studies, while a simplified approach for modelling hazard uncertainty is introduced and applied across Europe.

In addition to constructing frameworks that mitigate losses, earthquake engineering can provide guidance to help manage the incurred loss levels. Thus, the last part of this thesis looks at the seismic risk management via the mechanism of transfer of financial risk. A method to define loss-informed insurance premiums is presented and various investigations across Europe are performed to explore efficient insurance strategies.

Acknowledgements

The research for this thesis was funded by the University of Strathclyde “Engineering The Future” studentship, for which I am grateful. Supervision of the work was carried out by Dr. John Douglas and Dr. Enrico Tubaldi. I would like to express my deepest gratitude to both of them, for their continuous guidance and support through my PhD studies. Most of the work presented in this thesis has already being published. For this, I want to thank Prof. Jack Baker, Dr. Hing-Ho Tsang and Dr. Vitor Silva for reviewing part of this work and also the rest of the anonymous reviewers. Their useful feedback contributed to improve my research work. Thanks are extended to Dr. Flavia De Luca and Prof. Edoardo Patelli for being the examiners of this thesis. I want also to thank Prof. Daniele Zonta and Mr. Athanasios Antyras for their help in the early stages of my PhD. Last but not least, I want to express my deepest thanks to my family and my friends who always support me with their love, patience and encouragement.

Table of Contents

List of figures

List of tables

CHAPTER 1

Introduction

1.1 Background

Being one of the world's deadliest natural hazards, earthquakes challenge researchers from different scientific fields to assess future seismic activity and guide risk mitigation and management accordingly. Earthquake engineering is a relative new field, a development of the 20th century (Housner 1984), that has found its way into structural design regulations but is still under evolution.

Lessons learnt from past historical earthquakes have initiated significant advances in seismic design principles (Fajfar 2018; Landolfo et al. 2017; Bertero and Bozorgnia 2004). After the 1908 Messina-Reggio earthquake, the Italian Government Commission published the world's first seismic design code. For the first time the concept of the equivalent static approach (still in use nowadays) was introduced, with the seismic loading expressed as a percentage of the weight of the structure. In Japan, the 1855 Edo earthquake highlighted the need for increased shear-bearing capacity of the buildings, but the first Japanese seismic code was introduced only after the 1923 earthquake in Kanto. Similarly, in the US, the 1906 San Francisco earthquake was a devastating event, but earthquake engineering found its way into the regulations only after the 1925 Santa Barbara and the 1933 Long Beach earthquakes.

The continuous evolution of the seismic analyses is summarized in the gradual consideration of three key features that characterize the seismic response of structures, i.e. dynamics, inelasticity and randomness (Fajfar 2018). A first attempt for the consideration of dynamics was made in the Los Angeles city code in 1943, by relating

the seismic load to the number of storeys. The seismic forces are eventually related directly to the fundamental period of vibration of the structure in the 1956 San Francisco recommendations. Two significant advances are made in the following years: the modal response spectrum method, in the USSR's 1957 seismic code, which still remains at the basis of worldwide design regulations, and the consideration of energy dissipation in the inelastic range, in the 1959 SEAOC model code.

Modern codes have their start in 1978 (Fajfar 2018), when ATC 3-06 (ATC 1978) was released. This document included seismic hazard maps for a 475-years return period and also introduced the use of a reduction factor (response modification factor or behaviour factor of the American and European regulations, respectively) to account for the inelasticity of structural response. An elastic analysis can be performed with the seismic forces reduced by this factor, considering the energy dissipation in ductile structures and the inherent overstrength.

However, only nonlinear analyses allow a truly realistic assessment of the inelastic structural behaviour (Fajfar 2018). Response-history analysis was introduced in the seismic code of the former Yugoslavia (JUS 1981), while pushover-based techniques appeared in the 1970s, constituting the capacity spectrum method in the 1986 USA guidelines.

All these advancements in design codes have contributed to increase the safety levels of structures under extreme seismic events. However, many past earthquakes showed that the economic losses due to damage of structural and non-structural components of modern buildings designed to seismic codes could still be devastating. Notable examples of destructive events are the 1989 Loma Prieta, the 1994 Northridge and the 1995 Kobe earthquakes. This initiated the development of performance-based design techniques, introducing different design criteria that need to be met in order to achieve various design objectives (not only collapse prevention). This philosophy has found its way in various documentations such as Vision 2000 report (SEAOC, 1995), ATC-40 (ATC, 1996), FEMA-273 (BSSC, 1997), and FEMA-356 (ASCE, 2000). Similarly, two performance objectives were introduced within Eurocode 8 (CEN 2004): 'no-collapse' under the design seismic action, and 'damage limitation' under a more frequent seismic scenario.

The performance assessment in the above procedures still remains essentially deterministic, however, with the uncertainty inherent in the seismic input, and the structural properties and behaviour taken into account in a crude way by introducing some concepts from probabilistic seismic hazard analyses such as the uniform hazard spectrum, and by adding a series of safety factors. This approach however fails to explicitly control the risk levels the designed structures are exposed to (e.g. Collins et al. 1996; Tubaldi et al. 2012; Silva et al. 2016; Iervolino et al. 2018).

Acknowledging the above limitations, the philosophy of risk-based design has entered the US regulations: first for nuclear facilities (ASCE 2005), and later suggested as a design framework for standard structures (ASCE 2010). The approach was also adopted by the Indonesian regulations (Sengara et al. 2020). Apart from this approach, alternative simplified probabilistic techniques for applying risk targeting are also available. In Europe, the implementation of probabilistic concepts for performance assessment in Eurocode 8 is still under consideration (Fajfar 2018).

The focus of current research efforts is now turning to the development of tools for assessing and explicitly controlling the loss levels attained from damage of structural and non-structural components due to the expected future events, in addition to the construction cost. It is crucial that the developed frameworks use probabilistic methods to consider the uncertainties inherent in the hazard and response estimates. For example, a robust probabilistic performance-based framework was developed by the Pacific Earthquake Engineering Research (PEER) Center (see Günay and Mosalam 2013). The PEER framework considers explicitly the uncertainties inherent in the intensity, the ground-motion characteristics, the structural response, the damage, the financial implications and the casualties. As a complement, a cost-efficient framework has also to be established, for the management of these losses, for example, by transferring costs through loss-informed earthquake insurance.

1.2 Motivations

In most current seismic design regulations the design actions are defined based on a uniform-hazard spectrum with predefined exceedance frequency. This uniform-hazard approach is simple to apply and well-established, but it comes with the drawback of

uncontrollable levels of risk for different structures and locations characterized by different seismicity (e.g. Collins et al. 1996; Tubaldi et al. 2012; Silva et al. 2016; Iervolino et al. 2018).

In an attempt to explicitly control the risk levels a structure is exposed to, more rigorous design philosophies have emerged, that use fully probabilistic approaches in the design stage. A risk-targeting technique has been suggested, for example in the American regulations, while alternative risk-targeting techniques are also available (e.g. based on the use of risk-targeted behaviour factors or using directly hazard curves for inelastic response of single-degree-of-freedom systems).

Experience from the devastating losses (human and financial) of past earthquakes (e.g. 1989 Loma Prieta, 1994 Northridge or 1995 Kobe) has shown that there is also the need for loss considerations in earthquake engineering. This can be achieved with two mechanisms: mitigation and transfer. At first, design techniques with life-cycle cost considerations (balancing between the cost of seismic design and the benefit from loss reduction) should be established. Secondly, loss-informed earthquake insurance can provide risk-management solutions to reduce the financial burden of future seismic events.

These techniques generally involve a series of tasks that can be assigned to different experts, i.e. hazard analyses, structural analyses, damage (fragility) analyses and risk and loss analyses (see Figure 1.1). It is important to mention that, apart from the design of new structures and the retrofitting of the existing ones, the above analyses can find application in other sectors, as well. For example, insurance companies can estimate the expected losses due to structural and non-structural damage from future seismic events and determine the insurance premium accordingly.

A summary of the analyses involved in each design philosophy is presented in Figure 1.1. It is obvious that the more advanced the technique, the higher the complexity in its application. For example, besides its limitations, the uniform-hazard approach is easy to apply, while the US risk-targeting approach with its assumptions can confuse engineers and clients (Fajfar 2018). In the figure it is noticed that the uniform-hazard approach requires the definition of a hazard model and then the design is based on the

results of structural analyses. In risk-targeting, the fragility of the system needs to be defined in addition. Also, the minimum-cost design, which is the most developed, demands additional data for the fragility and the costs of every component of the structure (structural and non-structural).

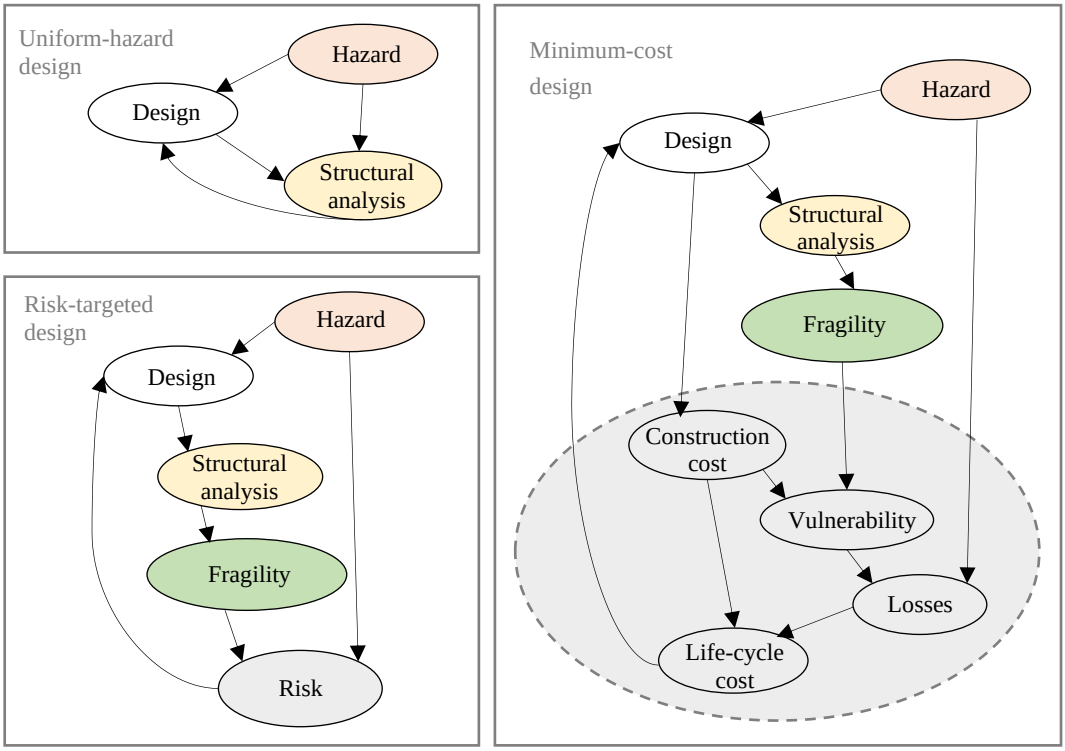

Figure 1.1 Summary of the basic steps of the three seismic design approaches

The above techniques require at first the definition of a hazard model. Due to the randomness in the nature of earthquakes, aleatory variabilities are present in the hazard estimates. Apart from these, uncertainties associated with the modelling approach, i.e. epistemic uncertainties, also affect the definition of the hazard input, which can be controlled based on the modelling assumptions and the available data (McGuire 1993). This is noticeable for example in the significant variations in the hazard data provided from different studies for the same region (e.g. Belvaux et al. 2014; Grünthal et al. 2014; Pavel et al. 2016), and the differences in the available ground motion prediction equations used for describing the seismic attenuation from the source to the site (e.g. Grünthal et al. 2018; Douglas et al. 2014; Stucchi et al. 2011; Bradley 2009). It can be understood from Figure 1.1, that this uncertainty will also be reflected in the performance assessment and the design output.

1.3 Aim and objectives

The thesis aims to critically evaluate available seismic design techniques, by identifying strengths and limitations, and highlighting possible paths that could be considered for updating the seismic design approaches of current codes. After all, according to Cornell and Krawinkler "*the final challenge is not in predicting performance or estimating losses; it is in contributing effectively to the reduction of losses and the improvement of safety*" (as quoted in ATC 2012).

Acknowledging this, the first objective of this study is to investigate the various risk-targeting approaches proposed for the seismic design of structures, since the risk-targeting philosophy has already been applied in practice and has gained intense research interest. Subsequently, the levels of safety and the costs associated with the uniform-hazard approach are investigated, given that this is the main technique found in most of the current design regulations. Then, life-cycle cost optimization criteria are analysed, by looking at how they are/can be implemented in seismic design. More specifically this dissertation aims to:

- Review the currently applied risk-targeting approach, investigate the assumptions made, discuss the limitations and suggest improvements.
- Discuss methods to define acceptable risk targets.
- Compare different approaches to undertake risk-targeting, with the aim of understanding the differences and limitations of each approach and suggest updates.
- Investigate three seismic design techniques (uniform-hazard, risk-targeting and minimum-cost) through case studies and demonstrate their application across Europe. In short, the aim here is to investigate the risk and life-cycle cost implications of the uniform-hazard method and to understand how the design will change when implementing the risk-targeting and the minimum-cost approaches.

Also, with the randomness remaining one of the most challenging and influential features of the seismic response, an additional aim is to:

- Investigate the effect of the epistemic uncertainties inherent in the hazard model on the structural performance.

The above objectives aim to explore risk mitigation tools and potential applications in the seismic design of structures. In addition, a final objective of this thesis is to:

- Investigate an alternative risk-management technique, and in particular the transfer of financial risk through earthquake insurance.

1.4 Outline

This thesis is a compilation of research articles (cited at the beginning of each chapter) and it is organized in the same order as they were written. This justifies some repetition in the thesis, so that each chapter can be read as a standalone study without needing to refer to the other chapters in detail.

In general, the first part of the thesis focuses on the risk-targeting approach, which is the latest trend in seismic design regulations. Then the uniform-hazard method, which is the current design philosophy, is evaluated. Subsequently, the minimum-cost approach is introduced. The final part of the thesis tries to provide some guidance on future research regarding hazard uncertainty and transfer of costs through earthquake insurance. In particular:

- Chapter 2 begins with an introduction of the risk-targeting philosophy and its application in the seismic design of structures. The approach presented is based on recent American regulations. The most important documents from the literature are considered to review how the input parameters vary in different regulations and studies. The concept of acceptable risk is also discussed, first by reviewing different approaches to justify tolerable levels for the risk target. A possible framework to define realistic bounds on the risk levels that can be regarded as tolerable is presented later, after a discussion of the limitations and possible improvements of the technique.
- An important input for the aforementioned technique is the fragility of the considered structures. This is the main focus of Chapter 3. In particular, different reinforced-concrete frame structures are considered to investigate the effect of the

number of storeys and bays on the fragility curves. First, 2D finite element models are developed and their design is done based on European design principles. Then various nonlinear time-history analyses are performed to generate the fragility curves of the designed models.

- Chapter 4 focuses on the most well-known approaches for risk targeting, one proposed in the American design regulations, one based on the use of risk-targeted behaviour factors (RTBF), and one based on direct estimation of hazard curves for inelastic response of single-degree-of-freedom systems. First, the sensitivity of risk-targeting on the linearization of the hazard curve is investigated. Then, a validation of the RTBF approach is presented, regarding risk-targeted design spectra for single-degree-of-freedom systems. After that, the risk-targeting framework applied in the American codes is investigated and recommendations for future modifications are provided. In the last part, the RTBF approach is implemented across Europe, for the derivation of uniform-risk hazard maps, showing how the seismic design levels change when moving from a uniform-hazard to a uniform-risk concept. The procedure is repeated for Italy using a hazard model from a different study.
- The main objective of Chapter 5 is to evaluate the three aforementioned design approaches, i.e. the uniform-hazard, the risk-targeting, and the minimum-cost approaches. The comparison is performed by quantifying the levels of safety (risk of collapse) and the costs (construction cost and life-cycle cost) associated with each technique, for a four-storey reinforced concrete frame building. First, the building is designed for different levels, following European practices and then the performance is assessed through time-history and fragility analyses. The collapse risk levels when designing with the uniform-hazard approach are estimated across Europe. Risk targeting is subsequently applied, followed by an evaluation of the design levels that minimize the life-cycle cost, considering the construction costs and the future losses caused by structural and non-structural damage. Subsequently, additional losses due to fatalities, injuries, loss of personal contents and loss of function of the building are also considered.
- The results of the fifth chapter are used in Chapter 6 as well, in order to investigate the effect of the epistemic uncertainty inherent in the definition of the seismic

hazard on the seismic risk estimates, the losses and the insurance modelling across Europe. A study is performed to evaluate the level of accuracy that is necessary in the definition of the hazard model, based on the uncertainty introduced in the cost and safety levels.

- Chapter 7 focuses on the topic of insurance. The effect of the assumptions made for the insurance model properties on the resulting premium rates is first investigated. Then a procedure for defining these properties based on target limits for the loss coverage is suggested and applied across Europe.
- Chapter 8 presents a summary of the conclusions derived from this dissertation. The limitations of this work are also discussed, and possible future research paths are highlighted.

References

ASCE - American Society of Civil Engineers (2000) Prestandard and Commentary for the Seismic Rehabilitation of Buildings, Report No. FEMA-356, Washington, DC

ASCE - American Society of Civil Engineers (2005) Seismic Design Criteria for Structures, Systems and Components in Nuclear Facilities. American Society of Civil Engineers, ASCE Standard 43-05

ASCE - American Society of Civil Engineers (2010) Minimum Design Loads for Buildings and Other Structures, ASCE Standard 7-10. American Society of Civil Engineers, Reston, VA

ATC - Applied Technology Council (1996) Seismic Evaluation and Retrofit of Concrete Buildings, Report No. ATC-40, Volume 1–2, Redwood City, California

ATC - Applied Technology Council, FEMA P-58 (2012) Seismic Performance Assessment for Buildings, Volume 1 – Methodology, Federal Emergency Management Agency, Washington, DC

ATC - Applied Technology Council (1978) Tentative provisions for the development of seismic regulations for buildings, ATC 3-06. National Bureau of Standards, Washington

Belvaux M, Douglas J, Ulrich T (2014) Comparisons between SHARE and current national seismic hazard maps for France. In Seismic Hazard Harmonization in Europe (SHARE): DGEB-Workshop

Bertero VV, Bozorgnia Y (2004) The early years of earthquake engineering and its modern goal. In Earthquake Engineering: From Engineering Seismology to Performance-Based Engineering (edited by Y. Bozorgnia and VV Bertero), CRC Press, London, UK

Bradley BA (2009) Seismic hazard epistemic uncertainty in the San Francisco bay area and its role in performance-based assessment. Earthquake Spectra, 25(4), 733-753

BSSC - Building Seismic Safety Council (1997) NEHRP Guidelines for the Seismic Rehabilitation of Buildings, Report No. FEMA-273, Federal Emergency Management Agency, Washington, DC

CEN (2004) EN 1998-1:2004 Eurocode 8: Design of structures for earthquake resistance - Part 1: General rules, seismic actions and rules for buildings, European Committee for Standardization, Brussels

Collins KR, Wen YK, Foutch DA (1996) Dual-level seismic design: a reliability-based methodology. Earthquake Engineering & Structural Dynamics, 25(12), 1433-1467

Douglas J, Ulrich T, Bertil D, Rey J (2014) Comparison of the Ranges of Uncertainty Captured in Different Seismic-Hazard Studies. Seismological Research Letters, 85(5), 977-985, doi: 10.1785/0220140084

Fajfar P (2018) Analysis in seismic provisions for buildings: past, present and future. Bulletin of Earthquake Engineering, 16, 2567–2608, doi: 10.1007/s10518-017-0290-8

Grünthal G, Bosse C, Stromeyer D (2014) Building-Code Related Seismic Hazard Snalyses of Germany and their Relation to SHARE. In Seismic Hazard Harmonization in Europe (SHARE): DGEB-Workshop, Vol. 27, pp. 25-41

Grünthal G, Stromeyer D, Bosse C, Cotton F, Bindi D (2018) The probabilistic seismic hazard assessment of Germany—version 2016, considering the range of epistemic uncertainties and aleatory variability. Bulletin of Earthquake Engineering, 16, 4339-4395

Günay S, Mosalam KM (2013) PEER performance-based earthquake engineering methodology, revisited. Journal of Earthquake Engineering, 17, 829-858

Housner GW (1984) Historical view of earthquake engineering. In: Proceedings of the 8th world conference on earthquake engineering, post-conference volume: 25–39. San Francisco, CA

Iervolino I, Spillatura A, Bazzurro P (2018) Seismic reliability of code-conforming Italian buildings. Journal of Earthquake Engineering, 22(s2), 5-27

JUS (1981) Code of technical regulations for the design and construction of buildings in seismic regions. Official Gazette of SFR Yugoslavia, 31/81 (English translation in Earthquake resistant regulations, a world list—1992, IAEE)

Landolfo R, Mazzolani F, Dubina D, da Silva LS, D'Aniello M (2017) Design of Steel Structures for Buildings in Seismic Areas. ECCS

Pavel F, Vacareanu R, Douglas J, Radulian M, Cioflan C, Barbat A (2016) An updated probabilistic seismic hazard assessment for Romania and comparison with the approach and outcomes of the SHARE project. Pure and Applied Geophysics, 173, 1881-1905, doi: 10.1007/s00024-015-1223-6

SEAOC - Structural Engineers Association of California (1995) Vision 2000, conceptual framework for performance-based seismic design. Recommended Lateral Force Requirements and Commentary. Sacramento, CA

Sengara IW, Irsyam M, Sidi ID, Mulia A, Asrurifak M, Hutabarat D, Partono W (2020) New 2019 Risk-Targeted Ground Motions for Spectral Design Criteria in Indonesian Seismic Building Code. In E3S Web of Conferences, 156, 03010, doi: 10.1051/e3sconf/202015603010

Silva V, Crowley H, Bazzurro P (2016) Exploring risk-targeted hazard maps for Europe, Earthquake Spectra, 32(2), 1165-1186

Stucchi M, Meletti C, Montaldo V, Crowley H, Calvi GM, Boschi E (2011) Seismic Hazard Assessment (2003–2009) for the Italian Building Code. Bulletin of the Seismological Society of America, 101(4), 1885-1911, doi: 10.1785/0120100130

Tubaldi E, Barbato M, Ghazizadeh S (2012) A probabilistic performance-based risk assessment approach for seismic pounding with efficient application to linear systems. Structural Safety, 36, 14-22

CHAPTER 2

Risk targeting in seismic design codes: The state of the art, outstanding issues and possible paths forward

Over the past decade there have been various studies on the development of seismic design maps using the principle of "risk-targeting". The basis of these studies is the calculation of the seismic risk by convolution of a seismic hazard curve for a given location (derived using probabilistic seismic hazard analysis) with a fragility curve for a code-designed structure (ideally derived from structural modelling). The ground-motion level that the structure is designed for is chosen so that the structure has a pre-defined probability of achieving a certain performance level (e.g. non-collapse). At present seismic design maps developed using this approach are only widely applied in practice in the US but studies have also been conducted on a national basis for France, Romania, Canada and Indonesia, as well as for the whole of Europe using the European Seismic Hazard Model.

This chapter presents a review of the state of the art of this technique, highlighting efforts to constrain better some of the input parameters. In addition, the difficulties of applying this method in practice are discussed as well as possible paths forward, including an empirical method to estimate an upper bound for the acceptable collapse and yield risk. The chapter is based on the following published article (extended and updated where appropriate):

Douglas J, Gkimprixis A (2018) Risk targeting in seismic design codes: The state of the art, outstanding issues and possible paths forward, Seismic Hazard and Risk Assessment - Updated Overview with Emphasis on Romania, R. Vacareanu and C. Ionescu (eds), Springer, doi: 10.1007/978-3-319-74724-8_14.

2.1 Introduction

Current seismic building codes [e.g. Eurocode 8 (CEN 2004b)], based on results from a probabilistic seismic hazard analysis (PSHA), generally adopt a constant hazard approach to define the ground motions used for design. In other words, the peak ground acceleration (*PGA*, or other intensity measure, *IM*, e.g. spectral acceleration) used for design in one location has the same probability of being exceeded in a given time period as the design *PGA* in another location. Often this annual probability is 1/475=0.0021 (equivalent to 10% in 50 years or a return period of 475 years assuming a Poisson process). This approach, however, does not guarantee uniform distribution of the risk levels of the designed structures in different locations. In 2007, a new approach was proposed by Luco et al. (2007) that targets a constant risk level across a territory. This has three principal advantages over the use of design levels defined in the traditional way: transparency, a uniform risk level across a territory and the ability to compare (and ideally control) risk for different types of hazard (e.g. earthquake and wind). It does come, however, with the disadvantage of making more choices explicit, rather than implicitly assumed because of convention (e.g. the choice of 475 years as the design return period).

The procedure of Luco et al. (2007), although often using different input parameters (see below), has been applied to France (Douglas et al. 2013), Romania (Vacareanu et al. 2018), Indonesia (Sengara et al. 2020), Canada (Allen et al. 2015) and at a European scale (Silva et al. 2016), as well as in the current US seismic design code (ASCE 2010; FEMA 2009a). Despite its apparent benefits (see above) and the fact that it is a relatively simple procedure to implement, there are a number of outstanding issues. For example, Douglas et al. (2013) note that the collapse probabilities targeted by Luco et al. (2007) appear to be at least an order of magnitude too high when compared with observed damage in previous earthquakes (also see Section 2.4.4 of this chapter).

The next section presents an overview of the risk targeting approach and how to apply it in practice, while previous choices of the critical input parameters are discussed in Section 2.3. A summary of different approaches to set acceptable risk targets is then

presented in Section 2.4. Finally, Section 2.5 highlights outstanding problems and potential solutions.

2.2 Method and required inputs to risk targeting

The risk of collapse of a building, λ_c, at a given site from earthquake shaking can be estimated by convolving the seismic hazard curve, $H(IM)$, expressing the probability of different levels of ground motion, with the fragility curve, $P(C|IM)$, expressing the probability of collapse given these ground motions (e.g. Kennedy 2011). This so-called "risk integral" forms the basis of the risk-targeting approach, and can be evaluated from either of the two analytically equivalent equations (Kennedy 2011):

$$\lambda_c = -\int P(C|IM) \cdot \frac{dH(IM)}{dIM} \cdot dIM = -\int P(C|IM) \cdot dH(IM) \quad (2.1)$$

$$\lambda_c = \int H(IM) \cdot \frac{dP(C|IM)}{dIM} \cdot dIM = \int H(IM) \cdot dP(C|IM) \quad (2.2)$$

where the symbol "*d"* denotes the differential and the minus sign in the first equation is used because the derivative of the hazard curve is negative. When a lognormal distribution is assumed for the fragility curve, $P(C|IM)$ is the cumulative distribution function of the standard lognormal distribution. More information on risk estimation using Eqn.(2.1) and Eqn.(2.2) can be found in the literature, e.g. in Eads et al. (2013) and Luco et al. (2007).

For this approach to work there needs to be a link between the design acceleration and the fragility curve used to compute the risk of collapse. For a standard fragility curve based on the lognormal distribution, a single point on this curve (if the standard deviation is fixed) is required to define the building's fragility completely. A convenient choice is, for example, to use the design *IM* and the corresponding probability of a building attaining the considered damage state when subjected to that *IM*.

The general procedure for finding the risk-targeted value for the considered *IM* (e.g. *PGA*) is shown in Figure 2.1. The key input parameters, using the nomenclature of Douglas et al. (2013), are: β (the standard deviation of the fragility curve assuming a lognormal distribution), X (the probability of collapse at the risk-targeted *IM*) and Y

(the targeted annual probability of failure, e.g. collapse). Seismic design codes generally do not report these values and hence assessing them has been the focus of considerable efforts over the past decade (see following section).

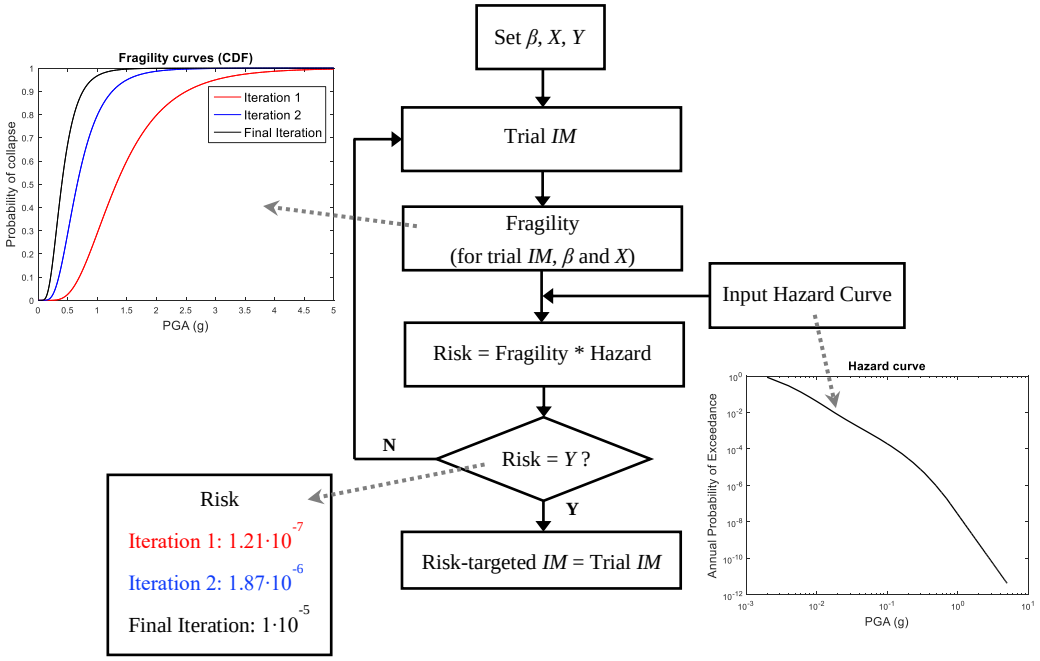

Figure 2.1 Flowchart of the method to find risk-targeted parameters

There is a closed-form solution for the risk given a hazard curve expressed as a power law and a lognormal fragility curve (see Chapter 4), which can be used to understand the influence of different parameters on the risk-targeted *IM*. For typical hazard curves, however, an iterative technique is required to determine the risk-targeted *IM* (Figure 2.1). First, a trial fragility curve is generated, based on the assumed β and for a trial *IM* value with a predefined collapse probability X. Then the risk is estimated by the convolution of the hazard and fragility curves. If the obtained risk differs from the target then a different trial *IM* value is chosen. The risk-targeted *IM* value is the one that gives a risk estimate equal to the target within a user-defined tolerance. We have found that a bisection method, which bounds the targeted risk from above and below until convergence to a given tolerance, is the best approach. The convolution is performed using the trapezium rule.

The seismic hazard curve used within the calculation needs to be defined down to potentially very low probabilities of exceedance because the probabilities of collapse

(or another damage state) defined by the fragility function are often much less than unity for large accelerations. This means that the hazard curve may need extrapolation, for which the power-law expression (based on the *IM*s for the smallest calculated probabilities) works well for most examples tested. A further investigation of this is presented in Chapter 4. The developed algorithm has been validated by comparison with results from the Risk-Targeted Ground Motion Calculator available on the USGS website (https://earthquake.usgs.gov).

2.3 The state of the art

A summary from the literature of the three key inputs to the procedure is given in this section, by reviewing the assumptions in the regulations and then in other important research works.

2.3.1 National regulations

ASCE 43-05 (ASCE 2005) provides design criteria for nuclear power plants and critical facilities based on a risk-targeting framework. The 'target performance goal' (mean annual frequency of exceeding a specified limit state) ranges from 10^{-5} to 10^{-4}, while for lower design categories values up to 10^{-3} are given in Braverman et al. (2007). To comply with the code, a nuclear plant must have a smaller than 1% chance of "unacceptable" performance (defined as the onset of significant inelastic deformation) at the design *IM* and less than 10% for 1.5 times the design *IM*.

Kennedy (2011) comments on the ASCE 43-05 approach and implements it for 28 US nuclear plants. With a β in the range 0.3 to 0.6, the Seismic Core Damage Frequencies (SCDFs) are between $6 \cdot 10^{-7}$ and $6 \cdot 10^{-6}$. Based on this, the United States Nuclear Regulatory Commission (2007) has set a target SCDF of 10^{-5}.

Luco et al. (2007) use generic fragility curves with β=0.8. They assume a probability of collapse of 10% under the Maximum Considered Earthquake (MCE) ground motion corresponding to a 2475-year return period. The ATC-63 project (see FEMA 2009b) initially proposed this value after analysing buildings designed with ASCE 7-05. Luco et al. (2007) find that designing for the 2003 NEHRP MCE ground motions led to non-uniform risk across US territory. By targeting the average collapse probability in

50 years, which they found to be around 1%, Luco et al. (2007) calculated new ground motions with ratios of 0.7 to 1.15 of the 2003 NEHRP MCE ground motions.

The results of that report were considered for the ASCE 7-10 and FEMA P750 (FEMA 2009a). The latter propose the convolution of a hazard curve with a fragility curve with β=0.8 (decreased to 0.6 in ASCE 7-10), X=0.1 and a target probability of collapse of 1% in 50 years. It should be clarified that these risk-targeted acceleration values should be reduced further for design purposes (see Chapter 4).

Following US practice, the philosophy of risk targeting has been followed by the new Indonesian Earthquake Resistance Building Code, SNI 1726-2012. By setting a target of 1% for the probability of collapse in 50 years, this code maps risk-targeted spectral response accelerations for 0.2s and 1.0s. The generic fragility curves follow a lognormal distribution with X=0.1. Considering the material properties and human-related parameters representative of the broader area of Indonesia, Sengara et al. (2016) report values of β around 0.7, which is adopted by SNI 1726-2012. Later on, modifications have been made in the Indonesian code, to derive risk-targeted ground motions, by reducing β to 0.65 and introducing a directivity factor (Sengara et al. 2020).

Although this approach has not yet been adopted in the European regulations, Eurocode 0 (CEN 2002) discusses structural reliability (i.e. ability of structures to comply with specified requirements during their working life) and defines the failure probability based on a "reliability index" for different building classes and reference time periods. For ordinary buildings (i.e. residential and office buildings) and one-year reference period, the reliability index is equal to 4.7, resulting in a value of $Y=10^{-6}$. Similarly, the Probabilistic model code (JCSS 2000), also provides values for the reliability index, based on the consequence class and the relative cost of the safety measure. For moderate consequences of failure and one-year period, the index is 4.2 and 3.3 (for seismic protection) if the relative cost of safety measures is normal or large, and thus Y equals to 10^{-5} and $5 \cdot 10^{-4}$, for the two cases respectively.

2.3.2 Investigation of the practice in US codes

Liel et al. (2015) comment on ASCE 7-10 and suggest modifications to consider subduction earthquakes and near-fault effects. With the same X and β as in the regulation, the probability of collapse in 50 years varied from 0.21% to 0.62%, for areas affected by subduction earthquakes, while at near-fault sites, the risk was much higher, reaching in some cases 6%.

Douglas et al. (2013) try to avoid significant changes in the existing design ground motions for France, which correspond to a 475-year return period. Considering previous studies, as well as the results of some sensitivity analyses, they finally choose β= 0.5 and X=Y=10^{-5}. Under these assumptions, the estimated risk-targeted *PGA*s are not very different from the values proposed by the current French code.

Allen et al. (2015) comment on the implementation of risk-targeting in Canada for future versions of its National Building Code (NBCC). For comparison, ground motion values derived from the risk-targeting approach of Luco et al. (2007) are divided by those proposed in 2015 NBCC (for a 2%-in-50-year exceedance probability). The resulting risk coefficients for spectral accelerations at 1.0s are between 0.84 and 1.00 in southwest Canada.

Silva et al. (2016) study the fragility curves derived by the European project Syner-G (www.syner-g.eu) and find an average value of β=0.5, which they consider as a lower bound. Assuming a 10% probability of collapse at the 2475-year ground motion and the hazard curves derived by the European project SHARE (www.share-eu.org), for two values of β (0.6 and 0.8) they find a probability of collapse at the 475-year design acceleration ranging from 10^{-3} to 10^{-2}. Choosing then a value of X=10^{-3} and Y= $5.0 \cdot 10^{-5}$ (by relating the risk of collapse to human losses), they propose new risk-targeted hazard maps for Europe.

In Vacareanu et al. (2018) the proposed values of Luco et al. (2007) and Silva et al. (2016) are used to investigate risk-targeting in Romania. Compared to previous uniform hazard maps, the distribution of the *PGA* changes significantly when targeting uniform risk. Vacareanu et al. (2018) also calculate the ratios between the *PGA* for a

mean return period of 475 years and those resulting from risk targeting for $Y = 2 \cdot 10^{-4}$, $\beta = 0.8$ and X equal to 0.1 and 0.001. For the lower X, the ratios were below 0.6 whilst for the higher X they were larger than 1.0. Then, the probability of collapse for the *PGA* corresponding to two mean return periods, 475 and 2475 years, is evaluated, considering the results of risk-targeting using X=0.1 and 0.001. They conclude that using X=0.001 leads to a less realistic distribution of the collapse probabilities. They suggest applying risk-targeting in Romania assuming X=0.1 for the *PGA* values with a return period of 2475 years, with an annual collapse risk target of $5 \cdot 10^{-4}$. They found that in the epicentral area of the Vrancea intermediate-depth seismic source the obtained risk-targeted *PGA*s for this risk target and for $\beta = 0.6$ and X=0.1, are equal to the uniform-hazard *PGA*s for a return period of 2475 years, while in the rest of the country they are lower. Finally, they continue with further comparisons between setting Y as $2 \cdot 10^{-4}$ versus $5 \cdot 10^{-4}$. For this they compare the ratios of each risk-targeting approach with the uniform-hazard *PGA*s for return periods of 225, 475 and 2475 years and discuss the noticeable differences in the distribution of the ratios for 41 locations across the country. From the various investigations they performed, they notice that the parameter β seems to play the role of a multiplying factor, at least for that study, in the sense that it just increases or decreases the values of the risk-targeted accelerations or collapse probabilities but does not change significantly the general distribution within the country. On the contrary, they found that the difference in the assumed X can significantly change the shape of the contours of the maps.

2.4 Defining acceptable risk

The definition of acceptable risk levels has raised many questions in the research and policy spheres. Some of the different approaches that can be used to justify the choice of a risk target are presented in the following subsections. The first approach presented is to assess the structural behaviour and evaluate the current risk levels modern structures are exposed to. A second way is by considering public opinion. Also, one can define the acceptable collapse risk through consideration of the consequences of a collapse. In the last part, we present a simplified approach to define an upper bound for the acceptable collapse risk, using earthquake damage databases.

2.4.1 Based on current risk levels

In Goulet et al. (2007) the performance of a code-conforming four-storey reinforced-concrete (RC) frame building was evaluated, examining different design solutions. The probability of collapse under a ground motion with 2%-in-50-years exceedance probability was found to range between 0 and 2%, considering only record-to-record variability; after structural uncertainties were included, the values increased to 2% to 7%. They also found a variation of Y between $0.1 \cdot 10^{-4}$ and $0.5 \cdot 10^{-4}$ and between $0.4 \cdot 10^{-4}$ and $1.4 \cdot 10^{-4}$, when they considered structural uncertainties.

Fajfar and Dolšek (2012) examined a three-storey RC building with no provisions for earthquake resistance. They found an annual probability of collapse equal to $0.65 \cdot 10^{-2}$. When designed with Eurocode 8 (CEN 2004b), this risk reduced to $2.22 \cdot 10^{-4}$ and to $2.7 \cdot 10^{-4}$ when the dispersion was increased to accounted also for epistemic uncertainties.

Ramirez et al. (2012) examine 30 buildings designed using the 2003 International Building Code (IBC) together with the ASCE provisions. They find the probabilities of collapse at the design basis earthquake (2/3 of the MCE) to be in the range 0.4% to 4.2% for these buildings.

Ulrich et al. (2014b) present fragility curves for three-storey RC buildings designed according to Eurocodes 2 and 8 (CEN 2004a and CEN2004b) for different levels of design *PGA*, PGA_d. They find yielding probabilities between 0.14 (for PGA_d=0.07g) and 0.85 (for PGA_d=0.3g) and in the range $1.7 \cdot 10^{-7}$ (PGA_d=0.07g) to $1.0 \cdot 10^{-5}$ (PGA_d=0.3g) for the probabilities of collapse at the PGA_d.

In Martins et al. (2015) fragility curves are also derived, firstly considering the spectral acceleration at the fundamental period of vibration $S_a(T_1)$. This results in β ranging from 0.35 to 0.45, which increased up to 0.8 when they used *PGA* instead. For a three-storey RC building, they found the X to be equal to $5.20 \cdot 10^{-3}$ and $2.21 \cdot 10^{-2}$ for design accelerations of 0.2 and 0.4g, respectively, which change to $3.95 \cdot 10^{-3}$ and $5.57 \cdot 10^{-2}$ for a five-storey RC building. Then, using $S_a(T_1)$ as the *IM*, the annual probabilities of collapse for the three-storey buildings were $9.50 \cdot 10^{-5}$, $1.67 \cdot 10^{-5}$ and $1.07 \cdot 10^{-5}$, and for

the five-storey buildings $1.78 \cdot 10^{-4}$, $7.34 \cdot 10^{-5}$ and $2.97 \cdot 10^{-5}$, for design accelerations of 0.0g, 0.2g and 0.4g, respectively. The investigation is further extended in Martins et al. (2018) by considering additional design acceleration levels. Also, they introduce uncertainties due to structural variability, by considering the span length and storey height as random variables. They conclude that the probability of collapse at the design acceleration is between 10^{-5} and 10^{-2}.

Likewise, the annual rates of collapse for five locations of different seismicity in Italy are investigated in the RINTC project (RINTC Workgroup 2018); a summary of the results can be found in Iervolino et al. (2018). The current version of the Italian seismic code was used for the design of structures of different typologies, considering two soil conditions. Concerning the regular three-, six-, and nine-story RC buildings, the results of their analyses indicate that annual collapse risk for code-conforming RC structures is roughly between 10^{-5} and 10^{-4}. For the case of one-storey precast RC structures (also designed with the seismic code) *Y* values are found roughly between 10^{-5} and 10^{-3}.

Tsang et al. (2017) investigate buildings with precast RC columns designed using the risk-targeted Maximum Considered Earthquake (MCE_R) ground motions proposed in IBC-2012 and ASCE 7-10, assuming five different soil sites. Theoretically, a 10% probability of collapse under the MCE_R in 50 years is expected. They estimate, however, probabilities that are in every case lower than 10% (a maximum of 6.1% was found). In addition, the average annual collapse risk was estimated as $2.5 \cdot 10^{-6}$ (with a maximum of $1.6 \cdot 10^{-4}$), while the regulation imposes $2 \cdot 10^{-4}$. Also, the value of 0.25% in a design life of 50 years ($5 \cdot 10^{-5}$ annually), as proposed in Silva et al. (2016), was in some cases exceeded. Judd and Charney (2014) state that "the assumed ASCE 7-10 fragility curve is conservative" and that "the conditional probability of collapse may exceed 10%".

Pavel et al. (2019) evaluate the collapse probability for a RC frame structure designed with current seismic regulations, at a site in Romania. Nonlinear analyses are performed for equivalent SDOF systems, with the properties defined from 1000 pushover analyses. The calculated annual probability of collapse of the designed frames is estimated through multiple-stripe analyses and is found between $3 \cdot 10^{-3}$ and $6 \cdot 10^{-5}$. Finally, a model is defined using all the derived data combined, giving an

annual collapse frequency of $2 \cdot 10^{-4}$. Also, the annual collapse frequencies for different levels of spectral acceleration are evaluated, with the mean and median values for the annual collapse frequency at the design $S_a(T_1)$ being close to 10%.

Pavel and Carale (2019) present a performance assessment for low-code high-rise soft-storey RC buildings in Romania. Fragility curves are derived for 42 buildings, using two approaches: static pushover-based and dynamic analyses. A Monte-Carlo simulated earthquake catalogue was generated for the Vrancea intermediate-depth seismic source considered. The results show a variation of the mean annual collapse probabilities from $1.3 \cdot 10^{-4}$ to $3.8 \cdot 10^{-3}$.

Marafi et al. (2020) study the impact of basin amplification on the collapse risk of buildings. The case study is comprised of 4- to 24-storey RC wall buildings designed with the American regulations, neglecting basin effects. Depending on the ground motions selected, the 50-years collapse risk was found to be two or three times higher than the 1% suggested by the regulations. Three alternative approaches are then suggested for the design to be risk consistent. In short, they suggest increasing the design lateral forces, reducing the design drift limits or modifying the slab-column connection rotational capacity.

2.4.2 Based on public opinion

A different way to justify the acceptability of a certain level of risk is by assessing the public's view on which levels of risk can be tolerated. Hunter and Fewtrell (2001) discuss the various difficulties encountered when trying to define the acceptable risk using this approach (e.g. bias, fright factors, perception of the nature of risk and available information). However, a 'public-opinion' approach can still provide a rough estimate of the level of acceptable risk.

The results of a public-based approach are always sensitive to the group of the people examined, and the degree of their understanding on the field. Wiggins (1972) states that it is possible to define the acceptable risk by evaluating the public opinion regarding the expected structural life and the building importance and occupancy rate.

For example, the acceptable risk for a hospital designed for 100 years is expected to be much higher than that of a warehouse built to be used for a short time period.

An interesting example of collecting data about public opinion can be seen in the case study given in Fajfar (2018). A survey was conducted in Slovenia for two opinion groups; a group of engineers who are considered as experts, and lay people. In particular, the groups were asked for their opinion regarding buildings that have been designed with the current seismic regulations. Surprisingly enough, the two groups seem to agree on the risk tolerance. A first question regarded the number of collapsed buildings that can be tolerated. For the probability of collapse in 50 years, the replies given by the experts indicated, after translation into a probability, a mean level of $5.62 \cdot 10^{-4}$ as being acceptable and from lay people a value of $5.75 \cdot 10^{-4}$. For the limit state where the total collapse has been avoided but the repairing cost is intolerable, there was only a small increase on these numbers. The mean values for the acceptable probability for this case were 10^{-3} and $7.58 \cdot 10^{-4}$, for the experts and the lay people, respectively.

2.4.3 Based on the consequences

A different way to define which collapse risk levels can be regarded as tolerable is by focusing on the consequences of a collapse. At first, the economic consequences (direct or indirect) can influence the acceptability criteria based on who the decision makers are (e.g. homeowner, engineer, insurance company and government). When a company makes a decision for the acceptable performance of a nuclear plant, for example, the risk of future damage should be very low to reduce the costs of repairing/reconstructing. Starr (1969) gives an example for a nuclear plant where for economic reasons the risk levels should be 200 times lower than the 'socially accepted' risk, related to electric power activities, or 1/40 the fatality risk of a coal-burning plant.

Other types of consequences can be regarded as well. Jonkman et al. (2003) present a review of different measures that are usually used in risk analyses, categorised based on the consequences they refer to, e.g. cost, structural damage, potential damage, integrated risks, environmental problems, injuries and deaths. The latter will be the objective of the following paragraph, as it is regarded as the most challenging.

Acceptable fatality risk

Referring to human life and trying to introduce the concept of acceptable fatality risk is a difficult task and has been questioned by some people. Yet it cannot be avoided when dealing with risk management, with the idea being introduced in modern regulations. The ISO standard (ISO 1998) for example, suggests an individual annual fatality risk due to collapse equal to 10^{-6}.

Wiggins (1972) suggests that the concept of risk of death should be considered by design codes. According to that work, an investigation was performed for the city of Long Beach in order to assess the seismic efficiency of the city building code. A link was defined between the structural capacity and the expected fatality rate, and the results were processed by community representatives. Based on the investigation as well as the opinion of the public and city officials, an annual individual fatality risk of 10^{-6} was considered acceptable by the city council.

Whitman et al. (1974) mention that the aforementioned study suggests that even lower values could be proposed in seismic regulations, of the order of 10^{-7}. In their study, Whitman et al. (1974) investigated the design of 5 to 20 storeys RC apartment buildings in Boston. For the case of no seismic provisions, the results show a distribution of the annual fatalities per person exposed from $2 \cdot 10^{-7}$ to $8 \cdot 10^{-5}$. With the fatality levels found to be much higher than 10^{-7} in many cases, they state that "the involuntary risk acceptable to the public apparently implies a very large value on human life".

According to Hunter and Fewtrell (2001), "any risk that is currently tolerated is considered to be acceptable". Following this 'currently tolerated' approach, evaluating the different risk levels an individual is exposed to constitutes the simplest way to understand which risk levels are considered acceptable by society.

Otway et al. (1970) provide some information for deaths caused by various accidents in the US. The highest annual probability of death per person for the considered accidents is 10^{-4}, for the case of falls, while for extreme natural hazards the rated are considerably lower (e.g. $5.5 \cdot 10^{-7}$ for deaths from lightning). A risk analysis performed in that work for a research reactor showed that the nearby community is exposed to an

annual fatality risk of $4.5 \cdot 10^{-4}$. In that paper it is also noted that accidents that provide an annual fatality risk of the magnitude of 10^{-3} per person are considered "uncommon". This level is considered unacceptable by the society, which demands immediate mitigation measurements to reduce this number. On the other hand, people are not much concerned about rarer events that can expose a person to a 10^{-6} annual probability of death, since they feel that they will not be exposed to so extreme scenarios.

In a similar manner, McGuire (2004) refers that events with 'annual probability of danger' lower than 10^{-5} can be ignored. He gives as an example the individual fatality risk from extreme weather events that people in the US are exposed to, which is, on average, equal to $5 \cdot 10^{-6}$, annually. On the other hand, risk values higher than 10^{-2} are considered unacceptable and should be reduced.

Likewise, a review of the annual fatality risk associated with different types of activities is also presented in Jordaan (2005). The values range from an order of 10^{-2} (for smoking) to 10^{-8} (venomous animals), with natural hazards such as lightning having statistics higher than 10^{-7}. It is also stated therein that typical targets for the annual probability of failure of an engineering system can range from 10^{-6} to 10^{-3}. They also present an illustrative example of risk perception circles to show that the personal experience can affect risk perception.

Fatality risk levels due to various hazards are also provided in Gulvanessian et al. (2012). The minimum value reported for the annual probability of deaths per exposed person refers to the fatalities caused by structural failure, which is equal to $1.4 \cdot 10^{-7}$, for the UK, while a value of $2 \cdot 10^{-6}$ is attributed to fatalities from earthquakes in California. The highest risk of death is given for deep sea fishing, with an annual rate of $2.8 \cdot 10^{-3}$ per exposed person.

For New Zealand, the GNS research institute suggests that the annual individual fatality risk due to rock falls should be between 10^{-3} to 10^{-5}, with a value of 10^{-4} proposed for Christchurch. This value has caused reaction by some researchers. For example, Enright (2015) discusses the tolerable risk levels for natural hazards in New Zealand in comparison with international regulations. The article explains why a value of 10^{-4} is regarded as very high and it is suggested that it be reduced to 10^{-5}. If other

hazards are also included, the 10^{-5} would still be suitable for existing buildings, while a value of 10^{-6} would be more sensible for new buildings.

Starr (1969) suggests that the risk tolerance is based on the type of the activity an individual is exposed to, by dividing them into voluntary (e.g. smoking) and involuntary (e.g. war). The risk tolerance for the first case depends mainly on the individual who adjusts his exposure to risk using a person value system to evaluate his experiences. For involuntary actions, more decision-makers have to be involved in the definition of the acceptability criteria. A significant difference between the acceptable risk levels for the two types of activities is noticed. In particular, as stated in that article, society seems to be willing to accept voluntary risk levels 1000 times higher than the ones attributed to involuntary activities.

An interesting example of an involuntary activity a person is exposed to is to be hit by space junk that re-enters Earth after a satellite has been launched. An article in 'The Economist' newspaper (The Economist, 2019) discusses this and states that a risk target for injury or death equal to 10^{-4} was regarded as acceptable by NASA in 1995, with the number later being adopted by other countries, too.

The same classification is referred also in Melchers and Beck (2018), where different risk levels are provided for various activities. The lowest value is given for the case of structural failures, equal to 10^{-7} per year. This type falls into the category of involuntary risks, since the residents demand a high level of safety. The highest risk of the studied activities is attributed to the case of mountain climbing, with an estimated annual fatality risk between $1.5 \cdot 10^{-3}$ and $2 \cdot 10^{-3}$.

An alternative connection between the acceptable fatality and the type of activity using a policy factor is presented in Vrijling et al. (1998). In particular, the acceptable individual fatality is considered equal to 10^{-4}, multiplied with a policy factor that depends on the type of the activity. This factor ranges from 10^{-2} for involuntary with no obvious benefits (e.g. living close to a liquid petroleum gas station) to 10^{2} for completely voluntary activities (e.g. mountaineering). For neutral activities, such as driving, a unit factor is set, which is ten times higher for (not completely) voluntary activities such as motorbiking. For involuntary activities with benefits (e.g. financial),

such as working at a factory, the policy factor is 10^{-1}. Being exposed to an earthquake can be seen as an involuntary activity with no benefit (i.e. policy factor equal to 10^{-2}), and thus the acceptable risk level is equal to 10^{-6}.

Apart from the individual risk, societal risk can also be useful as a risk measure (Jonkman et al. 2003). While individual risk refers to a specific location and gives the probability of death of an individual due to a hazard event, societal risk gives the death exceedance frequency for a whole area. For the individual risk, the Dutch law enforces an individual annual risk limit of 10^{-6} for new situations, increased to 10^{-5} for existing situations. For the societal risk the provided guidance suggests the use of an F-N curve, representing the frequency (F) of exceeding a number of deaths (N) within a year.

Various researchers have discussed the use of the F-N curves (Jonkman et al. 2003; Vrijling et al. 1998; Ale and Piers 2000; Tsang et al. 2020; Tsang et al. 2018; Helm 1996; Crowley et al. 2018). A limit line can be defined as:

$$F=k/N^n \tag{2.3}$$

where k is a constant that defines the position of the limit line, and n is the slope of the line. Different values are provided for the constant k in different countries, e.g. it is equal to 10^{-2} for the UK and Denmark, and 10^{-3} for Hong Kong and the Netherlands. The slope parameter is equal to 1 (same average annual fatality for any event) for the UK and Hong Kong and 2 (for high-consequence accidents accepted with lower probabilities) for Denmark and the Netherlands. These limit lines are presented in Figure 2.2.

A comparison of the limit line with the F-N curve of the assessed location will eventually provide the risk acceptability criterion. If the F-N curve is higher than the limit line, then the risk is unacceptable. Otherwise, it can be either in the acceptable risk region (negligible risk levels) or in the region between the two, which is usually called ALARP (as low as reasonably practicable) where there is a residual risk which is accepted due to other criteria, such as benefits (e.g. cost reduction or time saving).

An example is given in Figure 2.2, where it is observed how different these curves can be for different locations. Three characteristic examples are presented using the data

provided in Daniell et al. (2018) for various locations across Europe. In location A all standards are met, in contrast to the location C. The F-N curve of location B almost meets the UK standards but would be unacceptable by other regulations.

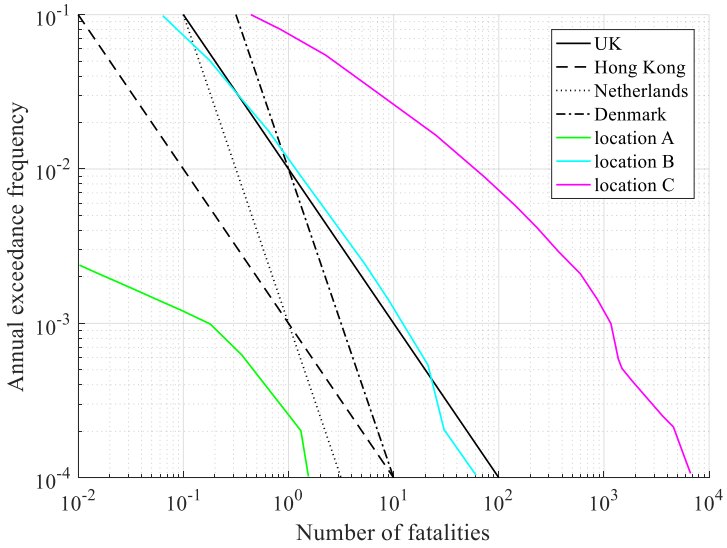

Figure 2.2 Example of F-N curves for three locations, together with the limit lines from different regulations

From fatality risk to collapse risk

Different techniques have been developed to establish a link between collapse and fatality and, thereby, obtain acceptable risk targets. In the CIRIA (1977) report, the acceptable annual collapse risk is expressed as a function of the acceptable individual annual probability of death (i.e. fatality risk), $P(D)$, the number of people in the exposed area, N, and a social criterion factor, K_s, as (Bhattacharya et al 2001):

$$Y = \frac{K_s}{N} \cdot P(D) \tag{2.4}$$

The social criterion factor depends on how voluntary the assessed hazard activity is, and a typical value of 5 is suggested in Bhattacharya et al (2001), together with $P(D)=10^{-4}$ in the UK.

A similar formula is proposed by Allen (1981) that relates the acceptable annual failure risk with the number of people exposed and the type of the activity, using a factor A, while an additional warning factor, W, is introduced, as:

$$Y = \frac{A}{W \cdot \sqrt{N}} \cdot 10^{-5} \tag{2.5}$$

The value 10^{-5} was obtained based on the statistics of collapse in Canada. The difference in the results obtained with the two approaches is noticeable.

In both Eqn.(2.4) and Eqn.(2.5) it is necessary to define the exposed number of people. Several methods have been proposed for this (e.g. Coburn et al. 1992; Yeo and Cornell 2002; Porter et al. 2008; Jaiswal and Wald 2010; ATC 2012; So and Spence 2013; Tsang et al. 2018), and information on this can be found in Sinković and Dolšek (2020), together with the introduction and application of a model for designing based on tolerated fatality risk.

Tsang and Wenzel (2016) suggest that the acceptable annual risk target for the limit state of complete structural damage (CSD) is equal to:

$$Y = \frac{P(D)}{P(D|CSD)} \tag{2.6}$$

where $P(D)$ is considered equal to 10^{-6} and $P(D|CSD)$ is the probability of dying due to complete structural damage. Values are provided based on the type of the building and the number of storeys (in the order of 10^{-4}). This probability is connected to the expected fatality rate given the *CSD* state, $\lambda_{d,CSD}$, as:

$$\mathrm{P}(D|CSD) = 1 - \mathrm{e}^{-\lambda_{\mathrm{d,CSD}}} \tag{2.7}$$

For a different limit state, the annual risk of "Real collapse" falls within the range $6 \cdot 10^{-6}$ to $8 \cdot 10^{-6}$.

A similar approach is followed by Silva et al. (2016), who divide the acceptable fatality risk with the fatality rate (number of fatalities over the number of occupants) to obtain an acceptable collapse risk. First, through a literature review they find that a value of $5 \cdot 10^{-6}$ for the annual fatality risk can be regarded as acceptable. Then, they mention that HAZUS (FEMA 2003) and ATC-13 (1985) give fatality rates between 5% to 10%, while Spence (2007) suggests fatality rates between 6% and 28%, based on the building type and using data from past earthquake events. Silva et al. (2016) select a

value of 10% for the fatality rate, giving an acceptable collapse risk is equal to $5 \cdot 10^{-5}$ per year.

2.4.4 Assessing risk using earthquake damage databases

One alternative technique is to estimate an upper bound on the risk that has been "accepted" historically based on the levels of observed damage in previous earthquakes, as attempted by Labbé (2010). This "risk" is an upper bound, as generally after every damaging earthquake the population lament the damage that occurred. Another potential solution to this problem is to target a damage state that is less severe than collapse, for example structural yielding. Targeting this limit state is less "morally" problematic and also has other benefits, e.g. it is generally easier to assess in numerical modelling when a structure yields rather than when it collapses. "Yield", however, is not as commonly included in databases of post-earthquake field investigations (because it is difficult to determine visually) as building collapse, which is obvious to field investigators and invariably recorded in the databases. The level of acceptable risk in this context could be defined using, for example, cost-benefit analysis based on the cost of reducing the risk further (perhaps adopting an ALARP "as low as reasonably practicable" philosophy).

In this subsection, we use field observations of building damage from recent earthquakes and an empirical Fermi-type approach to estimate an upper bound on the "acceptable" probability of collapse (Y) discussed above. In particular, the number of RC buildings that collapsed due to earthquakes during recent time periods in Italy and Greece are used to estimate the observed annual collapse rate.

The technique relies on the ratio of the total number of observed cases of a given damage level in a given period of time to the total number of buildings that could have been affected by earthquakes, which is then normalized to give an annual rate. Estimating both of these totals for a given country requires: a) post-earthquake field mission reports that provide the number of cases of damage and b) building census data indicating how many structures were present when the earthquake occurred.

There are a number of difficulties and uncertainties in applying this approach. For example, in some reports the number of collapses of RC buildings is combined with the number of collapses of other structural types, e.g. masonry. In others only a general "damage" category is used without specifying, for example, the number of collapses or partial collapses. Sometimes the focus of post-earthquake field missions is on estimating the number of casualties and not on collecting accurate building damage statistics. Also damage records may be incomplete, either by not including all damaging earthquakes during a time period or by not totalling all incidences of damage for a given earthquake (e.g. damage within cities but not rural areas). For example, Colombi et al. (2008), when deriving empirical vulnerability curves from Italian data, state that roughly half of the available observations cannot be used because of a lack of information on the structural type and level of damage. In addition, when combining data from different databases it is necessary to assume equivalence between various damage scales (or convert between scales). The damage assessment can also be sensitive to its purpose and the stakeholders involved (e.g. if compensation is involved from government or insurance). Finally (and probably most important), the sample sizes available are small, both in terms of the number of collapsed buildings and the small number of possible earthquake scenarios (locations and magnitudes) that have been sampled during the time period considered, which is relatively short given the recurrence interval of large earthquakes. Therefore, the annual collapse rates estimated here should be considered very rough.

We conduct a simplified analysis for Italy and Greece, for which the earthquake damage databases are roughly complete in recent years and easily accessible, and for a combined "total or partial collapse" damage state for RC buildings. It would be relatively simple to conduct such an analysis to other developed countries with good databases, such as the USA, Japan and New Zealand.

The Cambridge Earthquake Impact Database (CEQID) (http://www.ceqid.org/CEQID/Home.aspx) reports the number of RC building collapses in Italian earthquakes from 1980 to 2009 inclusive (30 years) as: Irpinia 1980 (58 buildings), Eastern Sicily 1990 (3), Umbria-Marche 1997 (49), Umbria-Marche 1998 (0), Pollino 1998 (9), Molise 2002 (29) and L'Aquila 2009 (57), giving a total of

205 total or partial collapses. Colombi et al. (2008) gives an estimate of 842 collapses for almost the same period range, thereby demonstrating large uncertainty in this total.

Next it is necessary to estimate the total number of RC buildings in Italy. EPISCOPE (2014) estimates that 24.7% of Italian residential buildings are of RC and Istat (2011, http://dati-censimentopopolazione.istat.it) states that there were 14,452,680 buildings in Italy of which 12,187,698 are residential. Therefore, it can be estimated that there are roughly 3.5 million RC buildings in total of which about 3 million are residential. We assume that this total has not changed over the 30 years covered by the collapse database, which given the slow population growth of Italy could be thought a reasonable assumption.

Dividing the total number of collapsed buildings by the building population and the number of years gives an estimate of the collapse rate. Using the two estimates of 205 and 842 in 30 and 23 years, respectively, and 3 or 3.5 million buildings (depending on whether the database covers all buildings or only residential) gives annual collapse rates of between $2 \cdot 10^{-6}$ and $1 \cdot 10^{-5}$, which is much lower than some of the probabilities assumed in previous risk-targeting exercises (e.g. Luco et al. 2007).

For the period 1978 to 2003 inclusive the following RC building collapses due to earthquakes in Greece have been reported: Thessaloniki 1978 (4 buildings) (CEQID), Gulf of Corinth 1981 (15) (Carydis et al. 1982), Kalamata 1986 (5), Aigion 1995 (1), Athens 1999 (69) (CEQID) and Lefkada 2003 (0) (Karababa and Pomonis 2011), giving a total of 94 total or partial collapses. Using information from the Greek statistical service (http://www.statistics.gr) and the TABULA project (www.building-typology.eu) for the total number of RC buildings in Greece, and assuming that the building total remained constant, leads to estimates of the collapse rate between $1 \cdot 10^{-6}$ and $2 \cdot 10^{-6}$, again much lower than some assumed probabilities for the targeted risk.

The accuracy of these estimates could be improved by using a more complete database both for the numerator (the damage) and the denominator (the number of buildings at risk) and by extending the time period covered so that more potential earthquake scenarios are considered. Nevertheless, such an analysis is constrained by the long

recurrence intervals of damaging earthquakes, which means that the assessed rates will always be associated with large uncertainties. In addition, variations due to building type (e.g. masonry versus reinforced concrete), location (e.g. developed versus less-developed countries) and damage level (e.g. collapse versus yield) could be studied as well.

The same procedure was repeated for the same two countries considering a different damage state. A broader class was defined to represent 'yield', as considered by Ulrich et al. (2014b), which includes the total number of RC buildings that are neither not-damaged nor collapsed (partially or in total). The same limitations discussed before are also the case here. In addition, complete data were available for a shorter period of 18 years for Greece (but still 30 years for Italy). With these assumptions, the annual percentage of yield is found equal to $3 \cdot 10^{-5}$ for Italy and $1 \cdot 10^{-4}$ for Greece. Apart from providing useful constraints on the inputs to risk-targeting this type of analysis could have other benefits as well. Firstly, they would provide an observational-based assessment of earthquake risk that can be compared to estimates from computer modelling, which require a large number of inputs and can be opaque to decision makers. If there are large differences in these estimates it may indicate that the computer models require calibration. Secondly, these estimates will enable differences in earthquake risk levels between countries to be judged more easily and used to understand what the impact of reducing risk could be in terms of the average number of buildings that could collapse per year, for example.

2.5 Outstanding issues and possible paths forward

As can be seen by the discussion in the previous paragraphs, there is a rapidly increasing number of studies that have attempted to apply the risk-targeting approach to different areas or sought to constrain the various inputs upon which this technique relies. Despite these many studies a number of problems remain, which we highlight in this section along with a brief discussion of potential solutions. Some of these potential issues are investigated further in later chapters of this thesis.

As noted above, when evaluating the risk integral, ground motions for very low probabilities of exceedance sometimes need to be estimated. A power-law

extrapolation appears to work well for most examples we have studied. Further research on the technicalities of the calculations, however, needs to be conducted to define a stable procedure that works for all possible inputs. Also, using a linear in log-log space approximation of the hazard curve simplifies the approach, enabling the use of closed-form solutions, but could affect the accuracy of the results. This topic is investigated in paragraph 4.3.1 of Chapter 4.

Targeting a non-zero value of collapse risk accepts that some buildings will collapse (potentially leading to human casualties) in earthquakes, even when they are designed in compliance with the building code. From a moral point of view this is problematic and it leads to the difficulty of trying to define what risk is "acceptable". Different techniques for this were discussed in paragraph 2.4, while an alternative cost-based approach that considers various damage states apart from collapse is presented in Chapter 5.

Once the targeted risk is chosen, unless great changes to the accelerations currently used for design are accepted by practicing engineers, the probability of collapse at the design acceleration is automatically implied, as shown by Figure 3 of Douglas et al. (2013). Here there is a trilemma: any two out of the three input parameters, risk-targeted *IM*, *X* and *Y*, can be chosen independently but not all three (see also paragraph 4.2.2 of Chapter 4). The solution to this potential problem is to check all three values are physically reasonable. This trilemma may be the reason for the apparently high target collapse probabilities (*Y*) used by Luco et al. (2007), as they were forced to adopt them once *X* had been defined and they did not want great modifications of the hazard maps of the previous code.

There is a need to derive fragility curves for a wide variety of code-designed structures with different geometries and materials. Previous studies have adopted generic fragility curves that scale constantly with the design acceleration so that the iterative procedure used to converge to the targeted risk is simple. As shown by Figure 3 of Ulrich et al. (2014a), however, this desired feature appears not to be true following current design practice, as they were not created with risk targeting in mind. It is possible, however, to generate a suite of fragility curves for all potential design accelerations and then to use the appropriate ones when iterating to find the actual

design acceleration for a location. As an example, a preliminary study is presented in Chapter 3.

2.6 Conclusions

Crowley et al. (2013) propose that 'Risk-targeted seismic design actions' should be considered for future versions of the Eurocodes. A call echoed by Formichi et al. (2016) in a report on the background and application of Eurocodes, published on behalf of the European Commission. This report also proposes that changes made in other international seismic design codes should be considered when updating the Eurocodes. It is, therefore, clear that application of the risk-targeting approach is being seriously discussed in Europe. In consequence, additional research effort to this end would provide valuable input for the development of risk-targeted design maps for new buildings in Europe.

This chapter discusses some critical issues that need to be solved before the risk-targeting approach for the development of seismic design codes can be employed in practice. Some of these (e.g. development of appropriate fragility functions) solely require engineering calculations but others (e.g. choice of the acceptable level of risk) need input from other domains, including decision makers. These issues are further investigated in the following chapters.

References

Ale BJM, Piers M (2000) The assessment and management of third party risk around a major airport. Journal of Hazardous Materials, 71, 1-16

Allen DE (1981) Criteria for design safety factors and quality assurance expenditure. In Proceedings of the Third International Conference on Structural Safety and Reliability, Trondheim, Norway

Allen TI, Adams J, Halchuk S (2015) The seismic hazard model for Canada: Past, present and future. Proceedings of the Tenth Pacific Conference on Earthquake Engineering Building an Earthquake-Resilient Pacific, Sydney, Australia. Paper number 100

ASCE (2005) Seismic Design Criteria for Structures, Systems and Components in Nuclear Facilities. American Society of Civil Engineers, ASCE Standard 43-05

ASCE (2010) Minimum Design Loads for Buildings and Other Structures, ASCE Standard 7-10. American Society of Civil Engineers, Reston, VA

ATC - Applied Technology Council, ATC-13 (1985) Earthquake Damage Evaluation Data for California, Report ATC-13, Redwood City, CA

ATC - Applied Technology Council, FEMA P-58 (2012) Next-generation Seismic Performance Assessment for Buildings, Volume 1 – Methodology, Federal Emergency Management Agency, Washington, D.C

Bhattacharya B, Basu R, Ma KT (2001) Developing target reliability for novel structures: the case of the Mobile Offshore Base. Marine structures, 14, 37-58

Braverman JI, Xu J, Ellingwood BR, Costantino CJ, Morante RJ, Hofmayer CH (2007) Evaluation of the Seismic Design Criteria in ASCE / SEI Standard 43-05 for Application to Nuclear Power Plants. Agencywide Documents Access and Management System (ADAMS) - USNRC

Carydis PG, Tilford NR, Brandow GE, Jirsa JO (1982) The central Greece earthquakes of February-March 1981, Report No. CETS-CND-018 of the Earthquake Engineering Research Institute, Berkeley, CA, National Academy Press, Washington, DC

CEN (2002) EN 1990:2002 Eurocode: basis of structural design. European Committee for Standardization, Brussels

CEN (2004a) EN 1992-1-1:2004 Eurocode 2: Design of concrete structures - Part 1-1: General rules and rules for buildings, European Committee for Standardization, Brussels

CEN (2004b) EN 1998-1:2004 Eurocode 8: Design of structures for earthquake resistance - Part 1: General rules, seismic actions and rules for buildings, European Committee for Standardization, Brussel

CIRIA - Construction Industry Research and Information Association (1977). Rationalization of safety and serviceability factors in structural codes. Report No. 63, London, 1977

Coburn AW, Spence RJS, Pomonis A (1992) Factors determining human fatality levels in earthquakes: mortality prediction in building collapse. In Proceedings of the 10th world conference on earthquake engineering

Colombi, M, Borzi B, Crowley H, Onida M, Meroni F, Pinho R (2008), Deriving vulnerability curves using Italian earthquake damage data, Bulletin of Earthquake Engineering, 6(3), 485-504, doi: 10.1007/s10518-008-9073-6

Crowley H, Silva V, Martins L (2018) Seismic design code calibration based on individual and societal risk. In Proceedings of 16th European conference on earthquake engineering, Thessaloniki, Greece

Crowley H, Weatherill G, Pinho R (2013) Suggestions for Updates to the European Seismic Design Regulations. SHARE Deliverable 2.6. Universita degli Studi di Pavia

Daniell JE, Pomonis A, Tsang HH, Wenzel F, Gunasekera R, Schaefer A (2018) The top 100 fatal earthquakes: examining fatality risk reduction globally with respect to seismic code implementation. In Proceedings of 16th European conference on earthquake engineering, Thessaloniki, Greece

Douglas J, Ulrich T, Negulescu C (2013) Risk-targeted seismic design maps for mainland France. Natural Hazards 65(3): 1999-201

Eads L, Miranda E, Krawinkler H, Lignos DG (2013) An efficient method for estimating the collapse risk of structures in seismic regions. Earthquake Engineering & Structural Dynamics, 42, 25-41

Enright PA (2015) Is there a tolerable level of risk from natural hazards in New Zealand?, Georisk: Assessment and Management of Risk for Engineered Systems and Geohazards, 9:1, 1-8, doi: 10.1080/17499518.2014.1000341

EPISCOPE (2014) Inclusion of new buildings in residential building typologies: Steps towards NZEBs exemplified for different European countries, EPISCOPE Synthesis Report no. 1 (Deliverable D2.4). Contract N°: IEE/12/695/SI2.644739. ISBN 978-3-941140-42-4

Fajfar P (2018) Analysis in seismic provisions for buildings: past, present and future. Bulletin of Earthquake Engineering, 16, 2567–2608, doi: 10.1007/s10518-017-0290-8

Fajfar P, Dolšek M (2012) A practice-oriented estimation of the failure probability of building structures. Earthquake Engineering and Structural Dynamics 41: 531–547

FEMA - Federal Emergency Management Agency (2003) Multi-Hazard Loss Estimation Methodology, Earthquake Model, HAZUS. Federal Emergency Management Agency and National Institute of Buildings Sciences, Washington, D.C

FEMA - Federal Emergency Management Agency (2009a) NEHRP Recommended Seismic Provisions for New Buildings and Other Structures (FEMA P750). Federal Emergency Management Agency

FEMA - Federal Emergency Management Agency (2009b) Quantification of Building Seismic Performance Factors (FEMA P695). Federal Emergency Management Agency

Formichi P, Danciu L, Akkar S, Kale O, Malakatas N, Croce P, Nikolov D, Gocheva A, Luechinger P, Fardis M, Yakut A, Apostolska R, Sousa ML, Dimova S, Pinto A (2016) Eurocodes: background and applications. Elaboration of maps for climatic and seismic actions for structural design with the Eurocodes. EUR, doi: 10.2788/534912

Goulet C, Haselton C, Mitrani-Reiser J, Beck J, Deierlein G, Porter K, Stewart, J (2007) Evaluation of the seismic performance of a code-conforming reinforced-concrete frame building - from seismic hazard to collapse safety and economic losses. Earthquake Engineering and Structural Dynamics 36: 1973–1997

Gulvanessian H, Calgaro JA, Holický M (2002) Designer's guide to EN 1990 Eurocode: basis of structural design. Thomas Telford Publishing

Helm P (1996) Integrated risk management for natural and technological disasters. Tephra, 15(1), 5-19

Hunter PR, Fewtrell L (2001) Acceptable risk. In Water Quality: Guidelines, Standards and Health. Assessment of risk and risk management for water-related infectious disease. London: IWA Publishing, 207-227

ICC IBC (2003) International Building Code (IBC), International Code Council (ICC), IL, USA

ICC IBC (2012) International Building Code (IBC), International Code Council (ICC), IL, USA

Iervolino I, Spillatura A, Bazzurro P (2018) Seismic reliability of code-conforming Italian buildings. Journal of Earthquake Engineering, 22(s2), 5-27

ISO - International Organization for Standardization (1998) ISO 2394:1998. General Principles on Reliability for Structures. Geneva, Switzerland

Jaiswal K, Wald D (2010) An empirical model for global earthquake fatality estimation. Earthquake Spectra, 26(4), 1017–37

JCSS (2000) Probabilistic model code—part 1: basis of design. Joint Committee on Structural Safety

Jonkman SN, Van Gelder PHAJM, Vrijling JK (2003) An overview of quantitative risk measures for loss of life and economic damage. Journal of hazardous materials, 99, 1-30

Jordaan I (2005) Decisions under uncertainty: probabilistic analysis for engineering decisions. Cambridge University Press

Judd JP, Charney FA (2014) Earthquake risk analysis of structures. In: Proceedings of the 9th International Conference on Structural Dynamics, EURODYN 2014, 2929–2938.

Karababa FS, Pomonis A (2011) Damage data analysis and vulnerability estimation following the August 14, 2003 Lefkada Island, Greece, earthquake, Bulletin of Earthquake Engineering, 9:1015-1046, doi: 10.1007/s10518-010-9231-5

Kennedy RP (2011) Performance-goal based (risk informed) approach for establishing the SSE site specific response spectrum for future nuclear power plants. Nuclear Engineering and Design, 241:648–656

Labbé PB (2010) PSHA outputs versus historical seismicity: Example of France. In: Proceedings of Fourteenth European Conference on Earthquake Engineering

Liel AB, Luco N, Raghunandan M, Champion, CP (2015) Modifications to risk-targeted seismic design maps for subduction and near-fault hazards. In: 12th International Conference on Applications of Statistics and Probability in Civil Engineering, ICASP12, Vancouver, Canada

Luco N, Ellingwood BR, Hamburger RO, Hooper JD, Kimball JK, Kircher CA (2007) Risk-targeted versus current seismic design maps for the conterminous United States. In: SEAOC 2007 convention proceedings

Marafi NA, Makdisi AJ, Berman JW, Eberhard MO (2020) Design strategies to achieve target collapse risks for reinforced concrete wall buildings in sedimentary basins. Earthquake Spectra, doi: 10.1177/8755293019899965

Martins L, Silva V, Crowley H, Bazzurro P, Marques M (2015) Investigation of structural fragility for risk-targeted hazard assessment. In: 12th International Conference on Applications of Statistics and Probability in Civil Engineering, ICASP12, Vancouver, Canada

Martins L, Silva V, Bazzurro P, Marques M (2018) Advances in the derivation of fragility functions for the development of risk-targeted hazard maps. Engineering Structures, 173, 669-680

McGuire RK (2004) Seismic hazard and risk analysis. Earthquake Engineering Research Institute

Melchers RE, Beck AT (2018) Structural reliability analysis and prediction. John Wiley & Sons

Otway HJ, Battat ME, Lohrding RK, Turner RD, Cubitt RL (1970) A Risk Analysis of the Omega West Reactor (No. LA-4449). Los Alamos Scientific Laboratory of the University of California, New Mexico

Pavel F, Carale G (2019) Seismic assessment for typical soft-storey reinforced concrete structures in Bucharest, Romania. International Journal of Disaster Risk Reduction, 41, 101332, doi: 10.1016/j.ijdrr.2019.101332

Pavel F, Pricopie A, Nica G (2019) Collapse Assessment for a RC Frame Structure in Bucharest (Romania). International Journal of Civil Engineering, 17, 1373-1381, doi: 10.1007/s40999-019-00398-2

Porter KA, Jaiswal KS, Wald DJ, Earle PS, Hearne M (2008) Fatality models for the U.S. geological survey's prompt assessment of global earthquakes for response (PAGER) system. In Proceedings of the 14th world conference on earthquake engineering, Beijing, China

Ramirez CM, Liel AB, Mitrani-Reiser J, Haselton CB, Spear AD, Steiner J, Deierlein GG, Miranda E (2012) Expected earthquake damage and repair costs in reinforced concrete frame buildings. Earthquake Engineering and Structural Dynamics, 41: 1455–1475

RELUIS and EUCENTRE (2014-2018) Research Project DPC – RELUIS/EUCENTRE, Technical Report and Deliverables

RINTC Workgroup (2018) Results of the 2015-2017 Implicit seismic risk of code-conforming structures in Italy (RINTC) project. ReLUIS report, Rete dei Laboratori Universitari di Ingegneria Sismica (ReLUIS), Naples, Italy, available at http://www.reluis.it/

Sengara IW, Irsyam M, Sidi ID, Mulia A, Asrurifak M, Hutabarat D, Partono W (2020) New 2019 Risk-Targeted Ground Motions for Spectral Design Criteria in Indonesian Seismic Building Code. In E3S Web of Conferences, 156, 03010, doi: 10.1051/e3sconf/202015603010

Sengara IW, Sidi ID, Mulia A, Muhammad A, Daniel H (2016) Development of risk coefficient for input to new Indonesian seismic building codes. Journal of Engineering and Technological Sciences, 48(1): 49–65

Silva V, Crowley H, Bazzurro P (2016) Exploring risk-targeted hazard maps for Europe, Earthquake Spectra, 32(2):1165-1186

Sinković NL, Dolšek M (2020) Fatality risk and its application to the seismic performance assessment of a building. Engineering Structures, 205, 110108

SNI (2012) Tata cara perencanaan ketahanan gempa untuk struktur bangunan gedung dan non gedung. Badan Standardisasi Nasional, ICS 91.120.25;91.080.01. Report 1726:2012. In Indonesian

So E, Spence R (2013) Estimating shaking-induced fatalities and building damage for global earthquake events: a proposed modelling approach. Bulletin of Earthquake Engineering, 11(1), 347–63

Starr C (1969) Social benefit versus technological risk. Science 165 (3899), 1232–1238

The Economist (2019) Stopping a hard rain, print issue Aug 10th, 2019. URL: https://www.economist.com/science-and-technology/2019/08/10/no-one-has-yet-been-killed-by-re-entering-space-junk

Tsang HH, Daniell JE, Wenzel F, Werner AC (2018) A semi-probabilistic procedure for developing societal risk function. Nat Hazards 92, 943–969, doi: 10.1007/s11069-018-3233-z

Tsang HH, Daniell JE, Wenzel F, Wilson JL (2020) A universal approach for evaluating earthquake safety level based on societal fatality risk. Bulletin of Earthquake Engineering, 18(1), 273-296, doi: 10.1007/s10518-019-00727-9

Tsang HH, Lumantarna E, Lam NTK, Wilson JL, Gad E (2017) Annualised collapse risk of soft-storey building with precast RC columns in Australia. Mechanics of Structures and Materials: Advancements and Challenges, 1681–1686

Tsang HH, Wenzel F (2016) Setting structural safety requirement for controlling earthquake mortality risk. Safety science, 86, 174–183

Ulrich T, Douglas J, Negulescu C (2014a) Seismic risk maps for Eurocode-8 designed buildings, In: Proceedings of the Second European Conference on Earthquake Engineering and Seismology

Ulrich T, Negulescu C, Douglas J (2014b) Fragility curves for risk-targeted seismic design maps. Bulletin of Earthquake Engineering 12(4): 1479-1491

United States Nuclear Regulatory Commission (2007) A performance-based approach to define the site specific earthquake ground motion. Technical report 1.208

Vacareanu R, Pavel F, Craciun I, Coliba V, Arion C, Aldea A, Neagu C (2018) Risk-targeted maps for Romania. Journal of Seismology, 22, 407–417, doi:10.1007/s10950-017-9713-x

Vrijling JK, Van Hengel W, Houben RJ (1998) Acceptable risk as a basis for design. Reliability Engineering and System Safety, 59, 141-150

Whitman RV, Biggs JM, Brennan, JE III, Cornell CA, de Neufville R, Vanmarcke, EH (1974) Seismic Design Decision Analysis, Report No. 9, Report R73-58, Structures Publication No. 381

Wiggins JH (1972) Earthquake safety in the City of Long Beach based on the concept of balanced risk. In: Perspectives on Benefit-Risk Decision Making. National Academy of Engineering, Washington, DC, US, pp. 87–95

Yeo GL, Cornell CA (2002) Building-specific seismic fatality estimation methodology. In the fourth US-Japan workshop on performance-based earthquake engineering methodology for reinforced concrete building structures. Earthquake Engineering Research Center, Toba, Japan

Žižmond J, Dolšek M (2017) The formulation of risk-targeted behaviour factor and its application to reinforced concrete buildings, Proceedings of the 16th World Conference on Earthquake Engineering, Santiago, Chile, 9-13 January. Paper no. 1659

CHAPTER 3

Development of fragility curves for use in seismic risk targeting

In this chapter, we design, based on Eurocodes 2 and 8, a set of six 2D reinforced concrete buildings corresponding to different geometries and two levels of design peak ground acceleration (0.1g and 0.3g). The response of these buildings to earthquake shaking is modelled numerically using state-of-the-art computer software to develop fragility curves for different limit states. We find that while the design acceleration has some influence on the fragility curves, other parameters such as the number of storeys also affect them. These preliminary results highlight the significant variability in the seismic structural performance and the resulting challenges that this poses for modern performance-based design philosophies, such as risk targeting. This chapter is based on the following publication:

Gkimprixis A, Douglas J, Tubaldi E, Zonta D (2018) Development of fragility curves for use in seismic risk targeting. In 16th European conference on earthquake engineering, Thessaloniki, Greece.

3.1 Introduction

A key input when designing a new structure using Eurocode (EC) 8 (CEN 2004b), the European seismic design code, is the design acceleration. This acceleration is used to construct the design response spectrum, which also depends on the site class (A, B, C, etc.). The general aim of EC8 is that the higher the design acceleration, the more resistant to earthquake shaking is the designed structure. In this study we conduct a

preliminary investigation of the impact of the design acceleration on the fragility of reinforced-concrete (RC) structures designed using Eurocodes 2 and 8 (CEN 2004a and CEN 2004b). The purpose of this investigation is to improve our understanding of whether the design acceleration dominates over other factors affecting fragility, in our case the number of storeys and number of bays.

In this section a brief introduction to the approach of risk-targeting for the development of seismic design maps is provided alongside a summary of previous studies providing the critical input to this approach that is further investigated here, i.e.: fragility curves for different design accelerations. Section 3.2 presents the structures that we have designed using EC2 and EC8 for our study. Next the procedure used to construct the fragility curves of those structures is presented. In Section 3.4 the results of these calculations are shown and compared to curves derived in previous studies. The article ends with some brief conclusions and recommendations for future work.

3.1.1 Risk-targeting

As discussed in the previous chapter, in the approach for the development of seismic design maps commonly known as risk-targeting, rather than mapping the design acceleration from a probabilistic seismic hazard assessment (PSHA) for a constant return period (e.g. 475 years), the design accelerations that lead to a constant level of risk of collapse (or other damage level) are mapped. To calculate these accelerations an iterative approach is used herein where, for each location, the hazard curve from the PSHA is convolved with a fragility curve expressing the probability of collapse given an acceleration to evaluate the annual probability of collapse for a structure designed to that standard. The iteration continues until this probability of collapse equals the chance of collapse that is considered acceptable.

Risk-targeting has three principal advantages over the use of design levels that are defined in the traditional ‘uniform hazard’ way, i.e. for a given return period (e.g. 475 years). These advantages are: transparency, a risk level that is uniform across a territory (so that the population is equally protected throughout the territory, which is fairer than the current situation where different populations are more vulnerable to earthquakes) and the ability to compare (and ideally control) risk for different types of

hazard (e.g. earthquake versus wind). It does, however, come with the disadvantage of making more choices explicit, rather than implicitly being assumed through convention (e.g. the choice of 475 years as the design return period).

3.1.2 Previous studies presenting fragility curves for code-designed structures

In a risk-targeting approach, seismic risk is calculated by convolving the seismic hazard curve of a given location with a fragility curve for a code-designed structure (ideally derived from structural modelling). The ground-motion level that the structure is designed for is chosen so that the structure has a pre-defined probability of achieving a certain performance level (e.g. non-collapse). Determining fragility curves for structures designed with modern codes for different levels of ground motion is, therefore, a prerequisite for the application of the method. In this section, we briefly summarize previous studies proposing fragility curves for code-designed structures for different levels of design acceleration. Only studies that have derived fragility curves for two or more levels of design acceleration are summarized here. This is because the large dispersion between fragility curves from different studies makes drawing conclusions on the effect of design accelerations on the fragility of the structure difficult. For example, if one study presents a fragility curve for a 3-storey RC building designed for a 0.1g peak ground acceleration (*PGA*) and another study presents a curve for a comparable building but designed for 0.3g, the differences could be due to the design acceleration or they could be due to (minor) differences in the design approach or fragility curve derivation (e.g. selected strong-motion records, damage thresholds and fitting technique).

In a previous study, Ulrich et al. (2014) developed fragility curves in terms of *PGA* for EC8-designed RC structures but only for a single building geometry (3 storey-3 bay) and a handful of design accelerations: 0.0 (gravity loads only), 0.7 m/s^2, 1.1 m/s^2, 1.7 m/s^2, 2.3 m/s^2 and 3.0 m/s^2. One of the conclusions reached was that the fragility curves for design accelerations of 1.1 m/s^2 or lower were similar and overall the impact of the design acceleration on the fragility was quite low. This suggests that using code design procedures even without considering earthquake loading leads to robust structures and the correlation between design acceleration and fragility is weak.

Martins et al. (2015) consider 3-storey and 5-storey RC 3-bay-4-frames structures designed for 0.0g, 0.2g and 0.4g. They present the fragility curves for these six structures both in terms of spectral acceleration at the fundamental period of vibration, $S_a(T_1)$, and *PGA*. One observation that can be made from the presented curves is that the effect of the number of storeys on the fragility curves derived for the same design accelerations is high. The curves of Martins et al. (2015) show a higher effect of the design acceleration on the fragility of the structures than the curves of Ulrich et al. (2014).

A similar work is presented in Martins et al. (2018), where structural variability is introduced, by considering the span length and storey height of the 3- and 5-strorey buildings as variables (10 combinations per building, randomly selected) and the buildings were designed for a *PGA* equal to 0.05g, 0.1g, 0.2g, 0.3g, and 0.4g. Fragility curves are then generated in terms of *PGA* and $S_a(T_1)$ for both the collapse and yield damage states. They highlight the slight increase of the standard deviation of the fragility cures when structural variation is considered and suggest investigating other sources of uncertainty (e.g. variability of damage state thresholds).

3.2 Design of structures according to Eurocodes

In this section the approach for the design of the case-study structures and their characteristics are presented.

3.2.1 Structures considered

The modelled structures are standard RC buildings (Importance class II), which are symmetrical in plan and elevation. The buildings are chosen so that the influence of the design acceleration, the number of bays and the number of storeys on the fragility curves can be investigated. In particular, 2-storey-2-bay buildings are designed for two design *PGA*s (a_g): 1m/s^2 (0.1g) and 3m/s^2 (0.3g) and 4-storey-2-bay and 2-storey-4-bay buildings for the same design *PGA*s are considered as well. A medium ductility class is assumed for all models. The buildings are square in plan, with bay lengths of 5m. The length of the columns is also constant and equal to 3m. The material properties, which are the same for all the models, are presented in Table 3.1.

Table 3.1 Properties of concrete and steel used in modelled structures

Concrete		**Steel**	
Characteristic strength (MPa)	25	Characteristic strength (MPa)	450
Mean compressive strength (MPa)	33	Mean strength (MPa)	517.5
Mean tensile strength (MPa)	2.6	Modulus of elasticity (MPa)	$2.0 \cdot 10^5$
Modulus of elasticity (MPa)	$3.1 \cdot 10^4$	Strain hardening parameter (-)	0.005
		Fracture/buckling strain (-)	0.106

3.2.2 Design approach

The considered structures are all designed to be compliant with the EC2 and EC8 regulations. Since the models are regular both in plan and elevation, the codes allow the use of a simplified 2D design and modelling approach. To be conservative, an internal frame is considered, by neglecting torsional effects. The 2D numerical models are shown in Figure 3.1.

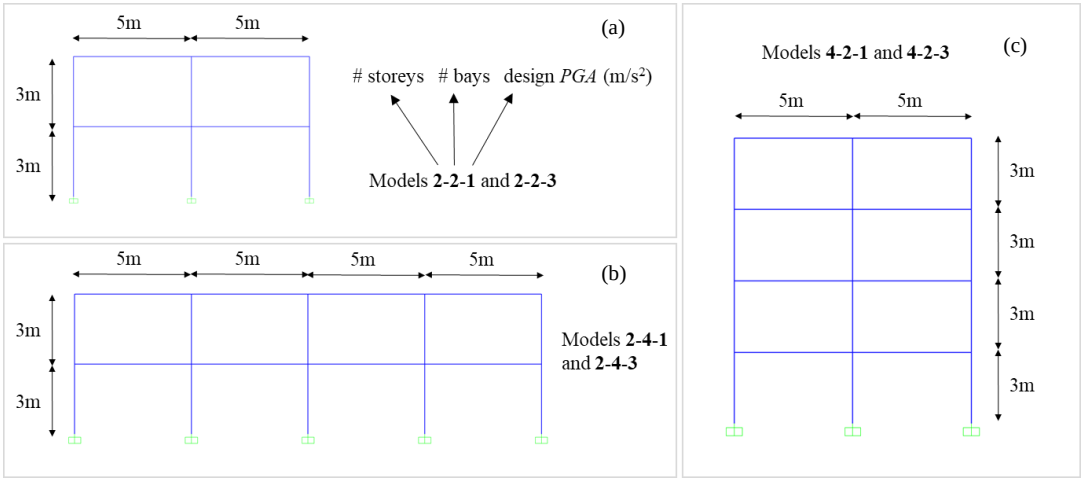

Figure 3.1 Representation of the numerical models for (a) 2-storey-2-bay buildings, (b) 2-storey-4-bay buildings, and (c) 4-storey-2-bay buildings

The simplified approach of EC8-1-4.3.1(7) is implemented to take into account the effect of cracking. To this end, a 50% reduction of the materials' modulus of elasticity is considered for the elements of all the models. For the structural design, the characteristic values of Table 3.1 are used for the concrete and steel properties. A value of 25 KN/m^3 was assumed for the specific weight of reinforced concrete. The assumptions of fixity at base and of rigid diaphragms in each storey are also made. The

contribution of the slab (15 mm thick) to the lateral stiffness was considered by assuming T-shaped beams, an approach compliant with the codes. For more information on this point, the reader is referred to EC2-1.1-5.3.2.1, which deals with the estimation of the effective beam width (b_{eff}).

The first step of the design procedure is to define minimum dimensions for the sections. It is noted that both the columns and the beams have the same section for all storeys. The models are analysed both for gravitational and earthquake loading. Regarding the permanent load, 1KN/m^2 was assumed for the finishing weight and 1.5 KN/m^2 and 3.25 KN/m^2 for the internal and external walls of the intermediate storeys, respectively. In the perimeter of the roof, a load of 3.75 KN/m was assumed instead. The distributed live load (Q) was taken equal to 2 KN/m^2 and 2.5 KN/m^2 for the roof and intermediate storeys, respectively.

The following two load combinations are considered for the design: 1.35·G+1.5·Q and G+0.3·Q+E, where G, Q and E are the permanent, live and earthquake loads respectively. It is highlighted that the first load combination (gravity loads only) needs to be checked, since it could control the section dimensions and reinforcement for low design acceleration values. Assuming soil class B conditions and 5% for the damping ratio, the EC8 Type 1 horizontal design acceleration spectrum is calculated. To define the design spectrum, a behaviour factor q = 3.9 is considered, as suggested in EC8-1-5.2.2.2 for multi-storey, multi-bay frame systems regular in plan and elevation with medium ductility, and a modal response spectrum analysis is then performed.

The required reinforcement area (longitudinal and shear) for beams and columns is then calculated, according to the requirements of the codes. An additional check is made manually according to EC8-1-4.4.2.2(2) regarding the second-order effects. The limitation of inter-storey drift (maximum 0.5% storey drift) is also checked, in accordance with the criterion of paragraph EC8-1-4.4.3.2, by employing a value of 0.5 for the reduction factor v. The beneficial contribution of the infills in terms of added stiffness and strength for low seismic intensities is disregarded.

If the structure fails any of the above criteria, the sections are increased by the user. Otherwise, the design procedure is complete, and the resulting maximum values are

considered for simplicity. The results of this procedure are summarized in Table 3.2. Our calculated dimensions are comparable with those presented by Fardis et al. (2012) for similar structures designed using EC2 and EC8.

Table 3.2 Properties of the designed structures

Model	Beams						Columns		First modal period (s)
storeys-bays-design PGA(m/s^2)	Str.	H (cm)	W (cm)	b_{eff} (m)	Top reinf. (mm)	Bottom reinf. (mm)	H=W (cm)	Reinf. (mm)	
2-2-1	1	30	25	1.65	2Φ24	2Φ16	35	4Φ20	0.37
	2	30	25	1.65	2Φ18+3Φ14	4Φ12			
2-2-3	1	35	30	1.70	4Φ20	3Φ16	40	8Φ16	0.28
	2	35	30	1.70	2Φ24	2Φ16			
2-4-1	1	25	25	1.65	3Φ22	2Φ18	35	8Φ14	0.40
	2	25	25	1.65	2Φ24	2Φ16			
2-4-3	1	35	30	1.70	5Φ18	5Φ12	40	4Φ24	0.29
	2	35	30	1.70	3Φ18	3Φ12			
4-2-1	1	30	25	1.65	3Φ20	2Φ16	35	8Φ14	0.76
	2	30	25	1.65	2Φ24	2Φ16			
	3	30	25	1.65	4Φ16	2Φ16			
	4	30	25	1.65	4Φ14	3Φ12			
4-2-3	1	50	45	1.85	7Φ18	6Φ16	50	8Φ20	0.38
	2	50	45	1.85	2Φ22+2Φ24	4Φ18			
	3	50	45	1.85	3Φ18+2Φ16	3Φ16			
	4	50	45	1.85	3Φ16	3Φ16			

3.3 Construction of fragility curves

In this section, the method used to model numerically the code-design structures is discussed.

3.3.1 Dynamic modelling

The finite element software Seismostruct (Seismosoft 2018) is used to perform the seismic analyses. The software uses the fibre approach to distribute plasticity across an element's section. In particular, the sectional stress-strain state derives from the integration of the nonlinear uniaxial stress-strain response of the individual fibres into which the section is subdivided. Herein, 150 fibres are employed, based on accuracy and computational efficiency criteria. A forced-based formulation is used to model the elements and the plastic-hinge method is employed to distribute plasticity across the

elements' length (Calabrese et al. 2010), using the inelastic plastic hinge force-based frame element type. The length of the plastic hinge (L_p) is calculated according to the Paulay and Priestley (1992) formula:

$$L_p = 0.08 \cdot L + 0.022 \cdot f_y \cdot d_b \quad (3.1)$$

where L is the element's length and f_y and d_b the yield strength and diameter, respectively, of the longitudinal reinforcing steel. This is a widely used expression, although various alternative equations can be found in the literature (Fardis 2009; Bae and Bayrak 2008; Mortezaei and Ronagh 2013).

Regarding the material properties, the Kappos and Konstantinidis (1999) nonlinear concrete model was used alongside a steel model based on Menegotto and Pinto (1973). In the design approach described in the former section, the characteristic values were used. However, for the performance of nonlinear analyses, the mean values of Table 3.1 are used instead, as stated in EC8-1-4.3.3.4.1(4). Once again, we should highlight that the masonry infills were not considered in the nonlinear modelling.

A Rayleigh damping matrix, built based on the tangent stiffness approach, is employed to model the damping inherent to the structure and its contribution to the seismic energy dissipation. A 5% damping ratio is considered for the first two transitional modal periods (estimated via eigenvalue analysis). Finally, the seismic combination includes both the permanent loads (G+0.3·Q, where G denotes the permanent loads and Q the live ones) and the seismic excitation (acceleration in the horizontal direction) at the base nodes.

3.3.2 Strong-motion records

The structures modelled in this study are assumed to be located in a high seismicity area in the Mediterranean region, where near-source moderate and large crustal earthquakes are possible (e.g. central Italy or Greece), but not at a specific site. A set of strong-motion records reflecting the earthquake shaking that the structures could be subjected to was selected from RESORCE (Akkar et al. 2014) using these selection criteria: epicentral distance between 0 and 30km, moment magnitude between 5 and 7 and focal depth less than or equal to 30km. 24 records (see Appendix A), with unscaled

peak ground accelerations (*PGA*) from 2.1m/s^2 to 8.7m/s^2, were selected. For the calculation of the fragility curves the records were all scaled to a set of 26 roughly logarithmically-spaced *PGA*s between 0.15m/s^2 and 60m/s^2. The linear elastic response spectra for 5% critical damping of the 24 records scaled to a common *PGA* of 5m/s^2 are shown in Figure 3.2, along with the average spectrum and the first modal periods of the designed structures.

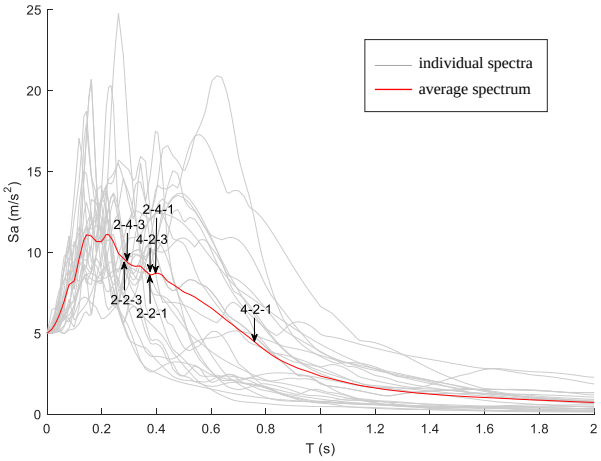

Figure 3.2 Linear elastic response spectra (5% damping) of the selected records scaled to a common *PGA* of 5m/s^2 (grey), the average spectrum (red) and the first modal periods of the designed structures

3.3.3 Fitting of fragility curves

Incremental dynamic analyses (IDAs) (Vamvatsikos and Cornell, 2002) were performed with the selected records. As stated above, for each model the 24 selected records were scaled at 26 different intensity levels and used as input. From the results of the analyses, the maximum inter-storey drift was selected for each *PGA* level, thus creating a cloud of 24 × 26= 624 points, for each model.

Similar to Ulrich et al. (2014), two limit states are considered in this study, namely the 'no damage' and 'severe damage' of Ghobarah (2004). The first limit state corresponds to some fine cracks forming in plaster, whereas the second corresponds to partial collapse of lateral and gravity load carrying elements. These limit states are controlled by the interstorey drift ratios limits, equal to 0.2% and 1.8% respectively for the 'no damage' and 'severe damage' limit state. The limit state of 'light damage', with a 0.4%

threshold, is also examined since it is regarded by the author to be more representative of the yield scenario (compared to the conservative 0.2%).

When estimating the response of structures to extreme ground motions, it is common that the numerical simulations do not converge due to numerical instabilities, giving numerically infinite values for the response parameters (e.g. Vamvatsikos and Cornell 2002). Therefore, particularly for the 'severe damage' level, it is not possible to obtain accurate drift estimates for all strong-motion records scaled to high *PGA*s. In this situation, the standard least-squares (LS) regression on the results of dynamic analyses cannot be used (since the response parameters are inaccurate) and the maximum-likelihood estimation (MLE) (Shinozuka et al., 2000) is preferable because it does not use the response parameters directly (e.g. Gehl et al. 2015). This is despite the higher uncertainties in the derived fragility curves for the same number of dynamic runs using MLE as opposed to LS regression (Gehl et al. 2015). The likelihood function method requires only knowledge of whether the monitored limit state has been exceeded or not for the strong-motion record considered. We assume that simulations that do not converge indicate that the structure has collapsed, which is a common assumption (e.g. Vamvatsikos and Cornell 2002).

For consistency, results for every limit state are derived using the MLE method assuming a lognormal fragility curve with two free parameters: the median capacity, α, and the standard deviation, β. Comparisons between fragility curves derived using MLE and LS regression for 'no damage' limit state have been carried out, and the observed differences are minimal.

The following equation describes the probability of being at or exceeding a particular damage state (ds_i) for a given intensity ($IM=im$):

$$P(ds \geq ds_i | IM = im) = \Phi\left[\frac{ln(im/\alpha)}{\beta}\right] \tag{3.2}$$

where Φ is the cumulative distribution function of the standard normal distribution. This equation is used to fit the output of the dynamic analyses and generate the fragility curves.

3.4 Results

Figure 3.3 presents the fragility curves of the case study for the damage states of 'light damage' and 'severe damage'. The coefficients of the lognormal fragility curves according to Eqn.(3.2) are given in Table 3.3. In general, it is observed that by increasing the design *PGA*, the median capacity of the building increases. Moreover, the 2-storey and 4-storey buildings designed for the same *PGA*s are characterized by different fragilities. In particular, the 4-storey buildings experience lower inter-storey drift demands and hence are less fragile than the 2-storey ones, with similar trends observed also in relevant research works (e.g. Tsionis and Fardis 2014; Fardis et al. 2012; Martins et al. 2018). The difference between the fragility curves of the 2- and 4-storey buildings is larger for higher design *PGA* values. This can possibly be attributed to the clause of the codes that controls the inter-storey drifts at the damage limitation limit state, which results in a conservative design (i.e. sections with large dimensions) for the 4-2-3 model. The standard deviation, β, of the fragility curves, another critical parameter in the risk-targeting approach, shows consistent values with an average of 0.65 for the case of 'severe damage' (Table 3.3), which is close to the 0.6 proposed in ASCE 7-10. It should be noted that the obtained results are sensitive to the records selected to describe record-to-record variability effects (Figure 3.2).

Table 3.3 Coefficients of the fragility curves

Model	No damage		Light Damage		Partial Collapse	
	α	β	α	β	α	β
2-2-1	0.953	0.504	1.784	0.549	8.627	0.638
2-2-3	1.099	0.447	2.282	0.490	9.175	0.688
2-4-1	0.934	0.518	1.668	0.591	8.150	0.622
2-4-3	1.253	0.440	2.281	0.476	9.234	0.699
4-2-1	1.032	0.486	2.220	0.518	10.272	0.659
4-2-3	1.613	0.568	2.814	0.621	11.951	0.604

The results shown in Figure 3.3 and Table 3.3 also allow an evaluation of the influence of the geometry (in terms of number of bays only) on the fragility curves. It can be observed that the number of bays has a minor impact on these curves. This is expected, since if the span dimensions are kept constant, while the stiffness changes, so does the total mass, resulting in minor changes in the dynamic behaviour of the structure. This

last point can also be seen by comparing the modal periods of the structures (see Table 3.2).

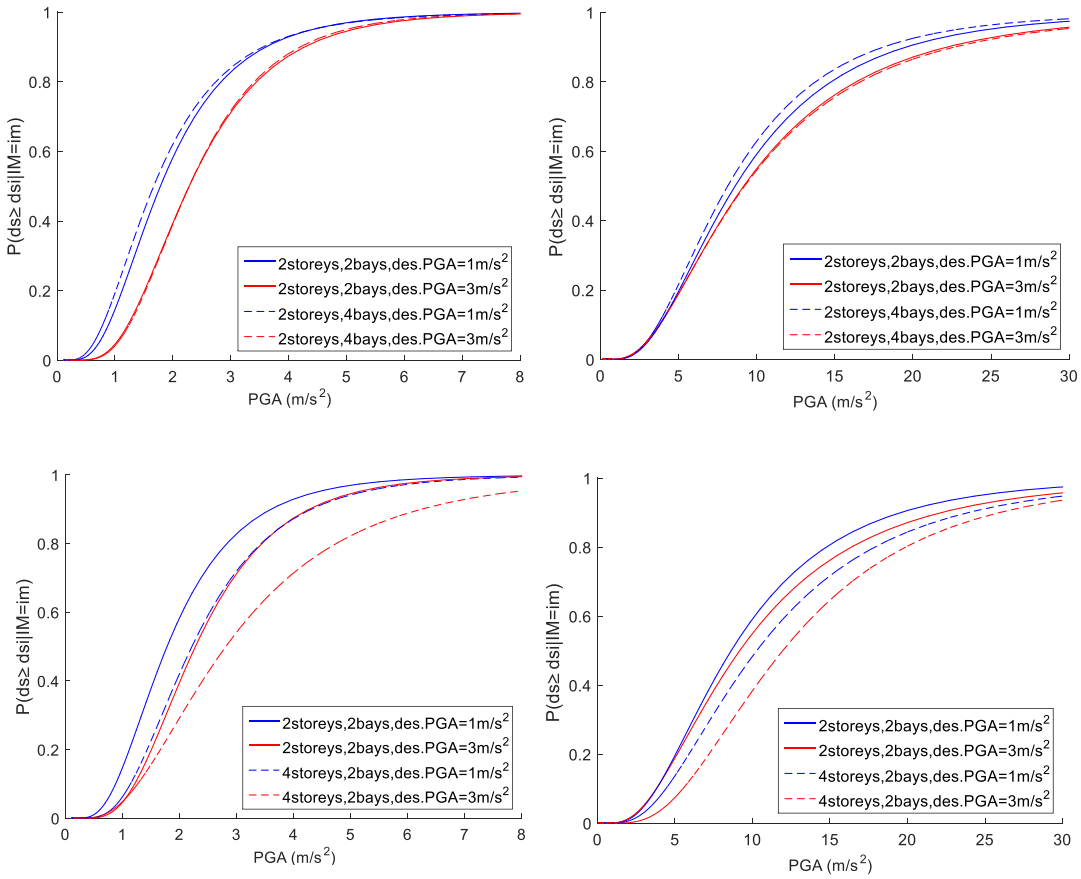

Figure 3.3 Influence of the number of bays (top figures) and storeys (bottom figures) on the fragility curves, for the 'light damage' (left) and 'severe damage' (right) limit states

Table 3.4 reports the probability of experiencing different damage levels at the design *PGA* obtained from the derived fragility curves. It is noticeable that there is an increase in that probability with the design acceleration, as seen also in other works (Martins et al. 2015; Ulrich et al. 2014). The probability of 'severe damage' when exposed to a *PGA* level equal to the design value is a necessary input when implementing the current risk-targeting approach (e.g. Douglas et al. 2013), although the approach could be modified to use fragility curves anchored to any *PGA* level. For the case study investigated here and under the assumptions discussed before, this probability is in the range 10^{-4} to 10^{-2} when designing for 0.1g and 0.3g, respectively.

As for the ‘no damage’ limit state, the average values are equal to 0.521 for 0.1g and 0.942 for 0.3g, quite close to the ones presented in Ulrich et al. (2014) for their yield damage state, which corresponds to the same inter-storey drift ratio limit of 0.2% as the one considered here. For ‘light damage’, an average value of 0.134 is observed for 0.1g and 0.657 for 0.3g. A direct comparison with the rest of the studies is not made here, due to the difference in the definition of the damage states.

Table 3.4 Probabilities of different levels of damage at the design *PGA*

Model	No damage	Light Damage	Severe Damage
2-2-1	0.538	0.146	$3.63 \cdot 10^{-4}$
2-2-3	0.988	0.712	$5.20 \cdot 10^{-2}$
2-4-1	0.552	0.193	$3.71 \cdot 10^{-4}$
2-4-3	0.976	0.718	$5.39 \cdot 10^{-2}$
4-2-1	0.474	0.062	$2.02 \cdot 10^{-4}$
4-2-3	0.863	0.541	$1.10 \cdot 10^{-2}$

3.5 Conclusions

The case study of this chapter is just a first step towards defining fragility curves that are useful for risk-targeting, which is a design philosophy currently attracting considerable research effort. The impact of the design acceleration and the number of bays and storeys on the probability of occurrence of different limit states is investigated herein. In future work it is recommended to investigate the influence of the strong-motion records selection and the choice of the damage state limits because these may have a significant impact on the derived fragility curves.

Some codes (e.g. ASCE) already use the risk-targeting approach and employ a simplified approach, by assuming a-priori values for the dispersion of the fragility curve (e.g. β=0.6) as well as for the probability of failure at the design *PGA*. The study results show that while the assumption of a constant β is realistic for the types of buildings investigated, the other assumption of a fixed probability of failure at the design *PGA* appears too strong. The buildings designed for 0.1g and 0.3g have probabilities of ‘severe damage’ roughly between 10^{-4} and 10^{-2}, i.e. with two orders of magnitude difference. Thus, future studies should investigate the effect of the assumption of a constant probability of failure at the design *PGA* on the final design

results. The error in the risk estimates resulting from the use of the simplifying assumption of generic fragility curves could be evaluated by performing extensive parametric analyses for different building and hazard scenarios and by comparing the results obtained using analytical fragility curves like those developed in this study.

References

Akkar S, Sandikkaya MA, Senyurt M, Azari Sisi A, Ay BÖ, Traversa P, Douglas J, Cotton F, Luzi L, Hernandez B, Godey S (2014) Reference database for seismic ground-motion in Europe (RESORCE), Bulletin of Earthquake Engineering, 12(1): 311-339, doi: 10.1007/s10518-013-9506-8

ASCE (2010) Minimum Design Loads for Buildings and Other Structures, ASCE Standard 7-10. American Society of Civil Engineers, Reston, VA

Bae S, Bayrak O (2008) Plastic hinge length of reinforced concrete columns. ACI Structural Journal, 105-S28, 290-300

Calabrese A, João PA, Pinho R (2010) Numerical Issues in Distributed Inelasticity Modeling of RC Frame Elements for Seismic Analysis, Journal of Earthquake Engineering, 14(S1): 38–68, doi: 10.1080/13632461003651869

CEN (2004a) EN 1992-1-1:2004 Eurocode 2: Design of concrete structures - Part 1-1: General rules and rules for buildings, European Committee for Standardization, Brussels

CEN (2004b) EN 1998-1:2004 Eurocode 8: Design of structures for earthquake resistance - Part 1: General rules, seismic actions and rules for buildings, European Committee for Standardization, Brussels

Computers & Structures, Inc. (2016) SAP2000, Integrated Solution for Structural Analysis and Design, Version 19.0.0, USA

Douglas J, Gkimprixis A (2018) Risk targeting in seismic design codes: The state of the art, outstanding issues and possible paths forward, Seismic Hazard and Risk Assessment - Updated Overview with Emphasis on Romania, R. Vacareanu and C. Ionescu (eds), Springer, doi: 10.1007/978-3-319-74724-8_14

Douglas J, Ulrich T, Negulescu C (2013) Risk-targeted seismic design maps for mainland France. Natural Hazards, 65: 1999-2013, doi: 10.1007/s11069-012-0460-6

Fardis MN (2009) Seismic design, assessment and retrofitting of concrete buildings: based on EN-Eurocode 8. Springer Science & Business Media

Fardis MN, Papailia A, Tsionis G (2012) Seismic fragility of RC framed and wall-frame buildings designed to the EN-Eurocodes, Bulletin of Earthquake Engineering, 10: 1767–1793

Gehl P, Douglas J, Seyedi D (2015) Influence of the number of dynamic analyses on the accuracy of structural response estimates, Earthquake Spectra, 31(1): 97-113, doi: 10.1193/102912EQS320M

Ghobarah A (2004) On drift limits associated with different damage levels, Proceedings of international workshop on performance-based seismic design concepts and implementation, June 28th–July 1st, 2004, Bled, Slovenia

Kappos A, Konstantinidis D (1999) Statistical analysis of confined high strength concrete, Materials and Structures, 32: 734-748

Luco N, Ellingwood BR, Hamburger RO, Hooper JD, Kimball JK, Kircher CA (2007) Risk-targeted versus current seismic design maps for the conterminous United States, SEAOC 2007 convention proceedings, 26-29 September, Squaw Creek, USA

Martins L, Silva V, Bazzurro P, Marques M (2018) Advances in the derivation of fragility functions for the development of risk-targeted hazard maps. Engineering Structures, 173, 669-680

Martins L, Silva V, Crowley H, Bazzurro P, Marques M (2015) Investigation of structural fragility for risk-targeted hazard assessment. Proceedings of 12th International Conference on Applications of Statistics and Probability in Civil Engineering (ICASP12), 12-15 July, Vancouver, Canada

Menegotto M, Pinto PE (1973) Method of analysis for cyclically loaded R.C. plane frames including changes in geometry and non-elastic behaviour of elements under combined normal force and bending, Symposium on the Resistance and Ultimate Deformability of Structures Acted on by Well Defined Repeated Loads,

International Association for Bridge and Structural Engineering, Zurich, Switzerland, 15-22

Mortezaei A, Ronagh HR (2013) Plastic hinge length of reinforced concrete columns subjected to both far-fault and near-fault ground motions having forward directivity. The Structural Design of Tall and Special Buildings, 22, 903-926, doi: 10.1002/tal.729Paulay T, Priestley MJN (1992) Seismic design of reinforced concrete and masonry buildings, John Wiley & Sons, New York

Seismosoft (2018) SeismoStruct 2018 – A computer program for static and dynamic nonlinear analysis of framed structures, available from https://seismosoft.com

Shinozuka M, Feng Q, Lee J, Naganuma, T (2000) Statistical analysis of fragility curves, Journal of Engineering Mechanics, 126: 1224–1231

Tsionis G, Fardis MN (2014) Seismic fragility curves for reinforced concrete buildings and bridges in Thessaloniki, Second European Conference on Earthquake Engineering and Seismology, 25-29 August, 2014, Turkey

Ulrich T, Negulescu C, Douglas J (2014) Fragility curves for risk-targeted seismic design maps. Bulletin of Earthquake Engineering, 12(4): 1479-1491, doi: 10.1007/s10518-013-9572-y

Vamvatsikos D, Cornell CA (2002) Incremental dynamic analysis. Earthquake engineering & structural dynamics, 31, 491-514, doi: 10.1002/eqe.141

CHAPTER 4

Comparison of methods to develop risk-targeted seismic design maps

The seismic design of structures according to current codes is generally carried out using a uniform-hazard spectrum for a fixed return period, and by employing a deterministic approach that disregards many uncertainties, such as the contribution of earthquake ground motions with return periods other than that assumed for the design. This results in uncontrolled values of the failure probability, which vary with the structure and the location. Risk targeting has recently emerged as a tool for overcoming these limitations, allowing achievement of consistent performance levels for structures with different properties through the definition of uniform-risk design maps. Different countries are implementing the concepts of risk targeting in different ways, and new methods have recently emerged.

In the first part of this chapter, the most well-known approaches for risk targeting are reviewed, with particular focus on the one implemented in recent American design codes, the one based on the use of risk-targeted behaviour factors (RTBF), and an approach based on direct estimation of hazard curves for inelastic response of single-degree-of-freedom systems. The effect of the linearization of the hazard curve is investigated first. A validation of the RTBF approach is then provided, based on comparison with the results of uniform-risk design spectral accelerations for single-degree-of-freedom systems with elastic-perfectly plastic behaviour for two different sites. The effectiveness of the current risk-targeting framework applied in the United States is also investigated. In the last part of the chapter, uniform-risk hazard maps for Europe are developed using the RTBF approach, showing how the seismic design

levels may change when moving from a uniform-hazard to a uniform-risk concept. The work presented in this chapter is based on the following publication:

Gkimprixis A, Tubaldi E, Douglas J (2019) Comparison of methods to develop risk-targeted seismic design maps. Bulletin of Earthquake Engineering, 17, 3727–3752 (2019), https://doi.org/10.1007/s10518-019-00629-w.

4.1 Introduction

The seismic assessment and design of structures is continuously evolving, as demonstrated by the rapid development of new procedures, best exemplified by the PEER performance-based earthquake engineering framework (Porter 2003). Numerous studies have aimed to incorporate probability concepts into seismic performance evaluation, with consideration of the uncertainties related to not only the seismic input, but also the structural properties, the capacity, and the model (e.g. Dolšek 2009; Liel et al. 2009; Tubaldi et al. 2011; Fib 2012). Moreover, increasing attention has been given to achieving an explicit control of the probability that a structure exceeds prefixed performance objectives during its design life (e.g. Collins et al. 1996; Wen 2001; Fragiadakis and Papadrakakis 2008; Barbato and Tubaldi 2013; Gidaris and Taflanidis 2015; Castaldo et al. 2017; Altieri et al. 2018; Franchin et al. 2018). It is widely acknowledged that in the long term, risk-based assessment and design criteria will be recommended, or will even be mandatory, in design codes (Vamvatsikos et al. 2015; Fajfar 2018). For instance, the United States has already incorporated such criteria in its seismic design codes ASCE 7-16 (2017) and FEMA P-750 (2009a); the new version of Eurocode 8 Part 1 will also include an Informative Annex on probabilistic assessment of structures (Fajfar 2018).

Probability concepts have already entered into current codes in the definition of the seismic action. The basis of the seismic input definition is often probabilistic seismic hazard analysis (PSHA) (e.g. McGuire 2008; Baker 2015), which estimates the probability distribution of a seismic intensity measure (IM), such as the peak ground acceleration (*PGA*) or the pseudo-spectral acceleration (S_a). This information can be used to build a uniform hazard response spectrum (UHS) for a given return period T_R or probability of exceedance in the design lifetime. The value of T_R depends on the

target performance objective and on the importance of the structure. For example, a return period T_R = 475 years, corresponding to a 10% probability of exceedance in 50 years (given the standard assumption of a Poisson process), is often associated with ultimate limit state conditions (e.g. in Eurocode 8-1-2.1, CEN 2004).

Having defined the seismic input, the structural response can be estimated by using various analysis methods, the most advanced one consisting in selecting a set of ground motions, and evaluating, via nonlinear time-history analysis, the mean or maximum demand for the considered records. The seismic code approach is still, however, essentially deterministic (Bradley 2011), and does not allow direct evaluation of the probability of exceedance of the engineering demand parameters (EDPs) of interest for the performance assessment. This is mainly a consequence of the dispersion in the EDP-IM relationship and in the system capacity (Cornell 2005). The consequence of this dispersion is that hazard levels corresponding to a probability of exceedance other than that of the UHS need to be considered (e.g. Cornell 1996; Iervolino et al. 2018; Tubaldi et al. 2015). Moreover, for design purposes, seismic codes prescribe the use of a UHS divided by a behaviour factor (or response modification factor) relevant to the structural system under study. This approach has been shown to result in inconsistent values of the risk of failure, which differ for systems with different vibration periods, and also for the same structure located in areas characterized by different hazard. Again, this inconsistency is the result of the record-to-record variability effects (i.e. the variability of the frequency content and other characteristics of the ground motion for a given IM level) that generally result in dispersion in the EDP-IM relationship for multi-degree of freedom (MDOF) or nonlinear structural systems. The many safety margins introduced by seismic codes (e.g. material design values, capacity design and minimum member sizes) are also responsible for the uncontrollable risk levels that are generally different from the hazard levels (e.g. Collins et al. 1996; Tubaldi et al. 2012; Silva et al. 2016; Iervolino et al. 2018).

Given these limitations, more advanced approaches have been developed to achieve an explicit control of the seismic structural performance in the assessment and design stage (Fragiadakis and Papadrakakis 2008; Barbato and Tubaldi 2013; Gidaris and Taflanidis 2015; Castaldo et al. 2017; Altieri et al. 2018; Franchin et al. 2018). Parallel

to these reliability-based assessment and design approaches, simplified methods have been proposed, fostering a gradual introduction of probability concepts into practice. Most of these methods are based on the probabilistic framework outlined in Kennedy and Short (1994) and Cornell (1996), which led to the development of the SAC-FEMA framework (Cornell et al. 2002) for structural design of steel moment resisting frames under seismic action, later enhanced by others (e.g. Lupoi et al. 2002; Vamvatsikos 2013). This framework introduces some simplifying assumptions to allow for a closed-form approximation of the mean annual frequency (MAF) of limit state exceedance. Based on the concepts and procedures developed by these methods, Fajfar and Dolšek (2012) introduced a practice-oriented approach for seismic risk assessment. This method employs pushover analysis instead of more time consuming dynamic analyses for response assessment and considers a default value of the dispersion to account for the record-to-record variability effects. Moreover, Žižmond and Dolšek (2017) developed the concept of risk-targeted behaviour factors, as a means to control the risk of exceedance of different limit states by the structure during the design procedure. Vamvatsikos and Aschheim (2016) introduced the concept of yield frequency spectra, enabling the direct design of a structure subject to a set of performance objectives. Such spectra can be used to provide the risk-targeted yield strength of a system that satisfies an acceptable ductility response level.

In the United States, following the work of Luco et al. (2007), the concept of risk-targeting has emerged, aiming to define ground motion maps adopting a "uniform risk" rather than a "uniform hazard" concept. With this approach, the seismic uniform-hazard ground motion maps are modified to obtain more consistent levels of the collapse probability across the country. While risk targeted design maps have been already implemented in American seismic design codes (see Luco et al., 2015), they have not yet been introduced in practice in, where the implementation of probabilistic behaviour factor concepts in Eurocode 8 is still under consideration (Fajfar 2018).

Finally, since the work of Sewell (1989), researchers have produced ground motion prediction equations (GMPEs) for predicting inelastic ductility demands of structural systems (e.g. Sewell 1989; Tothong and Cornell 2006; Ruphakety and Sigbjörnsson 2009; Bozorgnia et al. 2010a, 2010b; De Luca et al., 2011). Such GMPEs depend on

the actual yield strength of the system and are more structure specific than typical GMPEs for *PGA* or S_a. Thus, they have often been developed for elasto-plastic single degree of freedom (SDOF) systems only, since it is not feasible to derive them for every type of MDOF system. Nevertheless, they could be used within PSHA to construct uniform-risk inelastic spectra, ensuring consistent probabilities of exceeding different ductility demand levels. In this way, it is possible to avoid over- or under-design associated with the use of displacement reduction factors, at least for structures behaving as SDOF systems.

This chapter aims to review and compare the abovementioned approaches for the implementation of uniform-risk concepts in the performance-based design of structures. This is the first time that approaches employed in different fields (structural engineering and engineering seismology) and different countries are compared in a systematic way. In the first part of the paper, the risk-targeted behaviour factor (RTBF) approach, Luco's risk-targeting approach and the inelastic GMPEs approach are introduced together with their simplifying assumptions. A unified notation is adopted by changing, when necessary, the symbols used in the original papers and providing slightly different but equivalent derivations of the relevant equations. In the second part of the chapter, the effect of the linearization of the hazard curve, at the base of the framework developed by Kennedy and Short (1994) and Cornell (1996), is investigated. Subsequently, an elastic-perfectly plastic SDOF system is used to validate the RTBF approach for generating risk-targeted design spectra. Then, the choices made when applying risk-targeting in practice are examined, by giving suggestions for future revisions. In the final part of the chapter, risk-targeted design maps for Europe are generated using the RTBF approach, showing how existing maps may change if this approach was adopted.

4.2 Critical review of various risk-targeting approaches

The aim of any risk-targeting approach is to control the risk of exceeding a limit state related to an unsatisfactory performance of the structure. This risk can be expressed in terms of the MAF of exceedance of the limit state, λ_{LS}. Obviously, the event of limit state exceedance may result from the occurrence of earthquakes of different intensities

(Cornell 2005). Herein, we consider the spectral acceleration $S_a(T,\xi)$ at the fundamental period of vibration of the structure and for the damping ratio ξ as the IM. The MAF of limit state exceedance λ_{LS} can be expressed through the total probability theorem (e.g. Benjamin and Cornell 1970) as:

$$\lambda_{LS} = \int P\left(C|S_a\right)\cdot|dH(S_a)| \tag{4.1}$$

where the symbol "d" denotes the differentiation operator, $H(S_a)$ is the hazard curve, providing the MAF of exceeding S_a, from PSHA (Cornell 1968; McGuire 2008; Baker 2015), and $P\left(C|S_a\right)$ corresponds to the conditional probability of exceeding the limit state under an earthquake with intensity S_a. This probability is given by:

$$P\left(C|S_a\right) = P\left[S_a > S_a^C\right] \tag{4.2}$$

where S_a^C is the limit state capacity, i.e., the value of the spectral acceleration causing the exceedance of the limit state. It is noteworthy that this probability must account for the so called record-to-record variability effects (reflected in the variability of S_a^C, which assumes different values for different records) and the effect of the uncertainty in the structural capacity, as done in Cornell (1996).

In the following subsections, alternative approaches for risk-targeting are reviewed.

4.2.1 The risk-targeted behaviour factor (RTBF) approach

This approach is based on the work of Kennedy and Short (1994) and Cornell (1996), who developed a simple and practice-oriented way for estimating the seismic risk of a structural system and for designing the system's strength corresponding to a target reliability level. In particular, a closed-form expression of the MAF of failure of the system λ_{LS} can be obtained by introducing a series of simplifying assumptions, reviewed below. In the following, reference is made to the formulation of Cornell (1996), and the limit state definition is based on a measure of the global ductility of the system, μ. This entails defining explicitly a yield condition and an ultimate or "failure" condition, which can be kinematically related to each other. Different choices

can be made when defining these conditions, which may require identifying an elasto-plastic SDOF system equivalent to the structure under investigation (Cornell 1996; Aschheim, 2002). Hereinafter, the condition of "failure" corresponds to the ductility demand μ_d imposed by the earthquake exceeding the ductility capacity μ_c. The corresponding MAF of limit state exceedance is denoted hereinafter as λ_c, to highlight the fact that failure corresponds to exceedance of the ductility capacity. Obviously, other engineering demand parameters can be employed to describe the system performance, as done e.g. in Cornell et al. (2002) and Lupoi et al. (2002).

An important assumption concerns the seismic hazard, $H(S_a)$, which is represented by a linear equation in log-log space:

$$H(S_a) = k_0 \cdot S_a^{-k_1} \tag{4.3}$$

According to Cornell (1996), the limit state capacity S_a^c, can be expressed in terms of the following product:

$$S_a^c = q_{\mu_c} \cdot S_a^y \cdot \varepsilon_{\mu_c} \tag{4.4}$$

where S_a^y is the spectral acceleration inducing yielding of the system, q_{μ_c} is the ductility-dependent contribution of the behaviour factor, denoting the factor by which a specific acceleration time history capable of causing incipient first yield must be scaled up to produce a ductility demand equal to the median capacity $\hat{\mu}_c$, and ε_{μ_c} is a lognormal random variable with unit mean and lognormal standard deviation β_{μ_c} that captures the variability of the ductility capacity in spectral acceleration terms.

It is noteworthy that S_a^y and q_{μ_c} are also generally random variables, due to record-to-record variability effects. In fact, the seismic intensity corresponding to the yield limit state or other more severe limit states for a MDOF system is different for different records due to higher mode effects. Cornell (1996) assumes that these two random variables follow a lognormal distribution, with median values equal to $\hat{S}_a^y$ and $\hat{q}_{\mu_c}$

respectively, and lognormal standard deviation, or dispersion, $\beta_{S_a^y}$ and $\beta_{q_{\mu_c}}$. Moreover, in the case of a deterministic SDOF system, if the pseudo-spectral acceleration is used as the *IM*, then the yield acceleration has zero dispersion, i.e., $\beta_{S_a^y}$=0, because it is directly related to the yield displacement u_y through the relation $S_a^y = \omega^2 \cdot u_y$. This is generally not true in the more general case of MDOF systems, due to the influence of higher modes of vibration (Luco and Cornell 2007).

The product of lognormal random variables is also a lognormal random variable. Thus, based on the previous assumptions, the limit state capacity S_a^c follows a lognormal distribution with median $\hat{S}_a^c = \hat{q}_{\mu_c} \cdot \hat{S}_a^y$ and lognormal standard deviation $\beta = \sqrt{\beta_{S_a^y}{}^2 + \beta_{q_{\mu_c}}{}^2 + \beta_{\mu_c}{}^2}$. Under the assumptions discussed above, the MAF of limit state exceedance, can be expressed as (Kennedy and Short 1994; Cornell 1996):

$$\lambda_c = H\left(\hat{S}_a^c\right) \cdot e^{0.5\cdot(k_1\cdot\beta)^2} = k_0 \cdot \left(\hat{S}_a^y\right)^{-k_1} \cdot \hat{q}_{\mu_c}{}^{-k_1} \cdot e^{0.5\cdot(k_1\cdot\beta)^2} \tag{4.5}$$

It is noticeable in this equation that the risk estimates are sensitive to the assumptions made for k_1 and β. In particular, as observed in Figure 4.1 the factor $e^{0.5\cdot(k_1\cdot\beta)^2}$ increases significantly in cases of very steep hazard curves and high values of β.

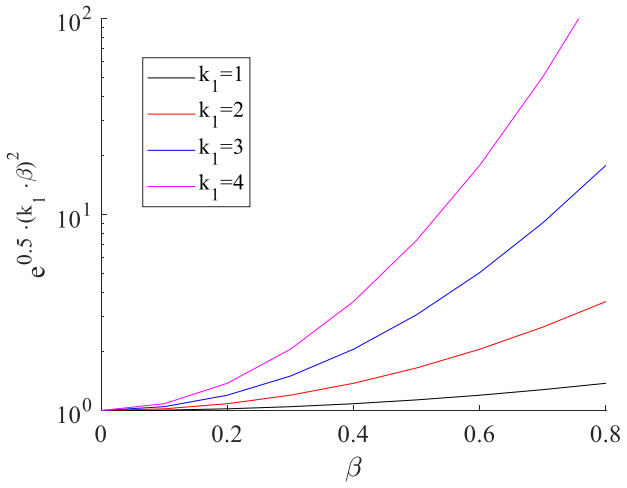

Figure 4.1 Sensitivity of risk estimates on k_1 and β

Eqn.(4.5) can be inverted to find the median value of $\hat{S}_a^y$ corresponding to a prefixed value of the MAF of failure. However, in order to exploit this formulation for design purposes, it is better to introduce the overstrength of the system q_s, similarly to Žižmond and Dolšek (2017). This overstrength is defined as the ratio between the spectral acceleration at yield of the system and the design spectral acceleration S_a^d (Kappos 1999):

$$q_s = \frac{\hat{S}_a^y}{S_a^d} \tag{4.6}$$

Substituting Eqn.(4.6) into Eqn.(4.5) gives the following expression of the MAF of failure, where now the dependence on the design spectral acceleration is made explicit:

$$\lambda_c\left(S_a{}^d\right) = H\left(S_a{}^d\right) \cdot f_{hc} \tag{4.7}$$

where $f_{hc} = \hat{q}_{\mu_c}{}^{-k_1} \cdot q_s{}^{-k_1} \cdot e^{0.5\cdot(k_1\cdot\beta)^2}$.

A risk curve $\lambda_c\left(S_a{}^d\right)$ can be built by plotting the values of λ_c against the values of the design spectral acceleration $S_a{}^d$. Figure 4.2a plots and compares the relation between the hazard curve $H\left(S_a{}^d\right)$ and the risk curve $\lambda_c\left(S_a{}^d\right)$. The hazard curve for $S_a{}^d$ is obtained by linearizing the site hazard curve (more insight into the effect of the linearization is given in Section 4.3.1). If the hazard curve is linear, then so is the risk curve by virtue of Eqn.(4.7).

Figure 4.2a also plots the yield curve $\lambda_y\left(S_a{}^d\right)$ corresponding to the MAF of yielding for a system designed with a spectral acceleration $S_a{}^d$. This can be obtained by setting $\hat{\mu}_c$ =1, which also corresponds to $\hat{q}_{\mu_c}$ =1 in Eqn.(4.7):

$$\lambda_y\left(S_a{}^d\right) = H\left(S_a{}^d\right) \cdot f_{hy} \tag{4.8}$$

where $f_{hy} = q_s^{-k_1} \cdot e^{0.5\cdot(k_1\cdot\beta)^2}$.

Again, if the hazard curve is linear, then so is the risk and yield curves by virtue of Eqn.(4.7) and Eqn.(4.8). While the analytical equation for risk calculation, Eqn.(4.5), is provided in the literature, it has been rearranged here into Eqn.(4.7) and Eqn.(4.8) to make the relation between hazard and risk and their dependence on the design spectral acceleration more explicit.

The design pseudo-spectral acceleration corresponding to a target value of the MAF of collapse λ_c for a system with median ductility capacity $\hat{\mu}_c$, can be obtained from Eqn.(4.7) as:

$$S_a^d = \frac{\hat{S}_a^c}{\hat{q}_{\mu_c} \cdot q_s} = \frac{1}{\hat{q}_{\mu_c} \cdot q_s} \cdot \left(\frac{k_0}{\lambda_c}\right)^{1/k_1} \cdot e^{0.5\cdot k_1\cdot\beta^2} \tag{4.9}$$

By plotting the values of S_a^d against T for a given ductility capacity and MAF of collapse, the uniform-risk design spectrum for a site can be obtained. In contrast to the inelastic spectrum in design codes, this spectrum provides a consistent level of the risk of failure for systems with different vibration periods.

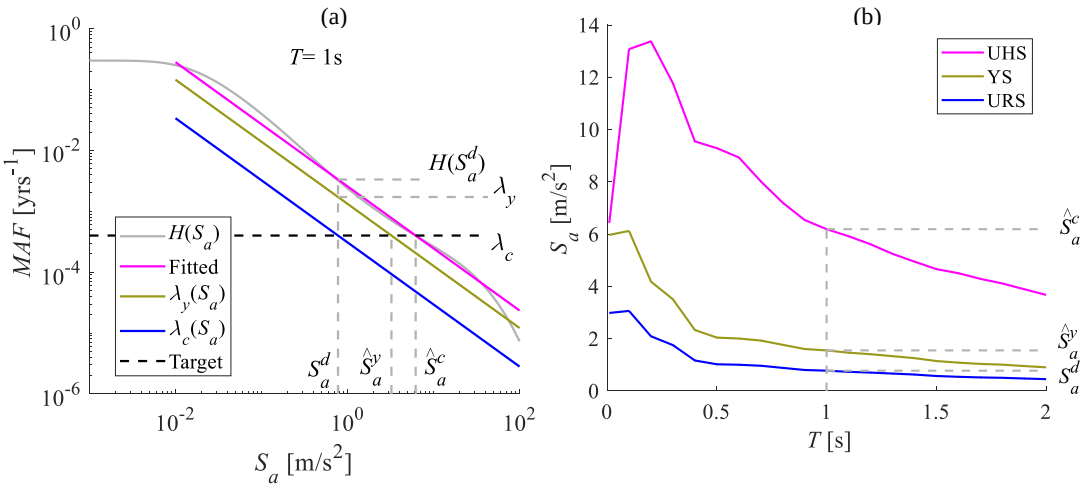

Figure 4.2 (a) Risk, yield and hazard curves for a system with T=1s; (b) uniform hazard spectrum (UHS), uniform risk spectrum (URS) and yield spectrum (YS) for a MAF of exceedance of 1/2500

Figure 4.2b shows the uniform hazard spectrum (UHS), the corresponding uniform risk spectrum (URS) and the yield spectrum (YS), derived for the same target MAF of exceedance (i.e. 1/2500), assuming q_s =2 and a ductility level of 4, for an example site (see following section). The values of these spectral ordinates for *T*=1s can be obtained by intersecting the hazard and risk curves with a horizontal line at target MAF of 1/2500 in Figure 4.2a.

In seismic codes, the design seismic input is often expressed in terms of a UHS for a given reference MAF of its exceedance, λ_{ref} , which does not necessarily coincide with the target MAF of limit state exceedance λ_c. Let $S_a^{ref} = \left(\frac{k_0}{\lambda_{ref}} \right)^{1/k_1}$ denote the spectral ordinate of the system with period *T*, obtained by inverting the hazard curve of S_a for the MAF of exceedance λ_{ref} . After dividing S_a^{ref} by S_a^d , the expression for the risk-targeted behaviour factor (Žižmond and Dolšek 2017; Fajfar 2018) is obtained:

$$q = \frac{S_a^{ref}}{S_a^d} = \frac{\hat{q}_{\mu_c} \cdot q_s}{\gamma_{IM}} \tag{4.10}$$

where $\gamma_{IM} = \frac{\hat{S}_a^c}{S_a^{ref}} = \left(\frac{\lambda_{ref}}{\lambda_c} \right)^{1/k_1} \cdot e^{0.5 \cdot k_1 \cdot \beta^2}$ is a factor accounting for the difference between the MAF of the seismic design input and the target MAF of collapse.

To summarize, the spectral ordinate S_a^{ref} , corresponding to the elastic response spectrum and the MAF of exceedance λ_{ref} , should be divided by *q* to design a system reaching the target performance, i.e., a MAF of collapse equal to λ_c . This factor is equal to the product of three components: q_s accounting for the system's overstrength, $\hat{q}_{\mu_c}$ for the system's ductility capacity, and $\gamma_{IM} = \hat{S}_a^c / S_a^{ref}$ for the difference in the MAF of exceedance of the input and of collapse. Figure 4.3 illustrates the relation between the spectral ordinates and the various components of *q* in the acceleration-displacement response spectrum plane.

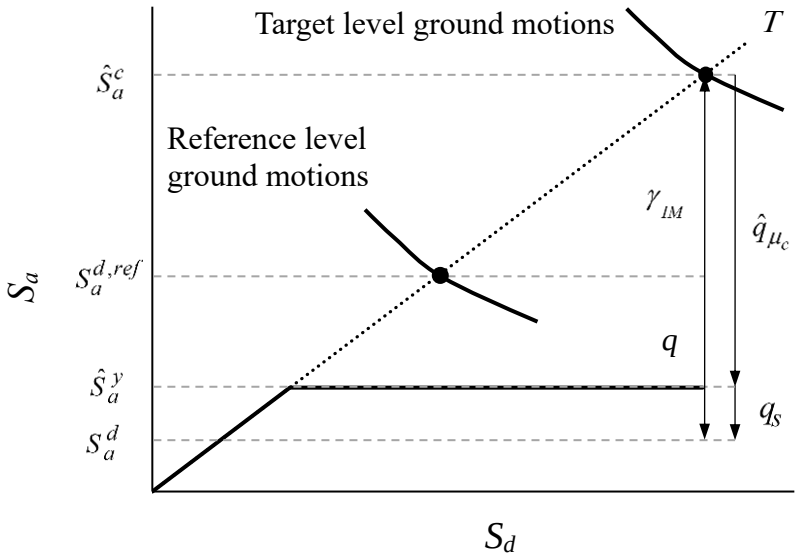

Figure 4.3 Relation between the spectral ordinates and the various components of q for a system with vibration period T

4.2.2 Luco's approach

Luco et al. (2007)'s approach for risk targeting was introduced to ensure a uniform collapse probability for structures located in regions across the United States characterized by different shapes of the hazard curve. The approach was developed from the seminal work of Kennedy and Short (1994) and is based on the assumption that the structural capacity follows a lognormal distribution with median $\hat{S}_a^c$ and dispersion β. The value of $\hat{S}_a^c$ corresponding to the target MAF of collapse for the structure can be evaluated through an iterative procedure, having made an assumption on the value of β. For example, β = 0.8 and 0.6 are used in FEMA P-750 (2009a) and ASCE 7-16 (2017), respectively. These values are quite high because they also account for epistemic uncertainties and the uncertainty in the capacity. The risk-targeted spectral acceleration, to be considered for design purposes, is the value of the spectral acceleration $S_a^{c,X}$ corresponding to a probability of failure X (Figure 4.4).

Under the assumption of a lognormally-distributed capacity curve, the relation between the median capacity $\hat{S}_a^c$ and the risk-targeted spectral acceleration $S_a^{c,X}$ can be expressed as follows (see Kennedy and Short, 1994):

$$S_a^{c,X} = \hat{S}_a^c \cdot \mathrm{e}^{\Phi^{-1}(X)\cdot\beta} \tag{4.11}$$

where $\Phi^{-1}(X)$ is the inverse of the standard normal cumulative distribution function (also called the probit function) for a probability X, such that $\Phi^{-1}(0.5) = 0$ and $\Phi^{-1}(0.1) = -1.2816$.

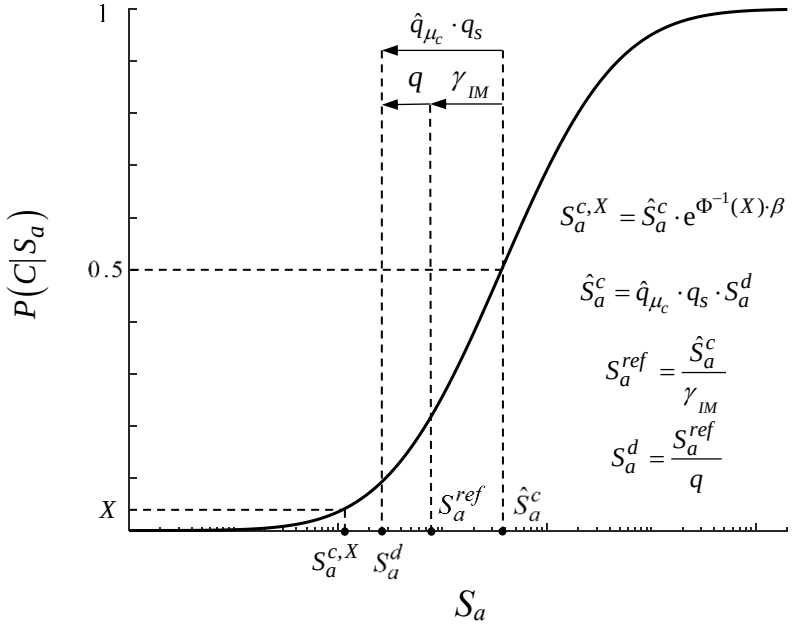

Figure 4.4 Conditional probability of failure and design accelerations obtained with Luco's ($S_a^{c,X}$) and RTBF (S_a^d) approaches

Both Luco et al. (2007) and the aforementioned American regulations prescribe the use of X=0.1 when implementing risk-targeting. This value was based on the results of previous studies where different structural systems were analysed (NIST 2012; FEMA 2009b; NIST 2010; Kircher et al. 2014). However, this assumption was questioned by some studies. For example, the review of Chapter 1 presents a summary of the literature suggesting lower values of X (between $10^{-5} \sim 10^{-1}$). It is noteworthy that $S_a^{c,X}$ cannot be compared directly with the risk-targeted design acceleration S_a^d introduced in the previous section, since it needs to be reduced further for design purposes. For example, according to the ASCE 7-16 (2017), the risk-targeted acceleration values should be multiplied by 2/3 and then divided by a response modification coefficient, which accounts for the ductility and overstrength of the

system (see ASCE 7-16-C12.1.1, 2017). Application of these coefficients may again result in an uncontrolled level of the risk of failure. This issue is investigated more in detail in Section 4.3.

Analytical solution

Under the assumption of a linear hazard curve in the log-log plane, a closed-form expression of $S_a^{c,X}$ can be obtained. Recalling the definition of γ_{IM} given in Section 4.2.1, $\hat{S}_a^c$ can be expressed as:

$$\hat{S}_a^c = \gamma_{IM} \cdot S_a^{ref} \tag{4.12}$$

After substituting this into Eqn.(4.11), the following expression of $S_a^{c,X}$ is obtained:

$$S_a^{c,X} = \gamma_{IM} \cdot S_a^{ref} \cdot \mathrm{e}^{\Phi^{-1}(X)\cdot\beta} = \left(\frac{k_0}{\lambda_c}\right)^{1/k_1} \cdot e^{0.5\cdot k_1\cdot\beta^2+\Phi^{-1}(X)\cdot\beta} \tag{4.13}$$

Dividing $S_a^{c,X}$ by S_a^{ref}, the following expression for the risk coefficient C_R can be obtained:

$$C_R = \frac{S_a^{c,X}}{S_a^{ref}} = \gamma_{IM} \cdot \mathrm{e}^{\Phi^{-1}(X)\cdot\beta} = \left(\frac{\lambda_{ref}}{\lambda_c}\right)^{1/k_1} \cdot e^{0.5\cdot k_1\cdot\beta^2+\Phi^{-1}(X)\cdot\beta} \tag{4.14}$$

From Eqn.(4.14), it is found that for $X = 0.5$, $C_R = \gamma_{IM}$ and $S_a^{c,X} = \hat{S}_a^c$. In other words, under the assumption of a linear hazard curve in log-log space, Luco's approach can be seen as the first step of the RTBF approach to design: it provides the risk-targeted spectral acceleration $\hat{S}_a^c$ by starting from S_a^{ref} and taking $X = 0.5$.

Eqn.(4.14) can also be rearranged to provide an expression for the MAF of failure:

$$\lambda_c = \lambda_{ref} \cdot e^{0.5\cdot k_1^2\cdot\beta^2+\Phi^{-1}(X)\cdot\beta\cdot k_1-\ln(C_R)\cdot k_1} \tag{4.15}$$

Setting C_R=1 in Eqn.(4.15), which corresponds to assuming $S_a^{c,X} = S_a^{ref}$ and $\lambda_c = \alpha \cdot \lambda_{ref}$ one obtains:

$$\lambda_c = \alpha \cdot H\left(S_a^{c,X}\right) \tag{4.16}$$

where $\alpha = e^{0.5 \cdot k_1^2 \cdot \beta^2 + \Phi^{-1}(X) \cdot \beta \cdot k_1 - \ln(C_R) \cdot k_1}$.

This equation is at the base of the "Simplified Hybrid Method" of Kennedy (1999), providing an estimate of the seismic risk directly from the value of the hazard level of the spectral acceleration corresponding to a failure probability *X*. According to Kennedy (1999), α can always be taken equal to 0.5 for X = 0.1, given its low sensitivity with respect to k_1 and β. Later on, Hirata et al. (2012) provided a similar expression, with the same aim of obtaining a simple risk estimate without recourse to the convolution between the hazard and the conditional probability of failure. According to that study, α ranges between 0.5 and 1, depending on the value of *X* and the desired degree of conservativeness.

Similarly to Kennedy (1999) and Hirata et al. (2012), it is possible to find the value of *X* such that α=1, i.e., $\lambda_c = H\left(S_a^{c,X}\right)$. This value of *X* corresponds to:

$$X = \Phi(-0.5 \cdot k_1 \cdot \beta) \tag{4.17}$$

where $\Phi(\cdot)$ is the standard normal cumulative distribution function.

4.2.3 Inelastic GMPEs approach

In engineering seismology, research efforts often focus on estimating the ground motion at the site of interest, often defined in terms of IMs, resulting from a future earthquake. Usually this is achieved by application of GMPEs. GMPEs provide, via a relatively simple closed-form function, the distribution of an IM given the magnitude, the source-to-site distance and other parameters such as the local site conditions and the faulting mechanism. IMs are generally assumed to be lognormally distributed given magnitude, distance and the other independent parameters of the GMPEs.

Therefore, a GMPE provides an estimate of the median IM and its standard deviation, which is often roughly 0.7 in terms of natural logarithms for response spectral IMs [see e.g. Figure 10 of Gregor et al. (2014) for elastic spectral accelerations and Figure 11 of Bozorgnia et al. (2010a) for inelastic spectral accelerations].

PSHA provides the MAF of exceeding different levels of a given IM by combining models of the probability of different earthquake scenarios (defined in terms of magnitude, geographical location and other source parameters, e.g. faulting mechanism) with GMPEs providing estimates of the probabilities of different levels of the IM at the considered site given these scenarios (e.g. McGuire 2008; Baker 2015). The probabilities of different earthquake scenarios are often estimated using Gutenberg-Richter power laws expressing the annual chances of different size earthquakes (i.e. $\ln N = a - b \cdot M$, where N is the number of earthquakes of magnitude M or larger per year and a and b are empirical coefficients derived from analysis of the seismicity of the region surrounding the site) coupled with polygonal area sources where the chance of an earthquake occurring anywhere within the polygon is uniform.

Many hundreds of GMPEs are available in the literature (Douglas 2019), but most of them predict *PGA* or $S_a(T, \xi)$. In contrast, Sewell (1989), Bozorgnia et al. (2010a), Rupakhety and Sigbjörnsson (2009) and De Luca et al. (2011), for example, have developed GMPEs for the capacity demand of SDOFs systems with elastic-perfectly plastic behaviour and constant ductility, using the same functional form as for the elastic demand in terms of $S_a(T, \xi)$. These GMPEs depend on the actual yield strength of the SDOF systems and hence are more structure-specific than GMPEs for *PGA* or $S_a(T, \xi)$. PSHA can be conducted for a given site using these GMPEs, as in Bozorgnia et al. (2010b), to obtain uniform-risk spectra directly.

4.3 Investigation of the assumptions in the various approaches

Each of the methods presented in the former paragraphs is based on different assumptions, which affect to some extent the estimates of the seismic risk of structural systems. In this section, the effect of the hazard curve linearization, which is at the base of the RTBF approach, is investigated first, by considering two example sites. Subsequently, one of these sites is considered to calculate uniform-risk design spectral

accelerations for SDOF systems with elastic-perfectly plastic behaviour via the inelastic GMPEs approach. The obtained results are compared to those obtained via the RTBF approach, in order to evaluate the accuracy of the latter. Subsequently, the problem of the choice of X when applying Luco's risk targeting approach is investigated, together with the consequences of the choice of X on the value of the response modification factor to be employed for the simplified design. Finally, risk-targeted design maps for Europe are developed using the analytical RTBF approach.

4.3.1 Effect of hazard curve linearization

Even though higher-order models have been proposed in the literature for approximating the hazard curve (Bradley et al. 2007; Vamvatsikos 2013), the power law model (Sewell et al. 1991) is still widely employed because of its simplicity. Several methods have been proposed for fitting this model to a hazard curve. For example, in Jalayer and Cornell (2003) it is suggested to fit the curve through seismic hazard estimates at the American codes' Design Basis Earthquake (DBE) and Maximum Considered Earthquake (MCE) intensity levels, with 10% and 2% probabilities of exceedance in 50 years, respectively. Cornell (1996) suggests fitting between two points: one equal to the targeted MAF and one with a MAF ten times higher.

This subsection investigates the impact of the linearization of the hazard curve of Rhodes (Figure 4.5a) and of Lourdes (France) (Figure 4.5b) on seismic risk estimates. The hazard curve of Rhodes refers to the spectral acceleration S_a (1s, 5%) (further information regarding its derivation is given in the next subsection), whereas the hazard curve of Lourdes is for the *PGA* (more details about its derivation are given in Douglas et al., 2013).

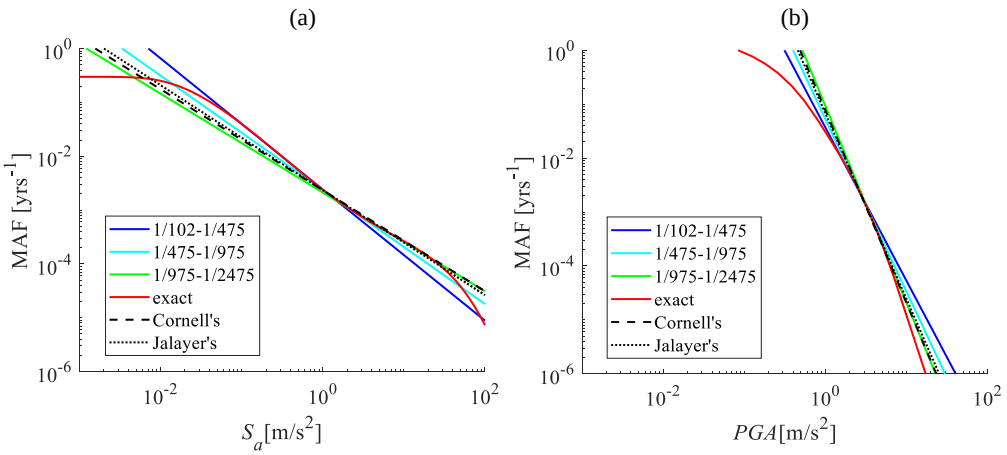

Figure 4.5 Hazard curve for: (a) Rhodes and (b) Lourdes, together with alternative fitting approaches

Risk targeting is carried out using the exact hazard curve (see e.g. Figure 2.1 of Chapter 2) for λ_c =2·10^{-4} yrs^{-1} and assuming different values of X: 10^{-5} according to Douglas et al. (2013), 0.1 according to the American codes (ASCE 7-16, 2017), and 0.5 following the discussion of Section 4.2.2. Figure 4.6 illustrates the resulting risk-targeted spectral acceleration values corresponding to different values of β. In the same figure, the acceleration values obtained by using Eqn.(4.13) and the linearized hazard curves fitted with different criteria are illustrated and compared. In particular, following Jalayer's (Jalayer and Cornell 2003) and Cornell's (Cornell 1996) approaches, the fitting is carried out between the MAF levels 1/475 – 1/2475 and 1/475 – 1/4975, respectively.

It is observed that Cornell's linearization approach provides in general the best approximation for the different cases considered, with a solution very close to that obtained without making any assumption on the hazard curve shape. Other values of X (in the range between 10^{-5} to 0.1) and λ_c (2·10^{-3} and 2·10^{-5}) have also been investigated for various sites across Europe using the 2013 European seismic hazard model (ESHM) (Giardini et al. 2013; Woessner et al. 2015), showing similarly good results when using Cornell's recommendation for the fitting. It is worth noting that depending on the hazard curve shape, there are cases were the linearized curve is above the exact and others where it is below. In general, if the part that contributes more in the convolution is above the exact one, the MAF is overestimated.

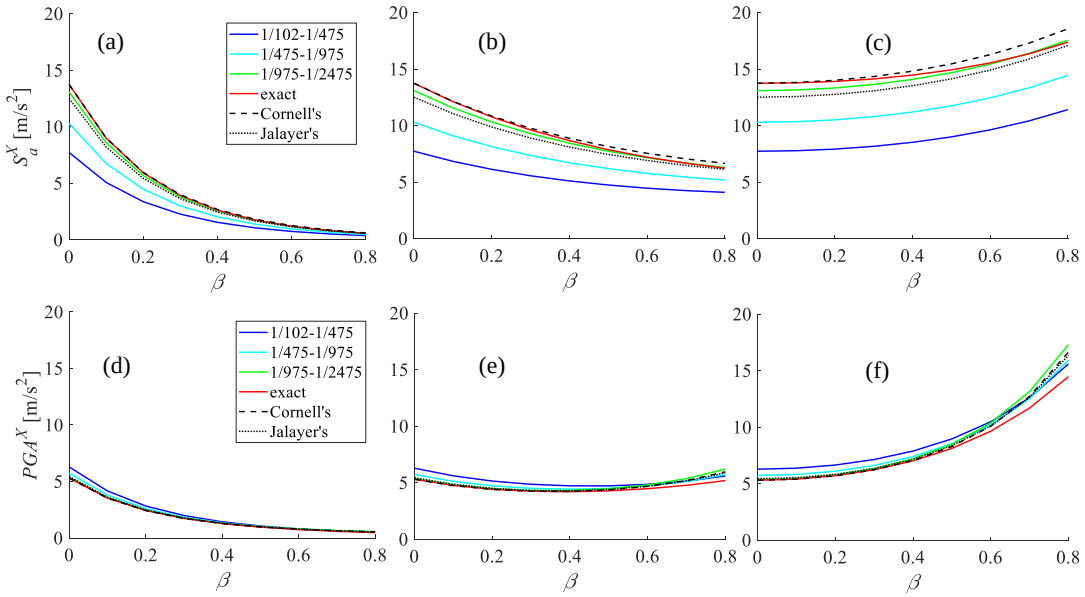

Figure 4.6 Variation of risk-targeted acceleration values with β for Rhodes (a, b, c) and Lourdes (d, e, f), for λ_c =2·10^{-4} yrs^{-1} and assuming X: 10^{-5} (a and d), 0.1 (b and e) and 0.5 (c and f). Comparison between the values obtained from convolution of the exact hazard curve and with analytical solution based on different fitting approaches

It is also interesting to observe in Figure 4.6 that the risk-targeted accelerations exhibit very different trends of variation with β. These can be better understood by looking at Eqn.(4.13) and noting that the argument of the exponent consists of two terms: a first order term in β, which is negative for cases of x lower than 0.5, and zero for X = 0.5, and a second order term in β, which can affect the concavity of the curve. When the second term is zero (i.e. for X= 0.5, Figure 4.6c and Figure 4.6f), the curve's sensitivity to β increases with k_1. Therefore, this sensitivity is higher for the case of Lourdes because it has a steeper hazard curve (higher k_1), compared to Rhodes.

4.3.2 Validation of the RTBF approach through comparison with the inelastic GMPEs approach

In this section, the RTBF and the inelastic GMPEs approaches are compared using PSHA results for the Greek island of Rhodes as an example. In order to make the comparison, a deterministic SDOF system with vibration period T and ductility capacity μ_c is considered. Other structural systems cannot be considered since inelastic GMPEs have been developed only for SDOF models.

Application of the inelastic GMPEs approach

The seismic source model (geometries of the source zones, activity rates and maximum magnitudes) for the calculations presented in this section was provided in November 2011 by Dr Laurentiu Danciu (ETH, Zurich, Switzerland). This model was an extract, at that date, of the ESHM (Giardini et al. 2013; Woessner et al., 2015) developed for the wider Europe region. The seismic source model used for the definitive calculations of ESHM is likely slightly different from the one used here but these minor changes will not affect the conclusions of this study. The model consists of the nine source zones closest to the Greek island of Rhodes (36.445°N-28.225°E), an area of active shallow crustal seismicity close to a subduction zone (Hellenic Arc). The seismicity of this region is roughly typical of areas of moderate to high seismic hazard in Europe and hence it is used as an example here.

In order to apply risk-targeting with the inelastic GMPEs approach, the selected seismic source model is coupled with the GMPEs of Rupakhety and Sigbjörnsson (2009). These GMPEs are chosen because: they were derived for Europe and the Middle East (and hence are consistent with our seismic source model), they have a simple functional form (which is computationally convenient), and, finally, the data used to derive these GMPEs are freely available and can be used also for computing the uniform-hazard elastic spectrum which is used as input for the RTBF approach (see the following subsection). The GMPEs of Rupakhety and Sigbjörnsson (2009) are for structural periods between 0 (equivalent to *PGA*) and 2.5s, and for ductility levels of 1 (elastic), 1.5, 2 and 4. The software CRISIS 2015 (Ordaz et al. 2015) is used for the PSHA. For comparison purposes, the results are presented together with the results of the RTBF approach.

Application of the RTBF approach

The application of the RTBF approach for risk targeting requires performing a series of time-history analyses under a set of records representative of the most likely seismic scenarios. A disaggregation of the seismic hazard for a ductility level of 1, carried out for the MAFs of interest, shows that the hazard is dominated by moderate earthquakes (moment magnitudes between 5.0 and 6.5) close to Rhodes (source-to-site distances

less than 15km), which is common in areas of high seismicity. For consistency with the results of the disaggregation and the strong-motion data used by Rupakhety and Sigbjörnsson (2009) to derive their GMPEs, the database of Ambraseys et al. (2004) is used to select 25 strong-motion records (Appendix A) from earthquakes with $5.0 \leq M_w \leq 6.5$ and $R_{JB} \leq 15$km from Europe and the Middle East.

The software OpenSees (McKenna et al. 2006) is employed to run time-history analyses of inelastic SDOF systems with different properties in terms of period T and deterministic ductility capacity μ_c, using the selected records. In particular, 21 different values of T in the range between 0.01s and 2s, and values of μ_c equal to 1, 2, 4 and 6 are considered. For each combination of these parameters, 25 analyses (one for each of the strong-motion records) are performed, leading to a total of 2,100 time-history analyses. The median $\hat{q}_{\mu_c}$ and lognormal standard deviation $\beta = \beta_{q_{\mu_c}}$ are evaluated for each value of T and μ_c, and the results are illustrated in Figure 4.7. As expected, $\hat{q}_{\mu_c}$ is equal to 1 for very stiff systems and then increases and approaches the ductility capacity of the system for long periods (T>1s), for which the equal displacement rule holds. The dispersion β is equal to zero for T=0s, it increases and attains a maximum for periods in the range between 0.25s and 0.5s and then it decreases for higher values of T.

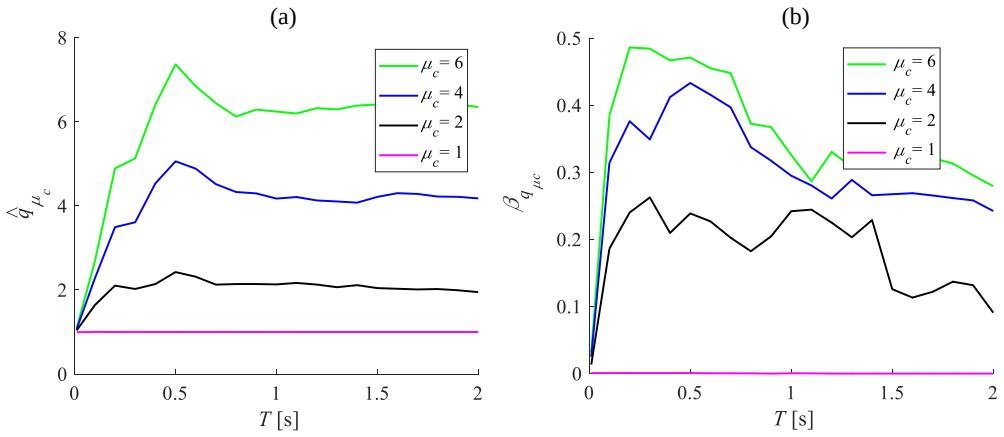

Figure 4.7 Results of the case study: (a) Median value $\hat{q}_{\mu_c}$ and (b) lognormal standard deviation $\beta_{q_{\mu_c}}$

FEMA P695 (2009b) provides a good introduction to different sources of uncertainty in the assessment of structural capacity, namely those of the ground motion records ($\beta_{RTR}=0.20 \sim 0.40$), those of the design requirements ($\beta_{DR}=0.10 \sim 0.50$), those inherent to the test data ($\beta_{TD}=0.10 \sim 0.50$) and to the modelling issues ($\beta_{MDL}=0.10 \sim 0.50$). The square root of the sum of the squares results in a global dispersion in the range 0.275 ~ 0.950. In our example, only the uncertainty due to record-to-record variability is considered, and the values of $\beta_{q_{\mu_c}}$, within the range 0 ~ 0.50 (Figure 4.7), are similar to those suggested by FEMA P695 (2009b) for β_{RTR}.

Figure 4.8 illustrates in log-log space the hazard curve of Rhodes for a system with natural period T=1s and 5% damping ratio, evaluated via PSHA, and the linearized approximation, which is fitted through the points corresponding to a MAF of exceedance of 1/250 and 1/2500. Using Eqn.(4.7) and the results of the time-history analyses, the risk curves $\lambda_c\left(S_a^d\right)$ can be built for different target ductility levels through the RTBF approach. For the purpose of comparison, the overstrength q_s is assumed equal to 1. As explained in Section 4.2.1, the risk curves for the different target ductility levels are parallel.

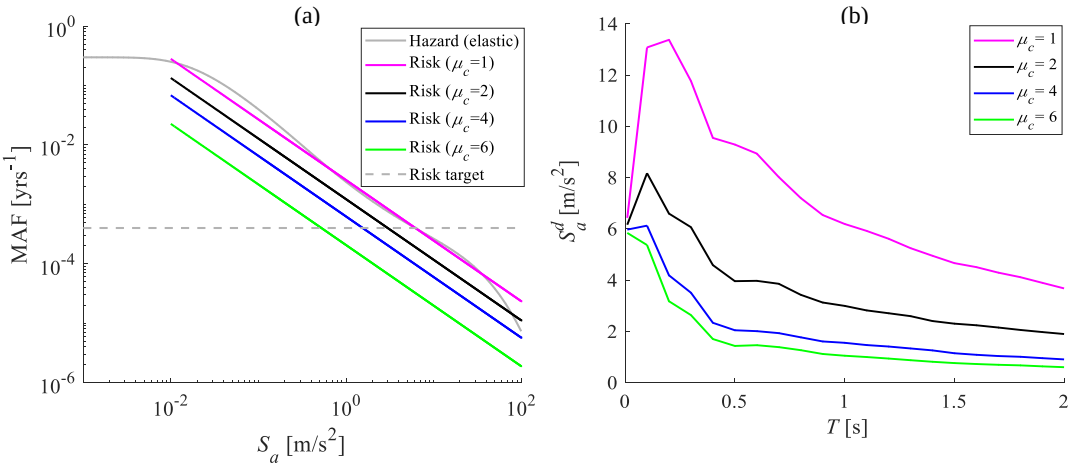

Figure 4.8 (a) Calculation of the risk curve for T=1s, q_s=1 and for various target ductility levels, using the RTBF approach, (b) corresponding design spectra

The curves in Figure 4.8a refer to a system with period T=1s. The same procedure can be repeated for systems with different vibration periods T to generate the design

spectra of Figure 4.8b for a target λ_c=1/2500 yrs^{-1}. Obviously, by increasing the ductility capacity, the design spectral acceleration reduces. Moreover, for high values of μ_c the risk-targeted spectrum does not exhibit a peak unlike for low μ_c values. The reduction is also much higher by passing from μ_c=1 to μ_c =2, than from μ_c=4 to μ_c =6.

Figure 4.9 compares the risk curves for two systems with periods T=0.4s and T=1s and ductility capacity μ_c=4, evaluated according to the RTBF and the inelastic GMPEs approaches. RTBF approach provides a very good approximation of the risk curve in the range of MAF of interest. It is also worth observing that the risk curve according to the inelastic GMPEs approach is almost parallel to the hazard curve, at least in the range of MAFs of interest. The discrepancy on the results of the two methods is due to the assumptions inherent to the RTBF approach, namely the linearity of the hazard curve and the lognormality of distribution of S_a.

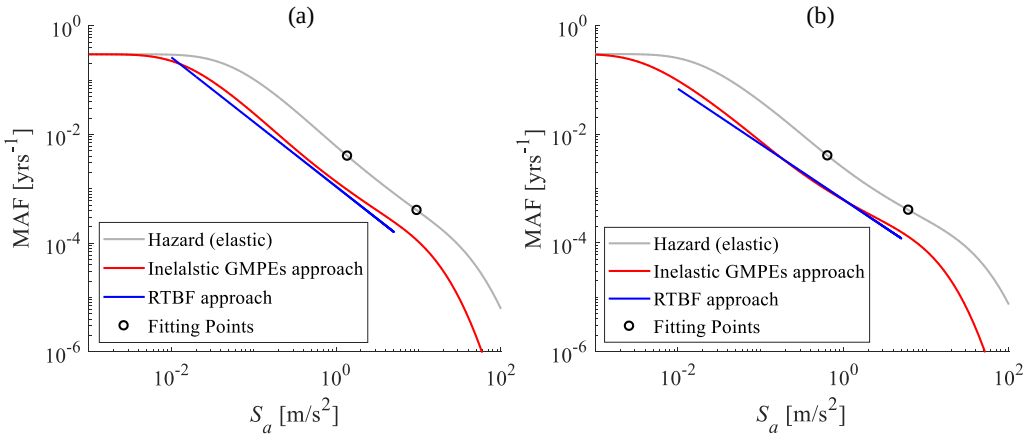

Figure 4.9 Comparison between the risk curves according to the RTBF and inelastic GMPEs approaches for μ_c= 4 and: (a) T=0.4s and (b) T=1s

To further demonstrate the accuracy of the RTBF method, in Figure 4.10 the uniform risk spectra according to the two approaches are compared. These spectra are generated by considering three different levels of the MAF of collapse, namely 1/250, 1/1000, and 1/2500, and two different levels of the ductility capacity (μ_c=2 and μ_c=4). It can be observed that the RTBF approach provides estimates of the risk-targeted spectral accelerations that are quite close to the estimates of the inelastic GMPEs

approach. The agreement between the two approaches is better for high values of the target MAF of exceedance.

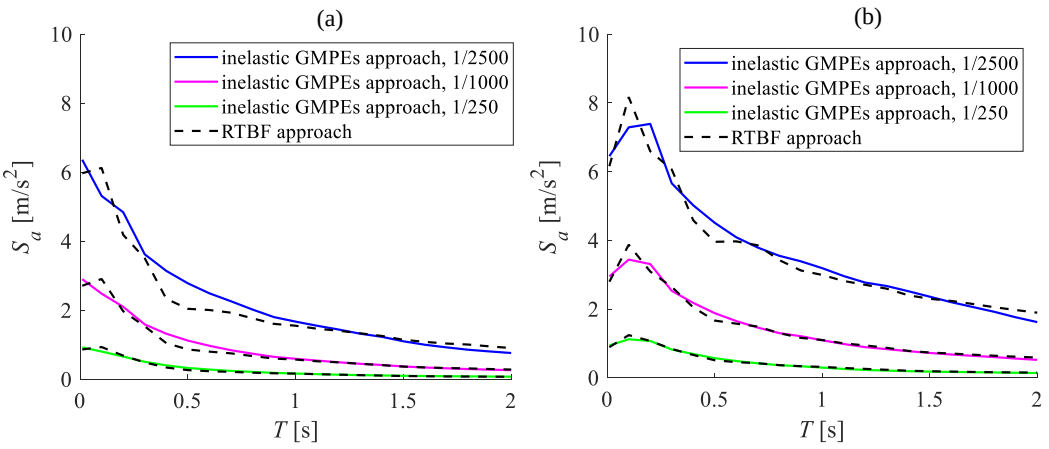

Figure 4.10 Comparison between uniform risk spectra according to the RTBF approach and to the inelastic GMPEs approach for: (a) μ_c=4 and (b) μ_c=2

4.3.3 Effect of the assumptions in Luco's approach

As stated before, Luco's approach has been implemented in many design codes, including ASCE 7-16 (2017). In this section, a study is performed to evaluate under which conditions the method can ensure a uniform-risk design. In particular, the choice of the value of X to be used for risk-targeting is examined, together with the implications of this choice on the values of the response modification factor to be employed when a simplified analysis/design procedure is implemented.

Which value of X?

As mentioned in Section 4.2.2, many researchers have tried to investigate the value of X to be used when applying Luco's approach for risk targeting in practice. For example, Kennedy and Short (1994) performed a sensitivity analysis for values of k_1 between 1.66 and 3.32 and found that the variation of the risk-targeted acceleration with β is minimized when X =0.1. This can also be observed in Figure 4.6 of Section 4.3.1, showing reduced variations of the risk-targeted acceleration with β varying from 0.5 to 0.8 when X=0.1 (Figure 4.6b,e), and higher variations when X=10^{-5} (Figure 4.6a,d) and X=0.5 (Figure 4.6c,f). It is noteworthy that this value of X also ensures

reduced deviations of the risk-targeted IM levels from the IM levels corresponding to T_R= 2475 yrs (λ_{ref} = 4·10^{-4} yrs^{-1}) which were employed for hazard maps in previous versions of the United States codes. In fact, assuming X= 0.1 and β = 0.6, and substituting the target risk level λ_c=2·10^{-4} yrs^{-1} set by the ASCE 7-16 (2017), and λ_{ref} =4·10^{-4} yrs^{-1} in Eqn.(4.14), the value of C_R is then close to unit for k_1 varying between 1 and 4. In other words, when using the value of 0.1, the risk-targeted acceleration values do not deviate significantly from the reference ones obtained via hazard analysis.

Figure 4.11 plots the values of λ_{ref} / λ_c against X obtained by solving Eqn.(4.15) for different values of k_1, C_R = 1 and β = 0.6. As already discussed, when targeting λ_{ref} / λ_c close to 2, then X is in the order of 0.1, irrespective of the slope of the hazard curve.

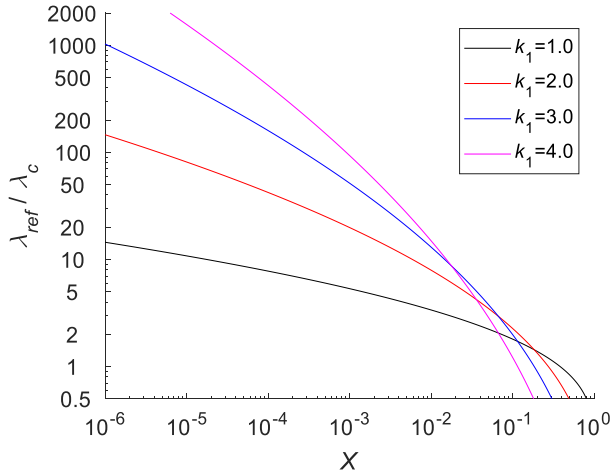

Figure 4.11 Variation of λ_{ref} / λ_c with X for different values for the hazard curve slope

In order to display the combined effects of β and k_1 on risk targeting, a nomogram can be drawn. Nomograms (e.g. Levens 1959) used to play the role of an analogue computer for complex equations, which is not a necessity nowadays; however, they can still help to understand visually the sensitivity of the results to the associated variables (Douglas and Danciu 2020).

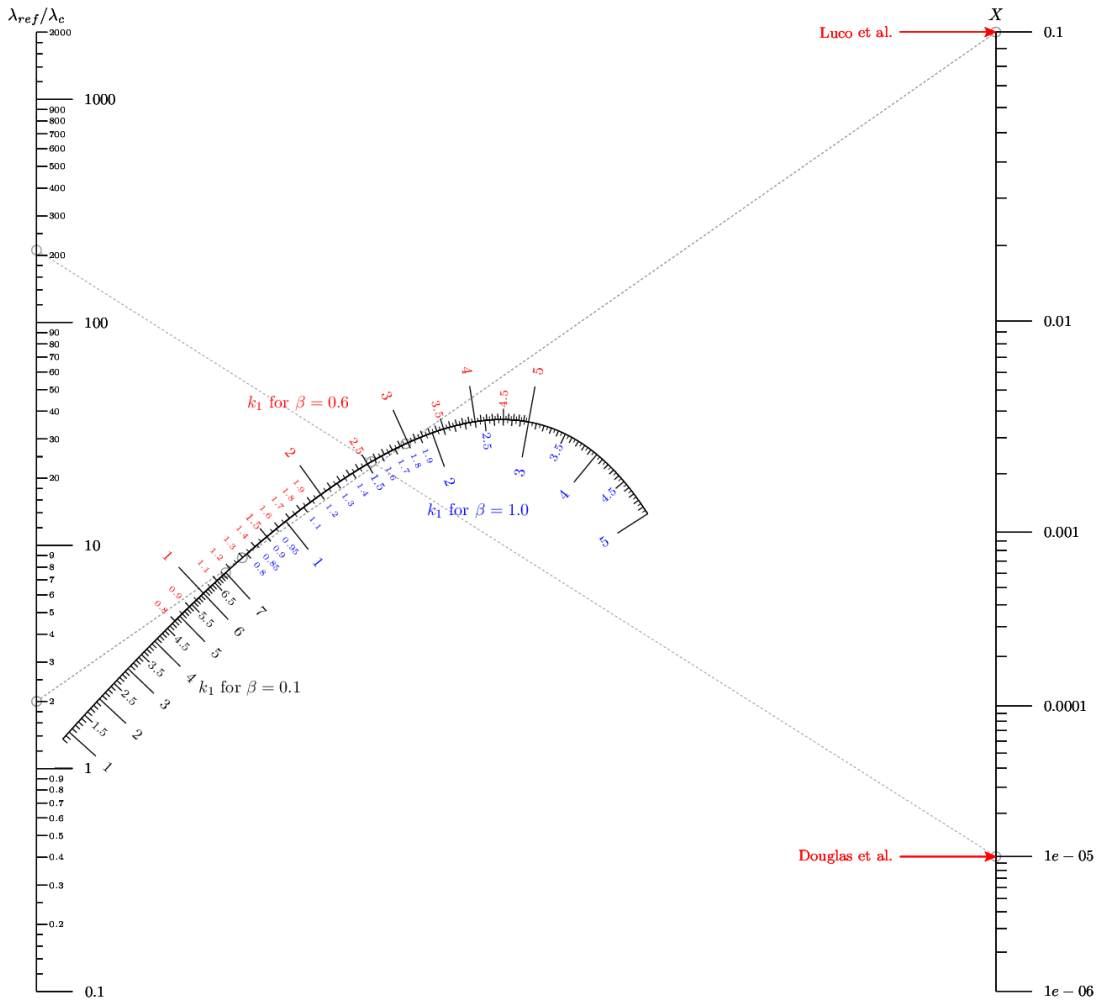

Figure 4.12 Nomogram showing the sensitivity of the ratio $\lambda_{ref} / \lambda_c$ to the values of X, β and k_1. The isopleths show two example calculations using this graph by connecting with straight lines choices of $\lambda_{ref} / \lambda_c$ and X and reading off the value of k_1

The nomogram shown in Figure 4.12 is built by setting $C_R = 1$ in Eqn.(4.14) and repeatedly solving for X, using different values of β and k_1. In the nomogram, the choices of Douglas et al. (2013) for France are compared to the ones of Luco et al. (2007). The line passing through $\lambda_{ref} / \lambda_c = 2$ and X=0.1 is almost parallel to the portion of the nomogram curve corresponding to β=0.6, confirming that the sensitivity of X to k_1 in this case is low. This is not the case for the values of Douglas et al. (2013), with the results changing significantly by varying k_1 and β. Moreover, the X values of Douglas et al. (2013) are very low. This is the consequence of the choice of targeting $\lambda_c = 10^{-5}$ yrs^{-1} (value of the MAF of collapse consistent with Eurocode 0, CEN 2002)

with λ_{ref} =2.1·10^{-3} yrs^{-1}. Overall, considering that the exact value of β is not known with precision, it would be preferable to choose low ratios of λ_{ref} / λ_c, in the range between 1 to 5. Thus, if very low values of λ_c need to be achieved, reference intensity levels higher than the ones currently suggested in the European codes would need to be considered, corresponding to MAF of exceedance λ_{ref} lower than 2.1·10^{-3} yrs^{-1} (Jack Baker, written communication, 2018).

Nevertheless, it should be noted here that ductility and overstrength factors are not considered in the development of risk-targeted acceleration maps of the United States. Thus, it is in design calculations that the risk-targeted acceleration is translated to a seismic load if some sort of simplified analysis is performed. For example, ASCE prescribes to multiply $S_a^{c,X}$ by 2/3 (ASCE 7-16-21.3, 2017) and then divide it by the response modification coefficient *R* (ASCE 7-16-C12.1.1, 2017). The risk levels achieved through this approach are investigated in the following paragraph, by considering the linearized hazard curve of Rhodes.

Effect of the choice of X on the response modification factors

This subsection aims to evaluate the risk of failure that is obtained if the simplified approach of ASCE 7-16 (2017), based on the use of response modification factors, is applied together with risk targeting for structural design. For this purpose, the case of a simplified SDOF system with *T*=1s and the hazard curve of Rhodes for S_a (1s, 5%) linearized according to Cornell's recommendations (Figure 4.5) are considered.

To define the design spectral acceleration of the system, $S_a^{c,X}$ must be evaluated first via Eqn.(4.13). The design spectral acceleration for the SDOF system under consideration is then set equal to $S_a^d = \frac{S_a^{c,X}}{R} \cdot \frac{2}{3}$, where *R* is the code's reduction factor (response modification coefficient). In general, the proposed values of *R* given by the code will differ from $\hat{q}_{\mu_c} \cdot q_s$. The corresponding MAF of failure of the system $\lambda_{c,calc}$ can be evaluated based on the median failure capacity $S_a^d \cdot \hat{q}_{\mu_c} \cdot q_s$. It can be shown that:

$$\lambda_{c,\text{calc}} = \lambda_{c,\text{target}} \cdot \left(\frac{\hat{q}_{\mu_c} \cdot q_s}{q^*} \right)^{-k_1} \cdot e^{-\Phi^{-1}(X) \cdot k_1 \cdot \beta} \tag{4.18}$$

where $q^* = \frac{3}{2} \cdot R$ is the factor by which $S_a^{c,X}$ is multiplied according to ASCE 7-16 (2017).

Figure 4.13 shows the variation of the ratio between the calculated and the targeted MAF of failure, for different values of q^* and different values of β. It can be observed that the calculated risk is very different from the targeted one, even when the actual value of the reduction factor $\hat{q}_{\mu_c} \cdot q_s$ is employed.

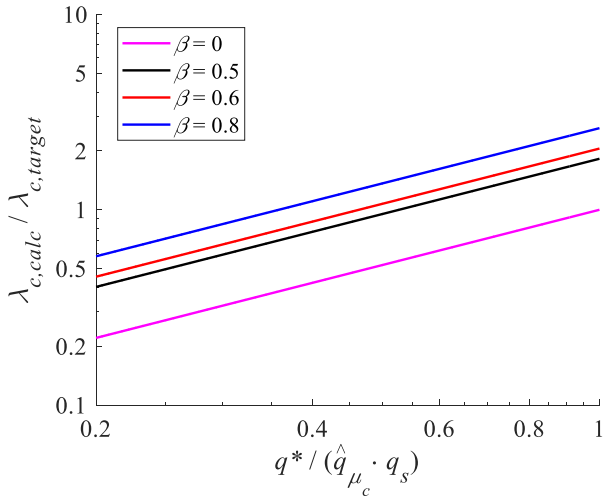

Figure 4.13 Variation between the calculated and the targeted MAF of failure for the case of Rhodes, for different values of $q^*/(\hat{q}_{\mu_c} \cdot q_s)$ and β

These results show that the application of the code may lead to non-consistent levels of the risk, which change for different locations and are sensitive to the choice of the reduction factor *R* and β. Again, this confirms that the development of risk-targeted maps must also involve a revision of the reduction factors to be employed for design if a simplified analysis or design approach using the reduction factors is to be employed in conjunction with risk-targeted hazard maps.

It is noteworthy that Kircher et al. (2014) have already acknowledged this issue. To clarify it, for risk targeting to be effective one must have $\lambda_{c,\text{calc}} = \lambda_{c,\text{target}}$. Based on Eqn.(4.18), this is only possible if:

$$q^* = \hat{q}_{\mu_c} \cdot q_s \cdot e^{\Phi^{-1}(X)\cdot\beta} \tag{4.19}$$

Figure 4.14 provides the relation between the value of X assumed in risk targeting, and the corresponding value of the reduction factor to be considered in order to achieve the targeted MAF of failure. As expected, if X=0.5, then the SDOF system should be designed with a reduction factor $q^* = \hat{q}_{\mu_c} \cdot q_s$. This is equivalent to carrying out the design according to the procedure outlined in Section 4.2.1. If X=0.1 and β = 0.6, as suggested in the American codes, then the reduction factor should be $q^* = 0.46 \cdot \hat{q}_{\mu_c} \cdot q_s$.

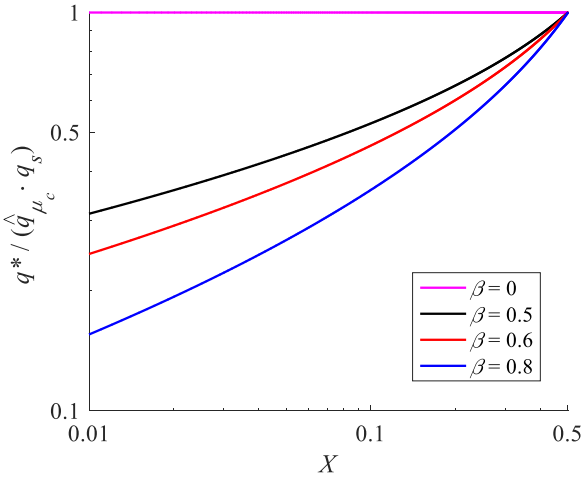

Figure 4.14 Variation of $q^*/(\hat{q}_{\mu_c} \cdot q_s)$ based on the assumptions made in the risk-targeting framework for X and β

It is noteworthy that the values of the behaviour factors suggested in current design codes are usually lower than the actual values of $\hat{q}_{\mu_c} \cdot q_s$, due to extra requirements and safety factors that usually serve to increase the strength and, therefore, reduce further the probability of collapse. For example, Žižmond and Dolšek (2013) designed an 11-storey and an 8-storey structure by gradually applying different criteria of compliance with the Eurocodes and reporting how each safety measure affects the final design. Assuming q^*=3.9, they found $q^*/(\hat{q}_{\mu_c} \cdot q_s)$ to range between 0.4 and 1, depending on the code requirements and factors of safety taken into account.

4.4 Risk-targeted maps for Europe

This section employs the analytical equations of the RTBF method to show some example risk-targeted maps for Europe. The target risk level is set equal to $2 \cdot 10^{-4}$ yrs^{-1}, a value proposed in ASCE 7-16 (2017), roughly corresponding to a 1% probability of exceedance in 50 years. The power law hazard model is fitted through two points (in accordance with the suggestions of paragraph 3.1): one corresponding to a MAF of exceedance equal to the target risk level, and one to a MAF of exceedance ten times higher, i.e., $2 \cdot 10^{-3}$ yrs^{-1} (roughly corresponding to a 10% probability of exceedance in 50 years). These points (acceleration versus probability of exceedance) are obtained for every location from the 2013 ESHM (Giardini et al. 2013; Woessner et al., 2015) project, which freely provides hazard information across Europe (see http://www.efehr.org/en/hazard-data-access/Intro/).

Figure 4.15a, Figure 4.16a and Figure 4.17a show the values of PGA^{ref} and $S_a^{ref}(T)$ according to PSHA (obtained from the 2013 ESHM project) and a reference return period of 475 years, whereas the values of k_1 corresponding to the slope of the fitted curve (between the two defined points) are plotted in Figure 4.15b, Figure 4.16b and Figure 4.17b. A high variation of the slope of the hazard curve is observed for different locations, even within the same country. There are cases were the curve is quite steep with $k_1 > 3$, whilst other locations have hazard curves with very low slopes, for instance 0.7.

Figure 4.15c, Figure 4.16c and Figure 4.17c show the risk-targeted values of the design acceleration, evaluated via Eqn.(4.10). For the case of the *PGA*, $\beta = 0$ and $\hat{q}_{\mu_c} = 1$, whereas for $S_a(T=0.5\text{s})$ and $S_a(T=1\text{s})$, $\hat{q}_{\mu_c}$ is assumed equal to 4 and $\beta = 0.6$, as per ASCE 7-16 (2017). In all cases the contribution of overstrength was considered as well, by assuming $q_S = 2$.

The values of the risk-targeted behaviour factor are given in the remaining figures. It is recalled that the factor q is the ratio of the reference design acceleration (MAF of exceedance of $2 \cdot 10^{-3}$ yrs^{-1}) and the risk-targeted design acceleration. A value higher

than one means that the reference design acceleration should be decreased in order to satisfy the risk acceptance criteria.

In general, very low values of q are obtained. However, it should be pointed out that this result is significantly affected by the assumed risk target, ($\lambda_c = 2 \cdot 10^{-4}$ yrs^{-1}), leading to values of γ_{IM} generally higher than 4 that tend to balance out the effect of $\hat{q}_{\mu_c} \cdot q_s$, which would yield design accelerations lower than the reference one. Of course, this conclusion is sensitive to the assumptions made for the ductility and overstrength of the system. A significant variation of the factor q in areas of low seismicity is noticed, but in any case the values of the accelerations remain low. This is discussed also by Silva et al. (2016), who considered only areas with acceleration values higher than 0.05g.

Focusing on the areas of high seismicity, for instance Italy, Greece, Romania and Turkey, for the case of $S_a(T = 0.5s)$, q is in the range between 1.31 to 2.16 and a similar range is noticed for T=1s, as well. For the case of the *PGA* though, the factor q is lower than one at all locations. This means that the reference *PGA* should be increased rather than decreased to achieve the target risk level.

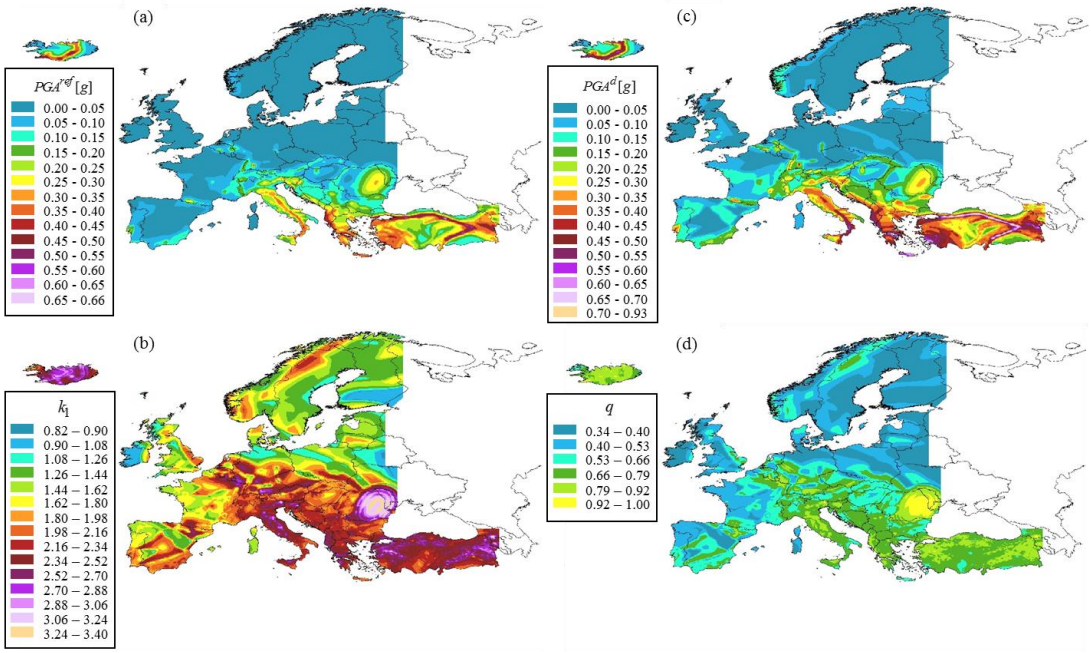

Figure 4.15 Seismic design maps for Europe in terms of *PGA*: (a) *PGA* at reference return period (475 years), (b) k_1 for the power-law approximation, (c) risk-targeted design *PGA* and (d) risk-targeted behaviour factor

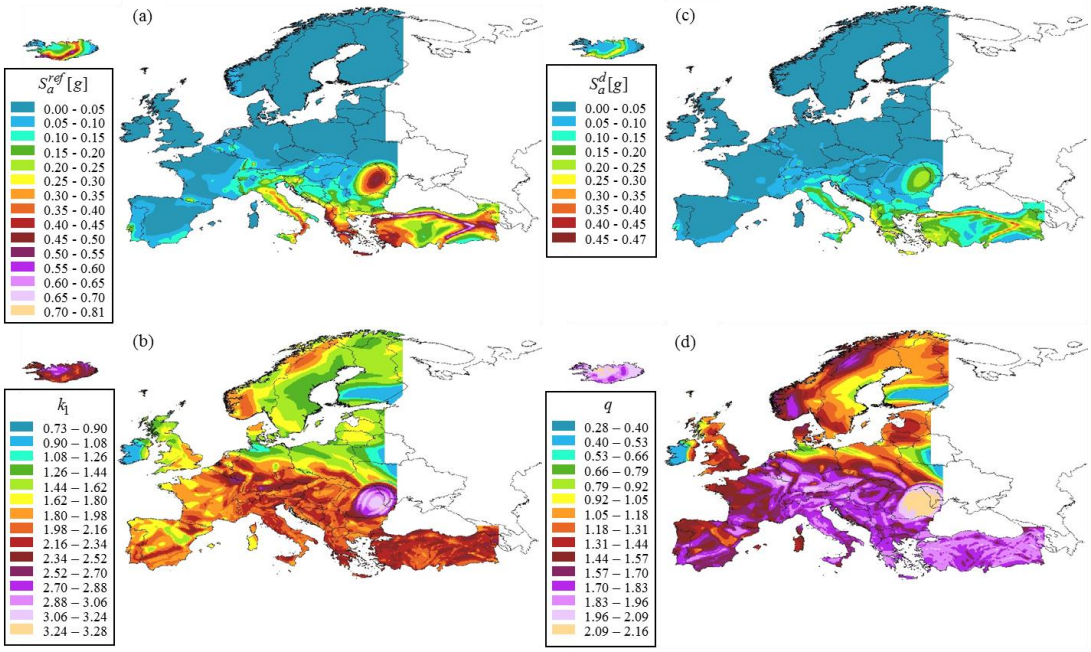

Figure 4.16 Seismic design maps for Europe in terms of S_a (T=0.5s): (a) Spectral acceleration for T=0.5s at reference return period (475 years), (b) k_1 for the power-law approximation, (c) risk-targeted design acceleration and (d) risk-targeted behaviour factor

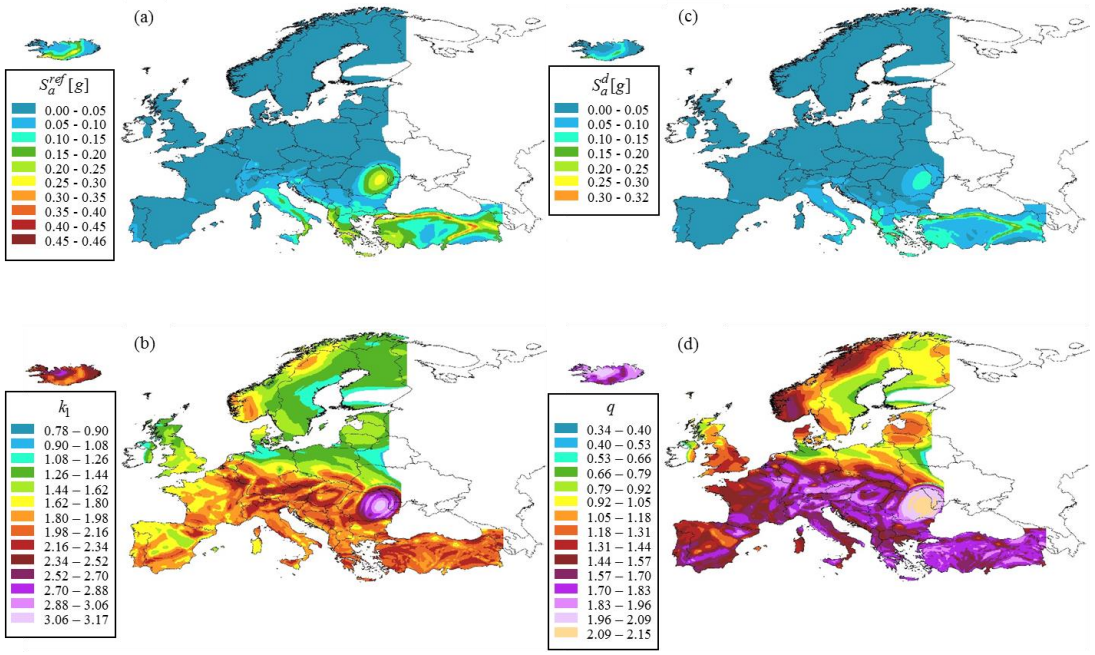

Figure 4.17 Seismic design maps for Europe in terms of S_a (T=1s): (a) Spectral acceleration for T=1s at reference return period (475 years), (b) k_1 for the power-law approximation, (c) risk-targeted design spectral acceleration and (d) risk-targeted behaviour factor

The above procedure is repeated using hazard data from a different study for Italy and the results are provided in Appendix B of the thesis.

4.5 Conclusions

The basic philosophy of current seismic design codes relies on the concept of 'uniform hazard spectrum'. This leads to structures exposed to inconsistent levels of risk, even when they are designed according to the same regulation. Acknowledging this, research efforts have proposed alternative design approaches aiming at controlling the risk of failure of structures. It can, however, be quite hard to follow the literature, due to inconsistent nomenclature amongst researchers and no single resource comparing the different approaches. The main goal of this chapter is to present using a consistent terminology and compare three widespread approaches for risk-targeting, highlighting the assumptions they are based on and their effect on the risk-targeting results. To the author's knowledge, this is the first time that approaches employed in different fields (structural engineering and engineering seismology) and different countries (US and those covered by Eurocode 8) are compared.

The probabilistic framework developed by Kennedy and Short (1994) and Cornell (1996), leading to the definition of risk-targeted behaviour factors (RTBFs), is discussed first, followed by Luco's approach, which is implemented in recent American design codes, and by the inelastic GMPEs approach, based on the use of ground motion prediction equations (GMPEs) for inelastic single-degree-of-freedom systems. It is shown that one of the main assumptions at the base of the RTBF approach, concerning the linearization of the hazard curve, does not significantly affect the accuracy of the risk-targeting results in most cases, if the fitting is carried out for mean annual frequencies of exceedance equal to the targeted level and ten times higher than this level. The inelastic GMPEs approach is innovatively used to validate the RTBFs approach, considering the case of a single-degree-of-freedom system. For the case study considered, it is shown that the RTBF approach provides accurate risk-targeted design results, if compared to the results obtained with the inelastic GMPEs approach. Luco's risk-targeting approach, if coupled with the response modification factors proposed in design codes, could lead to inconsistent risk levels for different

system properties. This is because these response modification factors of design codes (e.g. ASCE 7-16, 2017) are generally not based on probabilistic analyses. Thus, a revision of the reduction factors to be used for design purposes should be carried out, if a simplified analysis or design approach using reduction factors is to be employed in conjunction with risk-targeted hazard maps.

In the last part of the chapter, it is shown how seismic design spectra of Europe may change when moving from uniform-hazard to uniform-risk concepts. In the case studies, an overstrength factor equal to 2 is considered. The ductility-dependent component of the behaviour factor for the *PGA* is equal to 1, while for systems with period 0.5s and 1s it is considered equal to 4. It is found that to satisfy the commonly proposed risk-target of mean annual frequency of exceedance of $2 \cdot 10^{-4}$ yrs^{-1}, the design *PGA* should be increased compared to the uniform-hazard value corresponding to a return period T_R of 475 years. On the other hand, the values of the design spectral acceleration can be significantly lower compared to the reference values corresponding to T_R=475 yrs.

Given the importance that force-based seismic design still has in current design codes, it is anticipated that any of the approaches discussed in the paper could be employed to revise current values of behaviour factors based on risk-control criteria, helping to promote the use of probabilistic concepts in design practice.

References

Altieri D, Tubaldi E, De Angelis M, Patelli E, Dall'Asta A (2018) Reliability-based optimal design of nonlinear viscous dampers for the seismic protection of structural systems. Bulletin of Earthquake Engineering, 16(2), 963-982

Ambraseys NN, Douglas J, Sigbjörnsson R, Berge-Thierry C, Suhadolc P, Costa G, Smit PM (2004) Dissemination of European Strong-Motion Data, volume 2. Proceedings of 13th World Conference on Earthquake Engineering, Paper no. 32

ASCE (2017) Minimum Design Loads and Associated Criteria for Buildings and Other Structures, ASCE/SEI 7-16. American Society of Civil Engineers, Reston, VA

Aschheim M (2002) Seismic design based on the yield displacement, Earthquake Spectra, 18(4), 581-600. doi: 10.1193/1.1516754

Baker JW (2015) Introduction to Probabilistic Seismic Hazard Analysis, White Paper Version 2.1, 77 pp

Barbato M, Tubaldi E (2013) A probabilistic performance-based approach for mitigating the seismic pounding risk between adjacent buildings. Earthquake Engineering & Structural Dynamics, 42(8), 1203-1219

Benjamin JR, Cornell CA (1970) Probability, statistics, and decision for civil engineers, McGraw-Hill, New York

Bozorgnia Y Hachem MM, Campbell KW (2010a) Ground Motion Prediction Equation ("Attenuation Relationship") for Inelastic Response Spectra, Earthquake Spectra, 26(1), 1-23, doi: 10.1193/1.3281182

Bozorgnia Y, Hachem MM, Campbell KW (2010b) Deterministic and probabilistic predictions of yield strength and inelastic displacement spectra, Earthquake Spectra, 26(1), 25-40

Bradley BA (2011) Design seismic demands from seismic response analyses: a probability-based approach. Earthquake Spectra, 27(1), 213-224

Bradley BA, Dhakal RP, Cubrinovski M, Mander JB, MacRae GA (2007) Improved seismic hazard model with application to probabilistic seismic demand analysis. Earthquake Engineering & Structural Dynamics, 36(14), 2211-2225

Castaldo P, Amendola G, Palazzo B (2017) Seismic fragility and reliability of structures isolated by friction pendulum devices: seismic reliability-based design (SRBD). Earthquake Engineering & Structural Dynamics, 46(3), 425-446

CEN (2002) EN 1990:2002+A1 Eurocode – Basis of structural design, European Committee for Standardization, Brussels

CEN (2004) EN 1998-1:2004 Eurocode 8: Design of structures for earthquake resistance - Part 1: General rules, seismic actions and rules for buildings, European Committee for Standardization, Brussel

Collins KR, Wen YK, Foutch DA (1996) Dual-level seismic design: a reliability-based methodology. Earthquake Engineering & Structural Dynamics, 25(12), 1433-1467

Cornell CA (1968) Engineering seismic risk analysis. Bulletin of the seismological society of America, 58(5), 1583-1606

Cornell CA (1996) Calculating building seismic performance reliability: a basis for multi-level design norms. Proceedings of 11th World Conference on Earthquake Engineering, Acapulco

Cornell CA (2005) On earthquake record selection for nonlinear dynamic analysis. Proceedings of the Luis Esteva symposium, Mexico

Cornell CA, Jalayer F, Hamburger RO, Foutch DA (2002) Probabilistic basis for 2000 SAC Federal Emergency Management Agency steel moment frame guidelines. Journal of Structural Engineering, 128(4), 526-533

De Luca F, Iervolino I, Ameri G, Pacor F, Bindi D (2011) Prediction equations for nonlinear SDOF response from the ITalian ACcelerometric Archive: preliminary results. ANIDIS, Bari, Italy

Dolšek M (2009) Incremental dynamic analysis with consideration of modeling uncertainties. Earthquake Engineering & Structural Dynamics, 38(6), 805-825

Douglas J (2019) Ground motion prediction equations 1964–2018, http://www.gmpe.org.uk

Douglas J, Danciu L (2020) Nomogram to help explain probabilistic seismic hazard. Journal of Seismology, 24(1), 221-228. https://doi.org/10.1007/s10950-019-09885-4

Douglas J, Ulrich T, Negulescu C (2013) Risk-targeted seismic design maps for mainland France, Natural Hazards, 65(3), 1999–2013. https://doi.org/10.1007/s11069-012-0460-6

Fajfar P (2018) Analysis in seismic provisions for buildings: past, present and future. Bulletin of Earthquake Engineering, 16, 2567–2608, doi: 10.1007/s10518-017-0290-8Fajfar P, Dolšek M (2012) A practice-oriented estimation of the failure probability of building structures. Earthquake Engineering & Structural Dynamics, 41(3), 531-547

FEMA (2009a) NEHRP Recommended Seismic Provisions for New Buildings and Other Structures (FEMA P750). Federal Emergency Management Agency

FEMA (2009b) Quantification of Building Seismic Performance Factors (FEMA P695). Federal Emergency Management Agency

Fib. (2012) Probabilistic performance-based seismic design, Bulletin 68, International Federation of Structural Concrete, Lausanne, CH

Fragiadakis M, Papadrakakis M (2008) Performance-based optimum seismic design of reinforced concrete structures. Earthquake Engineering & Structural Dynamics, 37(6), 825-844

Franchin P, Petrini F, Mollaioli F (2018) Improved risk-targeted performance-based seismic design of reinforced concrete frame structures. Earthquake Engineering & Structural Dynamics, 47(1), 49-67

Giardini D et al. (2013) Seismic Hazard Harmonization in Europe (SHARE): Online Data Resource, doi: 10.12686/SED-00000001-SHARE

Gidaris I, Taflanidis AA (2015) Performance assessment and optimization of fluid viscous dampers through life-cycle cost criteria and comparison to alternative design approaches. Bulletin of Earthquake Engineering, 13(4), 1003-1028

Gregor N, Abrahamson NA, Atkinson GM, Boore DM, Bozorgnia Y, Campbell KW, Chiou BS-J, Idriss IM, Kamai R, Seyhan E, Silva W, Stewart JP, Youngs R (2014) Comparison of NGA-West2 GMPEs, Earthquake Spectra, 30(3), 1179-1197, doi: 10.1193/070113EQS186M

Hirata K, Nakajima M, Ootori Y (2012) Proposal of a simplified method for estimating evaluation of structures seismic risk of structures. Proceedings of 15th World Conference on Earthquake Engineering. Lisboa

Iervolino I, Spillatura A, Bazzurro P (2018) Seismic reliability of code-conforming Italian buildings. Journal of Earthquake Engineering, 22(s2), 5-27

Jalayer F, Cornell CA (2003) A Technical Framework for Probability-Based Demand and Capacity Factor Design (DCFD) Seismic Formats. PEER Report 2003/08, Pacific Earthquake Engineering Center, College of Engineering, University of California Berkeley, November

Kappos AJ (1999) Evaluation of behavior factors on the basis of ductility and overstrength studies. Engineering Structures, 21(9), 823-835

Kennedy RP (1999) Overview of Methods for Seismic PRA and Margin Analysis Including Recent Innovations. Proceedings of the OECD-NEA Workshop on Seismic Risk. Tokyo, Japan

Kennedy RP, Short SA (1994) Basis for seismic provisions of DOE-STD-1020. Rep. No. UCRL-CR-111478, Lawrence Livermore National Laboratory, Livermore, Calif., and Rep. No. BNL-52418, Brookhaven National Laboratory, Upton, NY

Kircher CA, Harris JL, Heintz JA, Hortacsu A (2014) ATC-84 Project: Improved Seismic Performance Factors for Design of New Buildings. Proceedings of 10th U.S. National Conference on Earthquake Engineering, Anchorage, Alaska

Levens AS (1959) Nomography, 2nd edn. Wiley, New York

Liel AB, Haselton CB, Deierlein GG, Baker JW (2009) Incorporating modeling uncertainties in the assessment of seismic collapse risk of buildings. Structural Safety, 31(2), 197-211. https://doi.org/10.1016/j.strusafe.2008.06.002

Luco N, Bachman RE, Crouse CB, Harris JR, Hooper JD, Kircher CA, Caldwell PJ, Rukstales KS (2015) Updates to Building-Code Maps for the 2015 NEHRP Recommended Seismic Provisions, Earthquake Spectra, 31(S1), S245-S271

Luco N, Cornell CA (2007) Structure-specific scalar intensity measures for near-source and ordinary earthquake ground motions. Earthquake Spectra, 23(2):357–392

Luco N, Ellingwood BR, Hamburger RO, Hooper JD, Kimball JK, Kircher CA (2007) Risk-targeted versus current seismic design maps for the conterminous United States. In: SEAOC 2007 convention proceedings

Lupoi G, Lupoi A, Pinto PE (2002) Seismic risk assessment of RC structures with the" 2000 SAC/FEMA" method. Journal of Earthquake Engineering, 6(04), 499-512

McGuire RK (2008) Probabilistic seismic hazard analysis: early history. Earthquake Engineering and Structural Dynamics, 37, 329–338, doi: 10.1002/eqe.765

McKenna F, Fenves GL, Scott MH (2006) OpenSees: Open System for Earthquake Engineering Simulation. Pacific Earthquake Engineering Center, University of California: Berkeley, CA

NIST (2010) Evaluation of the FEMA P-695 Methodology for Quantification of Building Seismic Performance Factors, NIST GCR 10-917-8. Prepared by the

NEHRP Consultants Joint Venture, a partnership of the Applied Technology Council and the Consortium of Universities for Research in Earthquake Engineering for the National Institute of Standards and Technology, Gaithersburg, Maryland

NIST (2012) Tentative Framework for Development of Advanced Seismic Design Criteria for New Buildings, NIST GCR 12-917-20. Prepared by the NEHRP Consultants Joint Venture, a partnership of the Applied Technology Council and the Consortium of Universities for Research in Earthquake Engineering for the National Institute of Standards and Technology, Gaithersburg, Maryland

Ordaz M, Faccioli E, Martinelli F, Aguilar A, Arboleda J, Meletti C, D'Amico V (2015) CRISIS 2015 software, https://sites.google.com/site/codecrisis2015/home

Porter KA (2003) An overview of PEER's performance-based earthquake engineering methodology, Proceedings of Ninth International Conference on Applications of Statistics and Probability in Civil Engineering.

Rupakhety R, Sigbjörnsson R (2009) Ground-motion prediction equations (GMPEs) for inelastic response and structural behaviour factors, Bulletin of Earthquake Engineering, 7, 637-659

Sewell RT (1989) Damage effectiveness of earthquake ground motion: Characterizations based on the performance of structures and equipment, PhD thesis, Stanford University, California, USA

Sewell RT, Toro GR, McGuire RK (1991) Impact of ground motion characterisation on conservatism and variability in seismic risk estimates. NUREG/CR-6467. U.S. Nuclear Regulatory Comission, Washingtion, DC

Silva V, Crowley H, Bazzurro P (2016) Exploring risk-targeted hazard maps for Europe, Earthquake Spectra, 32(2), 1165-1186

Tothong P, Cornell AC (2006) An Empirical Ground-Motion Attenuation Relation for Inelastic Spectral Displacement. Bulletin of the Seismological Society of America, 96, 2146-2164, doi: 10.1785/0120060018

Tubaldi E, Barbato M, Dall'Asta A (2011) Influence of model parameter uncertainty on seismic transverse response and vulnerability of steel–concrete composite bridges with dual load path. Journal of Structural Engineering, 138(3), 363-374

Tubaldi E, Ragni L, Dall'Asta A (2015). Probabilistic seismic response assessment of linear systems equipped with nonlinear viscous dampers. Earthquake Engineering & Structural Dynamics, 44(1), 101-120

Tubaldi E, Barbato M, Ghazizadeh S (2012) A probabilistic performance-based risk assessment approach for seismic pounding with efficient application to linear systems. Structural Safety, 36, 14-22

Vamvatsikos D (2013) Derivation of new SAC/FEMA performance evaluation solutions with second-order hazard approximation. Earthquake Engineering & Structural Dynamics 42(8), 1171-1188

Vamvatsikos D, Aschheim MA (2016) Performance-based seismic design via yield frequency spectra. Earthquake Engineering & Structural Dynamics, 45(11), 1759-1778

Vamvatsikos D, Kazantzi AK, Aschheim MA (2015) Performance-based seismic design: Avant-garde and code-compatible approaches. ASCE-ASME Journal of Risk and Uncertainty in Engineering Systems, Part A: Civil Engineering, 2(2), C4015008

Wen YK (2001) Reliability and performance-based design. Structural Safety, 23(4):407–428

Woessner J, Danciu L, Giardini D, Crowley H, Cotton F, Grunthal G, Valensise G, Arvidsson R, Basili R, Demircioglu MB, Hiemer S, Meletti C, Musson RW, Rovida AN, Sesetyan K, Stucchi M and The SHARE Consortium (2015), The 2013 European Seismic Hazard Model: Key components and results, Bulletin of Earthquake Engineering, 13(12), 3553-3596, doi: 10.1007/s10518-015-9795-1

Žižmond J, Dolšek M (2013) Deaggregation of seismic safety in the design of reinforced concrete buildings using Eurocode 8. Proceedings of 4th ECCOMAS Thematic Conference on Computational Methods in Structural Dynamics and Earthquake Engineering

Žižmond J, Dolšek M (2017) The formulation of risk-targeted behaviour factor and its application to reinforced concrete buildings. Proceedings of 16th World Conference on Earthquake Engineering, Paper no. 1659

CHAPTER 5

Evaluating alternative approaches for the seismic design of structures

The current design approach recommended by seismic codes is often based on the use of uniform-hazard response spectra, reduced to account for inelastic structural behaviour. This approach has some strong limitations that have been highlighted in many studies, including not allowing a direct control of the seismic risk and losses. This chapter aims at quantifying the levels of safety and the costs associated with this design approach, and to investigate alternative design approaches that have been developed in the last decades. In particular, a risk-targeting approach and a minimum-cost approach are considered. The first one, allowed by US codes, aims at designing structures with the same risk of collapse throughout regions of different seismicity. The second one aims to minimize the sum of the initial construction cost and the cost of expected losses due to future earthquakes. The comparison of the approaches is performed by considering, as an example structure, a four-storey reinforced concrete frame building located in different areas in Europe, and by looking at the implications in terms of achieved safety levels, initial costs, and future losses. The study's results provide useful information on how the design criteria and the different hazard levels throughout Europe affect the cost and safety levels of seismic design. The work presented in this chapter is based on the following publication:

Gkimprixis A, Tubaldi E, Douglas J (2019) Evaluating alternative approaches for the seismic design of structures. Bulletin of Earthquake Engineering, 18, 4331–4361 (2020). https://doi.org/10.1007/s10518-020-00858-4.

5.1 Introduction

Current seismic design regulations are often based on a uniform-hazard philosophy. This simplified design practice is essentially deterministic and employs a uniform-hazard spectrum, with predefined exceedance frequency depending on the performance objectives, to define the seismic action. Although this approach is simple, well established, and results in overall satisfactory performance (e.g. Jeong et al. 2012; Rivera and Petrini 2011; Panagiotakos and Fardis 2004; Mwafy 2001; Kappos 1997), it comes with the drawback of uncontrollable distribution of the risk levels in different locations (e.g. Collins et al. 1996; Tubaldi et al. 2012; Silva et al. 2016; Iervolino et al. 2018). This means that, although the structures are designed using the same regulation, they are exposed to different risk levels.

Acknowledging this, modern design philosophies have introduced the use of fully probabilistic approaches in the design stage to account explicitly for the risk level of the designed structure. A first official attempt to control the seismic risk across regions of different seismicity at a national level was made in the US, with regulations (ASCE 7-16 2017; FEMA P-750 2009) that proposed the use of risk-targeted ground motion maps, while alternative risk-targeting approaches are available in the literature (see previous chapters).

Observations on the effects of past historical earthquakes have shown that, while life safety is usually ensured by compliance with design codes, the economic losses due to damage in structural and non-structural components can be large (e.g. Perrone et al. 2019; Braga et al. 2011). This is mainly because structures are designed to undergo significant inelastic behaviour under major earthquakes to dissipate seismic energy, and there is insufficient attention paid to the behaviour of non-structural components in the design stage. Moreover, the behaviour of building components such as masonry infills, interacting with the frame structural components, is usually disregarded in the design stage, and very often these elements experience damage even under moderate earthquakes, leading to significant losses (e.g. De Risi et al. 2019, De Luca et al. 2014; Ricci et al. 2011; Romão et al. 2013; Braga et al. 2011).

It is understandable that seismic design has to serve a double goal and provide not only safe, but also economic design solutions. The two objectives can be conflicting, because in order to reduce the risk of loss of life the construction costs generally need to increase. Thus, there should be a compromise between construction costs and target levels of safety. This has motivated intense research in the development of design techniques that consider the benefit from the future losses reduction when the seismic design level, and consequently the initial construction cost, is increased (Cardone et al. 2019; Ordaz et al. 2017; Crowley et al. 2012; Padgett et al. 2010; Kappos and Dimitrakopoulos 2008; Lagaros 2007; Ellingwood and Wen 2005; Wen and Kang 2001).

The aim of this study is to quantify the levels of safety and the costs associated with the code design approach, and to investigate the effectiveness of the risk-targeted and minimum-cost design approaches. It is recalled that a simplified performance assessment procedure was displayed in Chapter 3, where buildings of different geometry were designed using 2D models and the fragility of the structural members was assessed. Herein, a more rigorous approach is followed, where 3D models are developed instead, and the performance of the various components (structural and non-structural) is assessed, in terms of achieved safety levels, initial costs, and future losses. Given the computational effort of this, no variability in the geometry was considered herein. In particular, the case study consists of a four-storey reinforced concrete (RC) frame building located in different regions in Europe, which exhibit a wide range of hazard levels.

After reviewing briefly the alternative design approaches, the RC structure is designed following the Eurocodes (ECs) for different values of the design peak ground acceleration (*PGA*). Using a nonlinear finite element model developed in Seismostruct (Seismosoft, 2020), time-history analyses are carried out to evaluate the performance of the building and establish a link between the seismic fragility and the design *PGA*. The distribution of the collapse risk rates obtained across Europe considering the uniform hazard *PGA* as design input is then assessed. Risk targeting is subsequently applied, followed by an evaluation of the design *PGA* levels minimizing the total costs of the building across Europe. In the calculations, the initial construction costs, the

future losses due to damage of both structural and non-structural components of the building and additional losses are considered. Finally, some comparisons are made among the results of the different approaches.

5.2 Review of design approaches

This section illustrates briefly the three design approaches considered in this study. Each approach provides a different value of the design seismic intensity at the site of interest, which is synthetically represented here by the design peak ground acceleration, PGA_{d}.

5.2.1 Uniform-hazard design

Modern seismic design codes generally follow a force-based approach in which the earthquake input is defined in terms of an acceleration response spectrum to be used in conjunction with simplified elastic analyses. The ductile behaviour of the structure is taken into account through the application of a reduction factor to transform the elastic spectrum into an inelastic design spectrum. In EC8 (CEN 2004b), this spectrum is anchored to a *PGA* value obtained from the hazard curve of the structure's site for a predefined probability of exceedance (e.g. 10% in 50 years for the 'no-collapse' objective associated with the 'ultimate limit state'), while the spectral shape is assumed to depend only on the local soil conditions. The application of this design framework establishes uniform hazard levels among different locations, meaning that the 'uniform-hazard' design *PGA* values, PGA_d^{UH} , share the same exceedance probability at every location. It is noteworthy that this approach leads to non-uniform levels of risk for different locations, as discussed in the previous chapters.

5.2.2 Risk-targeted design

This method aims to design a structure that will be exposed to an acceptable and controlled risk level, expressed as the mean annual frequency (MAF) of collapse, λ_C . This depends on the design acceleration, PGA_d , through the following expression (Kennedy 2011):

$$\lambda_C\left(PGA_d\right)=\int P\left(C|IM\right)\cdot\left|dH(IM)\right| \tag{5.1}$$

where $H(IM)$ is the hazard curve, obtained from PSHA (Cornell 1968; McGuire 2008; Baker 2015), providing the MAF of exceeding the seismic intensity measure (*IM*) used for risk assessment, and $P\left(C|IM\right)$ denotes the probability of collapse conditional on the *IM* level.

The solution of the risk-targeting problem requires an iterative approach (see Figure 5.1) that eventually leads to the risk-targeted design peak ground acceleration, PGA_d^{RT}, corresponding to the target risk level λ_C.

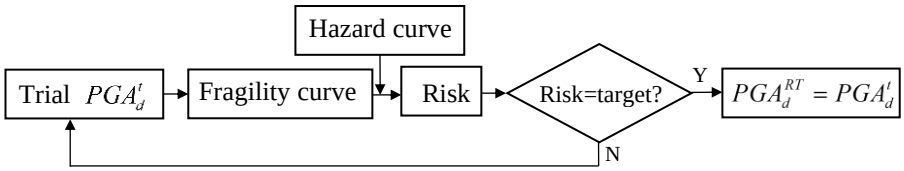

Figure 5.1 Risk-targeting design framework

5.2.3 Minimum-cost design

This approach aims to design a structure such that the total life-cycle cost is minimized. The costs of construction and seismic damage to structural and non-structural components are considered, while additional losses can be included. The methodology discussed herein is based mainly on the work of Wen and Kang (2001), while other articles have been considered as well (e.g. Kappos and Dimitrakopoulos 2008; Lagaros 2007; Ordaz et al. 2017; Crowley et al. 2012; Padgett et al. 2010). The variable to be minimized is the expected value of the life-cycle cost, *E*[*LCC*], over the time period *t*, which can be expressed as:

$$E\left[LCC\right]=C_0+E[FL] \tag{5.2}$$

where C_0 is the initial construction cost and $E[FL]$ is the expected cost due to future losses. The latter stems from the sum of the losses incurred for repairing (or replacing) the damaged structure and additional losses (e.g. from personal property damage, injuries or fatalities, and loss of function of the building).

The expected cost due to the future losses over a time period *t* is calculated as:

$$E\left[FL\right] = E[AL] \cdot (1 - e^{-\lambda \cdot t}) / \lambda \tag{5.3}$$

where λ is a constant discount rate/year, which converts the future losses into present monetary value. The expected value of the annual losses, $E[AL]$, is equal to:

$$E\left[AL\right] = \int_0^\infty E[AL \mid IM] \cdot dH(IM) \tag{5.4}$$

where $E[AL \mid IM]$ is the expected value of the losses given an *IM* level, usually referred to as vulnerability. The total vulnerability of the building derives from the sum of the vulnerability of each component at every storey, which is based on the fragility curves of the component for the various damage states and the costs associated with each damage state. If the collapse criterion is met at any storey, then it is assumed that the whole building has collapsed ('global collapse' case), and consequently it has to be replaced.

Following Ramirez et al. (2012), the collapse (C) and no-collapse (NC) cases are considered explicitly in the derivation of the vulnerability according to the following expression:

$$E[AL \mid IM] = E[AL \mid NC, IM] \cdot [1 - P(C \mid IM)] + C_r \cdot P(C \mid IM) \tag{5.5}$$

where the probability of collapse given the *IM*, $P(C \mid IM)$, is the fragility curve for the case of 'global collapse', and C_r is the associated cost.

The value of $E[LCC]$ depends on the PGA_d, which influences both the initial costs and the losses. An optimization technique can be employed to minimize $E[LCC]$, as shown schematically in the flowchart of Figure 5.2.

Starting with a trial PGA_d, the corresponding fragility curves of each component (structural and non-structural) of every storey are calculated, together with their cost. Based on the fragility curves and the costs associated with the various damage states, the vulnerability curves of the building are derived using Eqn.(5.5), by assembling the vulnerability of the various components and taking into account the building collapse

events. Then, $E[LCC]$ is calculated from Eqn.(5.2) This procedure is repeated for a range of trial PGA_d levels and the minimum-cost design acceleration, PGA_d^{MC}, is obtained as the one that minimizes $E[LCC]$.

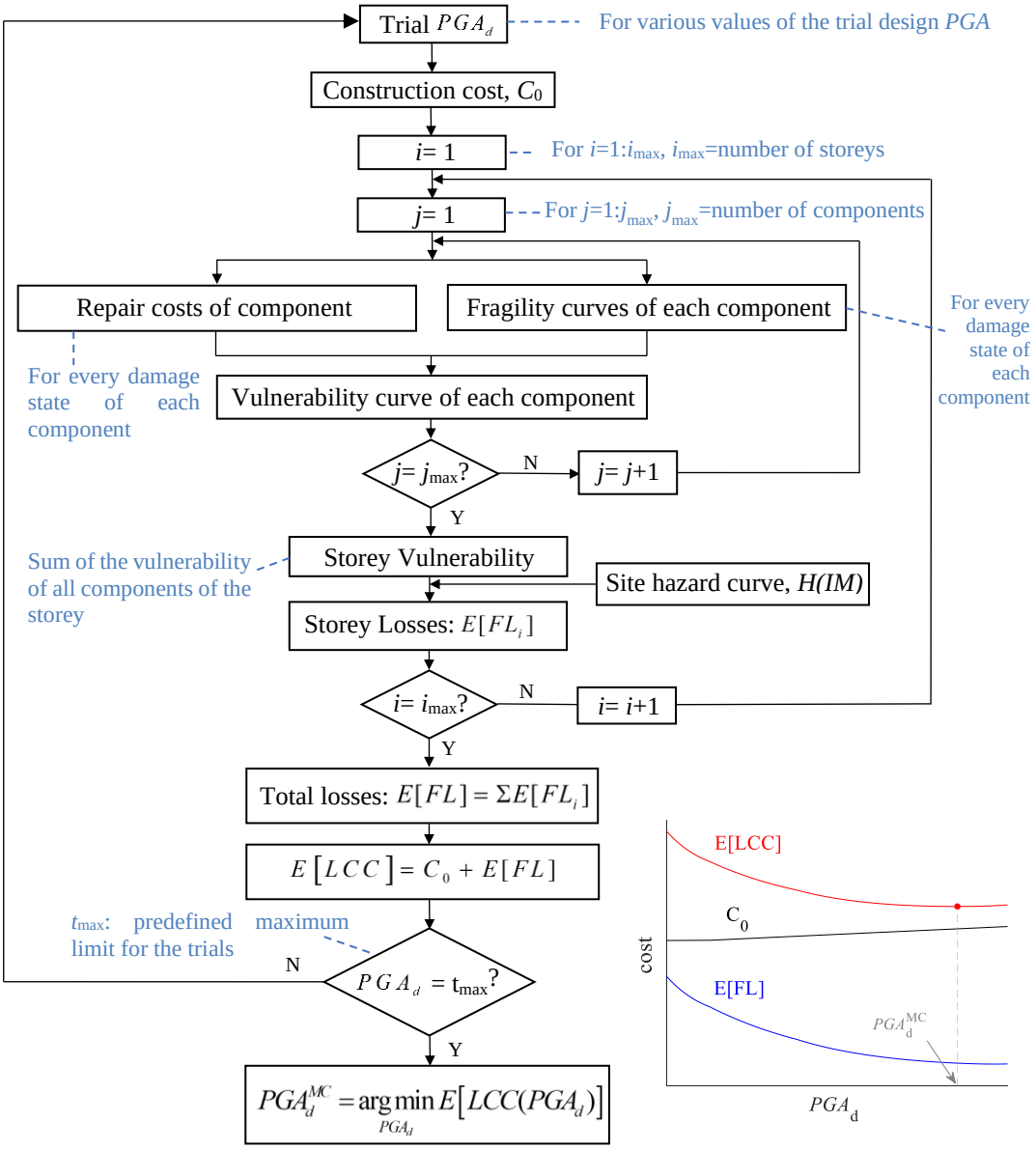

Figure 5.2 Flowchart of the developed minimum-cost design algorithm

5.3 Applications

A benchmark RC building is considered to evaluate and compare the design *PGA*s, risk levels, and losses corresponding to the application of the alternative design

approaches illustrated in the previous section. The case study is representative of many structures built across Europe, and consists in a 4-storey 3-bay RC frame building, symmetrical in plan and elevation, with span length and column height respectively equal to 5m and 3m (Figure 5.3).

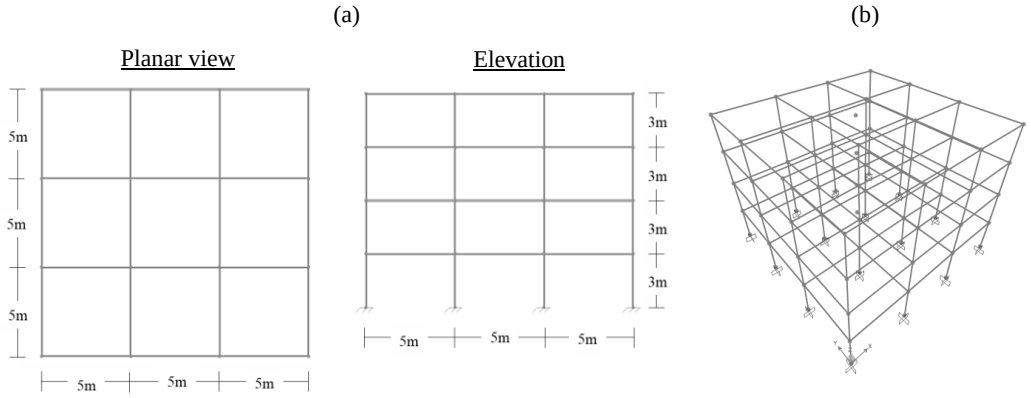

Figure 5.3 (a) Plan and elevation of the building, (b) 3D model of the building at the design stage

5.3.1 Seismic design according to Eurocodes

The building is designed following EC2 (CEN 2004a) and EC8 (CEN 2004b). Both the columns and the beams have the same section in all storeys. The concrete strength class is C25/30, corresponding to a characteristic compressive strength of 25 MPa, a mean compressive strength of 33 MPa, a mean tensile strength of 2.6 MPa, and a modulus of elasticity of $3.1 \cdot 10^4$ MPa. A B450C steel is assumed for the reinforcement, corresponding to a characteristic yield strength of 450 MPa, a mean strength of 517.5 MPa, and a modulus of elasticity of $2.0 \cdot 10^5$ MPa.

The self-weights of the concrete elements are derived assuming a specific weight of 25 KN/m^3. Regarding the permanent loads, 1 KN/m^2 is assumed for the floor finishing weight and 7 KN/m^3 for the weight of the masonry infills of the external frames. The influence of the structural elements dimensions and the presence of openings was considered in the calculation of the weight of the panel. An additional uniformly distributed load of 0.4 KN/m^2 is added to the floor loads to account for internal partitions, as per NTC-3.1.3 (NTC 2018). The live load (Q) is taken equal to 2 KN/m^2. The following load combinations are considered, according to EC8 (CEN 2004b) and

EC0 (CEN 2002): $1.35 \cdot G + 1.50 \cdot Q$ (gravity loads only), $G + 0.30 \cdot Q \pm E_x \pm 0.30 \cdot E_y$, $G + 0.30 \cdot Q \pm 0.30 \cdot E_x \pm E_y$, where G, Q and E are the permanent, live and earthquake loads respectively and x and y refer to the two horizontal directions.

Rather than considering the design spectra defined by national codes, the Type 1 horizontal design acceleration spectrum (EC8-1-3.2.2.2) is used for every location across Europe. The seismic design is carried out considering different design acceleration values, namely 0.0g, 0.1g, 0.3g and 0.5g, an importance class II, and a medium ductility class (EC8-1), corresponding to a behaviour factor $q = 3.9$, according to EC8-1-5.2.2.2 regarding multi-storey, multi-bay frame systems regular in plan and elevation with medium ductility. Class B is assumed for the soil conditions and 5% for the damping ratio. It should be noted that the EC8 Type 1 spectrum employed for the design is not strictly a uniform-hazard spectrum as its shape is constant for different locations (Tsang, 2015).

Two performance objectives are considered: 'no-collapse' under the seismic design action, and 'damage limitation' for a more frequent seismic event. Starting with 'the no-collapse' requirements, first an elastic analysis is performed, using the elastic response spectrum, modified by *q*. The contribution of the infills to the stiffness and strength of the frames is disregarded in the design stage, an approach usually followed in design practice. A modal response spectrum analysis is performed [EC8-1-4.3.3.1(2)P] to find the required reinforcement area for beams and columns. In the numerical model, a 50% reduction of the materials' modulus of elasticity is considered to account for the effect of cracking [EC8-1-4.3.1(7)]. Rigid diaphragms are considered at floor levels and the contribution of the slab (15 mm thick) to the lateral stiffness is taken into account by assuming T-shaped beams (EC2-1.1-5.3.2.1). The accidental eccentricity (EC8-1-4.3.2) is considered equal to $\pm 0.05 \cdot L_i$, where i is the floor-dimension perpendicular to the direction of the seismic action.

Capacity design rules are applied to design the required reinforcement area for beams and columns. This is to ensure that in every joint the sum of the moments of resistance of the columns are at least 1.3 times higher than that of the beams of the joint (EC8-1-

5.2.3.3). Following EC8-1-4.4.2.2(2), an additional check is made to ensure that second-order (P-δ) effects are not excessively high.

The 'damage limitation' criterion is satisfied by checking that the inter-storey drifts (ISDs) are less than 0.5% of the storey height (non-structural elements of brittle materials attached to the structure), in accordance with the criterion of paragraph EC8-1-4.4.3.2. To account for the reduced return period of the seismic action associated with this criterion, the design action is multiplied by a reduction factor of 0.5.

If the structure fails any of the above criteria, the sections are increased, otherwise the design procedure is complete. The results of this design procedure, in terms of RC member dimensions and total reinforcement, are summarized in Table 5.1, and are comparable to those of similar research works (e.g. Fardis et al. 2012, Ulrich et al. 2014).

Table 5.1 Properties of the structural members based on the design level

PGA_d [g]	Dimensions of RC members [m x m]		Total area of reinforcement steel [m^3]			
			Longitudinal		Transverse	
	Columns	Beams	Columns	Beams	Columns	Beams
0.0	0.30 x 0.30	0.30 x 0.30	0.17	1.72	0.07	0.25
0.1	0.40 x 0.40	0.40 x 0.30	0.31	1.49	0.08	0.22
0.3	0.55 x 0.55	0.55 x 0.30	0.59	3.14	0.16	0.41
0.5	0.70 x 0.70	0.65 x 0.30	1.04	4.28	0.32	0.63

It is clarified that wind and snow loads are not considered in the design because they may vary significantly from location to location and, therefore, they could complicate interpretation of the effect of the seismic hazard on the structural design. Thus, the case of PGA_d=0.0g refers to a design executed only under the gravity load combination. Further analyses have been carried out for the case-study building to confirm that the results are not significantly altered if the wind action is taken into account (for velocities up to 25 m/s).

5.3.2 Numerical models for nonlinear analyses

The finite element software Seismostruct (Seismosoft, 2020) is used to perform the nonlinear analyses. The inelastic plastic hinge force-based frame element type is used to describe the inelastic behaviour of beam and column elements. The plastic hinge

properties are derived based on the cross-sections at the extremes of the elements, employing 150 fibres to discretize the section (Calabrese et al. 2010; Scott and Fenves 2006). The length of the plastic hinge (L_p) is calculated according to Paulay and Priestley (1992), based on the element's length as well as the yield strength and the diameter of the longitudinal reinforcing steel. Beam-column joints are assumed to be rigid and their degradation is not explicitly taken into account, assuming that in newly-designed buildings these elements are not expected to be as critical as in existing buildings.

For the constitutive law of the RC members, the Mander et al. (1998) nonlinear concrete model and the Menegotto and Pinto (1973) steel model are used. While in the design approach the characteristic values were used, for the nonlinear analyses the mean values of Table 5.1 are used instead, as stated in EC8-1-4.3.3.4.1(4). A Rayleigh damping matrix with the tangent stiffness approach is employed to model the damping inherent to the structure and its contribution to the seismic energy dissipation (Chopra, 1995). A 5% damping ratio is considered for the first two transitional modal periods (estimated via eigenvalue analysis). Finally, the seismic excitation is applied only along the horizontal direction, while the permanent and live loads are considered with the combination G+0.30·Q.

The frames of the perimeter of the building are infilled with masonry panels made of 30cm-thick hollow bricks. Following the RINTC project (RINTC Workgroup 2018), the following properties of the infill are considered: σ_0= 0 MPa (vertical stress), σ_{m0}= 6 MPa (vertical compression strength), τ_{m0}= 0.775 MPa (shear strength), f_{sr}= 0.542 MPa (slide resistance in the joints), and E_m= 4312 MPa (elastic modulus of the infills).

The diagonal strut approach (Decanini et al. 2004) is followed to simulate the infills, using the above parameters to define the various failure mechanisms and the resulting constitutive law of the struts representing the infill panels. In order to account for the openings in the panels (doors or windows), the strut strength values are reduced by the factor proposed in Decanini et al. (2014). Generally, an opening of area 2.4 m^2 is assumed, (e.g. height 1.2m and width 2m for windows) corresponding to a 60%

strength reduction. More specifically, the reduction factor is equal to 0.44, 0.42, 0.40, and 0.38, for PGA_d equal to 0.0g, 0.1g, 0.3g and 0.5g, respectively. A further modification of the Decanini et al. (2004) model is introduced, to achieve a better agreement between predicted and observed ISD corresponding to infill damage, by using the drift values provided in the RINTC project. Recent researchers (Sassun et al. 2016; Hak et al. 2012) have investigated the relation between the drift capacity of an infill panel and the strain capacity of the equivalent strut. Using the analytical formulae of these works, the drift thresholds are used together with the geometry of the panel to obtain the strain values for the constitutive law of the strut. The constitutive laws of the struts and of the other materials are shown in Figure 5.4, together with the numerical model of the case-study buildings.

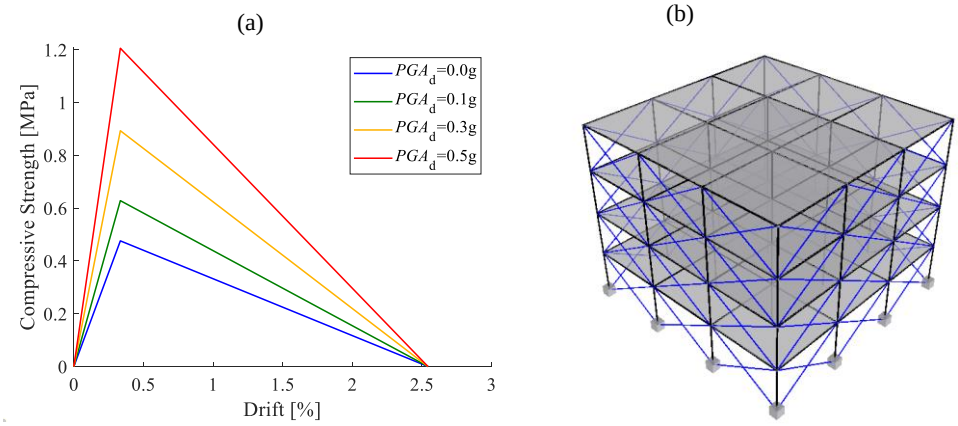

Figure 5.4 Summary of the modelling approach for the nonlinear analyses: (a) constitutive laws of the infills in terms of truss strength-storey drift, (b) numerical model in Seismostruct

It is noteworthy that increasing the PGA_d levels leads to a decrease of the contribution/impact of the infills. This is mainly because the columns section increases with PGA_d and thus the ratio of the infilled area to the area of the columns reduces. This ratio is one of the main parameters that controls the infill-frame interaction. In Seismostruct (Seismosoft, 2020), the infills are modelled with inelastic truss elements, using a trilinear concrete model with no residual strength.

5.3.3 Modal and pushover analyses

Modal analyses have been carried out on the numerical models corresponding to the various PGA_d levels considered. In the case of bare frames, the contribution of the

infills to the lateral strength is disregarded, while the mass is the same as in the infilled case. The fundamental vibration periods for the bare models are 0.73s, 0.47s, 0.29s and 0.22s, for PGA_d equal to 0.0g, 0.1g, 0.3g and 0.5g, respectively. These periods are reduced to 0.36s, 0.32s, 0.25s and 0.20s in the case of the infilled models. In general, the fundamental period of vibration reduces for increasing design acceleration levels, due to higher stiffness of the resisting components. Moreover, accounting for the stiffness of the infills results in a reduction of the fundamental period of vibration, as expected. This reduction is more significant for the frames designed for lower *PGA* levels, due to the higher infill-frame stiffness ratio, as discussed in the previous section.

Static pushover analyses are also performed by applying monotonically increasing horizontal loads and the resulting capacity curves, in terms of total base shear versus maximum (across the various storeys) ISD, are presented in Figure 5.5. It can be observed that the strength and stiffness of the infilled models are significantly higher than those of the corresponding bare models for low ISD levels. For high ISD levels, the infills are damaged and their contribution to the resistance reduces. The capacity curves of the models with and without infills coincide at high ISD levels, where all the infill frames are extensively damaged. The contribution of the infills to the global strength and stiffness of the buildings is rather low, in line with other studies on masonry infilled frames (see e.g. RINTC Workgroup 2018). This is mainly due to the use of hollow bricks for the infills, and the effect of the openings, which significantly reduce the infill capacity. It is noteworthy that the ISD levels at which the capacity curves of the infilled models attain their peak values tend to increase with the PGA_d levels. Moreover, the differences in terms of stiffness and strength between the infilled and bare frame models are more significant for low PGA_d levels, which is consistent with the observation of the previous subsection that the stiffness and strength of the strut elements modelling the infills reduces for increasing PGA_d. The ultimate ISD values of the capacity curves (3%) correspond to the failure of the RC members, as discussed below. Overall, the ductility capacity of the designed models is high, demonstrating the effectiveness of the employed capacity design criteria. Nonlinear geometric effects have been considered, but they are not significant for these buildings and the post-peak behaviour of the pushover curve is strongly affected by the constitutive law of the confined concrete.

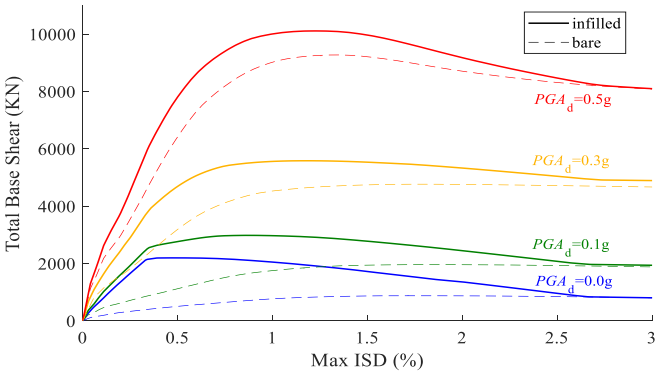

Figure 5.5 Effect of the PGA_d and the presence of infills on the pushover curves

5.3.4 Incremental dynamic analyses

Incremental dynamic analyses (IDAs) (Vamvatsikos and Cornell, 2002) are performed to derive fragility curves for the various models considered. To capture the uncertainties inherent to record-to-record variability effects, 22 records (see Appendix A) selected from RESORCE (Akkar et al. 2014) are considered. Since using a different set of records for each location of Europe would be too time-consuming, the considered records are not representative of any specific site, but have been selected based on generic criteria: epicentral distance between 0 and 30km, moment magnitude between 5 and 7, and focal depth less than or equal to 30km. It is noteworthy that the choice of the records selected to represent record-to-record variability effects may have an influence on the performance assessment, and other record sets, intensity measures, and nonlinear demand estimation methods may lead to different results. There is no perfect method for selecting the input ground motions for a Europe-wide study.

Figure 5.6 shows the linear elastic pseudo-spectral acceleration and displacement response spectra (Chopra 1995) of the records scaled to a common *PGA* value of 0.1g, for a damping ratio of 5%. In the same figure, the mean spectrum and the first modal periods of the bare and infilled models (see previous paragraph) are also plotted. It can be seen that increasing the design acceleration and/or accounting for the presence of infills, results in lower displacement demand and higher accelerations levels, due to the shortening of the building period.

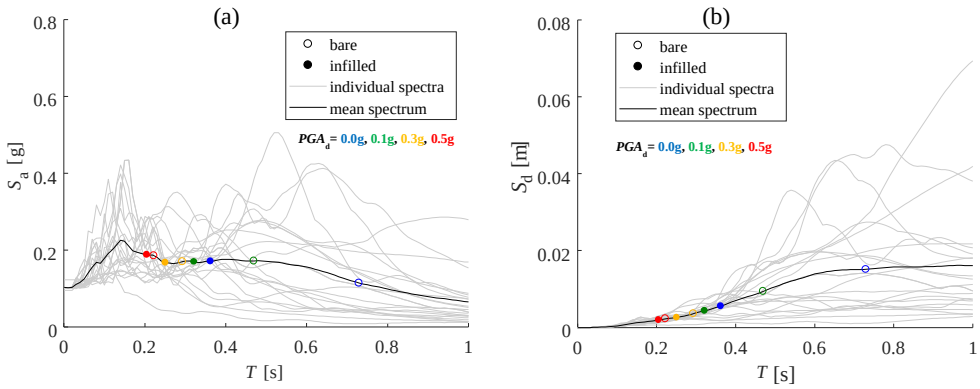

Figure 5.6 Linear elastic response spectra (5% damping) of the 22 selected strong-motion records scaled to a common *PGA* of 0.1g: (a) pseudo-spectral acceleration spectra, (b) displacement spectra

IDAs are performed by scaling the records to 29 different *PGA* levels, between 0.015g and 4g. It is noted that a common *IM* among the various structures is preferred in this study, to enable comparisons between the results from the different models. For this reason, *PGA* is selected as the *IM*, given also the fact that *PGA* is the *IM* used to scale the EC8 Type 1 design spectrum. Whenever numerical convergence issues arise, the structure is assumed to have failed.

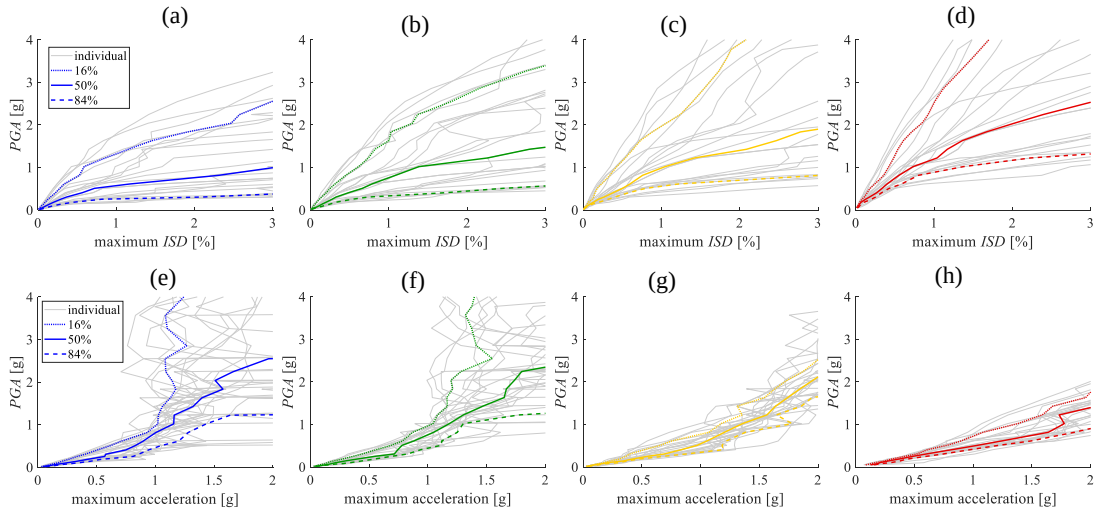

Figure 5.7 IDA curves in terms of maximum ISD (a to d) and maximum acceleration (e to h) for the models designed with: (a, e) 0.0g, (b, f) 0.1g, (c, g) 0.3g, (d, h) 0.5g

Figure 5.7 shows the IDA curves obtained for each record, in terms of *PGA* values versus maximum ISDs and maximum absolute accelerations observed across the storeys. The 50^{th}, 16^{th} and 84^{th} percentile IDA curves are also shown in the same figures. It can be observed that increasing the design acceleration results in decreased ISDs, and in higher absolute accelerations, since the structure becomes stiffer.

5.3.5 Fragility analyses

The results of the IDAs are used in this section to derive fragility curves for every component of each storey. The fragility curves are assumed to have a lognormal distribution and maximum-likelihood estimation (Shinozuka et al. 2000) is used for the fitting of the IDA results (e.g. Section 3.3.3 of Chapter 3). This approach, treating the IDA results as binary variables (corresponding to exceedance or not exceedance of the considered damage threshold), is particularly convenient for dealing with numerical convergence issues (e.g. Gehl et al. 2015).

All the components of the structure, have to be categorized in fragility groups (ATC, 2012a,b; Cardone et al. 2019; O'Reilly and Sullivan 2018; Cardone and Perrone 2017; O'Reilly et al. 2018). The RC members (columns, beams and slabs) are regarded as structural components, while the rest are defined as non-structural components. For the structural components, six damage states are considered, which are controlled by the ISD. For simplicity, the same ISD thresholds are considered for the different structures rather than use other criteria. These thresholds are based on the limits provided by Ghobarah (2004) for moment-resisting frames (Ductile MRF) and these limits have been employed in many other research works on RC building fragility assessment (Manoukas and Athanatopoulou 2018; Martins et al. 2018; Ulrich et al. 2014; Lagaros et al. 2007).

Based on the RINTC project, four damage states are defined for the damage of the infills explicitly, using ISD thresholds. In particular, the drift value at the peak strength of the panel is assumed equal to 0.334%. The cracking point is calculated at 80% of the peak strength, corresponding to a drift of 0.267%. Finally, it is considered that the infills reach the ultimate condition at a 50% drop of strength (Cardone and Perrone, 2015), leading to a value of 1.439% for the drift threshold. The number and distribution

of the internal partitions is estimated based on their distributed load assumed at the design stage, and the three limit states of Cardone and Perrone (2015) for partitions with doors are used.

The fragility of the rest of the non-structural components is evaluated by subdividing them into drift-sensitive and acceleration-sensitive ones, following FEMA P-58 (ATC 2012a,b). Table 5.2 summarizes the components considered in the study together with the assumptions made for the damage state definition.

Table 5.2 Damage states for the various components of the buildings

Type	Elements	Limit state thresholds	Damage levels (%)
S	Columns	0.10%, 0.20%, 0.40%, 1.00%, 1.80%, 3.00%	0.5, 5, 20, 45, 80, 100
	Beams	"	"
	RC slab	"	"
N/D	Flooring	"	"
	Infills, Plaster, Windows	0.27%, 0.33%, 0.78%, 1.44%	34, 37, 68, 100
	Insulation, Waterproofing	"	"
	Encasement, Skirting	"	"
	Aluminium/Iron Works	"	"
	Electrical system	"	"
	Partitions, Paint, Doors	0.08%, 0.20%, 0.50%	53, 82, 100
N/A	Flue, Drainage system	1.20g, 2.40g	14, 100
	Hydraulic system	0.55g, 1.10g	11, 100
	Gas system	"	"
	HVAC	1.50g	100
	Elevator	0.39g	100

Based on the results of the IDA and the damage state definition of Table 5.2, fragility curves are generated by considering explicitly the structural (S), non-structural drift-sensitive (N/D) and non-structural acceleration-sensitive (N/A) components at each storey (76 different fragility curves for each model). While the fragility of each components of every storey is considered separately, the case of collapse is defined ‘globally’. This means that when the 3% ISD limit is exceeded in any storey, then the whole building is assumed to collapse, and consequently both structural and non-structural components have to be replaced.

The results for the 'global collapse' condition for the four analysed models are presented in Figure 5.8. It can be observed that by increasing the PGA_d, the median value of the lognormal fragility increases roughly linearly.

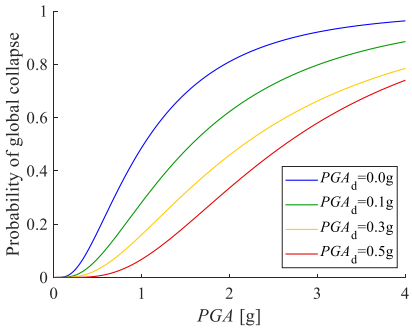

PGA_d [g]	median [g]	β
0.0	1.02	0.76
0.1	1.57	0.78
0.3	2.17	0.78
0.5	2.63	0.65

Figure 5.8 Fragility curves for the limit state of 'global collapse'

5.3.6 Risk analyses

In this subsection, the collapse risk levels corresponding to the uniform hazard design approach are evaluated across Europe. Then, the risk-targeting design approach is implemented to evaluate the design accelerations that will lead to a tolerable risk level. Finally, a comparison is made between the risk-targeted *PGA* levels and the uniform-hazard *PGA*s across Europe.

Risk levels associated with code-based design

The hazard curves for the different locations are based on the *PGA* values that correspond to 1%-, 2%-, 5%,- 10%-, 39%- and 50%-in-50-years exceedance probabilities according to the 2013 European Seismic Hazard Model (ESHM13,Giardini et al. 2013; Woessner et al. 2015). The second-order polynomial function in log-space proposed by Vamvatsikos (2013) is used to extrapolate the hazard data to a wider range of *PGA*. Figure 5.9 presents the *PGA* values for site class A that correspond to a 10%-in-50-years exceedance probability (MAF of exceedance $2.1 \cdot 10^{-3}$). As the seismic designs were undertaken using the EC8 spectrum for site class B, the *PGA*s for site class A from the ESHM13 hazard curves were multiplied by the soil factor 1.2, expressing the ratio between *PGA*s on site classes B and A in EC8.

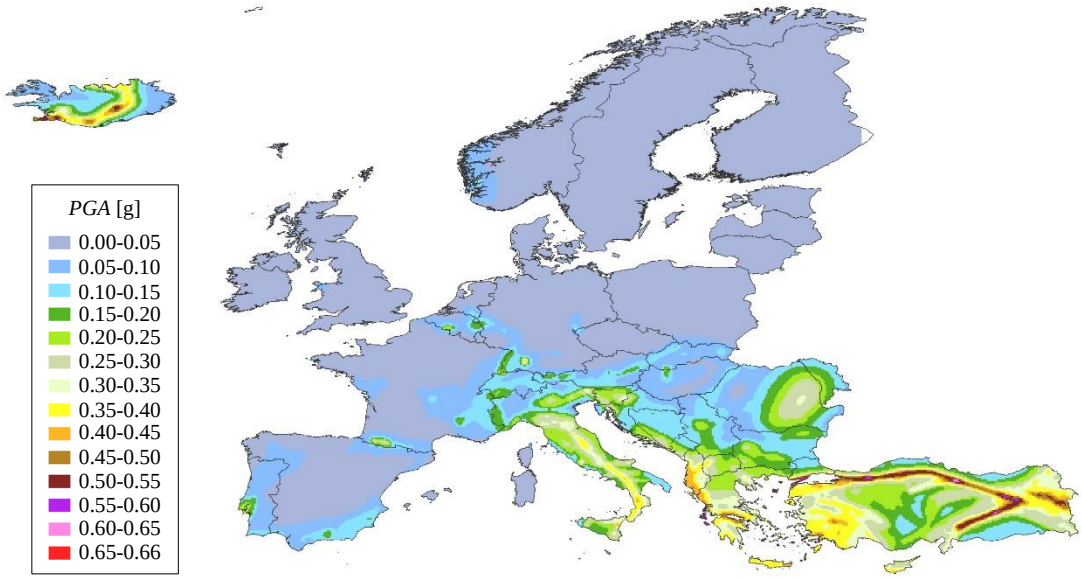

Figure 5.9 Design *PGA* values (site class A) with the uniform-hazard approach

Using the values of Figure 5.9 as the design acceleration, PGA_d^{UH} , a risk analysis is then performed to assess the levels of collapse risk obtained if the RC building is designed with the uniform-hazard (UH) approach. In future studies the design for each country could be done individually using the national design code. The parameters of the global-collapse fragility curves for a given PGA_d^{UH} value are obtained by interpolating the fragility parameter results of Figure 5.8. The annual collapse risk is obtained by convolution of the fragility and the hazard curves at each location, using Eqn.(5.1).

Figure 5.10 illustrates the obtained values of the collapse risk across Europe. In general, the probability of collapse is significantly lower than the probability of exceedance of the design hazard level ($2.1 \cdot 10^{-3}$), due to the various safety margins (e.g. safety factors, capacity design, minimum member size and detailing requirements) considered in the design. In areas of high seismicity, such as Italy and Greece, the values of the MAF of collapse are generally between 10^{-5} and 10^{-4}. This figure confirms the findings of other studies (e.g. Martins et al. 2018; Silva et al. 2016; Luco et al. 2007) that applying the UH approach leads to inconsistent risk levels.

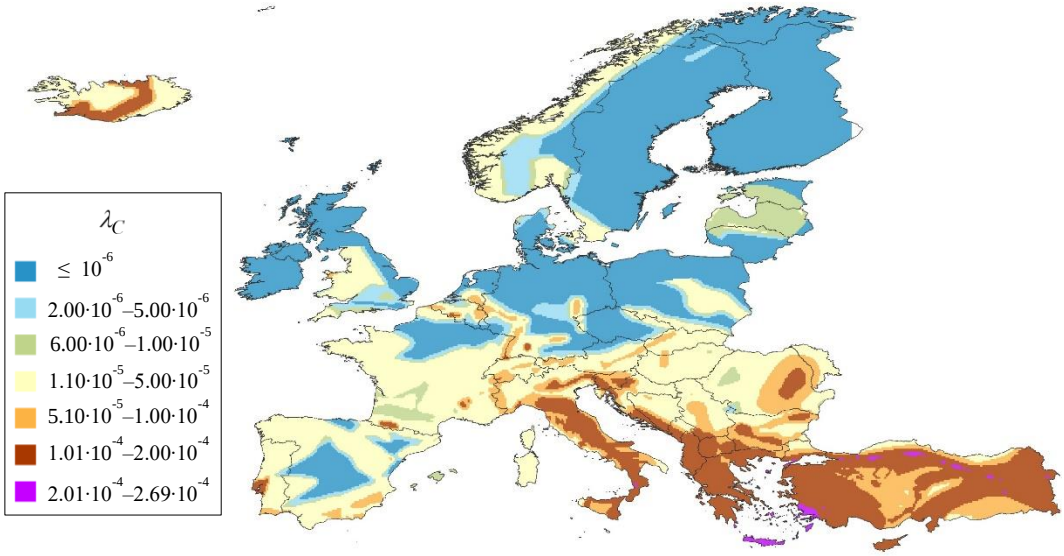

Figure 5.10 Annual collapse risk for the case-study building, designed with the UH approach

Comparisons with risk-targeting results

One of the key aspects of any risk-targeting framework is the choice of an acceptable collapse risk. Different values for this have been suggested in the regulations (Fajfar 2018) while other criteria (e.g. societal risk) have been proposed too (Tsang et al. 2020). First, following the recommendations of ASCE 7-16 (2017), the risk targeting design approach of Section 5.2.2 is applied considering a target annual collapse risk of $2 \cdot 10^{-4}$. Figure 5.11a presents the values of PGA_d^{RT} that lead to a uniform distribution of risk across Europe. These values are lower, except in the areas of highest hazard where they are the same or slightly higher, than those corresponding to the uniform-hazard approach, since the targeted risk value is higher than the actual risk levels obtained by designing with PGA_d^{UH} for almost all locations (Figure 5.10).

It is noteworthy that the obtained results may change significantly by considering different risk targets and structural systems. For instance, adopting the lower risk target of $5 \cdot 10^{-5}$ (following Silva et al. 2016) the PGA_d^{RT} values are significantly increased (Figure 5.11b).

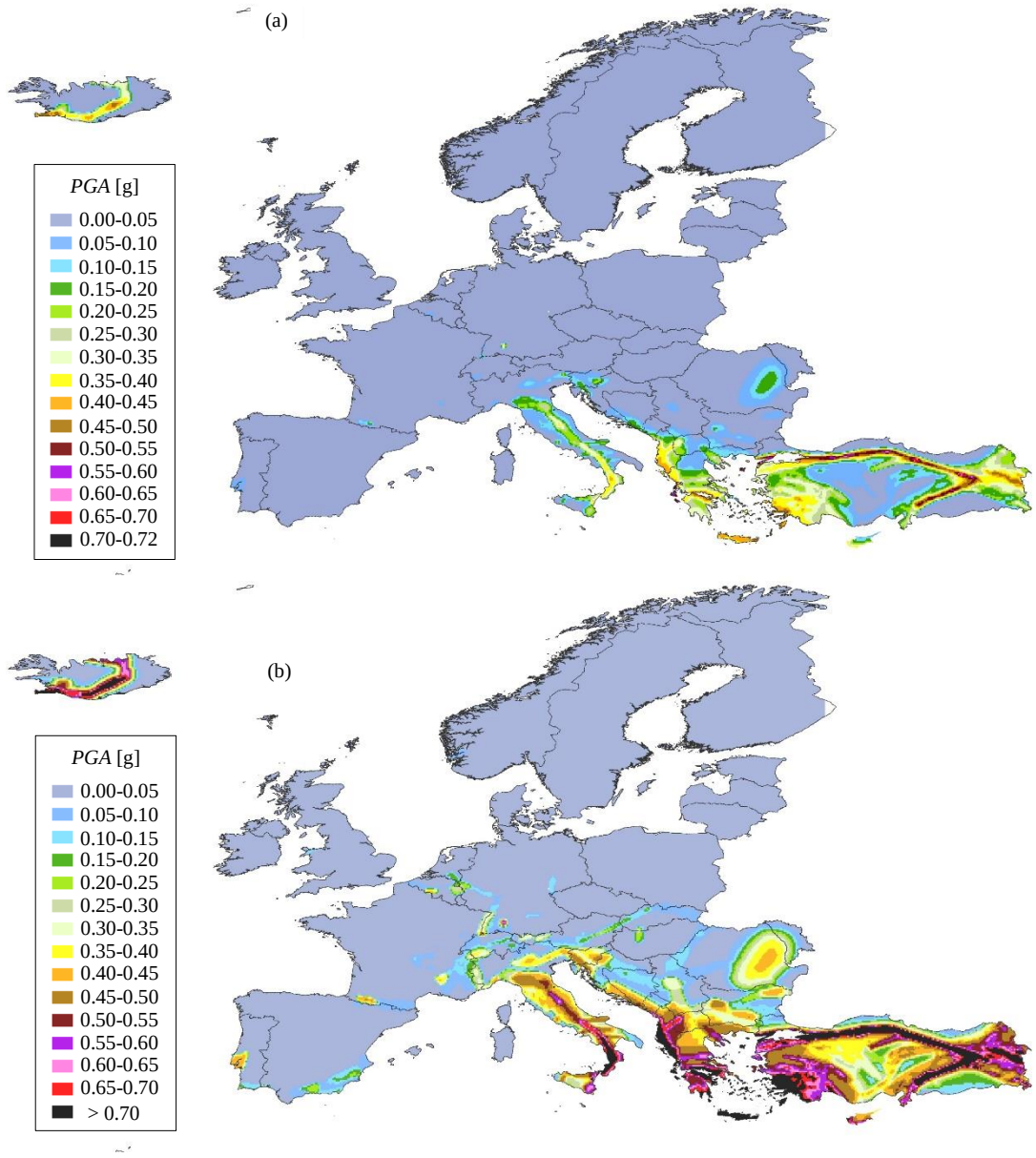

Figure 5.11 Design *PGA* values (site class A) with the risk-targeting approach, using annual collapse risk targets of (a) $2 \cdot 10^{-4}$, and (b) $5 \cdot 10^{-5}$

5.3.7 Initial construction costs

This subsection investigates the effect of the seismic design on the total construction costs. First, the cost of the structural members, i.e. columns, beams and slabs, is estimated based on the dimensions resulting from the application of the code design procedure (Table 5.1). Following Manoukas and Athanatopoulou (2018), the costs per unit weight of concrete and steel are assumed equal to 150 €/m^3 and 875 €/t, respectively. These costs include materials, labour cost and social security expenses.

The costs of non-structural components are based on data collected using personal contacts with engineers, construction price indices, as well as expert judgement, while they can be taken as a percentage of the replacement cost (Martins et al. 2016; Manoukas and Athanatopoulou 2018). Following FEMA P-58 (ATC 2012a,b), the cost of the foundations is not included in the analysis.

Table 5.3 Construction costs of the components of the four models

Components	€/m^2	% of total construction cost of each model			
		PGA_d=0.0g	PGA_d=0.1g	PGA_d=0.3g	PGA_d=0.5g
RC slab	100	13.72	13.70	13.33	12.98
Flooring	90	12.35	12.33	12.00	11.68
Aluminium/iron works	81	11.12	11.10	10.80	10.52
Encasement, Skirting	77	10.50	10.48	10.20	9.93
Plaster, Paint	67	9.16	9.14	8.89	8.66
Hydraulic system	52	7.16	7.15	6.96	6.78
Electrical system	45	6.18	6.17	6.00	5.84
Windows, Doors	44	6.05	6.04	5.88	5.72
Infills (0.0g/0.1g/0.3g/0.5g)	39/36/32/29	5.39	5.00	4.32	3.82
Heating system	38	5.19	5.18	5.04	4.91
Elevator	23	3.21	3.21	3.12	3.04
Columns & beams (0.0g/0.1g/0.3g/0.5g)	23/27/51/74	3.14	3.66	6.82	9.64
Partitions	18	2.41	2.41	2.34	2.28
Insulation, Waterproofing	14	1.85	1.85	1.80	1.75
Flue, Drainage system	9	1.24	1.23	1.20	1.17
Gas system	6	0.86	0.86	0.84	0.82
Doors	4	0.48	0.48	0.47	0.46

Table 5.3 reports the cost per m^2 (of the total area) of the building components for each PGA_d level considered. In addition, these costs are expressed as a percentage of the total construction cost (of each PGA_d level) in the same table. Similar to other research works (Taghavi and Miranda, 2003; Porter 2016) the structural elements are found to contribute to only 17% to 23% of the total cost, depending on the design level. The total construction cost of the structural and the non-structural components is found to be equal to 655,840 €, 656,778 €, 675,161 € and 693,205 € for PGA_d equal to 0.0g, 0.1g, 0.3g and 0.5g, respectively. With the total area of the building being equal to 900 m^2, this gives a range of the total cost between 729 €/m^2 and 770 €/m^2, which is similar to the values considered in other studies (Manoukas and Athanatopoulou 2018; Kappos and Dimitrakopoulos 2008; Lagaros 2007). An idea of the cost of seismic

design is obtained by normalizing the costs for different PGA_d levels by the cost for PGA_d= 0.0g. This gives a relative difference of 0.1%, 2.9% and 5.7% for the models designed for 0.1g, 0.3g and 0.5g, respectively, when compared to the total cost of the non-seismically-designed one (i.e. PGA_d= 0.0g).

The obtained values show that the cost of seismic design is not significant, compared to the total construction cost. Similar conclusions were made in the past by other researchers. Almost five decades ago, Whitman et al. (1974) investigated the change of initial cost for different seismic design levels. For low-rise RC buildings, it was found that the cost of seismic design was less than 5%. In NEHRP (2012), a construction cost increase of up to 3% with respect to the design for wind loads only was reported for six buildings in Memphis, Tennessee. In Porter (2016) a 50% upgrade from the life-safety minimum of the US codes increased the construction cost by only 1%.

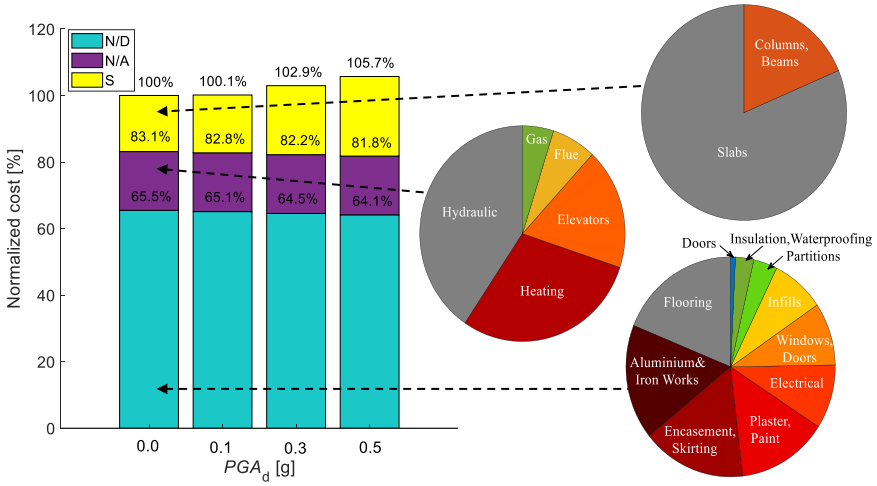

Figure 5.12 Contribution of each component to the initial construction cost

Figure 5.12 presents a disaggregation of the total costs into the various components, classified as structural (S), non-structural drift-sensitive (N/D), and non-structural acceleration-sensitive (N/A). It is evident that the majority of the cost is attributed to the non-structural drift-sensitive components (for the case study and the considered assumptions), while the cost of the acceleration-sensitive components is comparable to the cost of the structural elements.

Figure 5.13 presents the initial construction cost across Europe, when the building of the case study is designed using the PGA_d^{UH} values for the 475-yrs return period. The values are normalized to the initial cost at the site with the highest hazard (i.e. 707,609 €), and the difference at the site with lowest hazard is below 7%. This normalization is made because possible differences in construction costs across Europe are disregarded in this study.

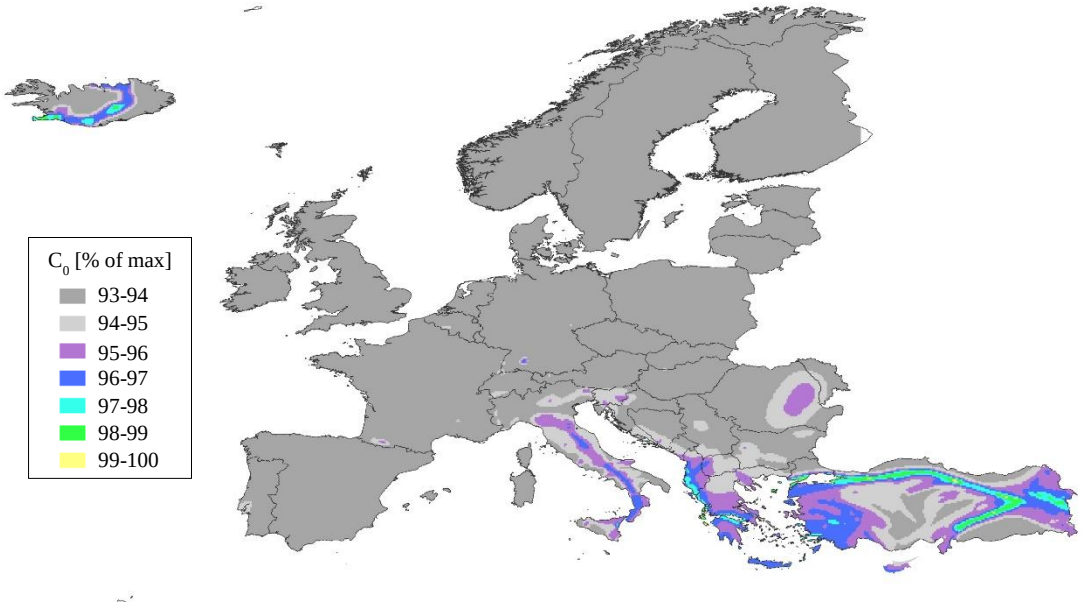

Figure 5.13 Normalized initial construction costs when designing with the UH approach

5.3.8 Future losses

According to Eqn.(5.4), the losses due to future earthquakes are a function of the vulnerability of the structural and non-structural components (probability of exceeding a given amount of loss conditional on the *PGA* level) and the hazard of the location. Thus, the fragility curves of each component are transformed into vulnerability curves with Eqn.(5.5), using the cost data of the previous sections and the damage percentages of Table 5.2, while alternatively specific repair interventions can be costed (Martins et al. 2016). The replacement cost is considered herein equal to the initial construction cost ($C_r = C_0$). The resulting vulnerability curves (normalized to the construction cost of each model) are presented in Figure 5.14a to Figure 5.14d, together with the contribution of the S, N/D, and N/A components. Generally, the N/D components

contribute most to the total vulnerability, while S and N/A have almost the same impact.

In Figure 5.14e to Figure 5.14h, the vulnerability is disaggregated into the two contributions of the non-collapse (NC) and collapse (C) cases, according to Eqn.(5.5). For low seismic intensities, the losses are dominated by the NC scenario, while at high intensities the losses are mainly dominated by the collapse scenario. As expected, by increasing the design acceleration the contribution of the C cases to the total vulnerability decreases. For instance, for *PGA*=2g, the percentage of the total losses that is attributed to the collapse cases is equal to 88%, 75%, 59% and 48% when the structure is designed with a PGA_d equal to 0.0g, 0.1g, 0.3g and 0.5g, respectively. Also, it is interesting to observe that the *PGA* level at which the C and NC cases contribute equally to the total losses increases for increasing PGA_d (i.e. *PGA* equal to 0.6g, 1.1g, 1.5g and 2.1g for PGA_d equal to 0.0g, 0.1g, 0.3g and 0.5g, respectively).

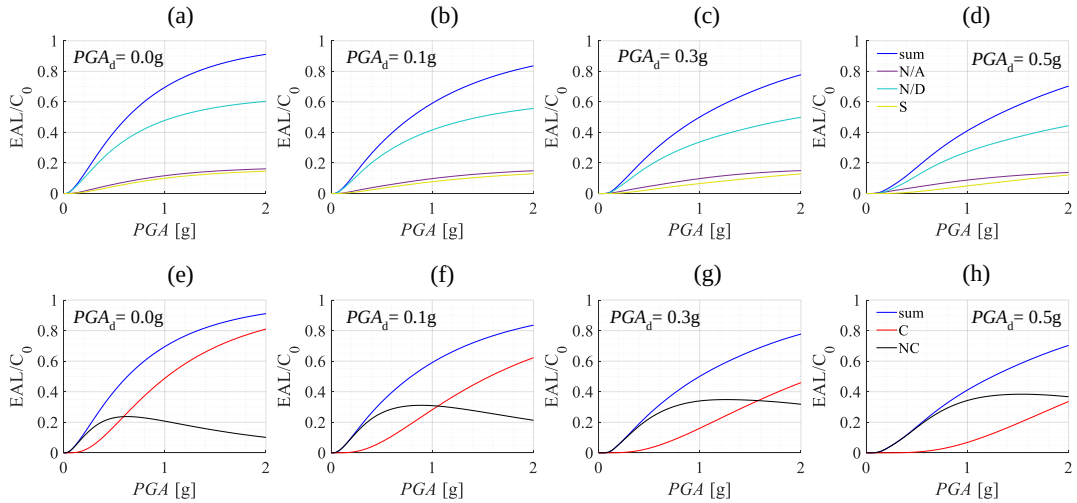

Figure 5.14 Disaggregation of the vulnerability curves of the models into: (a to d) S, N/D and N/A components, (e to h) C and NC cases

The expected annual losses (EAL) for the structure built considering different PGA_d at a particular location can be obtained via convolution of the hazard curve for the site and the vulnerability curves. Figure 5.15a shows the EAL obtained for Patras (21.75°E, 38.24°N), a Greek city of high seismicity. The EAL are normalized by dividing them by the EAL for PGA_d=0.0g, i.e., 4,850 €. A disaggregation of the losses at different levels of ground motion intensities, indicated that 90% of the total EAL

losses derive from *PGA* levels lower than 0.4g, 0.4g, 0.5g and 0.7g for the models designed with PGA_d equal to 0.0g, 0.1g, 0.3g and 0.5g, respectively. It can be observed that while the losses due to the drift sensitive components damage are decreased when increasing the PGA_d level, that is not the case for the acceleration sensitive components (see also Figure 5.14a to Figure 5.14d). This is reasonable, since the structure becomes stiffer and thus undergoes higher absolute accelerations (and lower displacements), as already observed in the response spectra of Figure 5.6. The loss disaggregation of Figure 5.15b highlights the importance of considering the NC case in the loss assessment process, since the contribution of the collapse scenario which is less frequent is only a small percentage of the total losses.

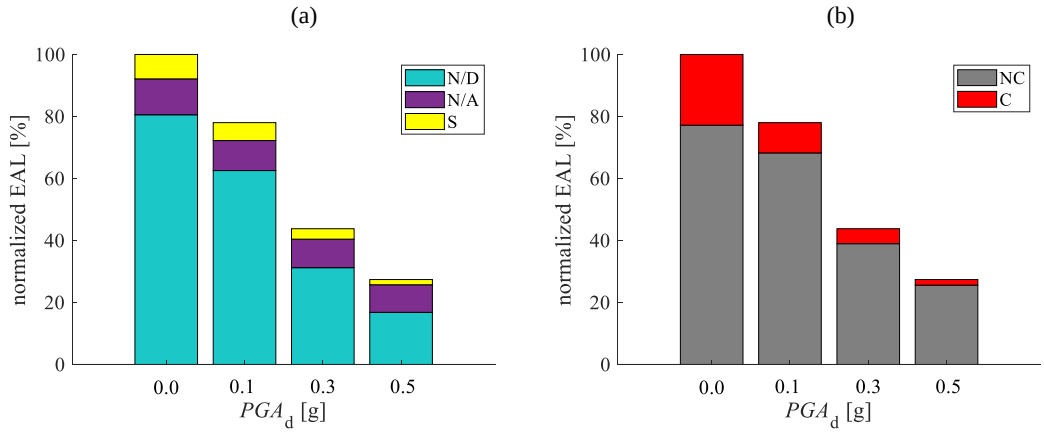

Figure 5.15 Expected annual losses for Patras: (a) contribution of S, N/D and N/A components, and (b) contribution of C and NC cases

Additional losses can also be considered when estimating future losses, usually from the following contributions (Lagaros, 2007): loss of contents (unit contents cost · floor area · mean damage index); rental loss (rental rate · gross leasable area · loss of function), which refers to the loss of rental income to the owner until functionality is restored; income loss (rental rate · gross leasable area · down time), which refers to buildings that are used for commercial reasons; cost of minor injuries, cost of serious injuries, and cost of human fatalities (cost per person · floor area · occupancy rate · expected rate).

It is noted that usually the losses are categorized as direct and indirect, but the terms can have different meanings within various projects [see e.g. the difference between

Kappos and Dimitrakopoulos (2008) and Kircher et al. (2006)]. Also, different stakeholders (e.g. engineers, homeowners, insurance companies) may focus on different types of losses (e.g. contents loss considered or studied separately). To avoid confusion, two extreme cases are studied herein: losses due to repair/replacement costs and additional losses.

The previous vulnerability analysis is repeated considering the repair/replacement costs and the additional losses in the minimum-cost design. Similarly to Lagaros (2007), 250 €/m^2 is assumed for the loss of contents, while the rates for the calculation of the rental and income losses are 7 €/m^2/month and 2,000 €/m^2/year, respectively. For the minor injury, serious injury and fatality cost rates, 5,000 €/person, 50,000 €/person and $2.5 \cdot 10^6$ €/person, are used, together with the assumption of 2 persons per 100 m^2. It is also assumed that the down time required in the extreme case of collapse is 18 months, based on Manoukas and Athanatopoulou (2018).

The contents are treated as acceleration sensitive components (FEMA P-58), and thus their damage states are defined based on acceleration thresholds. For simplicity, it is assumed that half of the losses are reached at a level of 0.55g, and the rest for accelerations higher than 1.2g. The rest of the additional losses are attributed to the structural damage, and thus they are calculated using the cost rates of Table 5.4, based on the damage state thresholds of the RC members.

Table 5.4 Cost rates depending on the damage state (Lagaros, 2007)

Damage state	Mean damage index [%]	Loss of function [%]	Down time [%]	Exp. minor injury rate [%]	Exp. serious injury rate [%]	Exp. death rate [%]
1	0	0	0	0	0	0
2	0.5	0.9	0.9	0	0	0
3	5	3.33	3.33	0	0	0.00074
4	20	12.4	12.4	0	0.032	0.009
5	45	34.8	34.8	2.6	0.35	0.09
6	80	65.4	65.4	27	3.6	0.9
7	100	100	100	35.7	35.7	18

The vulnerability curves of the case-study models considering both the repair/replacement costs and the additional losses are presented in Figure 5.16,

disaggregated into C and NC cases. The EAL are divided by the initial construction cost of each model.

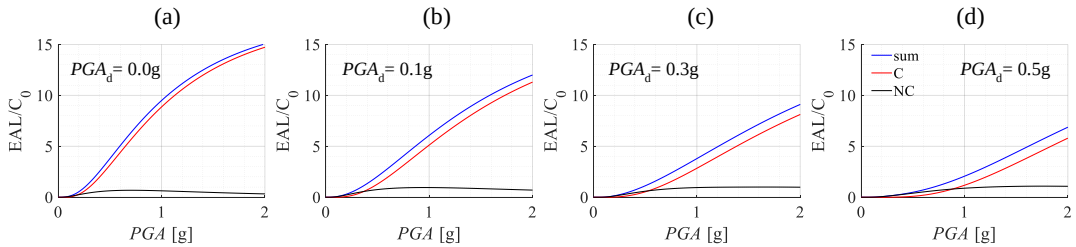

Figure 5.16 Normalized vulnerability curves including the additional losses, disaggregated into C and NC cases

The result of the loss analyses for the building located in Patras are shown in Figure 5.17a, where the repair cost and additional losses are presented separately, for each PGA_d (normalized to the total EAL for the 0.0g case, i.e. 28,603€). In this example, it can be observed that the fatalities, the income loss, and the repair cost contribute most to the overall EAL.

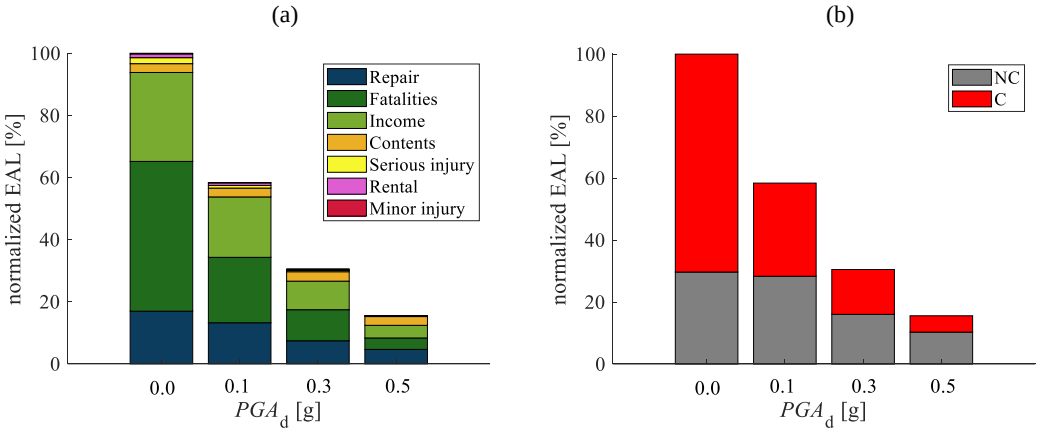

Figure 5.17 Consideration of additional losses: (a) contribution of repair cost and additional losses to the total EAL (normalized) and (b) contribution of C and NC cases, for different design levels

Figure 5.17b shows the contribution of the collapse and non-collapse scenarios to the total EAL. It can be observed that for a building designed with no seismic provisions the collapse scenario dominates the losses with a contribution of about 70%, whereas in the case of seismic design acceleration of 0.5g, the losses from the collapse scenario are about a third of the EAL. This is attributed to the fact that the annual collapse risk

levels for the two cases have an order of magnitude difference (10^{-3} and 10^{-4}) and the fatalities and income losses that contribute most (see Figure 5.17a) are linked with the collapse scenario, as mentioned above. A further disaggregation of the losses at different levels of ground motion intensities, indicates that 90% of the total expected annual losses derive from *PGA* levels lower than 0.8g, 0.8g, 0.9g, and 1g, for a PGA_d equal to 0.0g, 0.1g, 0.3g, 0.5g, respectively.

Figure 5.18a shows the EAL for repair/replacement across Europe for the building designed following the uniform hazard approach, i.e., based on the PGA_d^{UH} level that corresponds to a probability of exceedance of 10%-in-50-years. The EAL obtained considering also the additional losses are shown in Figure 5.18b. The areas with highest EAL are mainly in southern Europe (e.g. Greece, Turkey, Italy and Romania) and the maximum values for the EAL when considering only the repair cost is 2,455 €, which is increased to 7,609€ when additional losses are included.

The future losses for a period of t years and a discount factor λ can be easily estimated by multiplying the EAL of Figure 5.18 with the factor $(1-e^{-\lambda \cdot t})/\lambda$, according to Eqn.(5.3), and the expected life-cycle cost, *E*[*LCC*], can then be obtained by adding the initial construction costs, following Eqn.(5.2). Figure 5.19 shows the results obtained considering a design period of 50 years and a 3% discount rate. The maximum value of the *E*[*LCC*] calculated only with the repair/replacement costs is found to be 766,246€. This increases to 898,912 € when additional losses are considered.

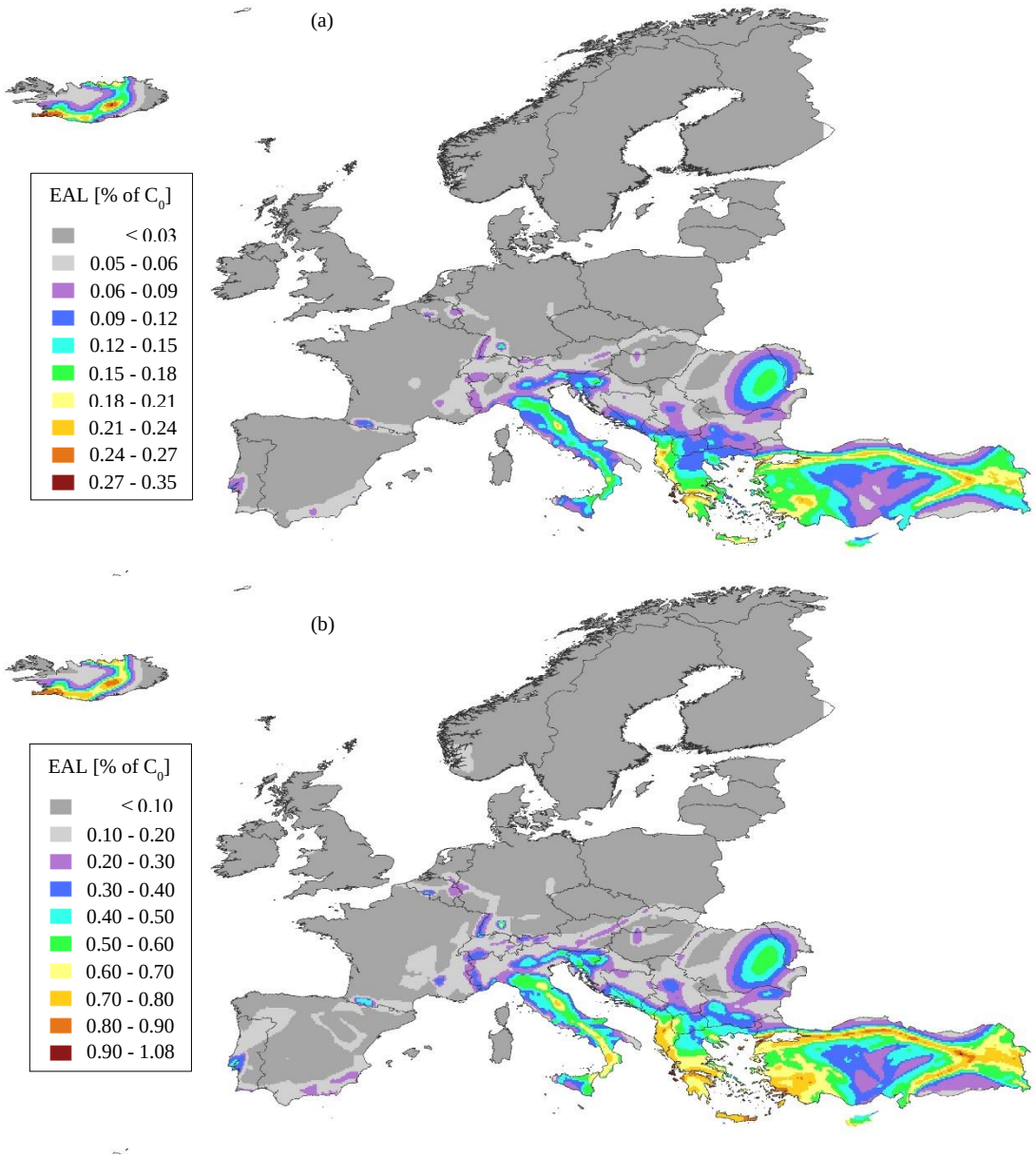

Figure 5.18 Expected annual losses across Europe (% the construction cost), for the building designed with the UH approach considering the repair costs (a) without, and (b) with additional losses (notice the scale difference)

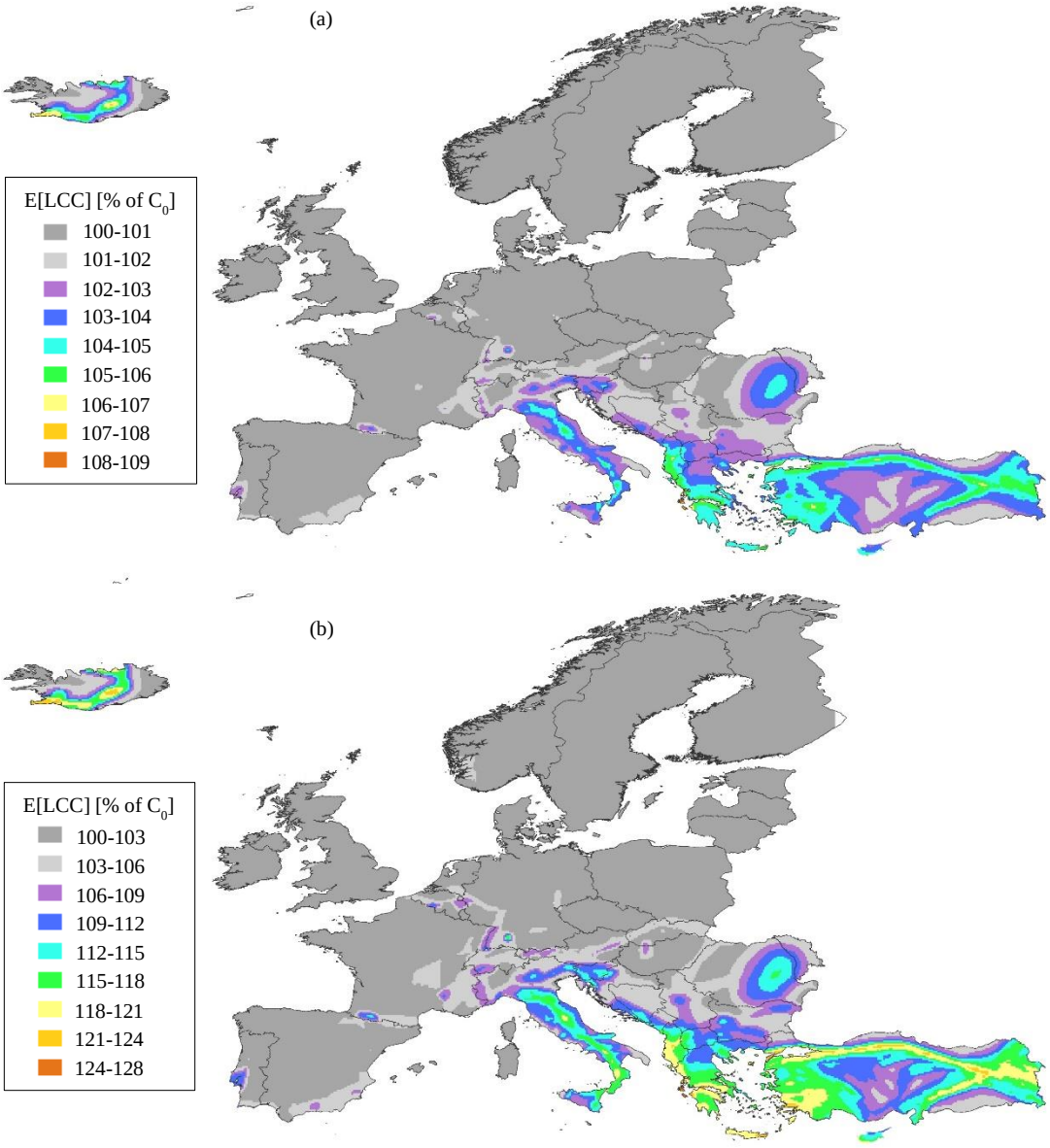

Figure 5.19 Expected life-cycle cost across Europe (% of the construction cost), obtained using the UH design approach, considering the repair costs (a) without, and (b) with the additional losses (notice the scale difference)

5.3.9 Minimum-cost analyses

This subsection shows the application of the minimum cost-based design approach of Figure 5.2 for the example building placed in different locations across Europe. Figure 5.20a shows the initial costs, the future losses and their sum, $E[LCC]$, for Patras for different values of PGA_d. The expected losses refer to a period of 50 years, while a discount factor 3% is applied. The minimum-cost design acceleration, PGA_d^{MC}, is the

one that minimizes the total cost, which is lower than the one that minimizes the total losses.

Figure 5.20a shows the effect of accounting for additional losses (see previous section) in the minimum-cost design, which results in an increase of the design *PGA*. In fact, when only the repair cost is considered, PGA_d^{MC} equals 0.42g, whereas a value of 0.67g is obtained if additional losses are considered. It is noteworthy that in the vicinity of PGA_d^{MC}, the losses have a small variation with PGA_d, which leads to small difference of the total costs obtained designing with UH and the minimum-cost approaches. The reduced variation of the total costs with the PGA_d is due to fact that they depend on the initial costs, which also exhibit a reduced variation. Also, while the losses attributed to the drift sensitive components are reduced when increasing the design level, this is not the case for the acceleration sensitive ones (see e.g. Figure 5.15).

Figure 5.20b provides an alternative illustration of the application of the method, where the cost of 'seismic design' is considered instead of the initial construction cost. The cost of seismic design is defined as the additional money one must invest to make the structure resistant to a given PGA_d level, compared to the case with no seismic provisions (0.0g). Of course, the representation of Figure 5.20b provides the same value of PGA_d^{MC} as the representation of Figure 5.20a, since the location of the minimum value of the total costs is not affected by a constant translation along the vertical axis.

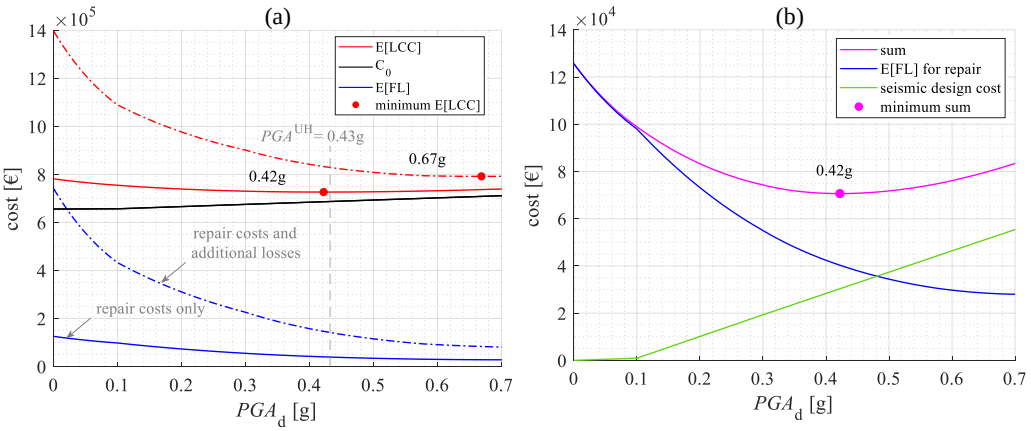

Figure 5.20 Minimum-cost design for Patras using: (a) the initial cost, and (b) the seismic design cost

The minimum-cost design is carried out for every location across Europe, and the obtained PGA_d^{MC} values are shown in Figure 5.21a. Comparing the results with the PGA_d^{UH} of Figure 5.9, a general reduction of the design acceleration values is observed when considering only the repair costs, while on the contrary the values are increased if the additional losses are included (Figure 5.21b).

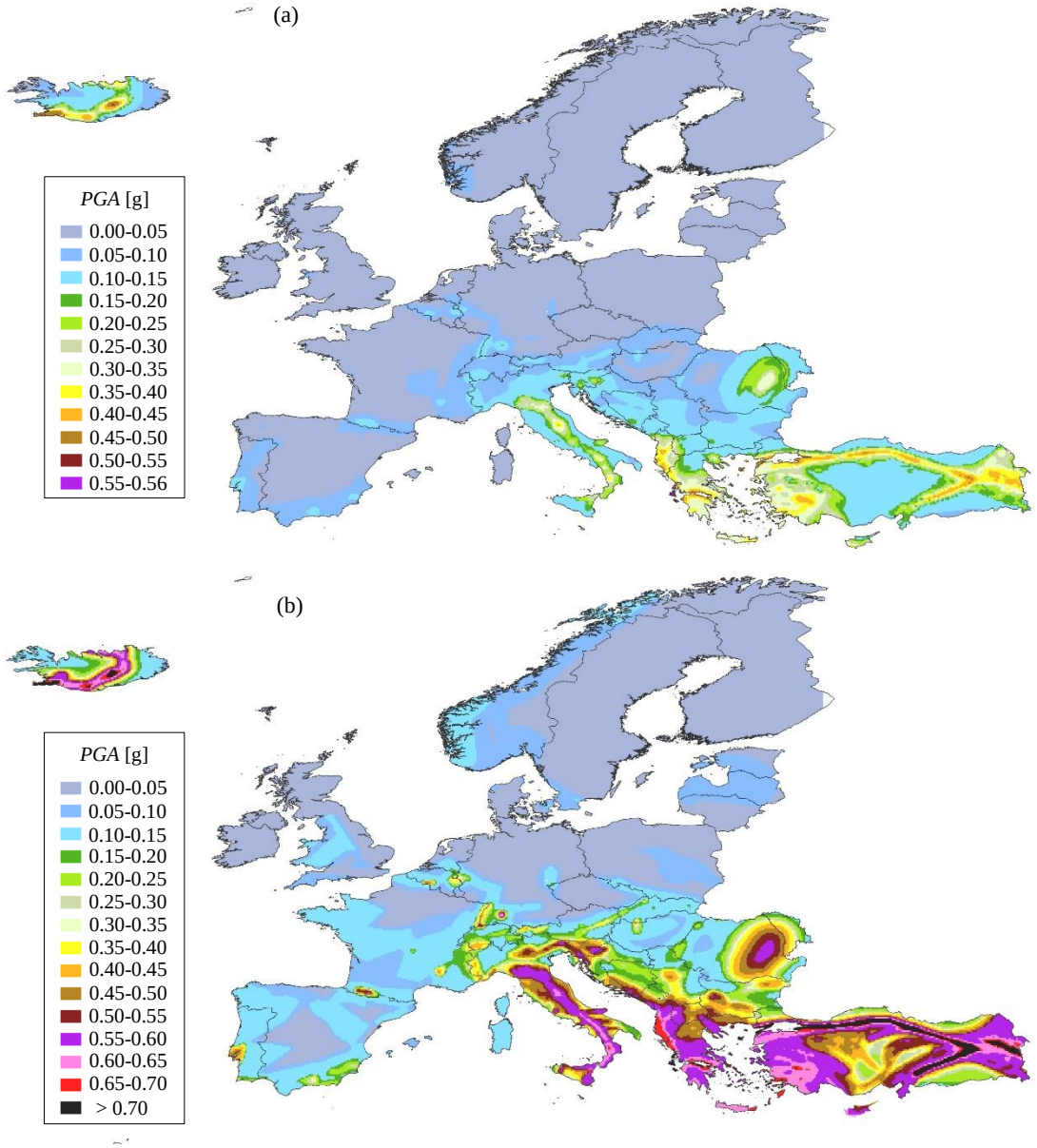

Figure 5.21 Design *PGA* values (site class A) obtained with the minimum-cost approach, considering the repair cost (a) without, and (b) with additional losses

It is highlighted that designing with PGA_d^{MC} does not guarantee that the MAF of collapse of the structure is below the predefined acceptable risk level. In this regard, it could be useful to combine the results of the minimum-cost and the risk-targeting approaches to find the acceleration that minimizes the total building costs, while also satisfying the constraint on the acceptable risk level. This 'minimum-cost risk-targeted' design acceleration corresponds for a given location to the maximum of the risk-targeted (Figure 5.11) and the minimum-cost value (Figure 5.21).

When only the repair costs are considered, the $E[LCC]$ with the minimum-cost approach is almost the same as that obtained with the UH approach (Figure 5.19). This is mainly the result of the reduced variation of the total cost in the surrounding of PGA_d^{MC}, as discussed above in the example for Patras (Figure 5.20a). Even when the additional losses are also included together with the repair costs, the differences are still lower than 6%. This can be observed in Figure 5.22, which illustrates the ratio of the $E[LCC]$ obtained when designing with the minimum-cost approach over that obtained with the uniform-hazard approach (Figure 5.19).

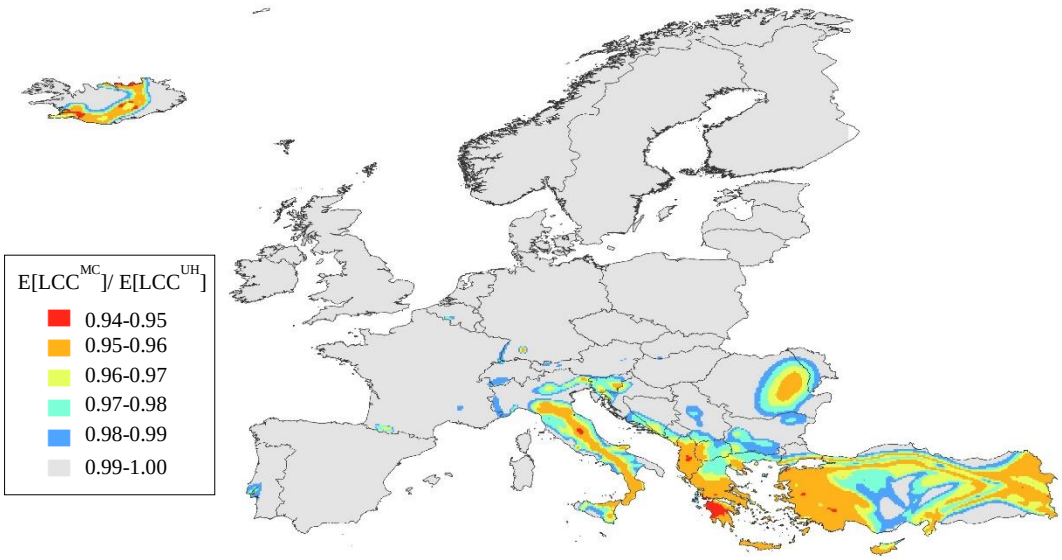

Figure 5.22 Comparison of the expected life-cycle cost obtained with the MC and UH approaches, considering the repair cost and additional losses

Studies on retrofit measures for existing structures consider the benefit-to-cost ratio (Calvi 2013; Padgett et al. 2010; Kappos and Dimitrakopoulos 2008) to compare the benefit from the loss reduction due to retrofitting to the cost of the intervention. The same concept can be used to evaluate the economic significance of minimum-cost design. The benefit to cost ratio in this case can be defined as the change of future losses when increasing the design acceleration from 0 to the PGA_d^{MC}, divided by the seismic design cost (increase in the initial construction cost due to this change). It is understandable that the higher the value of the ratio, the more beneficial is the implementation of minimum-cost design. In the example for the repair costs in Patras (Figure 5.20b) this ratio is roughly equal to 3, and is 4 times higher when additional losses are considered, too.

Figure 5.23 shows the values of benefit-to-cost ratios across Europe, considering a period of 50 years and a 3% discount rate. These ratios can provide decision makers with information on the benefit of seismic design, compared to the design carried out disregarding the seismic loads. It is noteworthy that for very low values of PGA_d^{MC} (close to 0.1g), the initial cost is not significantly increased compared to the no-seismic provision case. This explains why high values of the ratios are obtained for some regions (e.g. Belgium, Slovakia) with relatively low PGA_d^{MC} (see Figure 5.21). For the rest of Europe, it can be concluded that these ratios have roughly a maximum value of 10 for the repair costs case, and 25 if the additional losses are included.

A similar comparison between the results of the MC and UH approaches, not shown due to space constraints, gives much lower values of these ratios. For the areas of interest (PGA_d^{MC} higher than 0.2g), the ratios are close to unity when only the repair/replacement costs are considered and less than 2.5 when the additional losses are included as well.

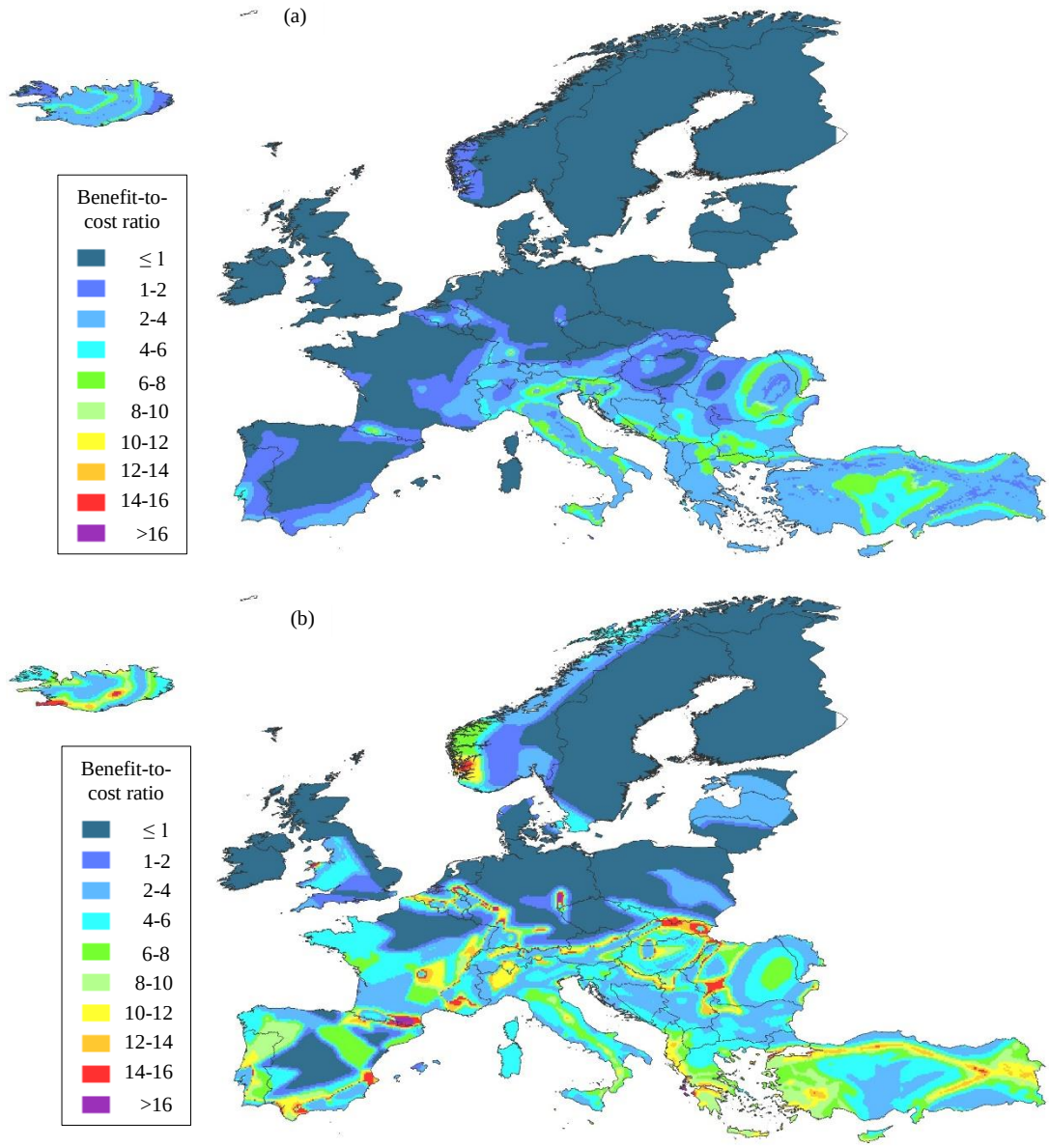

Figure 5.23 Benefit-to-cost ratios considering the repair cost (a) without, and (b) with the additional losses

5.4 Conclusions

The aim of this chapter is to review and compare three different approaches for seismic design, namely the uniform-hazard (UH), the risk-targeted (RT), and the minimum-cost (MC) approaches. For this purpose, an example 4-storey 3-bay reinforced concrete frame building placed in different locations across Europe is considered. First, the methodologies for implementing the three approaches are briefly reviewed. Then, a comparison of the effectiveness of the approaches is carried out based on safety

and costs considerations. The evaluation presented in this chapter is case-specific and therefore future studies on different building types are necessary to generalize the following conclusions:

- Using the UH design acceleration results in inconsistent levels of the risk across Europe, as already observed in past studies. The attained risk levels for the case-study building are generally within the acceptable risk limits proposed by the US regulations (except for some high hazard areas).
- The impact of the design seismic intensity (PGA_d) on the initial construction cost is small, due to the high contribution of the non-structural components, the cost of which is not dependent on the PGA_d.
- A small variation of the losses with the PGA_d levels has been noticed when only the damage of the structure is assessed. This variation is increased when additional losses are also included in the analysis.
- The life-cycle cost when designing with the UH approach is not far from that obtained using the MC method.
- A benefit-to-cost analysis has shown that there are many areas in Europe where seismic design is highly cost-beneficial in terms of life-cycle cost, compared to no seismic provisions.

The fact that the initial construction costs do not increase significantly by increasing the design *PGA* may suggest that higher performance levels could be targeted by seismic codes, since this would allow an increased safety to be achieved without increasing greatly the costs of the design. However, the economic benefits stemming from considering the optimal design *PGA* that minimizes the total life cycles costs instead of the *PGA* levels currently considered by seismic codes are not significant. Thus, a revision of design approaches in seismic codes is not warranted on the basis of the results of this study, given the fact that considering life-cycle cost analysis concepts in the design would make the design process more complicated to practicing engineers. It is recalled, however, that this conclusion is based on only a single example building type and hence it may not hold for other buildings.

References

Akkar S, Sandikkaya MA, Senyurt M, Azari Sisi A, Ay BÖ, Traversa P, Douglas J, Cotton F, Luzi L, Hernandez B, Godey S (2014) Reference database for seismic ground-motion in Europe (RESORCE), Bulletin of Earthquake Engineering, 12(1): 311-339, doi: 10.1007/s10518-013-9506-8

ASCE (2017) Minimum Design Loads and Associated Criteria for Buildings and Other Structures, ASCE/SEI 7-16. American Society of Civil Engineers, Reston, VA

ATC - Applied Technology Council, FEMA P-58 (2012a) Seismic Performance Assessment for Buildings, Volume 1 – Methodology, Federal Emergency Management Agency, Washington, D.C

ATC - Applied Technology Council, FEMA P-58 (2012b) Seismic Performance Assessment for Buildings, Volume 2 – Implementation Guide, Federal Emergency Management Agency, Washington, D.C

Baker JW (2015) Introduction to Probabilistic Seismic Hazard Analysis, White Paper Version 2.1, 77 pp

Braga F, Manfredi V, Masi A, Salvatori A, Vona M (2011) Performance of non-structural elements in RC buildings during the L'Aquila, 2009 earthquake. Bulletin of Earthquake Engineering, 9(1), 307-324

Calabrese A, Almeida JP, Pinho R (2010) Numerical issues in distributed inelasticity modeling of RC frame elements for seismic analysis. Journal of Earthquake Engineering, 14(S1), 38-68. doi: 10.1080/13632461003651869

Calvi GM (2013) Choices and Criteria for Seismic Strengthening. Journal of Earthquake Engineering, 17, 769-802

Cardone D, Gesualdi G, Perrone G (2019) Cost-benefit analysis of alternative retrofit strategies for RC frame buildings. Journal of Earthquake Engineering, 23(2), 208-241

Cardone D, Perrone G (2015) Developing fragility curves and loss functions for masonry infill walls. Earthquakes and Structures, 9(1), 257-279

Cardone D, Perrone G (2017) Damage and loss assessment of pre-70 RC frame buildings with FEMA P-58. Journal of Earthquake Engineering, 21(1), 23-61

CEN (2002) EN 1990:2002+A1 Eurocode – Basis of structural design, European Committee for Standardization, Brussels

CEN (2004a) EN 1992-1-1:2004 Eurocode 2: Design of concrete structures - Part 1-1: General rules and rules for buildings, European Committee for Standardization, Brussels

CEN (2004b) EN 1998-1:2004 Eurocode 8: Design of structures for earthquake resistance - Part 1: General rules, seismic actions and rules for buildings, European Committee for Standardization, Brussels

Chopra AK (1995) Dynamics of Structures: Theory and Applications to Earthquake Engineering, Prentice-Hall.

Collins KR, Wen YK, Foutch DA (1996) Dual-level seismic design: a reliability-based methodology. Earthquake Engineering & Structural Dynamics, 25(12), 1433-1467

Cornell CA (1968) Engineering seismic risk analysis. Bulletin of the seismological society of America, 58(5), 1583-1606

Crowley H, Silva V, Bal IE, Pinho R (2012) Calibration of Seismic Design Codes using Loss Estimation. In Proceedings of 15th World Conference on Earthquake Engineering, Lisbon, Portugal.

De Luca F, Verderame GM, Gómez-Martínez F, Pérez-García A (2014) The structural role played by masonry infills on RC building performances after the 2011 Lorca, Spain, earthquake. Bulletin of Earthquake Engineering, 12, 1999-2026, doi: 10.1007/s10518-013-9500-1

De Risi MT, Del Gaudio C, Verderame GM (2019) Evaluation of Repair Costs for Masonry Infills in RC Buildings from Observed Damage Data: the Case-Study of the 2009 L'Aquila Earthquake. Buildings, 9(5), 122

Decanini L, Mollaioli F, Mura A, Saragoni R (2004) Seismic performance of masonry infilled R/C frames. In 13th world conference on earthquake engineering (No. 165)

Decanini LD, Liberatore L, Mollaioli F (2014) Strength and stiffness reduction factors for infilled frames with openings. Earthquake Engineering and Engineering Vibration, 13(3), 437-454

Douglas J, Ulrich T, Negulescu C (2013) Risk-targeted seismic design maps for mainland France, Natural Hazards, 65(3), 1999–2013

Ellingwood BR, Wen YK (2005) Risk-benefit-based design decisions for low-probability/high consequence earthquake events in Mid-America. Progress in Structural Engineering and Materials, 7(2), 56-70

Fajfar P (2018) Analysis in seismic provisions for buildings: past, present and future. Bulletin of Earthquake Engineering, 16, 2567–2608, doi: 10.1007/s10518-017-0290-8

Fardis MN, Papailia A, Tsionis G (2012) Seismic fragility of RC framed and wall-frame buildings designed to the EN-Eurocodes. Bulletin of Earthquake Engineering, 10(6), 1767-1793

FEMA (2009) NEHRP Recommended Seismic Provisions for New Buildings and Other Structures (FEMA P750). Federal Emergency Management Agency

Gehl P, Douglas J, Seyedi D (2015) Influence of the number of dynamic analyses on the accuracy of structural response estimates, Earthquake Spectra, 31(1): 97-113, doi: 10.1193/102912EQS320M

Ghobarah A (2004) On drift limits associated with different damage levels, Proceedings of international workshop on performance-based seismic design concepts and implementation, June 28th–July 1st, 2004, Bled, Slovenia

Giardini D. et al. (2013) Seismic Hazard Harmonization in Europe (SHARE): Online Data Resource, doi: 10.12686/SED-00000001-SHARE.

Hak S, Morandi P, Magenes G, Sullivan TJ (2012) Damage control for clay masonry infills in the design of RC frame structures. Journal of Earthquake Engineering, 16(sup1), 1-35

Iervolino I, Spillatura A, Bazzurro P (2018) Seismic reliability of code-conforming Italian buildings. Journal of Earthquake Engineering, 22(s2), 5-27

Jeong SH, Mwafy AM, Elnashai AS (2012) Probabilistic seismic performance assessment of code-compliant multi-story RC buildings. Engineering Structures, 34, 527-537

Kappos AJ (1997) A comparative assessment of R/C structures designed to the 1995 Eurocode 8 and the 1985 CEB seismic code. The Structural Design of Tall Buildings, 6(1), 59-83

Kappos AJ, Dimitrakopoulos EG (2008) Feasibility of pre-earthquake strengthening of buildings based on cost-benefit and life-cycle cost analysis, with the aid of fragility curves. Natural Hazards, 45(1), 33-54

Kennedy RP (2011) Performance-goal based (risk informed) approach for establishing the SSE site specific response spectrum for future nuclear power plants. Nucl Eng Des 241:648–656

Kircher CA, Whitman RV, Holmes WT (2006) HAZUS earthquake loss estimation methods. Natural Hazards Review, 7(2), 45-59

Lagaros ND (2007) Life-cycle cost analysis of design practices for RC framed structures. Bulletin of Earthquake Engineering, 5(3), 425-442

Luco N, Ellingwood BR, Hamburger RO, Hooper JD, Kimball JK, Kircher CA (2007) Risk-targeted versus current seismic design maps for the conterminous United States. In: SEAOC 2007 convention proceedings

Mander JB, Priestley MJN, Park R (1988) Theoretical stress-strain model for confined concrete, Journal of Structural Engineering, Vol. 114, No. 8, pp. 1804-1826

Manoukas GE, Athanatopoulou AM (2018) Safety vs. Economy in Performance-Based Design of Buildings: Inevitable Compromise or False Dilemma?. Journal of Earthquake Engineering, 22(4), 687-707

Martins L, Silva V, Bazzurro P, Marques M (2018) Advances in the derivation of fragility functions for the development of risk-targeted hazard maps. Engineering Structures, 173, 669-680

Martins L, Silva V, Marques M, Crowley H, Delgado R (2016) Development and assessment of damage-to-loss models for moment-frame reinforced concrete buildings. Earthquake Engineering & Structural Dynamics, 45(5), 797-817

McGuire RK (2008) Probabilistic seismic hazard analysis: early history. Earthquake Engineering and Structural Dynamics, 37, 329–338, doi: 10.1002/eqe.765

Menegotto M, Pinto PE (1973) Method of analysis for cyclically loaded R.C. plane frames including changes in geometry and non-elastic behaviour of elements

under combined normal force and bending, Symposium on the Resistance and Ultimate Deformability of Structures Acted on by Well Defined Repeated Loads, International Association for Bridge and Structural Engineering, Zurich, Switzerland

Mwafy AM (2001) Seismic Performance of Code-designed RC Buildings. PhD thesis, Imperial College, London

NEHRP Consultants Joint Venture (2013) Cost Analyses and Benefit Studies for Earthquake-Resistant Construction in Memphis, Tennessee. NIST GCR 14-917-26. National Institute of Standards and Technology, Gaithersburg MD

NTC - Norme Tecniche per le Costruzione (2018) Aggiornamento delle Norme tecniche per le costruzioni, decreto 17-1-2018, Gazzetta Ufficiale 42, 20-02-2018, Ordinary Suppl. n. 8 (in Italian)

Ordaz M, Salgado-Gálvez MA, Pérez-Rocha LE, Cardona OD, Mena-Hernández U (2017) Optimum Earthquake Design Coefficients Based on Probabilistic Seismic Hazard Analyses: Theory and Applications. Earthquake spectra, 33(4), 1455-1474, doi: 10.1193/110116eqs189m

O'Reilly GJ, Sullivan TJ (2018) Probabilistic seismic assessment and retrofit considerations for Italian RC frame buildings. Bulletin of Earthquake Engineering, 16(3), 1447-1485

O'Reilly GJ, Perrone D, Fox M, Monteiro R, Filiatrault A (2018) Seismic assessment and loss estimation of existing school buildings in Italy. Engineering Structures, 168, 142-162

Padgett JE, Dennemann K, Ghosh J (2010) Risk-based seismic life-cycle cost–benefit (LCC-B) analysis for bridge retrofit assessment. Structural Safety, 32(3), 165-173

Panagiotakos TB, Fardis MN (2004) Seismic performance of RC frames designed to Eurocode 8 or to the Greek codes 2000. Bull of Earthquake Eng 2, 221-259

Paulay T, Priestley MJN (1992) Seismic design of reinforced concrete and masonry buildings, John Wiley & Sons, New York

Perrone D, Calvi PM, Nascimbene R, Fischer EC, Magliulo G (2019) Seismic performance of non-structural elements during the 2016 Central Italy earthquake. Bulletin of Earthquake Engineering, 17(10), 5655-5677

Porter K (2016) Not safe enough: the case for resilient seismic design. In Proc, 2016 SEAOC Convention

Ramirez CM, Liel AB, Mitrani-Reiser J, Haselton CB, Spear AD, Steiner J, Deierlein GG, Miranda E (2012) Expected earthquake damage and repair costs in reinforced concrete frame buildings. Earthquake Engineering & Structural Dynamics, 41(11), 1455-1475

Ricci P, De Luca F, Verderame GM (2011) 6th April 2009 L'Aquila earthquake, Italy: reinforced concrete building performance. Bulletin of Earthquake Engineering, 9, 285-305, doi: 10.1007/s10518-010-9204-8

RINTC Workgroup (2018) Results of the 2015-2017 Implicit seismic risk of code-conforming structures in Italy (RINTC) project. ReLUIS report, Rete dei Laboratori Universitari di Ingegneria Sismica (ReLUIS), Naples, Italy, available at http://www.reluis.it/

Rivera JA, Petrini L (2011) On the design and seismic response of RC frame buildings designed with Eurocode 8. Bulletin of Earthquake Engineering, 9(5), 1593-1616

Romão X, Costa AA, Paupério E, Rodrigues H, Vicente R, Varum H, Costa A (2013) Field observations and interpretation of the structural performance of constructions after the 11 May 2011 Lorca earthquake. Engineering Failure Analysis, 34, 670-692

Sassun K, Sullivan TJ, Morandi P, Cardone D (2016) Characterising the in-plane seismic performance of infill masonry. Bulletin of the New Zealand Society for Earthquake Engineering, 49(1), 100-117

Scott MH, Fenves GL (2006) "Plastic hinge integration methods for force-based beam–column elements", ASCE Journal of Structural Engineering, Vol. 132, No. 2, pp. 244-252

Seismosoft (2020) SeismoStruct 2020 – A computer program for static and dynamic nonlinear analysis of framed structures, available from https://seismosoft.com/

Shinozuka M, Feng Q, Lee J, Naganuma, T (2000) Statistical analysis of fragility curves, Journal of Engineering Mechanics, 126: 1224–1231

Silva V, Crowley H, Bazzurro P (2016) Exploring risk-targeted hazard maps for Europe, Earthquake Spectra, 32(2), 1165-1186

Taghavi S, Miranda E (2003) Response assessment of nonstructural building elements. Pacific Earthquake Engineering Research Center

Tsang HH (2015) Evaluation of codified elastic design spectrum models for regions of low-to-moderate seismicity. Soil Dynamics and Earthquake Engineering, 70, 148-152

Tsang HH, Daniell JE, Wenzel F, Wilson JL (2020) A universal approach for evaluating earthquake safety level based on societal fatality risk. Bulletin of Earthquake Engineering, 18(1), 273-296

Tsang HH, Wenzel F (2016) Setting structural safety requirement for controlling earthquake mortality risk. Safety science, 86, 174–183

Tubaldi E, Barbato M, Ghazizadeh S (2012) A probabilistic performance-based risk assessment approach for seismic pounding with efficient application to linear systems. Structural Safety, 36, 14-22

Ulrich T, Negulescu C, Douglas J (2014) Fragility curves for risk-targeted seismic design maps. Bulletin of earthquake engineering, 12(4), 1479-1491

Vamvatsikos D (2013) Derivation of new SAC/FEMA performance evaluation solutions with second-order hazard approximation. Earthquake Engineering & Structural Dynamics, 42(8), 1171-1188

Vamvatsikos D, Cornell CA (2002) Incremental dynamic analysis. Earthquake Engineering & Structural Dynamics, 31(3), 491-514

Wen YK, Kang YJ (2001) Minimum building life-cycle cost design criteria. II: Applications. Journal of Structural Engineering, 127(3), 338-346

Whitman RV, Biggs JM, Brennan JE III, Cornell CA, de Neufville R, Vanmarcke EH (1975) Seismic Design Decision Analysis.

Woessner J, Danciu L, Giardini D, Crowley H, Cotton F, Grunthal G, Valensise G, Arvidsson R, Basili R, Demircioglu MB, Hiemer S, Meletti C, Musson RW, Rovida AN, Sesetyan K, Stucchi M and The SHARE Consortium (2015) The 2013 European Seismic Hazard Model: Key components and results, Bulletin of Earthquake Engineering, 13(12), 3553-3596, doi: 10.1007/s10518-015-9795-1

CHAPTER 6

Sensitivity of seismic risk and loss estimates to the input hazard model

Different studies indicate the high sensitivity of seismic risk estimates for structures to the definition of the seismic hazard of a site. The uncertainty inherent in the hazard input model is transferred to and affects the results of the structural design and of the performance assessment. This chapter aims to investigate the impact of the epistemic uncertainty in the hazard model on the structural design and consequently the attained future losses and risk levels, for a benchmark four-storey reinforced-concrete frame building. First, a comparison is performed between the hazard data from two studies for different locations in Italy, in order to assess the possible range of variation of estimated hazard levels amongst different studies. The effects of these hazard variations on the seismic design and relevant risk and losses attained for the reference building are investigated afterwards for these sites. Then a simplified approach for modelling hazard uncertainty is introduced and the effects are investigated across Europe.

6.1 Introduction

The evaluation of the seismic risk of buildings is affected by significant sources of uncertainty of different natures, i.e. aleatory and epistemic uncertainties. Seismic hazard is one of the three key components of the seismic risk, alongside vulnerability and exposure. In addition to the randomness inherent to the occurrence of the earthquakes and their intensity, there is substantial epistemic uncertainty in the definition of seismic hazard curves for a site. This is also reflected in the significant

variation of the seismic hazard data obtained from different seismic hazard studies for the same region. For example, Belvaux et al. (2014) compared the results of two different hazard studies for France, showing that the values of the mean peak ground acceleration (*PGA*) for a 475-years return period from the 2013 European Seismic Hazard Model (ESHM13) (Giardini et al. 2013; Woessner et al., 2015) are on average half of those obtained by the MATE-02 project (Martin et al. 2002). Significant differences are noted also in Germany in Grünthal et al. (2014) between the results from ESHM13 and an older hazard map. An updated PSHA for Romania was performed by Pavel et al. (2016), using data from the recent project BIGSEES (http://infp.infp.ro/bigsees/default.htm). It was observed that ESHM13 gives on average significantly lower values of *PGA* for a mean return period of 475 years. This epistemic uncertainty is also influenced by the choice of the ground motion prediction equations used for describing the seismic attenuation from the source to the site (Grünthal et al. 2018; Douglas et al. 2014; Stucchi et al. 2011; Bradley 2009).

Considering the above, this chapter aims to investigate the effect of the epistemic uncertainties inherent in the definition of the seismic hazard on the design and consequently on the seismic risk estimates, the construction costs and the expected losses for a case-study building in Europe. The design and assessment results of the four-storey reinforced-concrete (RC) frame building studied in Chapter 5 are used in this investigation. Using these data, a study is performed to evaluate the level of accuracy that is necessary in the definition of the hazard model, based on the uncertainty introduced in the cost and safety levels.

6.2 Overview of the risk and loss assessment methodology

This section presents a brief summary of Chapter 5, the results of which are used in the investigations carried out in this chapter. The study concerns a 4-storey 3-bay RC building (Figure 6.1), designed according to Eurocodes (CEN 2004a; CEN2004b) considering different levels of the design peak ground acceleration (PGA_d), namely 0, 0.1g, 0.3g, 0.5g (infills considered only in the assessment).

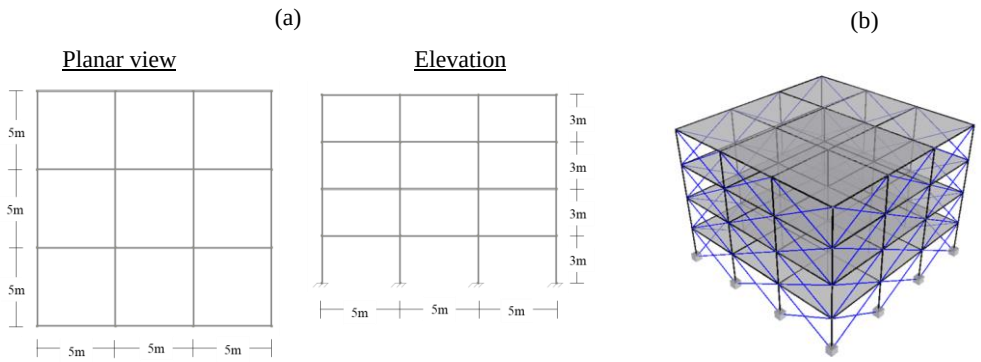

Figure 6.1 Case-study building: (a) geometry, and (b) numerical model used for nonlinear analyses

Then, using scaled ground motion records, incremental dynamic analyses (Vamvatsikos and Cornell, 2002) were performed for each model. The results were fitted using the maximum-likelihood approach (Shinozuka et al., 2000) to derive fragility curves for every component (structural and non-structural) of every storey explicitly (76 analyses for each model). A lognormal distribution function was used for the analytical expression of the fragility curves, and inter-storey drift and acceleration thresholds were defined to consider different limit state conditions of the drift-sensitive and acceleration-sensitive components.

A risk analysis was performed afterwards to evaluate the annual collapse risk of the designed models. The term risk refers to the mean annual frequency (MAF) of collapse, λ_C, and is obtained from the convolution of the fragility curve of the building (for global collapse) and the hazard curve of the assessed location, $H(IM)$. Analytically it can be expressed as (Kennedy 2011):

$$\lambda_C\left(PGA_d\right) = \int P\left(C|IM\right)\cdot\left|dH(IM)\right| \tag{6.1}$$

The hazard curve provides the MAF of exceeding various levels of the seismic intensity measure (*IM*) whereas the fragility, $P(C|IM)$, refers to the probability of collapse conditional on the *IM* level.

The construction costs for the four structures and a damage model were used to convert the fragility curves to vulnerability curves, expressing the expected value of annual losses conditional on the *IM*. Various studies were considered when conducting the

loss assessment (e.g. Wen and Kang 2001; Lagaros 2007; Kappos and Dimitrakopoulos 2008; Padgett et al. 2010; Crowley et al. 2012; Ramirez et al. 2012; Ordaz et al. 2017). The losses derive from the cost of repairing/replacing the damaged structure. In addition to these, additional losses (e.g. from personal property damage, injuries or fatalities, and loss of function of the building) can also be considered.

Following Ramirez et al. (2012), the collapse (C) and no-collapse (NC) cases are considered explicitly in the derivation of the vulnerability according to the following expression:

$$E[AL \mid IM] = E[AL \mid NC, IM] \cdot [1 - P(C \mid IM)] + C_r \cdot P(C \mid IM) \tag{6.2}$$

where the probability of collapse given the IM, $P(C \mid IM)$, is the fragility curve for the case of 'global collapse', and C_r is the associated cost.

The convolution of the vulnerability, $E[AL \mid IM]$, with the hazard gives the expected annual losses, $E[AL]$, as:

$$E[AL] = \int_0^\infty E[AL \mid IM] \cdot dH(IM) \tag{6.3}$$

The expected cost due to the future losses over a time period *t* is calculated as:

$$E[FL] = E[AL] \cdot (1 - e^{-\lambda \cdot t}) / \lambda \tag{6.4}$$

where λ is a constant discount rate/year, which converts the future losses into present monetary value.

Finally, the expected value of the life-cycle cost, $E[LCC]$, over the time period *t*, can be expressed as:

$$E[LCC] = C_0 + E[FL] \tag{6.5}$$

where C_0 is the initial construction cost and $E[FL]$ is the expected cost due to future losses.

The methodology and the results of the above study are used in the following paragraphs to investigate the effect of the hazard uncertainty on the risk and loss estimates.

In the following paragraphs the expected value of the annual losses and of the life-cycle cost when only the repair/replacement costs are considered will be referred to as EAL^r and $E[LCC^r]$, respectively. When the additional losses are also included in the estimates, the notation is changed to $EAL^{r,a}$ and $E[LCC^{r,a}]$.

6.3 Consequences of the uncertainty in the hazard data

Figure 6.2a and Figure 6.2b show the 84th percentile and 50th percentiles hazard maps obtained from the INGV project (Gruppo di Lavoro MPS 2004; Meletti and Montaldo 2007). The uncertainty results from multiple seismic source zonations and many ground-motion models within the logic tree of the seismic hazard assessment (see, e.g., Douglas et al. 2014 for a discussion of these uncertainties). The difference in the *PGA*s for a given site range between 0.005g and 0.063g, according to Stucchi et al. (2011), who give higher differences when comparing the 84th and 16th percentiles (up to 0.12g).

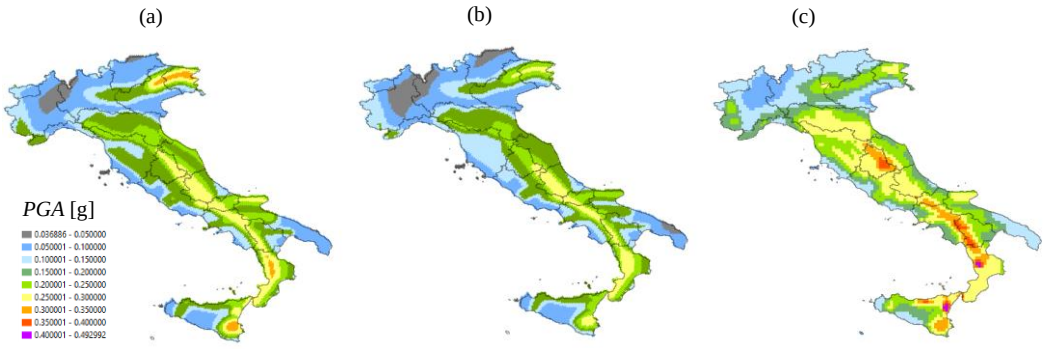

Figure 6.2 *PGA* (site class A) for 475-years return period: (a) 84th percentile from INGV, (b) median from INGV, (c) median from ESHM13

Differences can be observed between the results from different studies, too, as it can be inferred by comparing the results of Figure 6.2b with those of Figure 6.2c, showing the 50th percentile PGAs obtained from ESHM13 project. An investigation between the *PGA*s and response spectral accelerations at 1s obtained from different hazard

studies and for different percentiles can be found in Douglas et al. (2014). Thus, it is necessary to assess the impact of the hazard uncertainty on the safety of the designed structures and the cost implications. The topic is investigated in the following sections by looking at various case studies.

6.3.1 Epistemic uncertainty from different seismic hazard models for Italy

Four different locations are considered in Italy (Figure 6.3a), for which the hazard curves (50th percentiles) in terms of MAF of exceedance of the PGA (Figure 6.3b) are obtained from the INGV and ESHM13 projects. The latter gives higher values of *PGA*s for the 475-years return period, in the considered areas, as can also be noticed in Figure 6.2. That is not the case for the whole range of the *PGA* levels though, because the slopes of the INGV curves are generally steeper than those from the ESHM13 project.

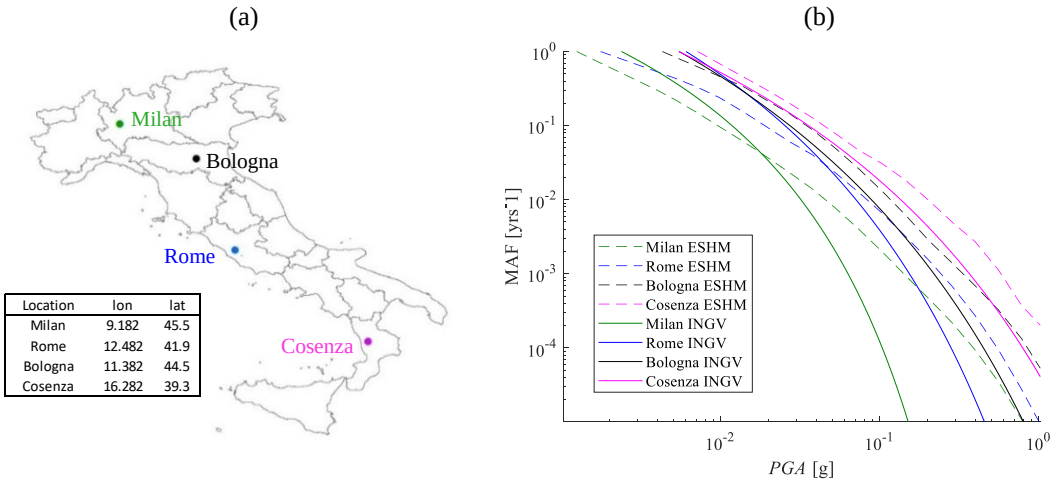

Figure 6.3 Case study for Italy: (a) selected locations, (b) hazard curves (site class A) of the locations from two projects

In the selected locations, the values of the *PGA*s corresponding to a 475-years return period are found to be 40% to 95% higher for the ESHM13 compared to INGV, as shown in Table 6.1. These differences in the hazard estimates result in a different design acceleration for the reference building, which is translated into different construction costs. The structural performance is also changed, and this affects the risk and loss levels from the expected future seismic activity. These are quantified following the procedure outlined in section 2 and the results are reported in Table 6.1.

It is clarified that class B is assumed for the soil conditions in every location, thus the hazard curves are multiplied by the soil factor 1.2, expressing the ratio between PGAs on site classes B and A in EC8.

Table 6.1 Comparison of the results for the hazard curves according to the INGV and ESHM13 hazard models

Location	Project	PGA^{UH} [g]	C_0 [€]	EAL^r [€]	$E[LCC^r]$ [€]	$EAL^{r,a}$ [€]	$E[LCC]^{r,a}$ [€]	Annual λ_C
	INGV	0.05	656323	62	657917	115	659294	$8.13 \cdot 10^{-7}$
Milan	ESHM13	0.10	656821	241	663049	821	678091	$2.61 \cdot 10^{-5}$
	dif. [%]	95.1	0.1	290.7	0.8	616.0	2.9	3110.1
	INGV	0.12	658626	438	669956	1070	686328	$1.53 \cdot 10^{-5}$
Rome	ESHM13	0.18	663719	541	677734	1829	711079	$5.78 \cdot 10^{-5}$
	dif. [%]	46.1	0.8	23.7	1.2	71.0	3.6	278.0
	INGV	0.17	662937	595	678333	1722	707538	$4.13 \cdot 10^{-5}$
Bologna	ESHM13	0.23	669049	887	692010	3246	753119	$1.17 \cdot 10^{-4}$
	dif. [%]	39.8	0.9	49.1	2.0	88.5	6.4	182.5
	INGV	0.27	672708	977	698016	3460	762300	$1.13 \cdot 10^{-4}$
Cosenza	ESHM13	0.44	687594	1379	723292	4818	812354	$1.49 \cdot 10^{-4}$
	dif. [%]	60.2	2.2	41.1	3.6	39.3	6.6	31.3

First, the initial construction cost is calculated considering as design acceleration, PGA_d, the PGA^{UH} values with a 10%-in-50-years exceedance probability. Given the fact that the initial construction costs are not very sensitive to the design acceleration, the relative differences for the two projects are less than 2.2% for the various sites. It is also important to mention that the variation of the initial cost in the vicinity of 0.1g is very low, as discussed in the previous chapter. This explains why the impact of the considered hazard uncertainty on the construction cost is negligible for Milan (low hazard) and more important for Cosenza.

The MAF of collapse, $\lambda_{C.}$, evaluated via Eqn.(6.1), is very sensitive to the hazard model choice, and the variations can be of two orders of magnitude from the estimates obtained considering the hazard from one project rather than the other. These results give a measure of the importance of considering the hazard uncertainty in risk assessment.

The life-cycle cost for a 50-years' time period, estimated based on the initial costs and the annual losses discounted by a factor of 3%, is less sensitive to the hazard

uncertainty than the risk. This is mainly because the construction cost (which is not very sensitive to the PGA_d) contributes more than the future losses to the E[LCC]. Nevertheless, the relative variation of E[LCC^r] (up to 4%) is higher than that of the construction cost. Higher variations in the life-cycle cost are observed if the additional losses are included.

6.3.2 Sensitivity analysis for Europe based on a simplified approach

This section investigates, through a sensitivity study, the effect of the uncertainty in the hazard input on the design and consequently on the risk and loss levels attained for the same reference building considered in the previous section. To demonstrate the approach, five locations of different seismicity are first studied in detail, and then the procedure is repeated for every location across Europe. Figure 6.4a shows the selected locations, together with the PGA^{UH} obtained from the ESHM13 project. These values refer to the uniform hazard *PGA* with a return period of 475 years (probability of exceedance 10% in 50 years). The hazard curves of the selected locations are plotted in Figure 6.4b.

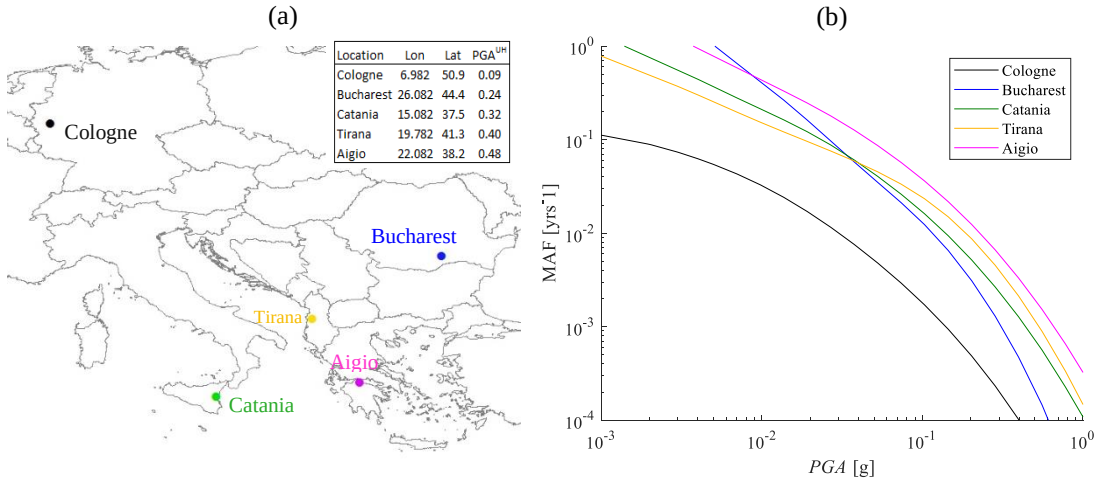

Figure 6.4 Case study for Europe: (a) selected locations, (b) hazard curves (site class A)

A simple approach is followed herein to investigate the effect of hazard uncertainty, by assuming that the hazard curves of Figure 6.4b, considered as the 'reference' ones, underestimate or overestimate the *PGA* levels by 50% at all the MAFs of exceedance. This corresponds to a translation of the hazard curves towards the left or the right. It

is clarified that the variation in the hazard curves is described by the variations of the *PGA* for a given MAF, rather than by variations of the MAF for a given *PGA*.

The varied curves are assumed to describe the actual hazard of the site, which is different than that described by the reference one, and thus will be referred to hereinafter as the 'true' curves. Having defined the 'reference' and the 'true' curves, the sensitivity of the annual risk of collapse λ_c and of C_0, EAL, E[LCC] are calculated for each site considering the following scenarios:

- the building is designed with the reference curve, and the performance is assessed by evaluating the output parameters of interest using the varied ones, which are assumed to be the true ones (case 1);
- the varied ('true') hazard curves are used both for the design and the assessment of the various output parameters (case 2), corresponding to the situation where we have better knowledge of the true hazard at a site;
- The design and assessment are performed using the reference curve (case 3).

The local sensitivity of the generic parameter p is defined as follows:

$$\Delta p[\%] = \frac{p_2 - p_1}{p_1} \tag{6.6}$$

where p_1 denotes the value of the parameters for case 1, and p_2 denotes the value of the parameters for case 2. The values of Δp provide useful information on the sensitivity of costs, losses, and safety to the hazard, for different sites, thus allowing quantification of the importance of obtaining more accurate hazard information.

The results of this sensitivity analysis for the five locations are presented in Figure 6.5. The red and blue points refer to the cases of respectively higher and lower 'true' hazards compared to the reference one (i.e. hazard underestimated and overestimated by the reference curve, respectively).

From the general trend, it is observed that if the design is carried out assuming an hazard level lower than the 'true' one (red points), then the initial construction cost increases, but on the other hand there is a reduction of the risk and loss levels attained.

The opposite applies in the case of the hazard assumed higher than the 'true' one (blue points). The life-cycle cost variations are influenced by the changes of both the initial cost and the future losses, and thus they do not follow a constant trend. It can also be observed that the parameter that is most sensitive to the hazard uncertainty is the risk. Of course, it is important to have in mind that the risk values are very small numbers. In Aigio, for example, if the "true" hazard is lower than the assumed one, the risk is $2.58 \cdot 10^{-5}$. If the design is performed using the "true" hazard curve, the risk changes to 10^{-4} (289% increase). For the rest of the parameters, it is clear that the differences are in general greater in higher hazard areas than in lower hazard areas (e.g. Cologne). This suggests that +/- 50% differences in hazard are relatively unimportant in low hazard areas, hence there is less need to refine hazard assessments there.

The EALs are very sensitive to the hazard, with a maximum difference of -30% and 98% in the case of underestimation and overestimation of the hazard, respectively. On the other hand, the sensitivity of the initial cost is lower than 4%, given that the initial cost does not present a significant variation for the different design levels (Figure 6.6a). Although the EALs are significantly affected, the actual numbers are quite small compared to the initial cost. Thus, the E[LCC] is affected mainly by the change of the initial cost, showing differences less than 2%.

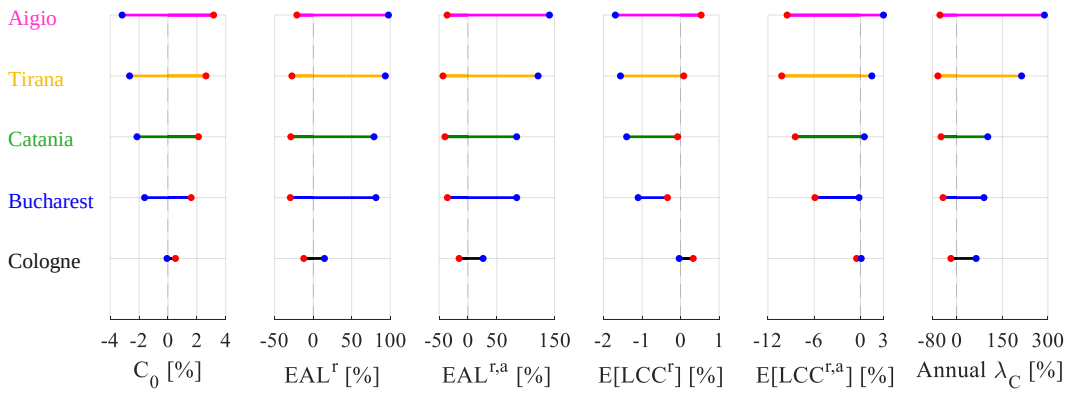

Figure 6.5 Variation of the studied parameters of the case study

The graph for the initial cost is almost symmetrical, meaning that hazard underestimations and overestimations have roughly the same effect in absolute terms. That is not the case for the other studied parameters. For example, the impact of

overestimating the hazard ("true" hazard curve 50% smaller than the design one) on the EALs is higher than when the hazard is underestimated.

To better understand these trends, the location of Catania is selected for further investigation. Figure 6.6a shows the relation between the initial cost C_0 (normalized to the one for PGA_d=0, i.e. 655,840€) and the design acceleration. This relationship is almost linear for PGA_d values higher than 0.1g. This is why the 50% increased or decreased hazard results in roughly 2% change of C_0 in both cases. Figure 6.6b shows the results in terms of EAL, normalized to those corresponding to PGA_d=0 for each case (i.e., 729€, 2,357€, and 4,362€ for -50%, reference, and +50% hazard). For reference, a black curve is also plotted which corresponds to considering the reference hazard curve both for design and assessment (case 3 above). The EAL are also evaluated again considering the reference hazard curve only for design while the assessment is done with the curve increased by 50% (red line) or decreased by 50% (blue line). Similarly, the colour of the dots shows which hazard curve was used for the design.

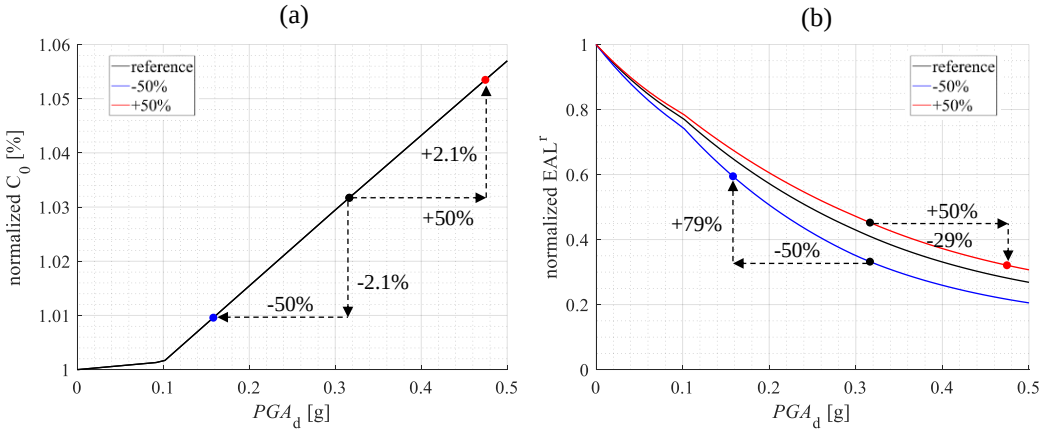

Figure 6.6 Impact of the difference between design and actual hazard on (a) C_0 and (b) *EAL*

The same sensitivity study is performed for the E[LCC] and the results are presented in Figure 6.7a and Figure 6.7b, with the additional losses disregarded or considered along with the repair/replacement cost, respectively. In this case, the hazard uncertainty does not affect the life-cycle costs in a consistent direction, as mentioned before. This is attributed to the fact that the relation of LCC with the PGA_d is not

monotonic, given that the initial cost and the future losses are affected in opposite ways by a change in the PGA_d.

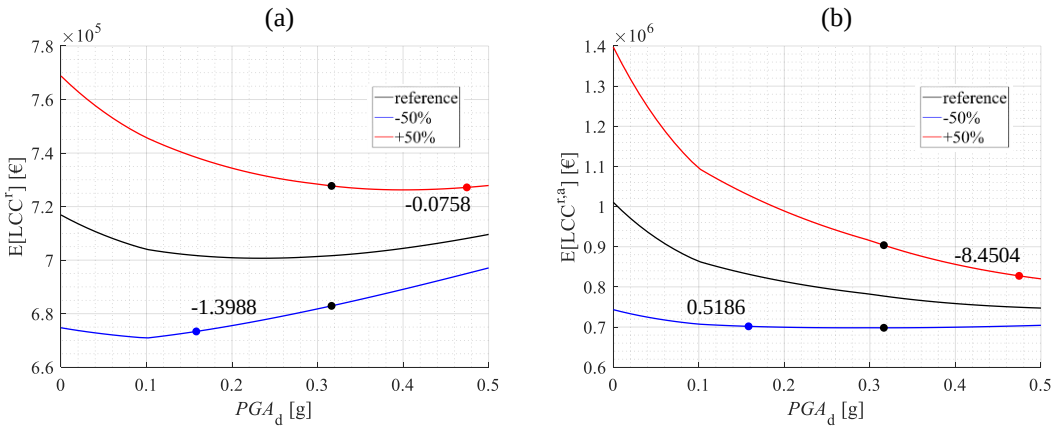

Figure 6.7 Impact of the difference between design and actual hazard curve on $E[LCC^{r,a}]$ considering (a) only the repair costs, and (b) the repair costs and additional losses

Next, the effect of the hazard uncertainty on the cost and performance of the structure is investigated for every location across Europe. First, the *PGA* values that correspond to 1%-, 2%-, 5%,- 10%-, 39%- and 50%-in-50-years exceedance probabilities for the different locations are obtained from the 2013 European Seismic Hazard Model (ESHM13,Giardini et al. 2013; Woessner et al. 2015). For example, Figure 6.8 presents the *PGA* values for site class A that correspond to a 10%-in-50-years exceedance probability (MAF of exceedance $2.1 \cdot 10^{-3}$).

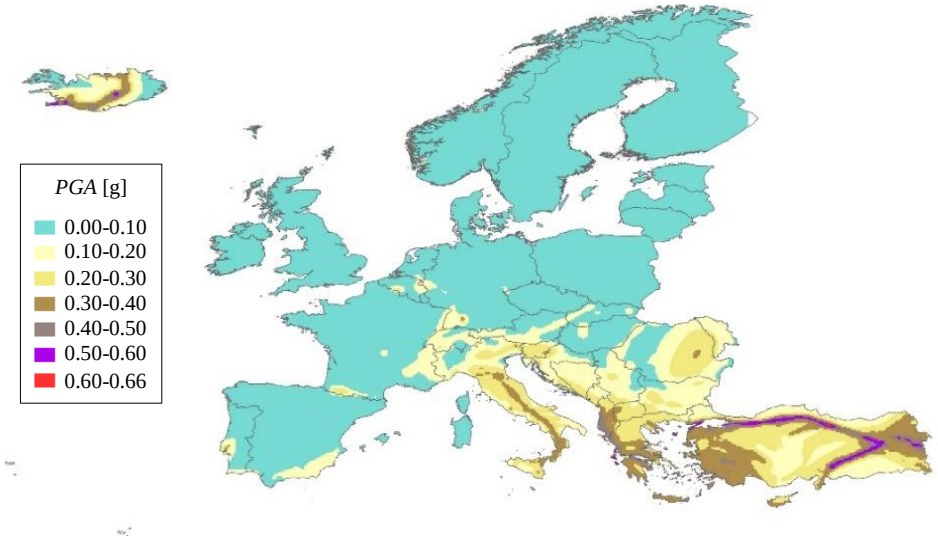

Figure 6.8 *PGA* values (site class A) with a 10%-in-50-years exceedance probability

The second-order polynomial function in log-space proposed by Vamvatsikos (2013) is used to extrapolate the hazard data to a wider range of *PGA*. As the seismic designs were undertaken using the EC8 spectrum for site class B, the *PGA*s for site class A from the ESHM13 are multiplied by the soil factor 1.2, expressing the ratio between PGAs on site classes B and A in EC8, to construct the 'reference' hazard curves. These *PGA*s are further increased or decreased by 50% to perform the sensitivity analyses.

The variations of C_0, EAL, E[LCC] and λ_c for all the considered locations across Europe are then calculated based on Eqn.(6.6). In particular, the parameters are evaluated for 'case 1' and 'case 2' (defined above), and the resulting variations are summarized in Figure 6.9 versus the value of the 475-years-return-period PGA^{UH} (each point refers to a given location across Europe. In order to avoid the uncertainties of extrapolating the vulnerability curves to very high values of *PGA* (e.g. 0.60g would become 0.90g for a 50% increased hazard) the results presented herein refer to *PGA*s up to 0.5g.

Overall, it can be observed that the effects of the hazard variations change significantly from location to location. For example, the changes in the observed parameters are negligible for low hazard sites with PGA^{UH} less than 0.1g. Thus, for these locations it appears unnecessary to achieve very precise estimates of the hazard, since the impact of the hazard uncertainty on the risk (given its low level) and losses is not significant. It should be clarified that this observation is based on analyses for a single example code-compliant structure and may not hold for other elements at risk.

The parameter that is more sensitive to the hazard uncertainty is the risk. Underestimating the actual hazard of the site can lead to underestimation of the risk of two orders of magnitude. As also discussed above for the case of Catania, the variations of the EAL increase monotonically with PGA^{UH}, while the E[LCC] does not exhibit a clear trend of variation. For PGA^{UH} values higher than 0.1g, the variations of C_0 due to increased or decreased hazards are almost symmetrical. This is a consequence of the relation between C_0 and the design acceleration, which is almost linear for PGA^{UH} values higher than 0.1g (Figure 6.9a). In the vicinity of 0.1g the change of C_0 when the hazard is reduced by 50% is smaller than when the hazard is

increased (Figure 6.6a). This is attributed to the minimum requirements the design code sets and the fact that for low levels of PGA_d the design is mainly influenced by the gravity load combination. This leads to an overdesign in the case of PGA_d=0, influencing the slopes of the C_0 and EAL curves (Figure 6.8a and Figure 6.8b).

From the results it is concluded that the necessary precision in the definition of the hazard curve depends on the parameter of interest. In other words, the need of investing in the accuracy of the hazard model depends on the stakeholder. For example, a study of the risk sensitivity can be of interest for updating design guidelines and defining the design seismic input and the target reliability levels to be achieved. On the other hand, the information on the sensitivity of the EALs would be more useful for insurance companies that cover losses from future earthquakes, since they affect the insurance premium (see Chapter 7).

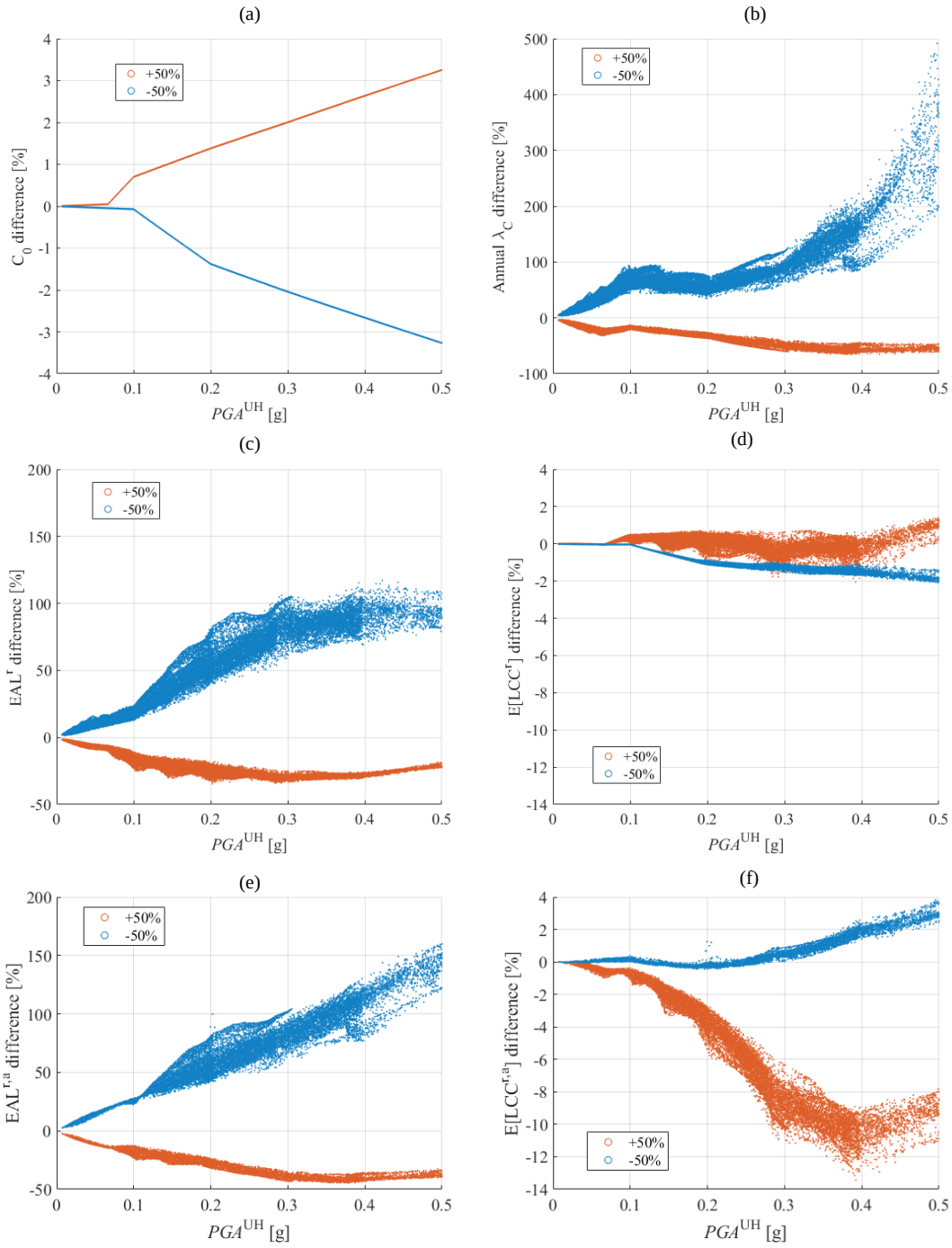

Figure 6.9 Effect of designing with the "true" hazard curves (obtained by increasing or decreasing by 50% the reference hazard curve) in terms of variation of: (a) initial cost, (b) annual collapse risk, (c) EAL (only repair costs), (d) EAL including additional losses, (e) life-cycle cost (repair costs only), and (f) life-cycle cost including additional losses

6.4 Conclusions

The aim of this chapter is to investigate the effect of the hazard input on the seismic design of structures and consequently on the construction cost, the life-cycle cost and the risk estimates. Based on the results obtained in this study it can be concluded that:

- Significant variations of the hazard input are noticeable between various seismic hazard studies;
- The parameters exhibiting the most significant variations from site to site are the annual collapse risk and the expected annual losses;
- The initial construction cost presents small variations and consequently the life-cycle cost also does not vary significantly;

It is highlighted that the results refer to a 4-storey 3-bay RC frame building assumed to be built in different locations across Europe and hence the conclusions may not hold for other types of structures or other elements at risk.

References

Belvaux M, Douglas J, Ulrich T (2014) Comparisons between SHARE and current national seismic hazard maps for France. In Seismic Hazard Harmonization in Europe (SHARE): DGEB-Workshop

Bradley BA (2009) Seismic hazard epistemic uncertainty in the San Francisco bay area and its role in performance-based assessment. Earthquake Spectra, 25(4), 733-753

CEN (2004a) EN 1992-1-1:2004 Eurocode 2: Design of concrete structures - Part 1-1: General rules and rules for buildings, European Committee for Standardization, Brussels

CEN (2004b) EN 1998-1:2004 Eurocode 8: Design of structures for earthquake resistance - Part 1: General rules, seismic actions and rules for buildings, European Committee for Standardization, Brussels

Cosenza E, Del Vecchio C, Di Ludovico M, Dolce M, Moroni C, Prota A, Renzi E (2018) The Italian guidelines for seismic risk classification of constructions:

technical principles and validation. Bulletin of Earthquake Engineering, 16, 5905-5935, doi: 10.1007/s10518-018-0431-8

Crowley H, Silva V, Bal IE, Pinho R (2012) Calibration of Seismic Design Codes using Loss Estimation. In Proceedings of 15th World Conference on Earthquake Engineering, Lisbon, Portugal.

Douglas J, Ulrich T, Bertil D, Rey J (2014) Comparison of the Ranges of Uncertainty Captured in Different Seismic-Hazard Studies. Seismological Research Letters, 85(5), 977-985, doi: 10.1785/0220140084

Giardini D et al. (2013) Seismic Hazard Harmonization in Europe (SHARE): Online Data Resource, doi: 10.12686/SED-00000001-SHARE

Grünthal G, Bosse C, Stromeyer D (2014) Building-Code Related Seismic Hazard Snalyses of Germany and their Relation to SHARE. In Seismic Hazard Harmonization in Europe (SHARE): DGEB-Workshop (Vol. 27)

Grünthal G, Stromeyer D, Bosse C, Cotton F, Bindi D (2018) The probabilistic seismic hazard assessment of Germany—version 2016, considering the range of epistemic uncertainties and aleatory variability. Bulletin of Earthquake Engineering, 16, 4339-4395

Gruppo di Lavoro MPS (2004) Redazione della mappa di pericolosità sismica prevista dall'Ordinanza PCM del 20 marzo 2003 n. 3274, All. 1. Rapporto conclusivo per il Dipartimento della Protezione Civile, aprile 2004, Istituto Nazionale di Geofisica e Vulcanologia (INGV), Milano-Roma, Italy, available at http://zonesismiche.mi.ingv.it/

Kappos AJ, Dimitrakopoulos EG (2008) Feasibility of pre-earthquake strengthening of buildings based on cost-benefit and life-cycle cost analysis, with the aid of fragility curves. Natural Hazards, 45(1), 33-54

Kennedy RP (2011) Performance-goal based (risk informed) approach for establishing the SSE site specific response spectrum for future nuclear power plants. Nucl Eng Des 241:648–656

Lagaros ND (2007) Life-cycle cost analysis of design practices for RC framed structures. Bulletin of Earthquake Engineering, 5(3), 425-442

Martin Ch, Combes P, Secanell R, Lignon G, Fioravanti A, Carbon D, Monge O, Grellet B, Révision du zonage sismique de la France, étude probabiliste. Ministère de l‟Aménagement du Territoire et de l‟Environnement. Rapport GEOTER GTR/MATE/0701-150, 2002, in French

Meletti C, Montaldo V (2007) Stime di pericolosità sismica per diverse probabilità di superamento in 50 anni: valori di ag. Progetto DPC-INGV S1, Deliverable D2, http://esse1.mi.ingv.it/d2.html

Ordaz M, Salgado-Gálvez MA, Pérez-Rocha LE, Cardona OD, Mena-Hernández U (2017) Optimum Earthquake Design Coefficients Based on Probabilistic Seismic Hazard Analyses: Theory and Applications. Earthquake spectra, 33(4), 1455-1474, doi: 10.1193/110116eqs189m

Padgett JE, Dennemann K, Ghosh J (2010) Risk-based seismic life-cycle cost–benefit (LCC-B) analysis for bridge retrofit assessment. Structural Safety, 32(3), 165-173

Pavel F, Vacareanu R, Douglas J, Radulian M, Cioflan C, Barbat A (2016) An updated probabilistic seismic hazard assessment for Romania and comparison with the approach and outcomes of the SHARE project. Pure and Applied Geophysics, 173, 1881-1905, doi: 10.1007/s00024-015-1223-6

Ramirez CM, Liel AB, Mitrani-Reiser J, Haselton CB, Spear AD, Steiner J, Deierlein GG, Miranda E (2012) Expected earthquake damage and repair costs in reinforced concrete frame buildings. Earthquake Engineering & Structural Dynamics, 41(11), 1455-1475

Shinozuka M, Feng Q, Lee J, Naganuma, T (2000) Statistical analysis of fragility curves, Journal of Engineering Mechanics, 126: 1224–1231

Stucchi M, Meletti C, Montaldo V, Crowley H, Calvi GM, Boschi E (2011) Seismic Hazard Assessment (2003–2009) for the Italian Building Code. Bulletin of the Seismological Society of America, 101(4), 1885-1911, doi: 10.1785/0120100130

Vamvatsikos D (2013) Derivation of new SAC/FEMA performance evaluation solutions with second-order hazard approximation. Earthquake Engineering & Structural Dynamics, 42(8), 1171-1188

Vamvatsikos D, Cornell CA (2002) Incremental dynamic analysis. Earthquake Engineering & Structural Dynamics, 31(3), 491-514

Wen YK, Kang YJ (2001) Minimum building life-cycle cost design criteria. II: Applications. Journal of Structural Engineering, 127(3), 338-346

Woessner J, Danciu L, Giardini D, Crowley H, Cotton F, Grunthal G, Valensise G, Arvidsson R, Basili R, Demircioglu MB, Hiemer S, Meletti C, Musson RW, Rovida AN, Sesetyan K, Stucchi M and The SHARE Consortium (2015) The 2013 European Seismic Hazard Model: Key components and results, Bulletin of Earthquake Engineering, 13(12), 3553-3596, doi: 10.1007/s10518-015-9795-1

CHAPTER 7

Loss-informed earthquake insurance of structures

The previous chapters investigated the alternative techniques to mitigate the seismic risk and loss levels that structures are exposed to. Apart from providing a control of these levels, earthquake engineering can also provide solutions to manage the financial implications of future seismic events. This chapter focuses on the management of the expected losses through the mechanism of transfer of the financial risk. Various insurance models are explained and applied in different case studies, and numerous analyses are performed across Europe, for a benchmark four-storey reinforced-concrete frame building.

7.1 Introduction

Regarding the financial implications of the seismic risk, two mechanisms are usually employed in earthquake risk management: mitigation and transfer (Goda et al. 2014). The first solution aims to reduce the risk levels a structure or facility is exposed to and thus mitigate the losses, while with the transfer mechanism a percentage of the losses is covered by a third party (e.g. an insurance or re-insurance company).

The previous chapters of the thesis focused more on the mechanism of mitigation, which can be achieved for example with seismic provisions in national regulations for the design of new buildings. Improving the seismic design standards can be sometimes difficult, since the future benefits are more uncertain compared to the immediate costs involved, but it is achievable (Olshansky, 2005). Moreover, attempts have been made at the national level to promote strengthening strategies with the benefit of tax

deduction, for instance in Berkeley (Spence 2007), or more recently in Italy with the Sismabonus project (Cosenza et al. 2018).

With the second mechanism, a level of risk is managed by the (re)insurance company. The homeowner will still have to cover losses from small events that happen frequently but will transfer the responsibility of dealing with the effect of more catastrophic events to the insurer. It is surprising though that even in seismically-active areas earthquake insurance is not very widespread. For example, in California fewer than 20% of the residential buildings are insured (Spence, 2007). As explained by Kunreuther (1993), one reason is that homeowners either question the benefits compared to the insurance cost or they feel that a disaster will not happen to them. Insurance companies can also be reluctant to promote this type of insurance, fearing the uncertainty of major seismic events, which can be devastating for the economic survival of the company. This is usually dealt with by reinsurance, which aims to transfer the risk of a very large loss from the (often national) insurance companies to the (international) reinsurance companies.

It is interesting that the earthquake insurance penetration rates (i.e. percentage of global insurance premiums over a country's gross domestic product) are unevenly distributed among different countries. Apart from the differences in the seismicity and exposure levels of the various regions, other factors can justify this heterogeneity, e.g. societal (income, educational level, and available information that can influence public willingness) or political (government involvement in the insurance sector). Globally, these rates vary from 1% to almost 100%, according to Michel (2014), while information for Europe can be found in Maccaferri et al. (2011). An interesting investigation is presented in Maccaferri et al. (2011), that shows significant variation of the penetration rates (from 5% to 90%) for the different EU member states. It is noticed that many regions of high seismicity (e.g. Greece and Italy) have very low penetration rates (below 10%) and insurance is offered as an extension of other policies (e.g. fire insurance). On the other hand, high penetration rates can be seen in locations of low seismicity (e.g. the UK). This is attributed to the fact that earthquake insurance is usually bundled with other policies (e.g. insurance for fire, personal accidents, life assurance and property loss) in those countries.

In the same article (Maccaferri et al. 2011) the importance of "risk-based" insurance is highlighted. They note that only six member states have applied a risk-based insurance policy. Acknowledging the importance of this, this chapter focuses on the topic of earthquake insurance with loss considerations. The effect of the assumptions made for the insurance model properties on the resulting premium rates is first investigated. Then a procedure for defining these properties based on a target limit for the loss coverage is suggested and applied across Europe. The design and assessment results of the four-storey reinforced-concrete (RC) frame building studied in Chapter 5 (see also a summary in Section 6.2 of Chapter 6) are used in this investigation.

7.2 Insurance strategies for seismic loss management

A typical insurance strategy in the market involves the definition of two quantities, namely the deductible (D) and limit (L), denoting respectively the minimum and maximum losses covered by insurance (Goda et al, 2014). Assuming that all the losses between D and L are covered by the insurer (i.e. there is no coinsurance), then the total amount covered (claim) is obtained based on the defined D and L for different levels of the losses as (Goda et al, 2014):

$$\text{claim} = \begin{cases} 0, & \text{for loss} \le D \\ \text{loss} - D, & \text{for } D \le \text{loss} \le L \\ L - D, & \text{for loss} \ge L \end{cases} \tag{7.1}$$

The claim sets the minimum (or pure) premium that the company should charge to cover the expected losses. Of course, the insurance premium must be increased for the company to have some profit. The insurance premium can be expressed as (Yucemen 2013):

$$\text{insurance premium} = \text{claim} / (1\text{-LF}) \tag{7.2}$$

where LF is a load factor introducing hidden uncertainties, other expenses and the profit of the insurer. For example, this factor is considered equal to 0.4 for Turkey (Yucemen 2013), which translates into an increase of the minimum claim by 67%.

With the deductible the insurance company avoids dealing with small damage claims that can happen more often and that can be covered directly by the owner. The aim of the limit point is to protect the insurance company from extreme scenarios that can jeopardize the economic survival of the company. These points are defined based on the needs of the involved stakeholders (e.g. property owners, insurance and reinsurance companies, capital market and government).

In a typical insurance scheme, D=10% and L=50% of the insured value (Yoshikawa and Goda, 2014), though different schemes can be defined. A review of the existing insurance systems applied in various countries can be found in Goda et al. (2014), and shows that deductible values between 1% and 15% are usually applied. Other techniques to define the deductible and limit points can be found in the literature, for example based on the return period (Pakdel-Lahiji et al., 2015).

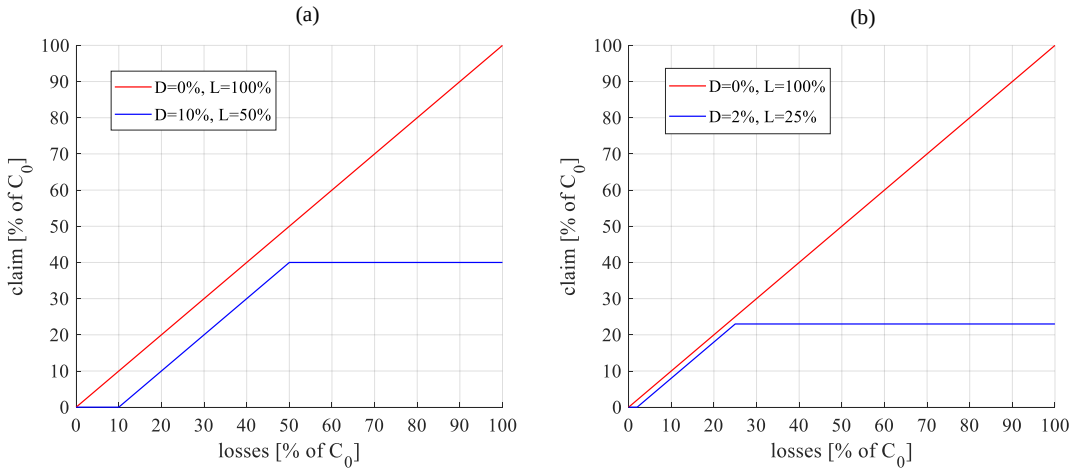

Figure 7.1 Claim for the case of full insurance (claim=losses) and partial insurance with: (a) D=10%, L=50%, (b) D=2%, L=25%

As an example, Figure 7.1a shows the insurance model for D and L set to 10% and 50% of the construction cost, respectively. With this model, the owner cannot claim anything if the losses are less than 10% of the construction cost, while for more extensive damage the company will pay the difference, with a maximum coverage of 50%-10%= 40% of the building's value. The extreme case of full insurance (D=0, L=100% of the construction cost) is given as well, which means that all losses are covered by the insurance. Also, a second example for the partial insurance model is

shown in Figure 7.1b, with D and L assumed equal to 2% and 25%, respectively. These models will be implemented in the case studies of the following section. It is clarified that the construction cost herein refers to the cost of structural and non-structural components only. No additional losses are included (e.g. due to personal contents loss, income and rental losses or injuries and fatalities) since they can be considered separately with different insurance models.

7.2.1 Application of the insurance models

This section presents an application of earthquake insurance modelling for a location in Aigio, Greece. The case study concerns the 4-storey 3-bay RC building which was designed and analysed in Chapter 5 (see also Section 6.2 of Chapter 6). First, the uniform hazard acceleration PGA^{UH} is obtained from the hazard curve of Aigio (see Figure 7.4 below) for a MAF of exceedance equal to 1/475 (10%-in-50-years probability of exceedance). Using this value (0.48g) as design acceleration, the corresponding vulnerability curve is derived based on the results of Chapter 5. Using the hazard curve of the location (multiplied by the soil factor 1.2 to consider class B soil conditions) and the vulnerability curve of the designed building, the loss exceedance curve (red curve) of Figure 7.2 is derived. This curve gives the MAF of exceeding different levels of losses and the area under the curve gives the EAL. The EALs accounting for repair costs only are equal to 1,584€ in this example.

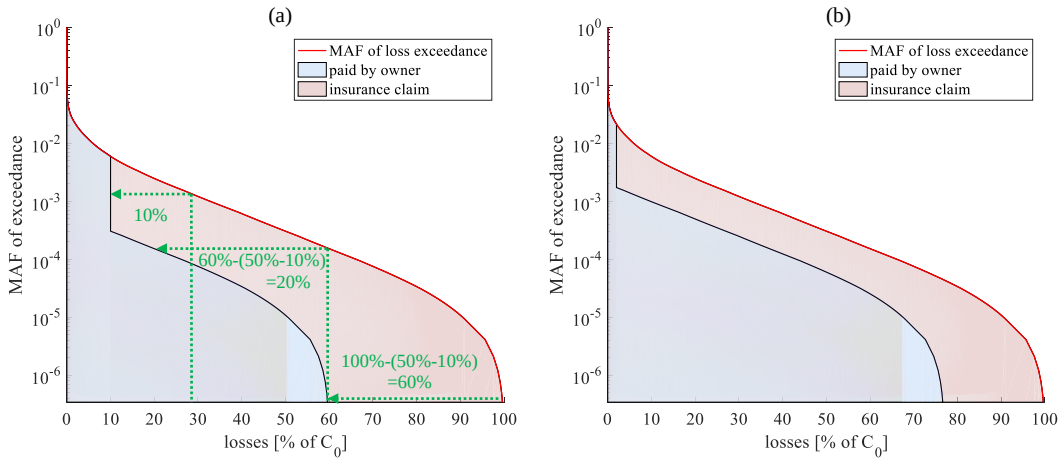

Figure 7.2 Loss exceedance curve for Aigio together with the part that is covered by partial insurance, assuming (a) D=10%, L=50%, and (b) D=2% and L=25%

In the case of a fully-insured building, these losses would all be covered by the insurance company (claim=EAL). If the model of Figure 7.1a (D=10%, L=50%) is applied instead, a new curve is derived (black curve), which refers to the owner, and in particular shows the percentage of the losses that can be claimed. This can be obtained by evaluating, for each loss level, the portion of costs covered by the owner and the insurer. The owner has to cover the losses that are under the black curve, while the rest are covered by the insurance contract and thus transferred to the insurance company. In other words, from the aforementioned 1,584€, 478€ are covered by the insurance, thus setting the minimum annual premium that the insurance should charge to 478€. The remaining repair costs (1,106€) would need to be covered by the homeowner alone.

Given that only 30% of the EAL are covered in this example, a different insurance model is investigated, by implementing the model of Figure 7.1b (D=2%, L=25%) and the results are presented in Figure 7.2b. With this change, 60% of the losses (945€) will be covered by the insurer, leaving the homeowner to deal with the remaining EAL (639€).

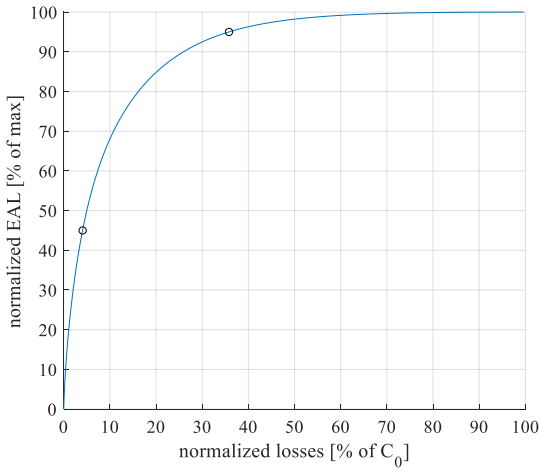

45% of EAL: 4% loss

95% of EAL: 36% loss

% of EAL covered		D [%]			
		0	2	5	10
L [%]	25	89	60	39	21
	50	98	69	48	30
	100	100	70	50	32

Figure 7.3 Disaggregation of the EAL and their coverage for characteristic D and L values

Figure 7.3 presents a disaggregation of the EAL (normalized to the maximum value, i.e. 1,584€) in terms of the different levels of the incurred losses. Almost 50% of the EAL is derived from losses that are smaller than 5% of the initial cost, which have

high MAF of exceedance (Figure 7.2), while the contribution of losses higher than 30% is negligible. A sensitivity analysis of the claim with regards to the values of D and L is also presented in the same figure. As stated before, the typical assumption of D=10% and L=50% gives a 30% coverage of the EAL by the insurance, i.e. the owner has to manage the remaining 70%.

Similar observations were made by other researchers. Yucemen (2013) mentions that the very small deductible (2% in contrast to the more usual value of 10%) suggested by the current insurance policy in Turkey leads to increased premium rates. This is because the small to moderate earthquake events that cause small losses but happen more frequently contribute more to the EAL. For example, earthquakes causing macroseismic intensity VI (corresponding to slight damage) can contribute from 29% to 64% to the EAL, depending on the seismic zone considered. By ignoring the contribution of macroseismic intensity V events (to account for the deductible point), the pure premium rates were found between 0.082% and 0.313%, for RC buildings that comply with the seismic regulation, increased to 0.155% and 0.85% for the case of no seismic provisions. Another study for the insurance modelling of residential buildings in Turkey (Bommer et al. 2002) suggested values of EAL less than 0.2% of the construction cost. Motamed et al. (2018) estimated EAL for residential buildings in Iran between 0.12% and 0.5% of the replacement cost. The review of the international insurance systems of Goda et al. (2014) showed that the maximum premium rates can vary from 0.018% to 0.9% of the construction cost, while Yucemen (2013) gave values of 0.525% for California, 0.43% for Japan and 0.727% for Mexico.

From the above it is clear that different insurance models can be defined based on national guidelines and other research works. Herein, a different way to define D and L is proposed, with the objective of sharing the EAL evenly between the insurer and the owner. Of course, this can be accomplished with various combinations of D and L, but the aim is to have a deductible between 2% to 5% of the initial cost. Therefore, we considered it more reasonable to set D and L as the points where 45% and 95% of the EAL are concentrated. This will result in the owner covering the 45% of EAL that come from small earthquake events and 5% of the losses that come from very rare event, leaving the other 50% (from 45% to 95%) to the insurer. If this scheme is

applied in the case study, the deductible and limit points are D=4% and L=36% (see Figure 7.3).

7.2.2 Investigation for Europe

This subsection investigates the sensitivity of the percentage of the EAL that is transferred to the insurer on the assumptions made for the deductible and limit points. Figure 7.4a shows the selected locations across Europe, together with the uniform hazard *PGA* with a return period of 475 years, PGA^{UH}, obtained from the 2013 European Seismic Hazard Model (ESHM13, Giardini et al. 2013; Woessner et al. 2015). The hazard curves of the selected locations are plotted in Figure 7.4b.

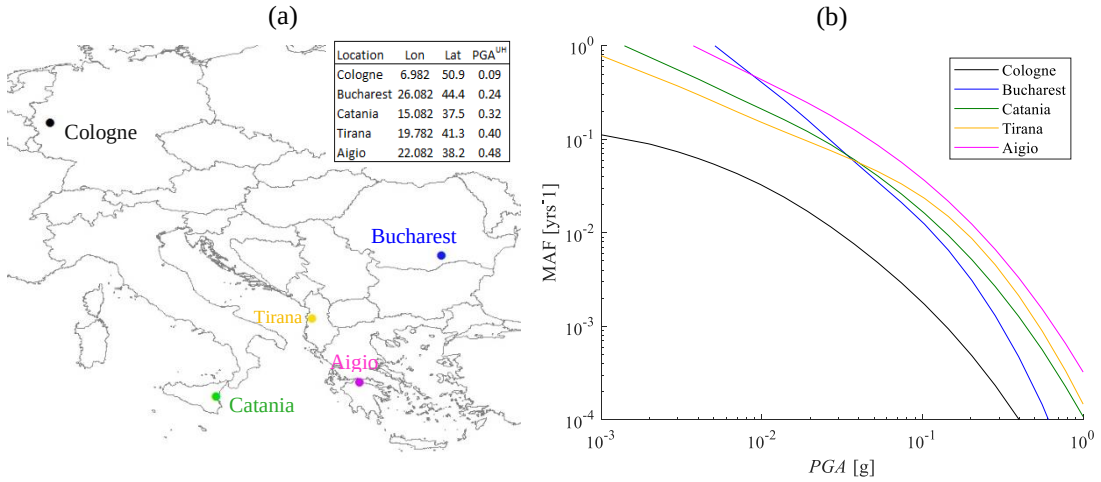

Figure 7.4 Case study for Europe: (a) selected locations and (b) hazard curves (site class A)

First, the vulnerability of the structure is estimated, based on the design acceleration, considered equal to the PGA^{UH} for a 475-year return period. Then, the EAL are calculated by convolving the vulnerability and hazard curves. The results are presented in Table 7.1 and are expressed as a percentage of the initial construction cost. It is observed that the EAL are increased in the regions of higher seismicity, even though the design acceleration is increased. A second case is also examined, which refers to buildings with no seismic provision (PGA_d=0), designed only with the gravity loads combination (1.35G+1.5Q).

Using the insurance model of Figure 7.1a (D=10%, L=50%) and the procedure explained in the previous subsection, the claim values are estimated for each location.

It is reminded that this parameter shows the percentage of the EAL that is covered by insurance, based on the insurance model applied. The results of Table 7.1 for the five locations show that the EAL covered by the insurance are small, and vary approximately between 20% and 40%.If the deductible and limit points change to 2% and 25%, respectively, then the percentage of the EAL that is covered by the insurance is increased, and is found in the range between 55% to 65%.

Table 7.1 Investigation for five locations in Europe for two design acceleration considerations (PGA_d equal to PGA^{UH} and 0)

Location	PGA_d [g]	C_0 [€]	EAL [% of C_0]	claim [% of EAL] D=10% L=50%	claim [% of EAL] D=2% L=25%	D for 45% of EAL [% of C_0]	L for 95% of EAL [% of C_0]
Cologne	0.09	656691	0.03	26	57	3.19	30.02
	0	655840	0.04	27	56	3.39	34.18
Bucharest	0.24	669255	0.12	22	61	3.02	23.43
	0	655840	0.27	23	56	2.78	27.59
Catania	0.32	676639	0.14	32	63	4.53	34.80
	0	655840	0.36	32	58	4.39	40.04
Tirana	0.40	684130	0.18	31	64	4.52	32.89
	0	655840	0.50	39	64	6.17	41.87
Aigio	0.48	691820	0.23	30	60	4.08	35.78
	0	655840	0.82	34	59	4.96	43.06

These results were expected, based on the conclusions of the previous subsection. In the previous section, it was also suggested to use as D and L the points where 45% and 95% of the total EAL are concentrated. Using this approach for the assessed locations, D is found roughly between 3% and 5% and L between 20% and 45% of the initial construction cost.

In order to repeat the procedure for every location across Europe, the *PGA* values that correspond to 1%-, 2%-, 5%,- 10%-, 39%- and 50%-in-50-years exceedance probabilities for the different locations are obtained from the ESHM13 model. The second-order polynomial function in log-space proposed by Vamvatsikos (2013) is used to extrapolate the hazard data to a wider range of *PGA*.

Figure 7.5 presents the *PGA* values for site class A that correspond to a 10%-in-50-years exceedance probability (MAF of exceedance $2.1 \cdot 10^{-3}$). As the seismic designs of the case study buildings were undertaken using the EC8 spectrum for site class B,

the *PGA*s for site class A from the ESHM13 are multiplied by the soil factor 1.2, expressing the ratio between PGAs on site classes B and A in EC8, to construct the 'reference' hazard curves.

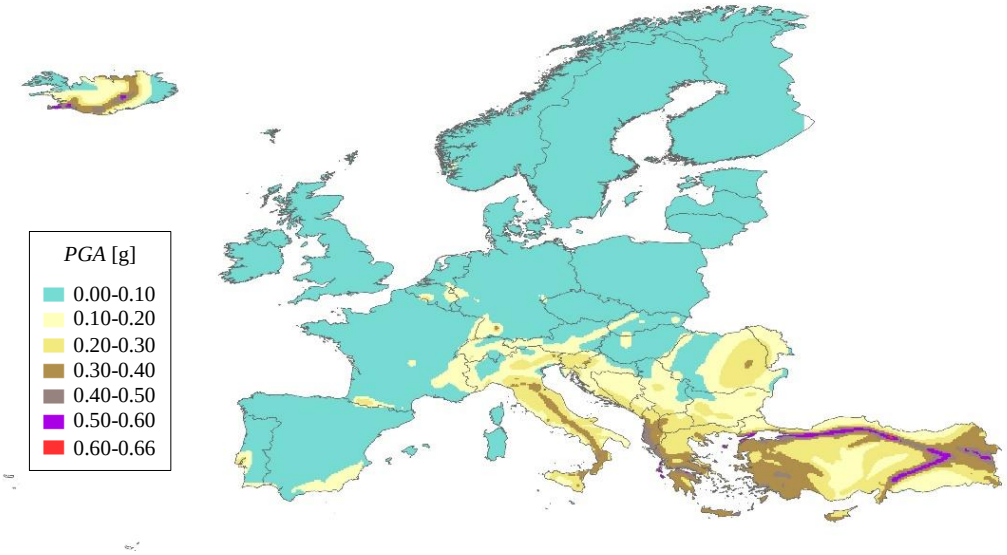

Figure 7.5 *PGA* values (site class A) with a 10%-in-50-years exceedance probability

Then for each location the EAL are calculated based on the design *PGA.* The insurance premium is set equal to the EAL (case of full insurance) and it is the minimum amount (no profit) the company should charge just to cover the expenses for the repair/replacement costs. Then the company can define a different model for the profit (e.g. a percentage of the losses). Two cases are plotted, for buildings designed with seismic provisions (Figure 7.6a) and for building designed for gravity loads only (Figure 7.6b).

The maximum value of the EAL for the case of seismically designed buildings is around 2,455€, which increases to 11,566€ in the case of no seismic provision, which are equal to 0.35% and 1.8% of the construction cost, respectively. These values are the expenses of the insurance company in the case of full insurance (D=0, L=100%) and can be seen as the minimum premium (no profit) the insurance company has to charge.

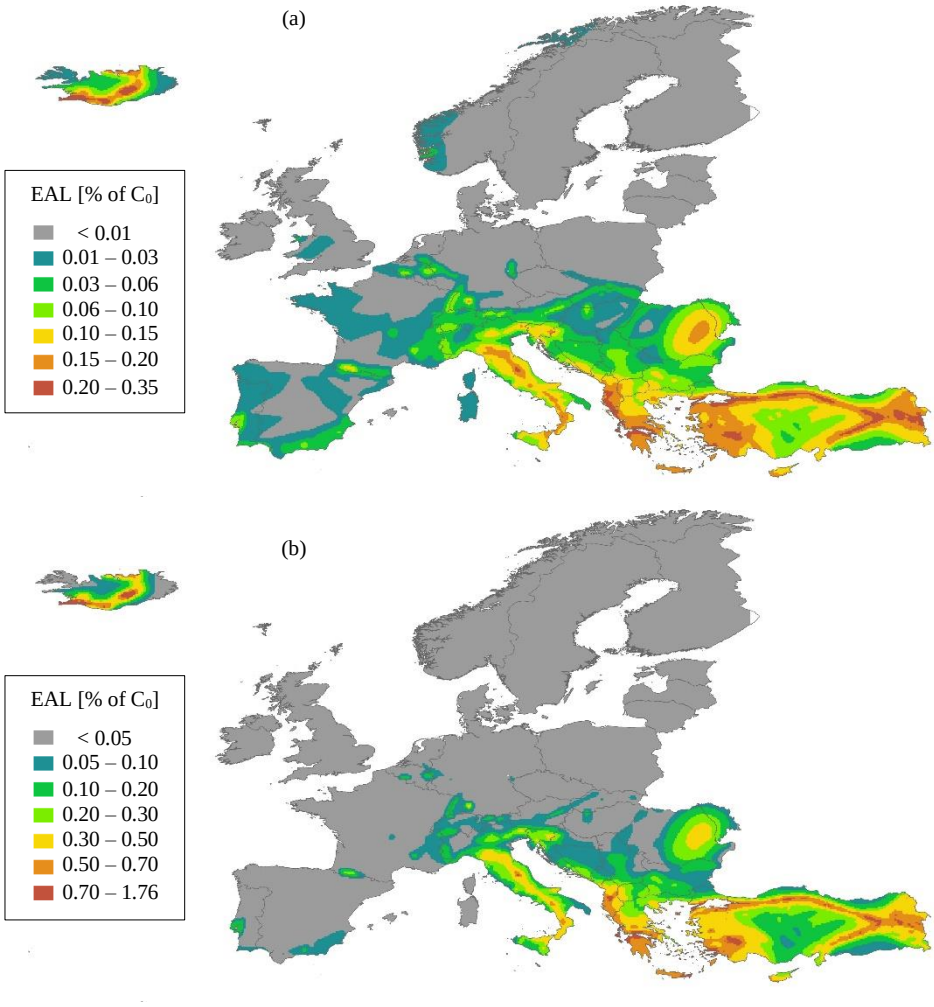

Figure 7.6 Minimum premium (% of construction cost) for full insurance when the building is designed considering the gravity loads and (a) with seismic provisions, and (b) without seismic provisions (notice the difference in the scale)

Next, the impact of the deductible and limit points on the EAL coverage is investigated, first for the case where seismic provisions are applied. In particular, for each location the EAL are assessed based on the hazard of the location, and the claim is defined for three insurance models: a) full insurance (D=0, L=100%), b) D=10% and L=50%, and c) D=2% and L=25%. Figure 7.7a summarizes the claim obtained for every considered location across Europe, in relation with the PGA^{UH} of all the locations (Figure 7.5). In the case of full insurance, the claim is equal to the EAL and as commented above, a maximum value of 0.35% of the construction cost is obtained in this case. For the insurance models b and c, the maximum claim is found to be 0.10% and 0.19% of the initial construction cost, respectively.

In the case of full insurance, 100% of the EAL are covered by the insurance company, while Figure 7.7b shows the percentage of the EAL that is covered when the other two models are applied instead. Each point on these graphs shows the value obtained for a given location across Europe, in comparison to the PGA^{UH} of this location (Figure 7.5). In general, it is observed that by applying model b, this percentage varies from 2% to 42% and for the model c from 19% to 70%. In total, it can be concluded that for the high seismicity regions the coverage is higher than 20% and 50%, when model b and model c are applied, respectively.

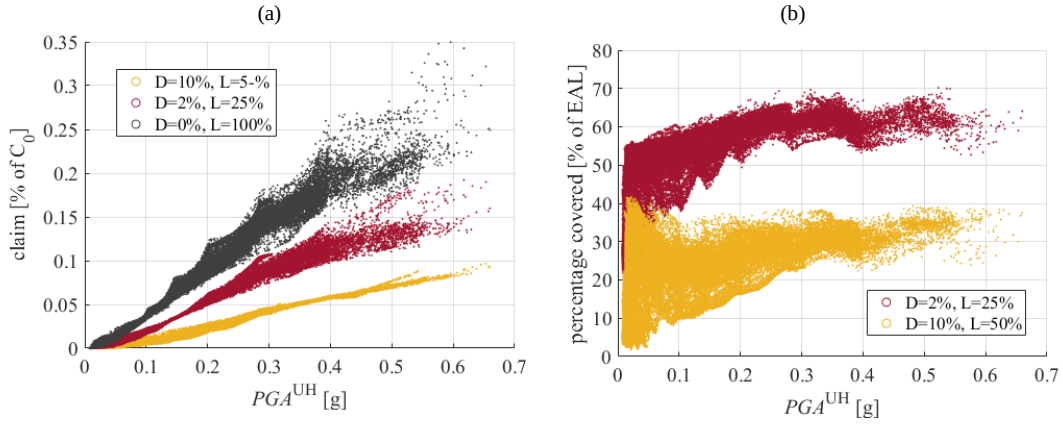

Figure 7.7 Impact of the insurance model on (a) the minimum premium, and (b) the percentage of the EAL that is covered, for Europe

In order for this percentage to become equal to 50% in every location, a disaggregation of the EAL is performed. The points where 45% and 95% of the EAL are concentrated are plotted in Figure 7.8a and Figure 7.8b, respectively. As explained in the previous paragraphs, if these values are used for the D and L, respectively, then half of the EAL are transferred to the insurance company. A further increase of the obtained L values in each location does not affect the minimum premium by more than 5%, though it would expose the insurer to higher financial risk.

As explained above, for low *PGA* levels the gravity loads combination defines the design and thus leads to over-designing in some cases. This results in a high discrepancy of the results in the vicinity of $PGA^{UH}=0$. Nevertheless, the losses (Figure 7.6a) in this area are quite small. In general, it can be concluded that values roughly

between 2% and 6% for the deductible point are more reasonable in high seismicity regions, whereas L can be set between 20% and 50%.

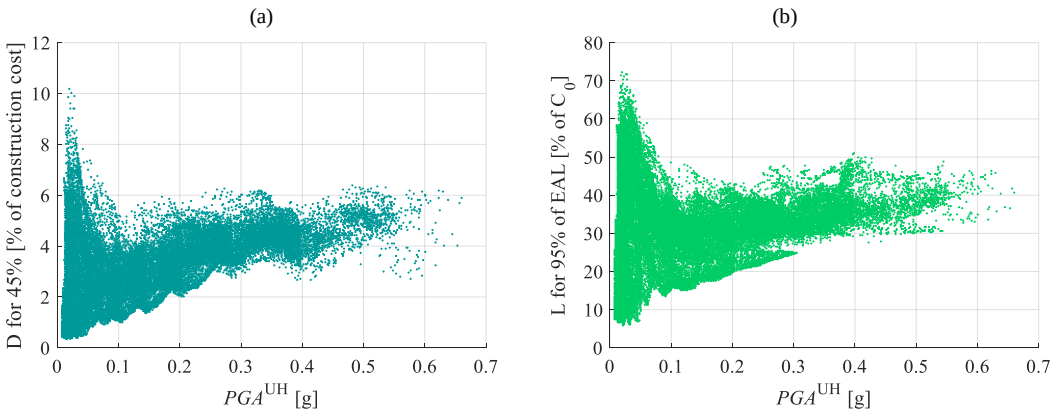

Figure 7.8 Points where the 45% (a) and 95% (b) of the EAL is concentrated

The above procedure is repeated considering now the structure designed in the various locations only with the gravity loads combination (PGA_d=0). The results are summarized in Figure 7.9. As expected, the claim (Figure 7.9a) is much higher than for the previous case study, with the maximum value for the full insurance being equal to 1.76%. When the partial insurance model b (D=10%, L=50%) and model c (D=2%, L=25%) are implemented, then this percentage is 0.51% and 0.96%, respectively. The percentage of the EAL covered (Figure 7.9b) ranges from 2% to 56% and 19% to 80%, for model b and c, and is generally higher than 15% and 40% in the high seismicity regions. The deductible (Figure 7.9c) and limit (Figure 7.9d) points vary from 0.4% to 12% for model b, and 6% to 73% for model c. The general trend suggests a value of D between 2% and 10%, and a value of L between 20% and 50%.

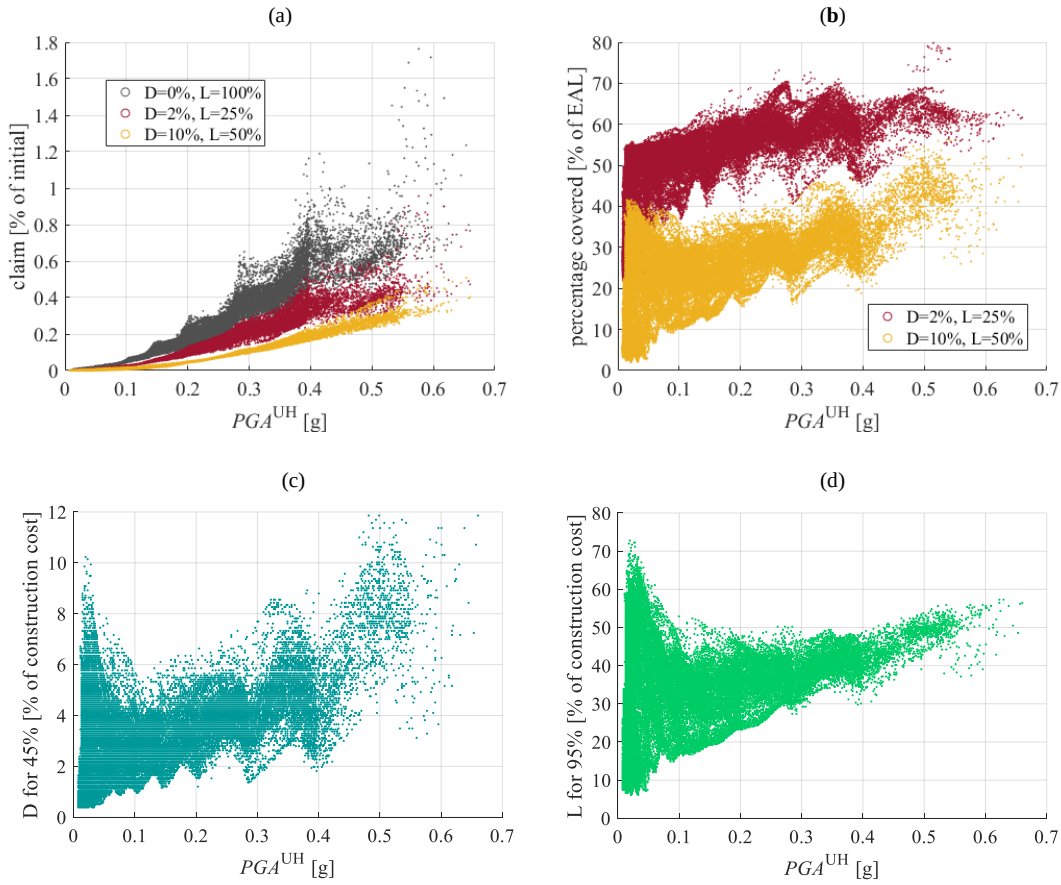

Figure 7.9 Results for the structure designed only for gravity loads: (a) claim and (b) percentage of EAL covered, for the different insurance models; points where the 45% (a) and 95% (b) of the EAL is concentrated

7.3 Conclusions

The aim of this chapter is to investigate how the expected annual losses can be applicable to earthquake insurance modelling. Based on the results obtained in this study it can be concluded that the expected annual losses are mainly defined by more frequent events that cause minor damage to the structure. This means that deductibles higher than 10% result in low insurance rates but at the same time the homeowner has to deal with most of the repair costs. Different sensitivity analyses suggest using low deductible points (between 2% and 5%) together with limit points between 25% and 50% to obtain a roughly equal share of the losses between the insurer and owner. It is highlighted that the results refer to a 4-storey 3-bay RC frame building assumed to be built in different locations across Europe and hence the conclusions may not hold for other types of structures or other elements at risk.

References

Bommer J, Spence R, Erdik M, Tabuchi S, Aydinoglu N, Booth E, Del Re D, Peterken O (2002) Development of an earthquake loss model for Turkish catastrophe insurance. Journal of Seismology, 6, 431-446

CEN (2004a) EN 1992-1-1:2004 Eurocode 2: Design of concrete structures - Part 1-1: General rules and rules for buildings, European Committee for Standardization, Brussels

CEN (2004b) EN 1998-1:2004 Eurocode 8: Design of structures for earthquake resistance - Part 1: General rules, seismic actions and rules for buildings, European Committee for Standardization, Brussels

Cosenza E, Del Vecchio C, Di Ludovico M, Dolce M, Moroni C, Prota A, Renzi E (2018) The Italian guidelines for seismic risk classification of constructions: technical principles and validation. Bulletin of Earthquake Engineering, 16, 5905-5935, doi: 10.1007/s10518-018-0431-8

Crowley H, Silva V, Bal IE, Pinho R (2012) Calibration of Seismic Design Codes using Loss Estimation. In Proceedings of 15th World Conference on Earthquake Engineering, Lisbon, Portugal.

Giardini D et al. (2013) Seismic Hazard Harmonization in Europe (SHARE): Online Data Resource, doi: 10.12686/SED-00000001-SHARE

Goda K, Wenzel F, Daniell J (2014) Insurance and reinsurance models for earthquake, in: M. Beer, E. Patelli, I.A. Kougioumtzoglou, S.K. Au (Eds.), Encyclopedia of Earthquake Engineering, Springer, Berlin, Germany, doi: 10.1007/978-3-642-36197-5_261-1

Kunreuther H (1993) Earthquake insurance as a hazard reduction strategy: The case of the homeowner. In 1993 National Earthquake Conference “Earthquake Hazard Reduction in the Central and Eastern United States: A Time for Examination and Action”, Central United States Earthquake Consortium (CUSEC)

Maccaferri S, Cariboni F, Campolongo F (2011) Natural Catastrophes: risk relevance and insurance coverage in the EU. European Commission, Joint Research Centre

Michel GW (2014) Decision making under uncertainty: insuring and reinsuring earthquake risk. In Earthquake hazard, risk and disasters (pp. 543-568). Academic Press, doi: 10.1016/B978-0-12-394848-9.00021-3

Motamed H, Calderon A, Silva V, Costa C (2019) Development of a probabilistic earthquake loss model for Iran. Bulletin of earthquake engineering, 17, 1795-1823

Olshansky RB (2005) Making a difference: Stories of successful seismic safety advocates. Earthquake spectra, 21(2), 441-464, doi: 10.1193/1.1902953

Pakdel-Lahiji N, Hochrainer-Stigler S, Ghafory-Ashtiany M, Sadeghi M (2015) Consequences of financial vulnerability and insurance loading for the affordability of earthquake insurance systems: evidence from Iran. The Geneva Papers, 40, 295-315, doi: 10.1057/gpp.2014.35

Spence R (2007) Saving lives in earthquakes: successes and failures in seismic protection since 1960. Bulletin of Earthquake Engineering, 5, 139-251, doi: 10.1007/s10518-006-9028-8

Vamvatsikos D (2013) Derivation of new SAC/FEMA performance evaluation solutions with second-order hazard approximation. Earthquake Engineering & Structural Dynamics, 42(8), 1171-1188

Woessner J, Danciu L, Giardini D, Crowley H, Cotton F, Grunthal G, Valensise G, Arvidsson R, Basili R, Demircioglu MB, Hiemer S, Meletti C, Musson RW, Rovida AN, Sesetyan K, Stucchi M and The SHARE Consortium (2015) The 2013 European Seismic Hazard Model: Key components and results, Bulletin of Earthquake Engineering, 13(12), 3553-3596, doi: 10.1007/s10518-015-9795-1

Yoshikawa H, Goda K (2014) Financial seismic risk analysis of building portfolios. Natural Hazards Review, 15(2), 112-120

Yucemen MS (2013) Probabilistic assessment of earthquake insurance rates for buildings. In Handbook of Seismic Risk Analysis and Management of Civil Infrastructure Systems (pp. 787-815), Woodhead Publishing

CHAPTER 8

Conclusions and Recommendations

The main objective of this thesis was the investigation and comparison of alternative approaches for the seismic design of structures. For this, the various techniques have been reviewed and their differences have been clarified. This review provided better understanding of the approaches, highlighted some limitations, and showed possible paths forward. Departing from the single-site applications (invariably for high seismicity locations) that have been published before, this thesis combined European-wide assessment (including low and moderate seismicity regions) with in-depth modelling for the evaluation of the structural performance. Subsequently, an approach to evaluate the impact of the epistemic uncertainties inherent in the hazard modelling on the resulting measures of the risk and loss was presented. Finally, the topic of loss-informed insurance for managing the financial impacts of earthquakes has been investigated, again at the European scale.

In the following, a summary is provided of the work performed in each chapter together with the main conclusions. In the second part, the limitations of the work are discussed together with recommendations for future research work that is necessary to generalize these conclusions. It is anticipated that this thesis can contribute to future directions for seismic design, accounting not only for the seismic hazard component, but also for the expected annual risk and the potential losses.

8.1 Summary and conclusions

In Chapter 2, the risk-targeting seismic design approach currently recommended by the American regulations (ASCE 7-16 2017; FEMA P-750 2009) was reviewed. A

methodology was presented to apply the method analytically, using the trapezium rule for the convolution of the hazard with the fragility, and the bisection method to reduce the computational effort. It was explained that the method results to a trilemma, since there are three parameters that must be defined, but they are not independent. The chapter presented some of the most important studies in the literature, to provide an insight into reasonable values for these parameters. Additional focus has been given to the topic of defining acceptable risk levels and categorizing the techniques into three groups, based on current risk levels, public opinion, and the consequences of failure. Then a simple approach was followed, to define a bound for the acceptable risk, based on observations of damage in past earthquakes. Given the "moral" questions deriving from accepting a non-zero collapse risk, it was suggested to consider also other damage levels (e.g. yield) when applying risk-targeting in seismic design.

The need to further investigate the fragility assumptions involved in risk-targeting was already highlighted in Chapter 2. Based on this, Chapter 3 presented a sensitivity analysis to understand how the fragility curves of reinforced concrete buildings can vary with the seismic design level and the geometry, considering additional damage states apart from global collapse. A simplified approach was followed, using 2D numerical models with different numbers of storeys and bays, designed for various seismic levels. For the performance assessment the hazard uncertainty was considered by selecting different ground-motion records in the numerical analyses. As expected, by increasing the seismic design level, the buildings become less fragile, which is translated to an increase of the median capacity. An interesting observation was that while the number of bays does not have a significant impact on the fragility curves, at least for the case study, this is not the case for the number of storeys. This highlights the difficulty and the uncertainty involved in the use of generic fragility curves.

Chapter 4 presented a more rigorous investigation of three risk-targeting techniques. First, analytical expressions were provided for each technique, assuming an elasto-plastic single-degree-of-freedom (SDOF) system. A unified notation has been adopted to make resemblances and differences clearer and enable comparisons. It was found that there is a connection between Luco's approach (the approach of the American regulations) and the risk-targeted behaviour factor (RTBF) approach. Another

interesting observation was that the analytical equations can be rearranged to derive the seismic risk directly from the value of the hazard level of the spectral acceleration corresponding to a predefined failure probability value. The third risk-targeting technique reviewed was based on the use of inelastic ground motion prediction equations (GMPEs). A comparison with the RTBF approach for SDOF systems showed a good match of the obtained spectra for different risk targets, with the agreement being better for high values of the risk target.

Beside these comparisons, further case studies were presented to investigate the assumptions inherent in the various approaches. A key element of the method is the hazard curve, which in the presented equations was described as being linear in log-log space. This raised the question of which points should be used for the fitting. For this, a comparison of the risk-targeted acceleration values obtained using the exact hazard curve and a linear equation in log-log space using different fitting points was performed. Fitting the curve for mean annual frequencies of exceedance equal to the targeted level and ten times higher than this level was found to be a reasonable choice. Also, the results were found to be very sensitive to the assumed standard deviation of the fragility curves. After that, the assumption for the probability of collapse at the risk-targeted ground motion was investigated, by critically reviewing the value chosen by the American regulations. It was also shown that this approach could lead to inconsistent risk levels for different system properties, because the response modification factors of the American design codes are generally not based on probabilistic analyses. In the last part, the analytical equations of the RTBF approach were applied across Europe to derive risk-targeted spectral acceleration values for different structural systems. The procedure was then repeated for Italy, with a hazard model obtained from a different study, to highlight the sensitivity of the results to the hazard input.

An evaluation of alternative seismic design techniques was performed in Chapter 5. First the methodology of each technique was presented. Then in order to enable comparisons, a four-storey three-bay building was designed for different acceleration levels and its performance was assessed through 3D nonlinear finite element modelling. Various time-history analyses were performed to generate the fragility

curves of the models, which were used in the risk and loss analyses across Europe. The uniform-hazard (UH) approach, which is the most common in regulations, uses the design values for a predefined exceedance frequency. As shown, this technique leads to uncontrollable risk levels across different locations, which has been commented by other researchers too. Although the risk distribution using the UH approach is not uniform for different locations, the attained risk levels for the case-study building were generally within the acceptable risk limits proposed by the American regulations (except for some high hazard areas). Generally, in the risk targeting (RT) approach, the design accelerations are selected so that they lead to a uniform distribution of the collapse risk levels across different regions. It was shown in this study that the accelerations obtained with RT can be either higher or lower than the UH approach, depending on the risk target defined. A last approach to the seismic design problem is to focus on the life-cycle cost, which includes the construction costs and the losses resulting from future seismic activity. The impact of the design acceleration on the initial construction cost was found to be small, due to the high contribution of the non-structural components, the cost of which is not dependent on the design level. The variation of the losses with the design acceleration was small when the losses only due to damage of the structure are considered. This variation was increased when additional losses (personal contents, rental, income, injuries and fatalities) were also included in the analyses. The minimum-cost (MC) approach was then applied in each location. The method targets the acceleration value that minimizes the life-cycle cost of the designed structure. It was found that the life-cycle cost when designing with the UH approach is not far from that obtained using the MC method. Finally, a benefit-to-cost analysis was performed to evaluate which areas will benefit more from the implementation of the MC approach, in comparison to designing with no seismic provisions.

Using the results of the fifth chapter, Chapter 6 presented different sensitivity analyses on the topic of hazard uncertainty. First, the differences between the hazard input provided from two different studies were evaluated, showing significant variations. Then specific locations of different seismicity across Italy were selected to evaluate the impact of these differences on the risk, cost and loss estimates. Subsequently, a simplified approach to consider hazard uncertainty was introduced and different sites

across Europe were selected to explain it. Subsequently, the method was implemented in all areas across Europe. The concluding remarks from the analyses were that the parameters that are the most sensitive to the hazard uncertainty are the annual collapse risk and the expected annual losses, while the initial construction cost and consequently also the life-cycle cost do not vary significantly.

In Chapter 7 the expected annual losses were further investigated to explore the applicability of different insurance models. Using the results obtained by the study of Chapter 5, different sensitivity analyses were performed across Europe. The results showed that events that cause small damage to the structure but occur more frequently actually contribute more in the total expected annual losses. Therefore, defining deductibles higher than 10% results in low insurance rates but at the same time the homeowner has to deal with most of the repair costs. It was found that using low deductible points (between 2% and 5%) together with limit points between 25% and 50% can lead to more even distribution of the losses between the insurer and owner.

8.2 Limitations and future work

The work presented in this dissertation can be further extended in future, given the assumptions made in each chapter and the limitations. In particular:

- Two issues concerning the fragility functions are: what value of β to use and, indeed, whether the lognormal distribution should continue to be used at all? Fragility curves that are used within the risk targeting calculations can imply very strong buildings [e.g. Table 1 of Douglas et al. (2013)] as well as non-negligible chances of collapse for very low ground accelerations. This is a consequence of the high values of β that need to be used to account for different types of structures of varying geometries. Two solutions to this problem are: a) adopt a different functional form for the fragility curve that equals zero for low ground accelerations and unity for very high accelerations, or b) move from generic fragility curves for all types and geometries to a curve covering only a small set of structures. The second of these changes would mean a change of philosophy of design codes to being associated with a single map giving the design accelerations for all structures to potentially many maps giving design accelerations for different structural types

and geometries. This additional complexity, however, appears to be necessary if the risk-targeting approach is to imply physically realistic buildings and levels of risk.

- A simplified approach to define an upper bound for the acceptable risk levels using building damage data from past seismic events was demonstrated in Chapter 2. An investigation was conducted for reinforced concrete buildings in Italy and Greece. Future studies could consider other developed countries with good databases, such as the USA, Japan and New Zealand. The aim of that preliminary study was just to demonstrate the approach and derive a rough estimate of an upper bound. Future studies are advised using more complete database both for the damage and the number of buildings affected and by extending the time period covered so that more potential earthquake scenarios are considered. In addition, variations due to building type (e.g. masonry versus reinforced concrete), location (e.g. developed versus less-developed countries) and damage level (e.g. collapse versus yield) could be studied as well. The available databases are limited, however, and hence it is likely that these analyses would not lead to precise estimates.

- Another way to avoid the "moral" questions resulting from accepting collapse (and consequently fatalities) is by targeting a damage state that is less severe than collapse, for example structural yielding (which also is easier to define numerically). For sure it will be politically easier to justify and accept a risk target that refers to a condition of slight damage, thus avoiding mentioning the collapse scenario which is directly linked to potential fatalities. However, the resulting collapse risk will still remain uncontrollable, given that the post-yield behavior is not considered in that case.

- The aim of Chapter 3 was to investigate the sensitivity of the fragility curves to the geometrical variation. In order to reduce the computational effort, 2D models were used to represent the structures assessed in Chapter 3. More rigorous approaches can be implemented in future studies. Also, future studies should investigate the effect of the assumption of a constant probability of failure at the design *PGA* on the final design results. The error in the risk estimates resulting from the use of the simplifying assumption of generic fragility curves could be evaluated by

performing extensive parametric analyses for different building and hazard scenarios and by comparing the results obtained using analytical fragility curves like those developed in Chapter 3.

- The comparison of the risk-targeting approaches and the maps presented in Chapter 4 refer to SDOF systems and the power-law equation is used for the fitting of the hazard curve in order to estimate risk analytically. Second-order solutions for hazard-fitting could be implemented, too (e.g. Vamvatsikos 2013).

- It would be interesting to use the principles of Chapters 4 and 5, to develop a simplified framework for minimum-cost design based on SDOF systems and closed-form solutions.

- Given the effort required to undertake the various analyses and the application across Europe, a single example building type was selected for the applications of Chapter 5, 6 and 7. The accuracy of the modeling assumptions and their limitations were not the main objective of this thesis. Future studies can assume different geometries (number and dimensions of storeys and bays, irregularities), structural systems (e.g. shear walls) and materials (e.g. steel). In addition, a useful idea would be to investigate the effect of considering the infills at the design stage. The same comments apply also for Chapter 3, which aims only to highlight some limitations of the risk-targeting assumptions.

- For simplicity, the Type 1 horizontal design acceleration spectrum of Eurocode 8 (CEN 2004) was used for every location across Europe, together with the assumption of soil class B for the design and assessment. Ideally, the design spectra defined by national codes could be used.

- An important aspect to be considered when applying a common design framework among different countries is data harmonization. For this reason, the ESHM13 project (Giardini et al. 2013; Woessner et al. 2015) was used herein, which provides a harmonized (during a three-year European project with inputs from hundreds of experts) seismic hazard model for Europe. Also, there is a move in Europe to define harmonized design standards through the adoption of the design

criteria in the Eurocodes. The risk-targeting philosophy has been found to contribute also to this end (Spillatura 2018). Data harmonisation becomes more difficult, however, when the involved construction costs are considered, e.g. in the minimum-cost design approach studied in this thesis. Material and labour costs can differ significantly between different countries. This subject needs further investigation in the future, if further harmonisation is sought.

- In an attempt to reduce the computational effort, the same set of records was selected for different locations to perform the nonlinear analyses, with the scaling assumption also assumed justified. Different methods could potential be applied (e.g. record selection for each location separately), though there is no perfect method for selecting input ground motions for a Europe-wide study. Of course, this choice affects the results of the performance assessment, and other record sets, intensity measures, and nonlinear demand estimation methods may lead to different results. This investigation was not the objective of this thesis.

- In some cases, it was found that the available hazard data did not cover a sufficient range of annual frequencies of exceedance, and assumptions were made for the fitting and extrapolation of the hazard curves. Alternatively, hazard maps could be derived for each location using a probabilistic event- based risk calculator (e.g. with the OpenQuake software, https://www.globalquakemodel.org/openquake). Also, future studies should be performed with the ESHM2020 (from SERA project, http://www.sera-eu.org/en/activities/joint-research/) which is due to be released soon.

- The fragility curves were fitted on the results of incremental dynamic analyses. This required strong ground motions to reach the collapse damage state, which are rarely recorded and thus scaling was considered a justified assumption. Other approaches can be investigated, such as cloud analysis combined with censored maximum likelihood estimation.

- For simplicity, the same thresholds were considered for the different structures to characterize the damage states and derive the fragility curves. Other approaches could be followed instead, e.g. based on the results from pushover analyses. The

sensitivity of the conclusions on this assumption has not been the focus of this work.

- Another topic that should be further investigated and clarified is the definition of direct and indirect losses, since the definitions of the terms vary among different studies [see e.g. the difference between Kappos and Dimitrakopoulos (2008) and Kircher et al. (2006)]. The terms direct and indirect losses have been avoided in this study, to avoid confusion. In the minimum-cost approach of Chapter 5 the two extreme cases considered are alternatively referred to as: losses related to the initial construction costs (structural and nonstructural damage) and additional losses, which refers to rental and income loss, injuries and fatalities, and personal contents. A different approach could consider the personal contents together with the damage of the nonstructural components.

- In some of the design approaches examined, the data had to be extrapolated to much higher design accelerations than the ones considered for the case-study models. What is more some very high design levels would be unrealistic, leading to extreme dimensions for the structural members. Therefore, future studies could consider additional design acceleration levels and potentially explore different structural systems to meet the need of such high levels.

- This thesis has focused on how safety and economy criteria affect the structural design, while other criteria can be explored in future. It would be useful in some facilities to set the performance targets based on the environmental impact of seismic upgrade, balanced with its cost and safety. This can be performed by assessing, for example, the levels of CO_2 emitted based on the material quantities used for each design level. Another approach that has been discussed in Chapter 1 is that of societal risk. For this additional data should be collected regarding the exposure, i.e. the buildings that are present in the considered area and the occupants affected. For this, hazard analyses are necessary (e.g. by using OpenQuake) to generate stochastic event catalogues and also an exposure model for the number of occupants affected (e.g. Kappos and Dimitrakopoulos 2008; Sinković and Dolšek 2020) is required.

- A simplified approach for modelling the hazard uncertainty was followed in Chapter 6. In particular, the uncertainty in the hazard curves was modelled by changing the acceleration values corresponding to each exceedance frequency. In future, further studies can be conducted, for instance by changing the exceedance frequency for each acceleration level, or by changing the slope of the hazard curve. Another useful investigation would be to use different fractiles from the same hazard model. This approach was not preferred in this thesis because the aim was to have the same level of uncertainty at every location, introduced by a constant change of the acceleration value by 50%.

- The work can be extended by considering also additional sources of uncertainty, e.g. in the material properties, the geometry, the damage state definition and the ground-motion record selection.

- This thesis focused on the design and performance assessment of new structures. The ideas could be adapted to design retrofitting solutions for existing structures so that they conform to a predefined performance target.

References

ASCE (2017) Minimum Design Loads and Associated Criteria for Buildings and Other Structures, ASCE/SEI 7-16. American Society of Civil Engineers, Reston, VA

CEN (2004) EN 1998-1:2004 Eurocode 8: Design of structures for earthquake resistance - Part 1: General rules, seismic actions and rules for buildings, European Committee for Standardization, Brussels

Douglas J, Ulrich T, Negulescu C (2013) Risk-targeted seismic design maps for mainland France. Natural Hazards 65(3): 1999-201

FEMA (2009) NEHRP Recommended Seismic Provisions for New Buildings and Other Structures (FEMA P750). Federal Emergency Management Agency

Giardini D et al. (2013) Seismic Hazard Harmonization in Europe (SHARE): Online Data Resource, doi: 10.12686/SED-00000001-SHARE

Kappos AJ, Dimitrakopoulos EG (2008) Feasibility of pre-earthquake strengthening of buildings based on cost-benefit and life-cycle cost analysis, with the aid of fragility curves. Natural Hazards, 45(1), 33-54

Kircher CA, Whitman RV, Holmes WT (2006) HAZUS earthquake loss estimation methods. Natural Hazards Review, 7(2), 45-59

Sinković NL, Dolšek M (2020) Fatality risk and its application to the seismic performance assessment of a building. Engineering Structures, 205, 110108

Spillatura A (2018) From record selection to risk targeted spectra for risk based assessment and design. Ph.D. Dissertation. Pavia, Italy: IUSS

Vamvatsikos D (2013) Derivation of new SAC/FEMA performance evaluation solutions with second-order hazard approximation. Earthquake Engineering & Structural Dynamics, 42(8), 1171-1188

Woessner J, Danciu L, Giardini D, Crowley H, Cotton F, Grunthal G, Valensise G, Arvidsson R, Basili R, Demircioglu MB, Hiemer S, Meletti C, Musson RW, Rovida AN, Sesetyan K, Stucchi M and The SHARE Consortium (2015) The 2013 European Seismic Hazard Model: Key components and results, Bulletin of Earthquake Engineering, 13(12), 3553-3596, doi: 10.1007/s10518-015-9795-1

Appendix A

In this appendix, tables A.1, A.2 and A.3 present information for the ground motions records selected in Chapters 3, 4 and 5 of this thesis, respectively.

Table A.1 Selected ground motion records used in Chapter 3 (source: Akkar et al. 2014)

Date Time	Station Code / Name	Network	Orientation
7/4/2009 17:47	3698 / Sant'Eusanio Forconese, Italy	DPC (Italian Civil Protection Authority)	WE
9/7/1998 5:19	2510 / Horta, Portugal	Portuguese strong-motion network	SN
9/1/1988 1:02	3169 / Tirana-Seismological Observatory, Albania	Strong-motion network of Seismological Institute of Academy of Sciences of Albania	EW
19/8/1976 1:12	2437 / Denizli Merkez Meteoroloji Mudurlugu, Turkey	National strong-motion network of Turkey	NS
23/11/1973 13:36	2895 / San Mateus, Portugal	Portuguese strong-motion network	NS
4/11/1973 15:52	2518 / Lefkada-O.T.E., Greece	Strong-motion network of National Observatory of Athens	N25W
1/5/2003 0:27	0229 / Bingol Merkez Bayindirlik Ve Iskan Mudurlugu, Turkey	National strong-motion network of Turkey	NS
23/1/1992 4:24	2493 / Argostoli-O.T.E., Greece	ITSAK strong-motion network	59
12/11/1999 16:57	0187 / Sakarya Karadere Koyu, Turkey	Temporary strong-motion network of LDEO	EW
15/9/1976 9:21	0013 / Breginj-Fabrika Igli, Italy	National strong-motion network of Slovenia	EW
24/2/1981 20:53	0982 / Korinthos-O.T.E., Greece	Strong-motion network of National Observatory of Athens	N120
20/6/1994 9:09	1494 / Zarrat, Iran	Iranian strong-motion network	148
6/4/2009 1:32	3614 / L Aquila - V. Aterno - Centro Valle, Italy	DPC (Italian Civil Protection Authority)	NS
12/11/1999 17:17	3253 / Irigm Station No. 496, Turkey	Temporary strong-motion network of Universite Joseph Fourier IRIGM	NS
19/9/1979 21:35	0017 / Cascia, Italy	DPC (Italian Civil Protection Authority)	WE
4/11/1973 15:52	2518 / Lefkada-O.T.E., Greece	Strong-motion network of National Observatory of Athens	N115
24/5/1979 17:23	2920 / Budva-Ptt, Montenegro	Strong-motion network of EnergoProject	EW
13/9/1986 17:24	0055 / Kalamata-O.T.E. (1), Greece	N/A	N265
28/2/1997 12:57	3558 / Kariq, Iran	Iranian strong-motion network	69
15/6/1995 0:15	2500 / Aigio-OTE, Greece	Strong-motion network of National Observatory of Athens	N/A
26/3/1993 11:58	2424 / Pyrgos-Agriculture Bank, Greece	ITSAK strong-motion network	TRAN
14/7/1993 12:31	2498 / Patra-Agios Dimitrios, Greece	ITSAK strong-motion network	TRAN
7/9/1999 11:56	2473 / Athens-Sepolia (Garage), Greece	Strong-motion network of National Observatory of Athens	LONG
26/9/1997 0:33	0122 / Nocera Umbra, Italy	DPC (Italian Civil Protection Authority)	NS

Table A.2 Selected ground motion records used in Chapter 4 (source: Ambraseys et al. 2004)

Date Time	Country	Station name	Station code	Earthquake code	Waveform code
4/11/1973 15:52:12	Greece	Lefkada-OTE Building	8	30	42
11/9/1976 16:31:11	Italy	Forgaria-Cornio	24	60	114
11/9/1976 16:35:03	Italy	Buia	33	61	122
15/9/1976 9:21:19	Italy	San Rocco	28	65	147
16/9/1977 23:48:08	Italy	Forgaria-Cornio	24	72	159
18/7/1979 13:12:02	Turkey	Dursunbey-Kandilli Gozlem Istasyonu	80	112	239
19/9/1979 21:35:37	Italy	Cascia	225	115	242
16/1/1981 0:37:47	Italy	Procisa Nuova	111	153	322
7/5/1984 17:49:42	Italy	Atina	140	175	365
11/5/1984 10:41:50	Italy	Villetta-Barrea	154	176	384
13/9/1986 17:24:34	Greece	Kalamata-Prefecture	164	192	413
26/3/1993 11:58:15	Greece	Pyrgos-Agriculture Bank	214	267	558
26/9/1997 0:33:16	Italy	Nocera Umbra	60	290	593
6/10/1997 23:24:00	Italy	Colfiorito-Casermette	236	291	651
11/9/1976 16:31:11	Italy	Tarcento	26	60	707
3/10/1997 8:55:22	Italy	Colfiorito	221	350	776
3/4/1998 7:26:00	Italy	Nocera Umbra-Biscontini	235	364	852
16/1/1981 0:37:47	Italy	Contrada Fiumicella-Teora	308	153	980
16/9/1977 23:48:08	Italy	Somplago Centrale-Uscita Galleria	309	72	982
7/9/1999 11:56:51	Greece	Athens-Sepolia (Garage)	1259	474	1715
26/8/1983 12:52:09	Greece	Ierissos-Police Station	1311	648	1882
25/2/1994 2:30:50	Greece	Lefkada-Hospital	126	282	1911
26/8/1983 12:52:09	Greece	Ouranoupolis-Seismograph Station	1328	648	1917
15/5/1995 4:13:57	Greece	Chromio-Community Building	1369	2033	6050
7/11/1999 16:54:41	Turkey	LDEO Station No. C0375 VO	3136	2158	6440

Table A.3 Selected ground motion records used in Chapter 5 (source: Akkar et al. 2014)

Date Time	Station Code / Name	Network	Orientation
1/5/2003 0:27	0229 / Bingol Merkez Bayindirlik Ve Iskan Mudurlugu, Turkey	National strong-motion network of Turkey	NS
9/7/1998 5:19	2510 / Horta, Portugal	Portuguese strong-motion network	SN
15/6/1995 0:15	2500 / Aigio-OTE, Greece	Strong-motion network of National Observatory of Athens	N/A
26/3/1993 11:58	2424 / Pyrgos-Agriculture Bank, Greece	ITSAK strong-motion network	TRAN
9/1/1988 1:02	3169 / Tirana-Seismological Observatory, Albania	Strong-motion network of Seismological Institute of Academy of Sciences of Albania	EW
15/9/1976 9:21	0013 / Breginj-Fabrika Igli, Italy	National strong-motion network of Slovenia	EW
19/8/1976 1:12	2437 / Denizli Merkez Meteoroloji Mudurlugu, Turkey	National strong-motion network of Turkey	NS
15/4/1979 6:19	2914 / Bar-Skupstina Opstine, Montenegro	Strong-motion network of EnergoProject	NS
14/7/1993 12:31	2498 / Patra-Agios Dimitrios, Greece	ITSAK strong-motion network	TRAN
7/9/1999 11:56	2473 / Athens-Sepolia (Garage), Greece	Strong-motion network of National Observatory of Athens	LONG
23/11/1973 13:36	2895 / San Mateus, Portugal	Portuguese strong-motion network	NS
4/11/1973 15:52	2518 / Lefkada-O.T.E., Greece	Strong-motion network of National Observatory of Athens	N25W
26/9/1997 0:33	0122 / Nocera Umbra, Italy	DPC (Italian Civil Protection Authority)	NS
1/5/2003 0:27	0229 / Bingol Merkez Bayindirlik Ve Iskan Mudurlugu, Turkey	National strong-motion network of Turkey	NS
15/9/1976 3:15	0013 / Breginj-Fabrika Igli, Italy	National strong-motion network of Slovenia	EW
6/4/1977 13:36	2906 / Naghan 1, Iran	National strong-motion network of Iran	LONG
12/11/1999 17:17	3253 / Irigm Station No. 496, Turkey	Temporary strong-motion network of Universite Joseph Fourier IRIGM	NS
19/9/1979 21:35	0017 / Cascia, Italy	DPC (Italian Civil Protection Authority)	WE
24/5/1979 17:23	2920 / Budva-Ptt, Montenegro	Strong-motion network of EnergoProject	EW
13/9/1999 11:55	3263 / Kocaeli Tepetarla Tepetarla, Turkey	National strong-motion network of Turkey	EW
28/2/1997 12:57	3558 / Kariq, Iran	Iranian strong-motion network	69
12/11/1999 16:57	3253 / Irigm Station No. 496, Turkey	Temporary strong-motion network of Universite Joseph Fourier IRIGM	NS

References

Akkar S, Sandikkaya MA, Senyurt M, Azari Sisi A, Ay BÖ, Traversa P, Douglas J, Cotton F, Luzi L, Hernandez B, Godey S (2014). Reference database for seismic ground-motion in Europe (RESORCE), Bulletin of Earthquake Engineering, 12(1): 311-339, doi: 10.1007/s10518-013-9506-8

Ambraseys NN, Douglas J, Sigbjörnsson R, Berge-Thierry C, Suhadolc P, Costa G, Smit PM (2004) Dissemination of European Strong-Motion Data, volume 2. Proceedings of 13th World Conference on Earthquake Engineering, Paper no. 32

Appendix B

This appendix employs the risk-targeted behaviour factor (RTBF) technique described in Chapter 4 to derive example risk-targeted maps for Italy. While the procedure is the same followed in Section 4.4, data from a different hazard study for Italy are used herein.

Application of the risk-targeted behaviour factor approach for Italy

The hazard input for the *PGA* is provided by Gruppo di Lavoro MPS (2004) for a 10%-in-50-years probability of exceedance, while data for other probabilities of exceedance are available in Meletti and Montaldo (2007). In addition, the spectral acceleration values for a period of 0.5s are obtained from Montaldo and Meletti (2007). The target risk level is set equal to $2 \cdot 10^{-4}$ yrs^{-1}, as proposed in ASCE 7-16 (2017), roughly corresponding to a 1% probability of exceedance in 50 years. The power law hazard model is fitted through two points (see Chapter 4, Section 4.3.1). Based on the available data, the fitting points refer to a probability of exceedance in 50 years roughly equal to 2% and 10%.

Figure A.1a and Figure A.2a show the values of PGA^{ref} and $S_a^{ref}(T)$ according to PSHA and a reference return period of 475 years, whereas the values of k_1 corresponding to the slope of the fitted curve are plotted in Figure A.1b and Figure A.2b. A high variation of the slope of the hazard curve is observed. There are cases where the curve is quite steep with $k_1 > 5$, while other locations have hazard curves with very low slopes, in some cases lower than 1.4.

Figure A.1c and Figure A.2c show the risk-targeted values of the design acceleration, evaluated via Eqn.(4.10). For the case of the PGA, $\beta = 0$ and $\hat{q}_{\mu_c} = 1$, whereas for S_a (T=0.5s), $\hat{q}_{\mu_c}$ is assumed equal to 4 and $\beta = 0.6$, as per ASCE 7-16 (2017). In both cases the contribution of overstrength is considered as well, by assuming $q_S = 2$.

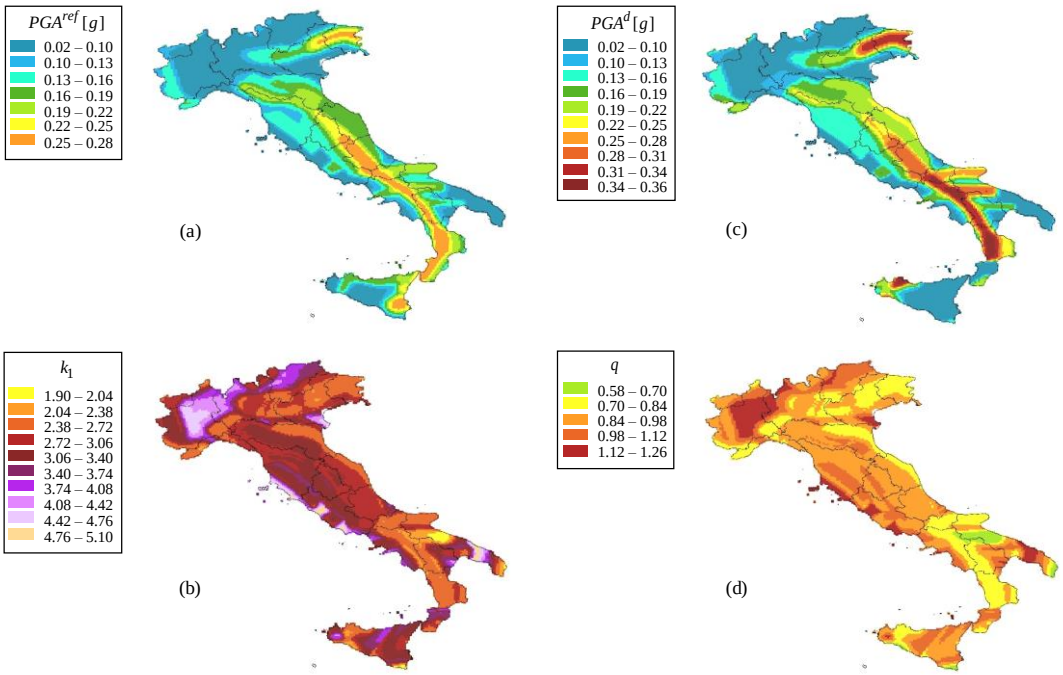

Figure A.1 Seismic design maps for Italy in terms of *PGA*: (a) *PGA* at reference return period (475 years), (b) k_1 for the power-law approximation, (c) risk-targeted design *PGA* and (d) risk-targeted behaviour factor

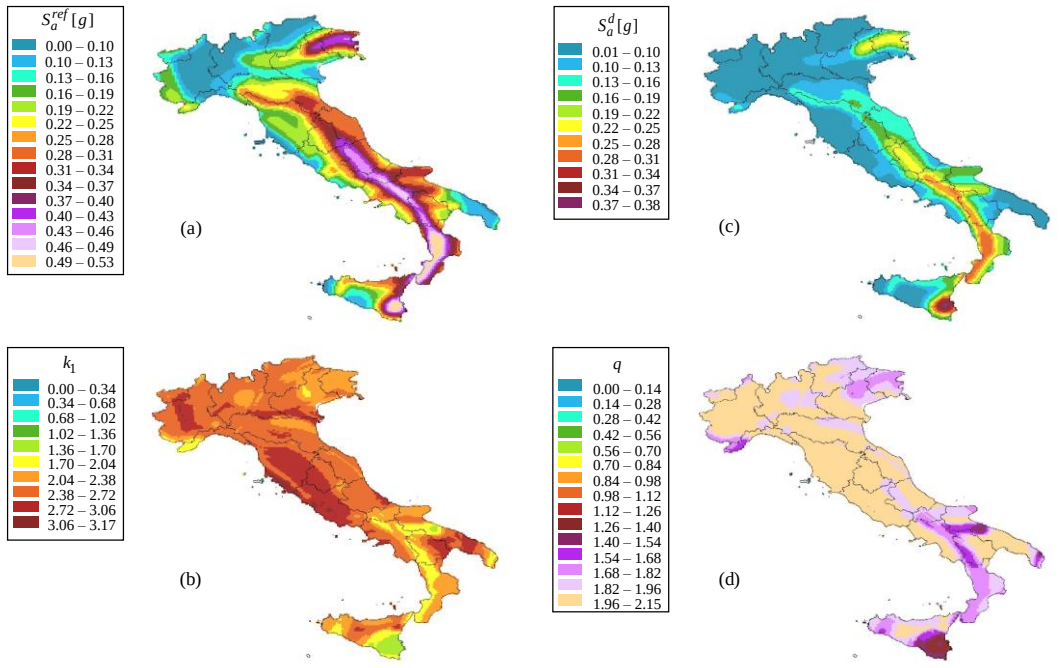

Figure A.2 Seismic design maps for Italy in terms of S_a (T=0.5s): (a) Spectral acceleration for T=0.5s at reference return period (475 years), (b) k_1 for the power-law approximation, (c) risk-targeted design *PGA* and (d) risk-targeted behaviour factor

The values of the risk-targeted behaviour factor q are given in Figure A.1d and Figure A.2d. This factor is derived by the ratio of the reference design acceleration and the risk-targeted design acceleration. A value higher than one means that the reference design acceleration should be decreased in order to satisfy the risk acceptance criteria.

In general, low values of q are obtained. Of course, this conclusion is sensitive to the assumptions made for the target risk level and the ductility and overstrength of the system. For the case of $S_a(T=0.5s)$, q is in general between 1.25 to 2.15. For the *PGA* though, q is lower than one in most areas, which means that the reference *PGA* should be increased to achieve the target risk level.

References

ASCE (2017) Minimum Design Loads and Associated Criteria for Buildings and Other Structures, ASCE/SEI 7-16. American Society of Civil Engineers, Reston, VA

Gruppo di Lavoro MPS (2004) Redazione della mappa di pericolosità sismica prevista dall'Ordinanza PCM del 20 marzo 2003 n. 3274, All. 1. Rapporto conclusivo per il Dipartimento della Protezione Civile, aprile 2004, Istituto Nazionale di Geofisica e Vulcanologia (INGV), Milano-Roma, Italy, available at http://zonesismiche.mi.ingv.it/

Meletti C, Montaldo V (2007) Stime di pericolosità sismica per diverse probabilità di superamento in 50 anni: valori di ag. Progetto DPC-INGV S1, Deliverable D2, http://esse1.mi.ingv.it/d2.html

Montaldo V, Meletti C (2007) Valutazione del valore della ordinata spettrale a 1sec e ad altri periodi di interesse ingegneristico. Progetto DPC-INGV S1, Deliverable D3, http://esse1.mi.ingv.it/d3.html